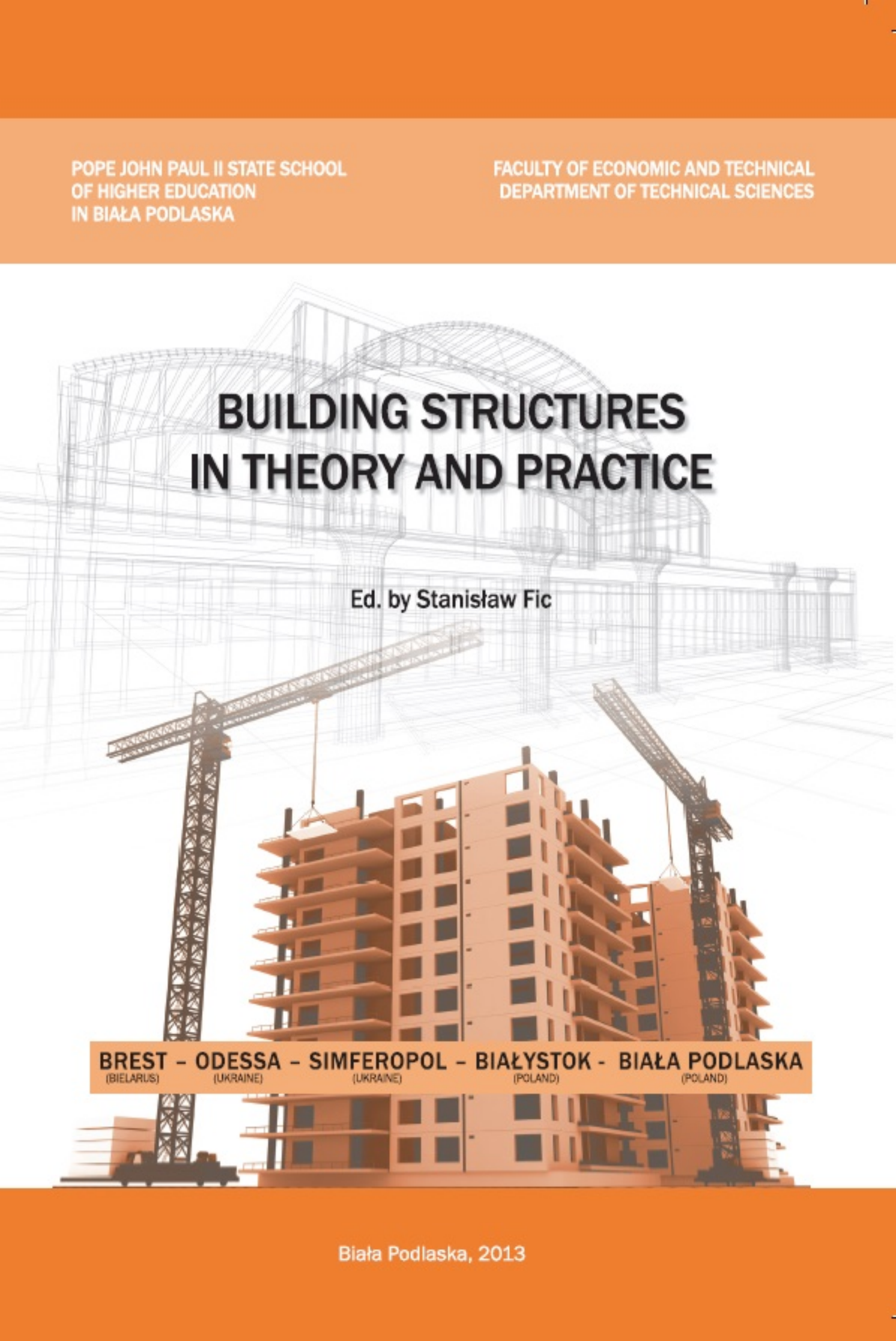


POPE JOHN PAUL II STATE SCHOOL
OF HIGHER EDUCATION
IN BIAŁA PODLASKA

FACULTY OF ECONOMIC AND TECHNICAL
DEPARTMENT OF TECHNICAL SCIENCES

BUILDING STRUCTURES IN THEORY AND PRACTICE

Ed. by Stanisław Fic



BREST – ODESSA – SIMFEROPOL – BIAŁYSTOK – BIAŁA PODLASKA

(BIELARUS)

(UKRAINE)

(UKRAINE)

(POLAND)

(POLAND)

Biała Podlaska, 2013

POPE JOHN PAUL II STATE SCHOOL
OF HIGHER EDUCATION
IN BIAŁA PODLASKA

FACULTY OF ECONOMIC AND TECHNICAL
DEPARTMENT OF TECHNICAL SCIENCES

BUILDING STRUCTURES IN THEORY AND PRACTICE

Edited by

Stanisław Fic

BREST – ODESSA – SIMFEROPOL – BIAŁYSTOK – BIAŁA PODLASKA
(BIELARUS) (UKRAINE) (UKRAINE) (POLAND) (POLAND)

Biała Podlaska, 2013

Reviewers:

prof. nadzw. dr hab. inż. Stanisław Fic
prof. dr hab. inż. Wiktor Tur
prof. dr hab. inż. Vadzim Nikitsin

The Scientific Council:

prof. nadzw. dr hab. inż. Stanisław Fic – chairman, PSW Biała Podlaska
prof. dr hab. inż. Wiktor Tur – vice-chairman, PSW Biała Podlaska, Technical University of Brest
prof. dr hab. inż. Vadzim Nikitsin – vice-chairman, PSW Biała Podlaska
prof. dr hab. inż. Andrzej Łapko – Białystok University of Technology
prof. dr hab. inż. Czesław Miedziałowski – Białystok University of Technology
prof. dr hab. inż. Bohdan Demczyna – National University Lviv Polytechnic
prof. dr hab. inż. Siergiej Fedorkin – Akademia PKB Krim
prof. dr hab. inż. Nikolai Lubomirskij – Akademia PKB Krim
prof. dr hab. inż. Valeri Vyrovoy – Odessa State Academy of Civil Engineering and Architecture
prof. dr hab. inż. Sergiej Koval – Odessa State Academy of Civil Engineering and Architecture
prof. dr hab. inż. Hrytsuk Mikhail – PSW Biała Podlaska
prof. dr hab. Jerzy Nitychoruk – PSW Biała Podlaska

Editorial Committee:

dr inż. Danuta Barnat-Hunek - chief editor

Organization unit:

dr Andrzej Misiejuk
dr Anna Jakubowicz
dr inż. Adam Wasilewski
mgr inż. Agnieszka Karwacka

MONOGRAPH

ISBN 978-83-61044-35-2

Liczba arkuszy wyd.: 10

Nakład: 110 egz.

Published by
Pope John Paul II State School of Higher Education
in Biała Podlaska

© Copyright by Państwowa Szkoła Wyższa im. Papieża Jana Pawła II
w Białej Podlaskiej



Wydawnictwo PSW JPII
ul. Sidorska 95/97, p. 231R
21-500 Biała Podlaska
www.pswbp.pl

Skład, druk, projekt okładki/ Printing, binding and cover design:

Agencja Reklamowa TOP, ul. Toruńska 148, 87-800 Włocławek,
tel.: 54 423 20 40, fax: 54 423 20 80, www.agencjatom.pl

Introduction

Theoretical and practical observations of the behaviour of the component or composite constructions made by many generations of engineers and scientists formed the basis for the design, simultaneously providing them with a safe bearing capacity, strength and deformability of materials. The accepted methods of calculations allow to determine the limit state of structural elements where the damage occurs or deformations exceed the limit value. This enables one to obtain the numerical values of strength and deformations of different materials under changing external interactions (computational bearing capacity and deformation characteristics). The resulting values are used to determine the load or other external impacts corresponding to a limit state (maximum load or impact). The adoption of the design process to the construction of the relevant requirements will ensure its safe use and durability over time. The correct dimensioning of steel, concrete, wood and composite structures is a difficult process, and hence in recent years, it has been assisted with computer programs. The use of computer software is so important for dimensioning components and structural systems that it is required regardless of experience or a careful analysis.

This monograph is a collection of 14 articles relating to components and structural systems made of different materials. The authors present theoretical considerations that occurred in the case of structural elements under the influence of internal and external impacts, often with the support of computer programs. Moreover, another group of articles refers to their own research conducted on different elements in the laboratory.

Solutions presented in the articles allow to obtain a range of information and knowledge on the behaviour of components and structural systems, and thus they have an important scientific and technical meaning. The achieved outcomes, resulting from a conducted research or theoretically relating to the area of scientific concern, are copyrighted.

The information and solutions described in the articles can be used as a study aid not only to students of architecture and civil engineering, but also for civil engineers involved in the design and construction of buildings and specialists in the area of engineering science.

Acknowledgments:

The initiative to publish the monograph is held under the patronage of His Magnificence Ph.D Full Professor Józef Bergier, Rector of Pope John Paul II State School of Higher Education in Biała Podlaska, whom I am very grateful.

I express sincere thanks to the authors of the articles, the reviewers and the Scientific Committee for their hard work and professional preparation. I wish you success in your personal and scientific life.

Sincerely
Stanisław Fic

Contents:

1. Łapko A., Łuniewska M. <i>Sectional design of r/c members using deformational model with inclined top branch of steel stress-strain relationship</i>	<i>7</i>
2. Naytchuk A., Malesza M., Miedzialowski Cz. <i>On selected directions of improvement in method of design of timber structures</i>	<i>26</i>
3. Smarzewski P. <i>Analysis of deformation states in high performance fibre reinforced concrete bent plates</i>	<i>42</i>
4. Tarasevich A., Tur V. <i>Calculation of the thin plates with the large deflections</i>	<i>51</i>
5. Jabłońska-Krysiewicz A., Sadowska-Buraczewska B. <i>Recent research and development in composite structures</i>	<i>57</i>
6. Oponowicz P., Michalska M. <i>Resistance of non-welded rhs connections</i>	<i>69</i>
7. Bąk G., Gosk W. <i>Numerical prediction of wave reaction of the layered elastic half-space.....</i>	<i>84</i>
8. Matulewicz S., Chyży T. <i>Effort analysis of structural elements of the high building subjected to large displacements.....</i>	<i>94</i>
9. Krętowska J. <i>A new subsoil model for the analysis soil-structure interaction.....</i>	<i>103</i>
10. Tur V., Malykha U. <i>Exerimental studies of concrete beams reinforced longitudinally with steel and GFRP bars</i>	<i>119</i>
11. Smarzewski P. <i>Modelling behaviour of high-strength concrete beams</i>	<i>129</i>
12. Matulewicz S., Miedzialowski C. <i>Modern computer methods of multivariant analysis of a tall building</i>	<i>144</i>
13. Jabłońska-Krysiewicz A., Waśniewska E. <i>Nonlinear elastic-plastic 3d-finite element modelling of semi-rigid steel end-plate connections.....</i>	<i>158</i>
14. Chyży T., Mackiewicz M. <i>Method of embankment modeling using one-dimensional layered finite elements.....</i>	<i>167</i>

15. Mackiewicz M.	
<i>Analysis of life cycle assessment of wooden construction</i>	<i>176</i>
16. Szafranko E.	
<i>Selection of a construction technology for a building object, analytical methods</i>	<i>192</i>
17. Pawłowicz J. A.	
<i>Possible applications of the 3d laser scanning technology in civil engineering</i>	<i>215</i>
18. Baszeń M., Miedziałowski C.	
<i>Experimental tests and analytical models of light wood-framed buildings.....</i>	<i>230</i>

SECTIONAL DESIGN OF R/C MEMBERS USING DEFORMATIONAL MODEL WITH INCLINED TOP BRANCH OF STEEL STRESS-STRAIN RELATIONSHIP

¹Andrzej Lapko, ²Monika Łuniewska

¹Chair of Building Structures, Faculty of Civil & Environment Engineering,
University of Technology, Wiejska Street 45e, 15-351 Białystok, Poland

E-mail: ¹lapko@pb.bialystok.pl;

²Design Office „KONSTRUKTOR”, gen. Maczka Street 52/ 2/13, 15-691 Białystok, Poland

E-mail: ²monika.lun@o2.pl

Summary:

The paper presents the analysis of advanced cross-sectional design models of R/C flexural members using inclined top branch of stress-strain relationship for flexural reinforcing steel. The analysis was performed having considered more effective way to use realistic properties of ductility of flexural steel. Workflow is based on a basic assumptions described in the Eurocode 2 and also in Model Code 2010.

For concrete in compression the two models were considered: parabola-rectangle relationship and bi-linear stress-strain relation and for reinforcing steel - inclined and horizontal top branch models.

There were derived and presented formulas for evaluation of cross-sectional parameters for the members with rectangular cross-section shape using the parabola-rectangle and bi-linear stress-strain relation for all the concrete classes and steel with inclined branch of strains. Adaptation in design of analytical formulas is very labour-consuming, therefore cross-sectional parameters for normal concrete and HSC were written using tabular coefficients and presented in the tables. As calculation examples of dimensioning of flexural beam are the areas of flexural reinforcement are compared for member with rectangular cross-section.

Keywords: stress-strain relationship, reinforced concrete, cross-sectional design, ductility of steel.

Introduction

The evaluation of flexural capacity of reinforced concrete members according to recent codes like EN 1992-1-1 (2004) and Model Code 2010 (2012) is based on assumptions of a non-linear stress-strain relationship for concrete in the compressive zone and bi-linear relationship representing steel behavior under loading till failure (Ultimate Limit State).

The exact formulas applied for computation of the ultimate bending moment, which can be resisted by the reinforced beams using deformational model are much more complex in comparison to simplified model using rectangular stress block, due to necessity of possible true approximation of concrete behavior in compression zone. Any approximation induces various parameters to the function representing the stress distribution in concrete compressive zone, which is strongly dependent from the stress-strain diagrams. Codes usually are providing certain parameters, which should be applied for the estimation of the stress distribution in compressive zone.

The paper presents the comparison of results of computations of the ultimate bending capacity for flexural members using non-linear model for concrete and bi-linear model for reinforcing steel with the inclined branch. For estimation of the resultant of stresses in compressive concrete zone different values of characteristics of the strain functions (ε_{c2} , ε_{cu2} , n , parameters of limit strain and exponent of stress – strain function respectively) are applied following European Standard EN 1992-1-1 (2004) and Model Code 2010 (2012). This comparison shows that the assumed and applied in different standards strain coefficients play a significant role on the magnitude of the computed ultimate flexural capacity.

Theoretical approach for flexural members

Functional stress-strain relationships for concrete in compression

Parabolic-rectangular compressive stress distribution shown in Fig.1a for ultimate flexural limit state design of reinforced concrete sections is recommended by recent European structural concrete codes (Eurocode 2 and Model code 2010). The three strain characteristics: n , ε_{c2} , ε_{cu2} defining the distribution of stresses in compression zone and recommended in standards are indicated and explained in the Fig.1a. The distribution of stresses in compression zone of considered section under bending is given by the formulas:

When the concrete strains are in the range $0 \leq \varepsilon_c \leq \varepsilon_{c2}$

$$\sigma_c = f_d \left[1 - \left(1 - \frac{\varepsilon_c}{\varepsilon_{c2}} \right)^n \right] \quad (1)$$

and for the range $\varepsilon_{c2} \leq \varepsilon_c \leq \varepsilon_{cu2}$

$$\sigma_c = f_d \quad (2)$$

where: f_d – design compressive strength for given concrete class,

ε_{c2} , ε_{cu2} , n – parameters of limit strain and exponent of stress – strain function respectively

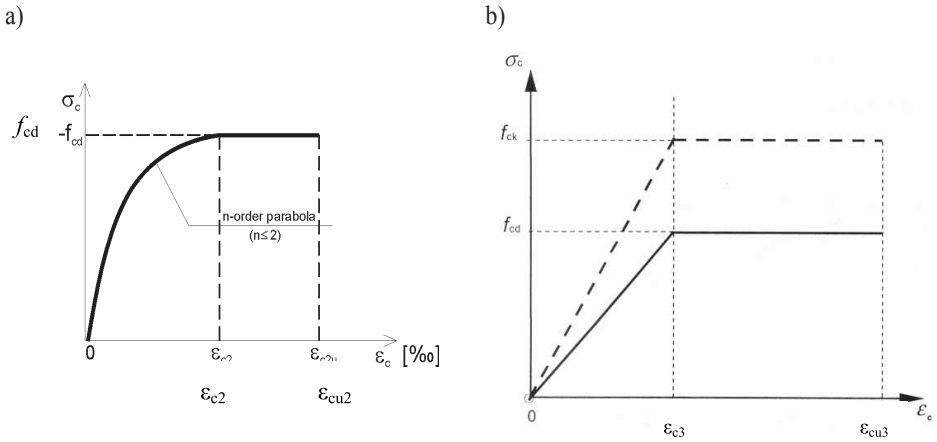


Fig.1. Stress - strain relationships for concrete used for ultimate limit state design (EC2 2004 Model Code 2010):

a) parabola-rectangle relation

b) bi-linear relation

The three strain characteristics are: n - exponent of stress - strain function and two values of strains: ϵ_{c2} representing strain at the border between curved and rectangular part of the stress strain diagram, and ϵ_{cu2} representing ultimate strain at failure (see Fig.1a).

In cross-sectional analysis could be used also bi-linear relationship for stress-strain function for concrete in compression. In Fig.1b there is presented design diagram of compressive stresses and strains with limited values of strains ϵ_{c3} and ϵ_{cu3} (Eurocode 2, Model Code 2010).

Reinforcing steel properties

Informations about behaviour of reinforcing steel may be found in Eurocode 2 in subsection 3.2 and in annex C. The rules presented there have general character and describing basic requirements and qualities of the product, specified in European Standard (EN 10080 2006).

The deciding influence in designs have: yield strength (f_{yk} or $f_{0.2k}$), designed yield strength f_{yd} and idealized stress-strain relation, taking into account reinforcing steel ductility, depending on ultimate deformation ϵ_u and ratio of tensile strength to the yield stress $(f_t/f_y)_k$.

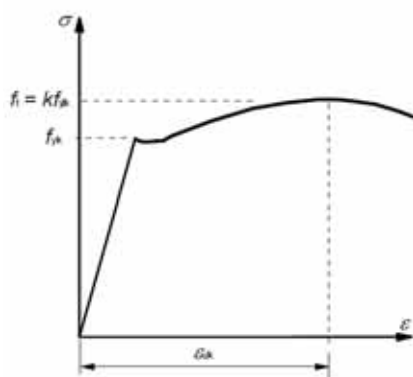
The application rules for design and detailings are specified in Eurocode 2. The yield strength f_{yk} ranges takes from 400 to 600MPa. In Poland the commonly used reinforcing steel has characteristic yield strength equal $f_{yk} = 500\text{MPa}$.

Table 1. Properties of steel used in Poland and theirs characteristics, according to Eurocode 2 (Strosolski 2011)

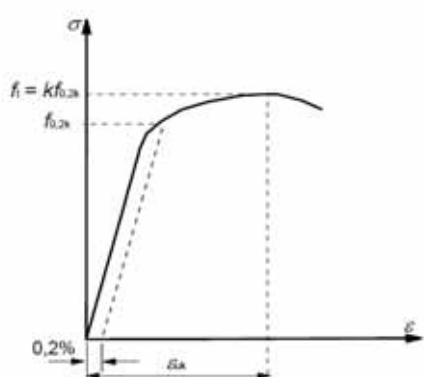
Steel class	Type	Yield strength [MPa]		Tensile strength f_t [MPa]	ε_{uk} [‰]	$k = (f_t/f_{yk})$
		f_{yk}	f_{yd}			
A	B500A	500	435	min 525	>2,5	>1,05
A	RB500	500	435	min 550	>2,5	>1,05
A	RB500W	500	435	min 550	>2,5	>1,05
B	RB400	400	347	min 440	>5	>1,08
B	34GS	410	356	min 590	>5	>1,08
B	BSt500S(B)	500	435	min 550	>5	>1,08
C	B500SP	500	435	min 575	>8	1,15-1,35

Ductility is understand as large strain capability of reinforcement after reaching yield strength: „Reinforcement ductility is defined by requirements on the elongation at maximum force ε_{uk} and by the ratio of tensile strenght to the yield stress” (Knauff 2006, 2012). It is specified by the two parameters: k and ε_{uk} (see Fig.2). The value of k denotes

$$k = \left(\frac{f_t}{f_y} \right)_k \quad (3)$$



a) hot rolled steel



b) cold worked steel

Fig. 2. Stress-strain diagrams of typical reinforcing steel (Eurocode 2, Model Code 2010)

In Table 2 there are presented properties of reinforcing steel, taken from Eurocode 2. It should be noticed, that k and ε_{uk} factors are given as a minimum values. It may be used when we don't have exact steel specifications given in certificates provided by the manufacturer.

Table 2. Properties of reinforcement (Annex C to Eurocode 2)

Property of steel	Bars and de-coiled rods			Wire Fabrics			Requirement of quantile value (%)
Class	A	B	C	A	B	C	-
Characteristic yield strength f_{yk} or $f_{0,2k}$ (MPa)	400 do 600						5,0
Minimum value of $k = (f_t/f_y)_k$	$\geq 1,05$	$\geq 1,08$	$\geq 1,15$ $< 1,35$	$\geq 1,05$	$\geq 1,08$	$\geq 1,15$ $< 1,35$	10,0
Characteristic strain at maximum force, ε_{uk} (%)	$\geq 2,5$	$\geq 5,0$	$\geq 7,5$	$\geq 2,5$	$\geq 5,0$	$\geq 7,5$	10,0

On the Polish market there are actually available many classes of high strength steels. However, only one of them is having the best ductility parameters: class B500SP with the EPSTAL quality mark. Material parameters of this steel allows to qualify it to class C (high ductility class). Today, most commonly used classes of steel are those with medium ductility.

For normal designs, Eurocode 2 allows to use one of the following assumptions (see Fig. 3):

- an inclined top branch: strain limit equals ε_{ud} and a maximum stress of $k f_{yk} / \gamma_s$
- a horizontal top branch: strain limit may not be checked.

The recommended value of ε_{ud} is $0,9 \varepsilon_{uk}$.

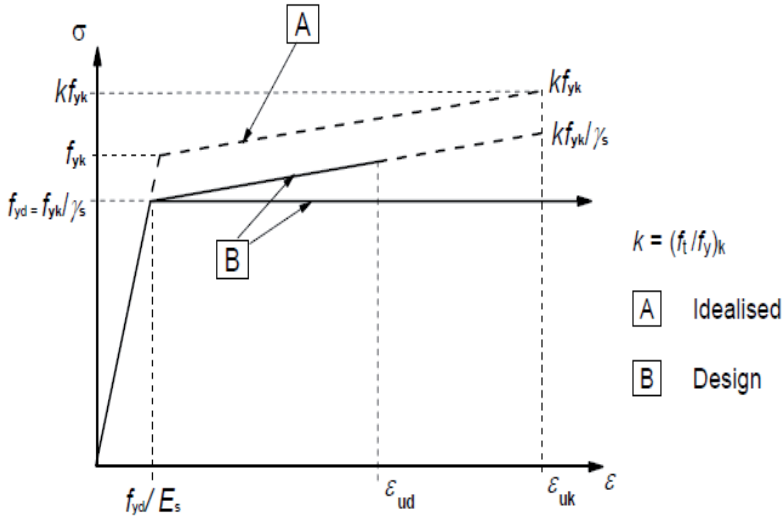


Fig. 3. Idealised (A) and design (B) stress-strain diagrams for reinforcing steel (Eurocode 2, 2004)

In model a) with inclined top branch, steel reaching yield strength at ultimate strain equals ε_{ud} . In b) model with horizontal top branch it was assumed that stress are constant and equal to design yield stress, and reinforcement strains are not limited. Commonly, design was based on model b) with horizontal top branch. Formerly, in both design models reinforcing steel strains ε_{uk} were limited for reinforcement bars to 10‰. There are no such limits in Eurocode 2.

In presented article will be analyzed model of steel with inclined top branch.

Analysis of cross-sectional forces for parabola-rectangular model for concrete

Main assumptions

According to Fig. 4 the external bending moment is balanced by following internal forces:

- resultant of compression stresses in concrete F_c
- resultant of stress in reinforcing steel tension F_s

Resultant of compression stress in concrete F_c may be computed as a volume of stress block, based on compression zone of the cross-section. The second parameter for volume evaluation depends of the shape of stress diagrams.

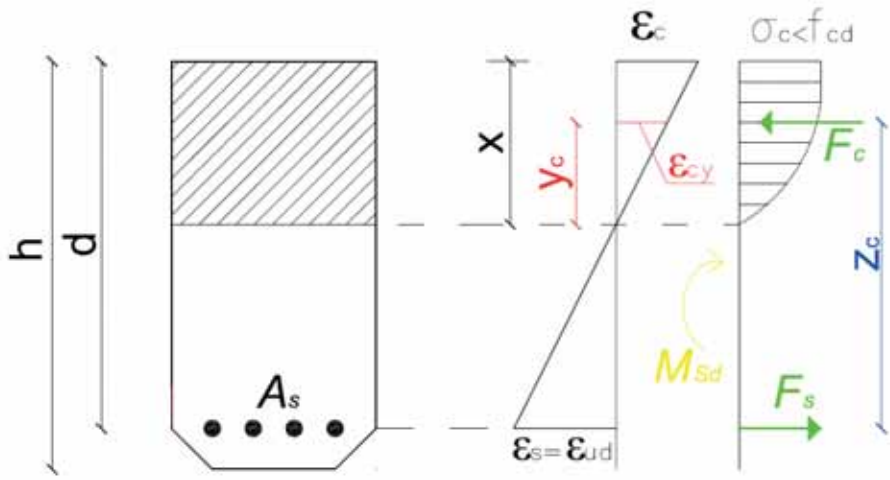


Fig. 4. Resultant of internal forces in any cross-section of flexural R/C member

For determination of internal forces moment M_{Rd} it is necessary to previously define internal level arm z_c – distance between resultants of forces F_c and F_s (according to Fig. 4).

$$z_c = d - x + y_c \quad (4)$$

y_c - distance between centre of gravity of stress block and the neutral axis of the element.

Resultant of stresses in flexural reinforcement may be written in following form:

$$F_s = A_s \sigma_s \quad (5)$$

$\sigma_s = f_{yd}$ – for variant with horizontal top branch for reinforcing steel deformations.

In variant with inclined top branch for reinforcing steel deformations, value σ_s can be designated from proportion, in which first should be determined range of deformations in reinforcing steel.

Ultimate limit state is determined on the basis of internal bending moment (flexural capacity):

$$M_{Rd} = F_c z_c \quad (6)$$

While range of the compression zone x in singly reinforced cross-section is defined from equation of internal forces:

$$F_c - F_s = 0 \quad (7)$$

Considering cross-section of the element and its bearing, independent of its shape may be made following assumptions:

1. Plane-sectional law according to Bernulli's rule (cross-section deformations are proportional to theirs distance to the neutral axis).
2. Deformations of reinforcement and concrete surrounding are the same for both materials $\varepsilon_s = \varepsilon_{cs}$
3. Concrete tensile strength f_{ct} is ignored
4. Stresses in concrete in compression is derived from the design relationship $\sigma_c - \varepsilon_c$
5. Stresses in the reinforcing steel are derived from the design curve $\sigma_s - \varepsilon_s$

Based on above assumptions there were derived formulas for evaluation of cross-sectional parameters for rectangular shape of elements. These formulas are depending on the combination of strain domains in concrete compression zone and in tension flexural steel (Lapko 2001, Lapko Jensen 2006). Because of concrete compressive strain conditions, the shape of the stress diagrams in the compressed zone can be different. Therefore, compression stress block F_c will be described with different functions according to the range of strains in concrete in compression (Lapko Jensen 2006).

Table 3. Strain domains assumed in the analysis (Lapko and Jensen 2006)

Strain Domain	1a	1b	2
Strains in concrete ε_c	$\varepsilon_c \leq \varepsilon_{c2}$	$\varepsilon_{c2} \leq \varepsilon_c \leq \varepsilon_{cu2}$	$\varepsilon_c = \varepsilon_{cu2}$
Strains in steel ε_s	$\varepsilon_s = \varepsilon_{ud}$	$\varepsilon_s = \varepsilon_{ud}$	$f_{yd}/E_s \leq \varepsilon_s \leq \varepsilon_{ud}$

Solutions for normal concrete classes for $f_{ck} \leq 50$ MPa

Combination of strains in domain 1a (see Fig.5)

$$\varepsilon_c \leq \varepsilon_{c2} = 2,0\text{‰} \quad \varepsilon_{cu2} = 3,5\text{‰} \quad n = 2 \quad \varepsilon_{ud} = \varepsilon_{su}$$

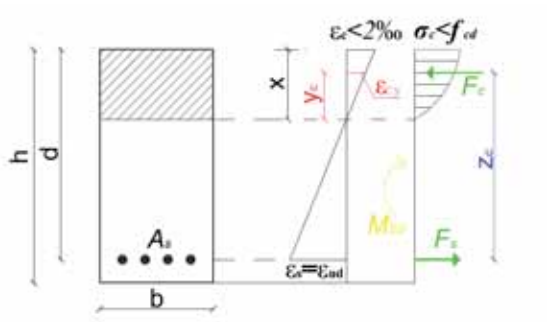


Fig. 5. Strain and stress diagrams in rectangular cross-section of flexural member in Domain 1a for normal concrete classes

The resultant of compressive stress block can be derived from the integral formula:

$$F_c = f_{cd} b \int_0^x \left[1 - \left(1 - \frac{\varepsilon_{cy}}{\varepsilon_{c2}} \right)^n \right] dy \quad (8)$$

Knowing, that $n=2$ we have:

$$F_c = f_{cd} b \int_0^x \left[1 - \left(1 - \frac{\varepsilon_{cy}}{2} \right)^2 \right] dy = f_{cd} b \int_0^x \left[\varepsilon_{cy} - \frac{\varepsilon_{cy}^2}{4} \right] dy \quad (9)$$

From linear proportions we obtain the value of ε_{cy} (see Fig.6)

$$\frac{\varepsilon_{cy}}{y} = \frac{\varepsilon_{su}}{d-x} \Rightarrow \varepsilon_{cy} = y \frac{\varepsilon_{su}}{d-x} \quad (10)$$

Substitution this value into the equation $\varepsilon_{cy} = y \frac{\varepsilon_{su}}{d-x}$ we obtain:

$$F_c = f_{cd} b \int_0^x \left[\varepsilon_{su} \frac{y}{d-x} - \left(\varepsilon_{su} \frac{y}{d-x} \right)^2 \frac{1}{4} \right] dy = f_{cd} b \left[\frac{\varepsilon_{su}}{2(d-x)} x^2 - \frac{\varepsilon_{su}^2}{(d-x)^2} \frac{x^3}{12} \right] \quad (11)$$

or for nondimensional value of neutral axis depth $\xi = x/d \Rightarrow x = \xi d$

$$F_c = f_{cd} b d \left[\frac{\xi^2 \left(\frac{1}{2} \varepsilon_{su} - \frac{1}{2} \varepsilon_{su} \xi - \frac{1}{12} \varepsilon_{su}^2 \xi \right)}{(1-\xi)^2} \right] \quad (12)$$

Internal lever arm can be obtained from the expression (see Fig.6):

$$z_c = d - x + y_c \text{ or } z_c = d - \xi d + y_c \quad (13)$$

y_c - location of stress block centre of gravity in compression zone of the member:

$$y_c = \frac{\xi \left[\frac{1}{3} - \frac{1}{3} \xi - \frac{1}{16} \varepsilon_{su} \xi \right]}{\frac{1}{2} - \frac{1}{2} \xi - \frac{1}{12} \varepsilon_{su} \xi} d \quad (14)$$

Finally we get:

$$z_c = d \left[\frac{\frac{1}{2} + \xi \left(-\frac{2}{3} - \frac{1}{12} \varepsilon_{su} \right) + \xi^2 \left(\frac{1}{6} + \frac{1}{48} \varepsilon_{su} \right)}{\frac{1}{2} - \frac{1}{2} \xi - \frac{1}{12} \varepsilon_{su} \xi} \right] \quad (15)$$

Internal bending moment is calculated as a product of resultant force F_c and lever arm z_c

$$M_{Rd} = F_c z_c \quad (16)$$

$$M_{Rd,1a} = f_{cd} b d^2 \left[\frac{\xi^2 \varepsilon_s \left[\frac{1}{2} + \xi \left(-\frac{2}{3} - \frac{1}{12} \varepsilon_s \right) + \xi^2 \left(\frac{1}{6} + \frac{1}{48} \varepsilon_s \right) \right]}{(1 - \xi)^2} \right] \quad (17)$$

Combination of strains in domain 1b

$$\varepsilon_{c2} = 2,0\text{‰} \leq \varepsilon_c \leq \varepsilon_{c2u} = 3,5\text{‰}, \quad \varepsilon_{ud} = \varepsilon_{su}$$

On the basis of above given assumption the following formulas were obtained in nondimensional value of neutral axis depth Resultant of compressive stresses is expressed as:

$$F_c = f_{cd} b d \left(\frac{3 \varepsilon_{su} \xi + 2 \xi - 2}{3 \varepsilon_{su}} \right) \quad (18)$$

Internal lever arm z_c

$$z_c = d \left[1 - \frac{3 \varepsilon_{su} \left[\frac{1}{2} \xi^2 - \frac{2}{3} \xi \frac{1 - \xi}{\varepsilon_{su}} + \frac{1}{3} \frac{(1 - \xi)^2}{\varepsilon_{su}^2} \right]}{3 \varepsilon_{su} \xi + 2 \xi - 2} \right] \quad (19)$$

Internal bending moment $M_{Rd,1b}$

$$M_{Rd,1b} = b d^2 f_{cd} \left[\frac{\xi^2 \left(-2 - \frac{3}{2} \varepsilon_{su} - \frac{1}{\varepsilon_{su}} \right) + \xi \left(3 \varepsilon_{su} + 4 + \frac{2}{\varepsilon_{su}} \right) - 2 + \frac{1}{\varepsilon_{su}}}{3 \varepsilon_{su}} \right] \quad (20)$$

Combination of strains in domain 2

$$\text{for } \varepsilon_c = 3,5\text{‰} \quad \varepsilon_{ud} \leq \varepsilon_{su}$$

The cross-sectional parameters are expressed as follows

$$F_c = f_{cd} b d \left(\frac{17}{21} \xi \right) \quad (21)$$

$$z_c = d \left(1 - \frac{9}{238} \xi \right) \quad (22)$$

$$M_{Rd,2} = b d^2 f_{cd} \left[\frac{17}{21} \xi \left(1 - \frac{99}{238} \xi \right) \right] \quad (23)$$

In shorter way all the above formulas may be written in following form, using functional coefficients depending on nondimensional neutral axis depth and the strains in flexural steel:

$$F_c = \omega(\xi) \cdot b d f_{cd} \quad z_c = \zeta(\xi) \cdot d \quad M_{Rd} = \mu(\xi) \cdot b d^2 f_{cd} \quad (24)$$

For the needs of design of flexural member with the rectangular cross-section using deformational model with the inclined branch of strains in steel the tables were elaborated. In any case the stresses in flexural steel depends on steel strain and its ductility characteristic (see Fig.3)

$$\sigma_s = f_{yd} + \frac{f_{yd} (k-1) \left(\varepsilon_s - \frac{f_{yd}}{E_s} \right)}{\left(\varepsilon_{ud} - \frac{f_{yd}}{E_s} \right)} \quad (25)$$

where k is steel ductility ratio, expressed in the formula (3) and ε_s is steel strain depending on the neutral axis depth as follows

$$\varepsilon_s = \varepsilon_c \frac{(1-\xi)}{\xi} \quad (26)$$

Table 4. Table for dimensioning of flexural member with rectangular shape for inclined top branch of reinforcing steel type of B500SP (Epstal)

Strain domains	Coefficients				Strains [‰]		σ_s
	ξ	ω	ζ	μ	ε_c	ε_s	
Domain 1a	0,01	0,003	0,997	0,003	0,73	72	500
	0,02	0,011	0,993	0,011	1,47	72	500
limit 1a / 1b	0,027	0,018	0,990	0,018	2,00	72	500
Domain 1b	0,03	0,021	0,989	0,021	2,23	72	500
	0,04	0,031	0,984	0,031	3,00	72	500
limit 1b / 2	0,0463	0,037	0,981	0,037	3,50	72	500
Domain 2	0,05	0,041	0,979	0,040	3,50	66,50	495
	0,06	0,051	0,974	0,050	3,50	54,83	484
	0,07	0,061	0,969	0,060	3,50	46,50	476
	0,08	0,065	0,967	0,063	3,50	40,25	470
	0,1	0,081	0,958	0,078	3,50	31,50	462
	0,12	0,097	0,950	0,092	3,50	25,67	457
	0,14	0,113	0,942	0,107	3,50	21,50	453
	0,16	0,130	0,933	0,121	3,50	18,38	450
	0,18	0,146	0,925	0,135	3,50	15,94	448
	0,2	0,162	0,917	0,148	3,50	14,00	446
	0,22	0,178	0,908	0,162	3,50	12,41	445
	0,24	0,194	0,900	0,175	3,50	11,08	443
	0,26	0,210	0,892	0,188	3,50	9,96	442
	0,28	0,227	0,884	0,200	3,50	9,00	441
	0,3	0,243	0,875	0,213	3,50	8,17	441
	0,32	0,259	0,867	0,225	3,50	7,44	440
	0,34	0,275	0,859	0,236	3,50	6,79	439
	0,36	0,291	0,850	0,248	3,50	6,22	439
	0,38	0,308	0,842	0,259	3,50	5,71	438
	0,4	0,324	0,834	0,270	3,50	5,25	438
	0,42	0,340	0,825	0,281	3,50	4,83	438
	0,44	0,356	0,817	0,291	3,50	4,45	437
	0,46	0,372	0,809	0,301	3,50	4,11	437
	0,48	0,389	0,800	0,311	3,50	3,79	437
	0,5	0,405	0,792	0,321	3,50	3,50	436
	0,52	0,421	0,784	0,330	3,50	3,23	436
	0,54	0,437	0,775	0,339	3,50	2,98	436
	0,56	0,453	0,767	0,348	3,50	2,75	436
	0,58	0,470	0,759	0,356	3,50	2,53	435
	0,6	0,486	0,750	0,364	3,50	2,33	435
	0,62	0,502	0,742	0,372	3,50	2,15	435
limit domain 2	0,631	0,511	0,738	0,377	3,50	2,05	435

Stress-strain diagram for steel type B500SP, depending on range of the depth of neutral axis may be presented also in Fig.6.

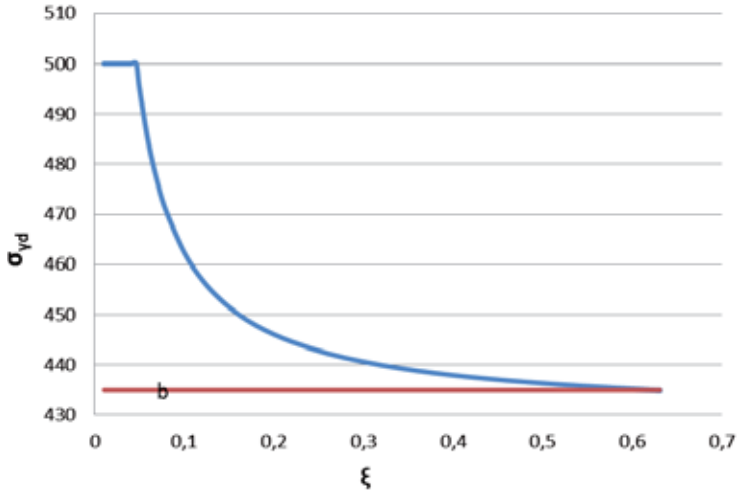


Fig. 6. Stress in steel versus neutral axis depth for B500P steel for the two models:
a) with inclined top branch, b) with horizontal top branch

Reinforcement ratios ρ diagrams in the cross-section of the flexural member depends on the depth of compression zone and concrete class for reinforcing steel are presented in Fig.7. Function $\rho(\xi)$ has been determined from the formula (32) using functional coefficients $\omega(\xi)$

$$\rho(\xi) = \omega(\xi) \frac{f_{cd}}{\sigma_s} \quad (27)$$

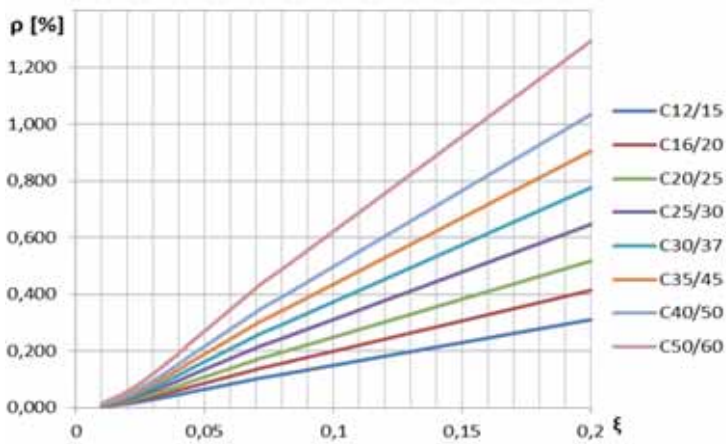


Fig. 7. Reinforcement ratios versus nondimensional neutral axis depth for given concrete classes

High Strenght Concrete classes

Algorithm used for calculation of assistance factors and dimensioning of rectangular cross-section of flexural R/C member made from High Strength Concrete (HSC) is analogous as for normal concrete classes (see p.3.2). However for this case that both limit concrete strain values ε_{c2} and ε_{cu2} are depending on HSC class. In the Eurocode 2 for highest concretes class C90/105 $\varepsilon_{c2} = \varepsilon_{cu2} = 2,6\%$ and in the Model Code for class C 100/115 these values are equal to $2,7\%$. Similarly, the values of n exponent of parabola function in formula (8) are depending on HSC class. Those formulas for cross-sectional parameters derived in paper of (Łapko Jensen 2006) are presented in Table 5.

Table 5. Overall method formulas, including variables strain of reinforcing steel in the flexural rectangular cross-section for high strength concrete (Lapko Jensen 2006)

Domain 1a	Auxiliar parameters
$F_c = [\xi + (1 - \xi)pA]bdf_{cd}$	$p = \frac{\varepsilon_{su}}{\varepsilon_{c2}}$
$z_c = \left\{ 1 - \xi + \frac{0,5\xi^2 - (1 - \xi)^2(B - A)}{\xi + (1 - \xi)pA} \right\} d$	$A = \frac{\left(1 - \frac{p\xi}{1 - \xi}\right)^{n+1} - 1}{p^2(n+1)}$
$M_{Rd,1a} = \left\{ (1 - \xi)[\xi + (1 - \xi)pA] + 0,5\xi^2 - (1 - \xi)^2(B - A) \right\} bd^2 f_{cd}$	$B = \frac{\left(1 - \frac{p\xi}{1 - \xi}\right)^{n+2} - 1}{p^2(n+2)}$
Domain 1b	
$F_c = \left[\xi - \frac{1 - \xi}{p(n+1)} \right] bdf_{cd}$	$p = \frac{\varepsilon_{su}}{\varepsilon_{c2}}$
$z_c = \left\{ 1 - \xi + \frac{0,5\xi^2 D - (1 - \xi)^2 C}{\xi(D+1) - 1} \right\} d$	$C = \frac{1}{p(n+2)}$
$M_{Rd,1b} = \left\{ \left(\xi - \frac{1 - \xi}{D} \right) \left[1 - \xi + \frac{0,5\xi^2 D - (1 - \xi)^2 C}{\xi(D+1) - 1} \right] \right\} bd^2 f_{cd}$	$D = p(n+1)$

Domain 2	
$F_c = \left\{ \xi \left[1 - \frac{1}{p_u(n+1)} \right] \right\} b d f_{cd}$	$p_u = \frac{\varepsilon_c 2u}{\varepsilon_c 2}$ $E = 0,5 p_u (n+1)$ $F = \frac{1}{p_u(n+2)}$
$z_c = \left[1 - \xi + \xi \left(\frac{E-F}{2E-1} \right) \right] d$	
$M_{Rd,2} = \left[\xi \left(1 - \frac{1}{2E} \right) \left(1 - \xi \frac{E+F-1}{2E-1} \right) b d^2 f_{cd} \right]$	

Bi-linear stress-strain relations for concrete

The procedures for cross-sectional design using bi-linear stress-strain relationship for concrete and bi-linear relationship for steel are analogous to previous case (see Fig.1b). The combinations of strain limits and stress diagrams are presented in Fig.8.

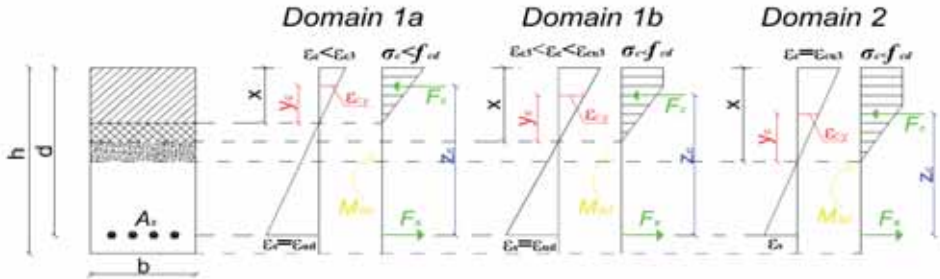


Fig. 8. Strains and stress diagrams for bi-linear model for concrete in strain domains 1a, 1b, 2.

From this analysis, there were derived the formulas, both for normal strength and High Strength Concrete classes. For normal concrete classes (for $f_{ck} \leq 50$ MPa) the formulas for cross-sectional parameters are listed in Table 6 and for HSC classes – are given in Table 7.

Table 6. Cross-sectional parameters derived using bi-linear model for normal strength concrete

Domain 1a	Domain 1b	Domain 2
$F_c = \frac{1}{2} \xi dbf_{cd}$	$F_c = \left(\frac{\varepsilon_{su} \xi - \frac{7}{8} (1 - \xi)}{\varepsilon_{su}} \right) dbf_{cd}$	$F_c = \frac{5}{4} \xi dbf_{cd}$
$z_c = \left(1 - \frac{1}{3} \xi \right) d$	$z_c = \left\{ 1 - \frac{\varepsilon_{su} \left[\frac{1}{2} \xi^2 - \frac{7}{8} \xi \frac{(1 - \xi)}{\varepsilon_{su}} + \frac{49}{384} \frac{(1 - \xi)^2}{\varepsilon_{su}^2} \right]}{\varepsilon_{su} \xi - \frac{7}{8} (1 - \xi)} \right\} d$	$z_c = \left(1 - \frac{7}{30} \xi^2 \right) d$
$M_{Rd,1a} = F_c z_c$	$M_{Rd,1b} = F_c z_c$	$M_{Rd,2} = F_c z_c$

Table 7. Cross-sectional parameters derived using bi-linear model for normal strength concrete

Domain 1a
$F_c = \frac{1}{2} \xi dbf_{cd}$
$z_c = d \left(1 - \frac{1}{3} \xi \right)$
$M_{Rd,1a} = \frac{1}{2} \xi \left(1 - \frac{1}{3} \xi \right) bd^2 f_{cd}$
Domain 1b
$F_c = f_{cd} bd \left(\frac{\varepsilon_{su} \xi - \frac{1}{2} \varepsilon_{c3} (1 - \xi)}{\varepsilon_{su}} \right)$
$z_c = \left[1 - \frac{\varepsilon_{su} \left[\frac{1}{2} \xi^2 - \frac{1}{2} \xi \frac{\varepsilon_{c3} (1 - \xi)}{\varepsilon_{su}} + \frac{1}{6} \frac{\varepsilon_{c3}^2 (1 - \xi)^2}{\varepsilon_{su}^2} \right]}{\varepsilon_{su} \xi - \frac{1}{2} \varepsilon_{c3} (1 - \xi)} \right] d$

$M_{Rd,1b} = f_{cd} b d^2 \left[\frac{\left(\xi - \frac{1}{2} \xi^2 \right) (\varepsilon_{su} + \varepsilon_{c3}) - \frac{1}{2} \varepsilon_{c3} + \frac{1}{6} \frac{\varepsilon_{c3}^2 (1 - \xi)^2}{\varepsilon_{su}}}{\varepsilon_{su}} \right]$
Domain 2
$F_c = f_{cd} b d \left[\frac{\xi (2 \varepsilon_{cu3} - \varepsilon_{c3})}{2 \varepsilon_{cu3}} \right]$
$z_c = \left[1 - \frac{2 \varepsilon_{cu3} \xi \left[\frac{1}{2} - \frac{1}{2} \frac{\varepsilon_{c3}}{\varepsilon_{cu3}} + \frac{1}{6} \frac{\varepsilon_{c3}^2}{\varepsilon_{cu3}^2} \right]}{(2 \varepsilon_{cu3} - \varepsilon_{c3})} \right] d$
$M_{Rd,2} = f_{cd} b d^2 \left\{ \frac{\xi \left(2 \varepsilon_{cu3} + \varepsilon_{c3} - 2 \varepsilon_{cu3} \xi^2 \left[\frac{1}{2} - \frac{1}{2} \frac{\varepsilon_{c3}}{\varepsilon_{cu3}} + \frac{1}{6} \frac{\varepsilon_{c3}^2}{\varepsilon_{cu3}^2} \right] \right)}{2 \varepsilon_{cu3}} \right\}$

Design procedures and example of calculation

For flexural members with rectangular cross-section loaded by design bending moment M_{Ed} dimensioning of area of flexural reinforcement may be performed using an algorithm presented in Table 8. As a first step we should assume concrete class and data for reinforcing steel, diameter of bars and then evaluate nominal thickness of the concrete cover.

Table 8. Design procedures for rectangular cross-section of flexural R/C member

1	Input data	$M_{Ed}, b, d, b, f_{cd}, \varepsilon_{uk}$
2	Calculation of strain limits	$\varepsilon_u = f_{yd} / E_s$ and $\varepsilon_{ud} = 0,9 \cdot \varepsilon_{uk}$
3	Calculation of tabular coefficient	$\mu = \frac{M_{Ed}}{f_{cd} b d^2}$
4	Coefficients read from specified tables	ω or ζ and ξ
5	Steel strain calculations (or read from tables)	$\varepsilon_s = \varepsilon_c \frac{(1 - \xi)}{\xi}$

6	Steel stress calculations (or read from tables)	$\sigma_s = f_{yd} + \frac{f_{yd}(k-1)\left(\varepsilon_s - \frac{f_{yd}}{E_s}\right)}{\left(\varepsilon_{ud} - \frac{f_{yd}}{E_s}\right)}$
7	Area of flexural reinforcement calculations	$A_{s1} = \omega db \frac{f_{cd}}{\sigma_s} \quad \text{or} \quad A_{s1} = \frac{M_{Ed}}{\zeta d \sigma_s}$
8	Checking the minimum area of reinforcement	$A_{s1,prov} \geq 0,26 \frac{f_{ctm}}{f_{yk}} bd$ $A_{s1,prov} \geq 0,0013 bd$

Calculation example of flexural reinforcement area for flexural beam

The beam with rectangular cross-section made of HSC class C70/85.

Data: $b = 0,25\text{m}$, $h = 0,35\text{m}$, $a_1 = 0,04\text{m}$, concrete class C70/85, steel BSt500SB.

The calculations are made for three values of bending moments: $M_{Ed} = 25 \text{ kNm}$, 50 kNm and 100 kNm using different models of cross-sectional analysis.

$$f_{cd} = \lambda \frac{f_{ck}}{\gamma_{c,HSC}} = 0,95 \frac{70}{1,56} = 43,6 \text{ MPa}$$

The results of calculations are presented in Table 9.

Table 9. Results of calculations of steel area for rectangular cross-section made of HSC

Model for concrete	Horizontal top branch		Inclined top branch	
	Parabola rectangle	Bi-linear	Parabola rectangle	Bi-linear
M_{Ed}	$M_{Ed} = 25 \text{ kNm};$			
F_c / bdf_{cd}	0,025	0,025	0,025	0,025
z_c / d	0,969	0,983	0,984	0,985
$A_{s1} [\text{cm}^2]$	1,94	1,89	1,71	1,78
M_{Ed}	$M_{Ed} = 50 \text{ kNm},$			
F_c / bdf_{cd}	0,050	0,050	0,050	0,049
z_c / d	0,956	0,967	0,972	0,973
$A_{s1} [\text{cm}^2]$	3,88	3,83	3,57	3,56
M_{Ed}	$M_{Ed} = 100 \text{ kNm}$			
F_c / bdf_{cd}	0,102	0,101	0,101	0,101
z_c / d	0,936	0,942	0,943	0,944
$A_{s1} [\text{cm}^2]$	7,92	7,85	7,63	7,81

Summary and conclusions

The presented above analysis was performed having considered more effective way to use realistic properties of ductility of flexural steel based on a basic assumptions described in Eurocode 2 and also in Model Code 2010. In the design procedures of flexural members with the use of steel stress-strain relationship with inclined top branch it could be reached saving of flexural steel areas. As it can be shown in the examples of design of flexural beam the influence of more realistic model on the required area of flexural steel depends on values of bending moment. The saving of steel area is larger for smaller depth of neutral axis zone. The results are also influenced on ductility of flexural steel. The more beneficial savings of required steel area can be reached for reinforcing steel with larger ductility ratio $k = f_{tk} / f_{yk}$ using strain model with inclined top branch.

In the examples there were used flexural steel with a ductility factor $k = 1,10$. For this case maximum savings of the reinforcing steel reaches to about 10%. Using steel class C ($k > 1,15$) reduction of required reinforcement area would be up to about 15%. However for steel class C with $k = 1,35$ we can expect reinforcing steel reduction up to about 35%.

References:

1. Lapko A, Jensen B. Ch.: *Podstawy projektowania i algorytmy obliczeń konstrukcji żelbetowych* wyd. Arkady, 2006.
2. Lapko A.: *Projektowanie konstrukcji żelbetowych*, Arkady, Warszawa 2003
3. Knauff M.: *Podstawy projektowania konstrukcji żelbetowych i sprężonych według Eurokodu 2*, PWN, 2013.
4. Knauff M.: *Obliczanie konstrukcji żelbetowych według Eurokodu 2*, PWN, 2006.
5. Starosolski W.: *Konstrukcje żelbetowe według Eurokodu 2 i norm związanych*, tom I, PWN, 2011.
6. Łuniewska M.: „*Application of deformational model in cross-sectional analysis of reinforced concrete beams*”, Proceedings of International Student Scientific Conference.
7. *Sovremennyye Tehnologii w Stroitelstvie*, Grodno, May. 2013.
8. PN-EN 1992-1-1:2004. *Design of Concrete Structures. Part 1-1. General Rules and rules for buildings*.
9. Appendix C for EN 1992-1-1:2004. *Design of Concrete Structures. Part 1-1. General Rules and rules for buildings*.
10. EN 10080. *Steel for the reinforcement of concrete. Weldable reinforcing steel. General*.
11. Model Code 2010. Final Draft. International Federation for Structural Concrete (fib), 2012.

ON SELECTED DIRECTIONS OF IMPROVEMENT IN METHOD OF DESIGN OF TIMBER STRUCTURES

¹Anatoly J. Naytchuk, ²Mikołaj Malesza, ²Czesław Miedziałowski

¹BelNIIS Republic of Belarus, e-mail: atnya@yandex.ru

²Białystok University of Technology, Wiejska Street 45E, 15-351 Białystok, Poland
email: m.malesza@wp.pl,

Summary:

Durability of timber structures depends on quality of design, conditions of manufacturing, transportation, assembling and exploitation. Any depart from the standard principle and requirements at any stage of structure preparation, as well as any abandon of specifications leads to commencement and progress of defects in the structure in process of exploitation and finally it causes the decrease of durability and sustainability and in effect decrease of life-service time. Load bearing capacity of timber structures decreases in time. Influence of load lasting time on strength parameters of timber derivative materials, and conditions of exploitation and common load action are included in application of partial modification factor k_{mod} , which was obtained in empirical way basing on experience of timber structure exploitation and wood parameters. This coefficient does not take into account state of stressing in structural element (bending, compression, tension parallel to the grain or perpendicular to the grain or shear). Wood considered as a solid body, undergoes failure in result of accumulation of sub-micro-defects. Factor k_{mod} in case of wood under static constant load tension perpendicular to grain within 50 years for service class 1 will give value of 0,15 what is four time lower than given in EN 1995. Work also consider some glulam defects and cracking under varying load action in the structures. Connections in glulam structures shall be designed to transfer the design load to and from structural element without causing local stress concentrations. These local stresses may initiate failure in the connection and then failure of whole structure. It is also important to design the connections isolating all timber elements from potential sources of potential moisture. The next part of the work refers to the cross laminated timber CLT as a new wood technology. This technology may soon open up the construction sector to wood building. There presented characteristic parameters of CLT and principles of design of modern timber structure using this new material.

Keywords: glulam, durability, cracks, cross laminated timber

Improvement in methods of design

Exploitation practice of timber structure specifically glued laminated timber (glulam) shows, that these structures not always fulfill conditions of durability and sustainability (long-life service) (Jasieńko 2003), (Kotwica et al. 2011), (Miedziałowski, Malesza 2006) due to varying natural wood defects, creation of cracks parallel to grain, delamination, splitting effect, deterioration in result of fungi, insects, bacterial or chemical attacks and weathering. It is known that within exploitation process is noticed lost of physical and functional wearing of timber structure. Lost of physical ability and wearing of timber structures become a main reasons leading to reconstruction and is resulted from physical, chemical and biological action on structures. All these action are taken into account in process of timber structure

design adopting requirements stated in standard documents and specifications. For this reason durability of timber structures depends on quality of design, conditions of manufacturing, transportation, assembling and exploitation. Any depart from the standard principle and requirements at any stage of structure preparation, as well as any abandon of specifications leads to commencement and progress of defects in the structure in process of exploitation and finally it causes the decrease of durability and sustainability and in effect decrease of life-service time. It is widely known, that load bearing capacity of timber structures decreases in time depending on type and time of loading, conditions of exploitation and kind of material.

In the EC countries and in some Custom Union Countries-CHT (Republic of Belarus, Kazakhstan, Ukraine) process of design of timber structures is conducted with accordance to adequate recommendations and requirements. According to (EN 1992) influence of load lasting time on strength parameters of timber derivative materials, as well as conditions of exploitation and common load action are included in application of partial modification factor k_{mod} , which was obtained in empirical way basing on experience of timber structure exploitation and wood parameters. The most acceptable approach in evaluation of k_{mod} has been described in work (Sorensen et al. 2005). This approach is based on the probability models securing the load bearing capacity of structure. Evaluation of these models is based on accumulation of defects according to Gerhardsa (Gerhards 1972), Barretta and Fosghi (Barrett, Foschi 1978) also Foschi and Yao (Foschi, Folz 1989). Indicated models are used for mathematic description for decrease of the load bearing capacity under sustained (long lasting) load in the form of function of load value and time of its application. Analyzing meaning of k_{mod} factor given in (EN 1992) it can be noticed, that this coefficient does not take into account state of stressing in structural element (bending, compression, tension parallel to the grain or perpendicular to the grain or shear). In our opinion this approach on evaluation of long-time duration of load influence on the wood strength parameters not completely includes specific of wood behavior. It is very well known, that wood, including also polymers considered physically as a solid body, undergoes failure in result of accumulation of sub-micro-defects. In this way equation of long-life of wood corresponding to concept of kinetic strength of solid body (EN 1992) can be described in the form:

$$t = \tau_0 \cdot e^{\frac{U_0 - \gamma \cdot \sigma}{R \cdot T}} \quad (1)$$

or

$$\lg t = \lg A - \alpha \cdot \sigma \quad (2)$$

where

$$\alpha = \frac{\gamma}{2,3 \cdot R \cdot T} \quad ; \quad \lg A = \frac{U_0}{2,3 \cdot R \cdot T} + \lg \tau_0 \quad (3)$$

U_0 – initial energy of activation in process of failure in kJ/mole

τ_0 – period of atom thermal vibration, c;

σ – stress, MPa;

t – time to failure (long-life), c;

γ – structure-чувствительный coefficient, kJ/[mole x MPa];

R – characteristic of thermal movement (gas constant), KJ/(mole x grad);

T – temperature, K.

In result of conducted analysis of experimental data on the base of principle equation of the kinetic concept of solid body strength according to Ivanov J.M. (Ivanov 1986), two mechanisms of failure for wood were discovered, which are strongly varying within time t up to destruction. Hence, for different timber materials under tensile, compression or shear stresses along the grain (Ivanov 1981), segment in varying tests under long-lasting load, being cut-off of the long term strength of wood from formula {2} along coordinate $\lg t$, equal 17,1, while under tension perpendicular to the grain it is equal 10,214 (Ivanov 1986) (Fig.1). In case of tension of wood under 45° to grain direction according to investigation in (Orlowicz, Naiczuk 1989-1), value of sectioned segment along coordinate $\lg t$ is 15,1. Using obtained results meaning of k_{mod} in case of wood under static constant load tension perpendicular to grain within 50 years for service class 1 will give value of 0,15 what is four time lower than given in (Zurkov 1957). In this way, fulfilling calibration of k_{mod} parameter in probability models shall take into account properties of failure of wood depending on type and conditions of stressing.

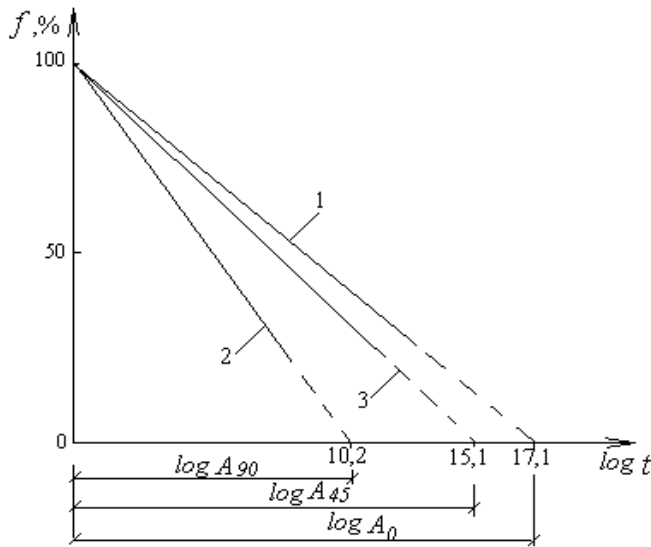


Fig.1. Dependence of long-term strength of wood under varying kind of stressing: 1-tension, compression and shear along the grain, 2-tension perpendicular to grain, 3-tension under 45 deg. to grain

Solution of this task is specifically actual for cases of evaluation of wood strength in the structure working in combined stressing conditions, taking into account criterial dependencies. Except this, in evaluation of technical state of timber structure with defects in the form of surface cracks, we are very often facing the question about evaluation of the final resources. Linking here methods of the failure mechanics in evaluation of the load bearing capacity or final resources of the structure with defects in the form of surface or sectional cracks is impossible without solving questions referring evaluation of formula depending changes of viscosity in failure of wood (velocity of freeing energy)

and form of failure and time of load lasting. It shall be noticed, that adopted in calibration of k_{mod} probabilistic models, and evaluation of their meaning at the same time can be used in evaluation of design strength and viscosity of failure of wood in the design of timber structure. As far as the use of their in evaluation of technical state (evaluation of final resources) is concerned, their application in our opinion is incorrect. In this case probably (if wood is not biologically defected) shall be used models basing on equation of kinetic concept of strength and principle of the linear summing of defects, where according to (Orlowicz, Naiczuk 1989-2) independence of final strength of wood in the function of loading has been stated. At the same time, action on structure within gone period of structure exploitation should be taken on the information and data of meteorological service for considered region.

In (EN 1992) analysis of at-supporting parts of timber beams under action of shear force Q shall be conducted with application of surface cracks. In this case effective (design) wide of cross-section in computer from formula

$$b_{ef} = k_{cr} \cdot b \quad (4)$$

where b_{ef} – effective (design) width of the cross-section of beam,
 b – width of the beam cross-section,
 k_{cr} – coefficient, for solid wood or glulam wood is taken in value of 0,67.

This requirement does not give the answer on the following questions: what shall be the surface cracks, one- or both-sides, what is the allowed depth b_{cr} and the length l_{cr} of the crack, how shall be accounted possible number of surface cracks and their geometry parameters (b_{cr} , l_{cr}) in analysis of beam under torsion load. According to given in (EN 1992) requirements additional investigations are to be conducted on specifying or evaluation of the load bearing capacity of the at-supporting sections of beam with defects in the form of surface cracking depending on geometric parameters crack itself and cross-sectional dimensions of beam (height h and span L). As far as the surface cracks are concerned, it shall be noticed, that at the supporting segments of the beams more of then for any other reasons, the cracks are appearing in result of cyclic temperature-moisture action in the process of exploitation due to improper isolation of beam end against moisture. Strength sectional cracks may appear in timber glulam beams if $h/b > 4$, at the distance $0,5h$ from the support and at the distance on the height of section $0,15h - 0,2h$ from neutral axis towards the tensile zone (Serov et al. 2010).

Influence of improper connections on creation of cracks and splitting in glulam elements – selected examples (Fruhval et al. 2007), (APA 2007)

Proper connection details are important to structural load bearing capacity and serviceability on any kind of timber framed structure constructed of solid or glulam wood. In case of longer span and larger cross section dimensions usually constructed as the glulam elements proper detailing connections is more critical than in case of solid wood elements. Consideration on the stage of design the moisture-related expansion and contraction characteristics of wood is essential in detailing glulam connections to prevent inducing tension perpendicular to grain stresses. Always in structure connections are to

be designed to transfer the design load to and from structural element without causing local stress concentrations. These local stresses may initiate failure in the connection and then failure of whole structure. It is also important to design the connections isolating all timber elements from potential sources of potential moisture. Wood expands in result of changes in its internal moisture content. In designing connections for glulam structure shrinkage effect cannot be restrained. In case of restrained shrinkage causing exceeding tension perpendicular to the grain stresses may cause split parallel do grain. Splitting failure reduces greatly shear and bending capacity of glulam elements. Improper beam notching can induce internal moment and tension stresses perpendicular to the grain.

There are several basic principles being leading to efficient, durable and structurally sound connections (APA 2007):

- load shall be transferred in compression bearing whenever possible,
- in glulam shall be allowed dimensional changes due to potential moisture cycling,
- details of connections inducing tension stresses perpendicular to grain shall be avoided,
- avoid moisture entrap in connection,
- glulam element shall not be placed in direct contact with masonry and concrete,
- eccentricity in joints details shall be diminished

Selected examples of improper detailing leading to failure and defects in connections:

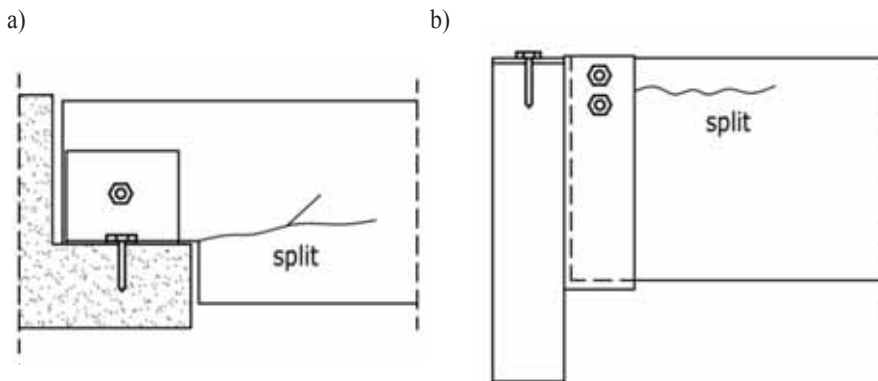


Fig. 2. a) Notching at the end of beam, b) Beam-to-beam connections

Notching at the end of beam can lead to splitting at inside corner due to shear stress concentrations and induced tensile stresses perpendicular to grain. The notch cannot exceed of 1/10 of the beam depth and result of lateral restrain at the top of the glulam beam, shrinkage of the beam can cause splitting at the top of connection because load is transferred from the bearing seat to connecting bolt. Splitting can occur also when restrain does not allow the beam for rotation in result of deflection.

Beam-to-beam connections. Shrinkage of supported beam causes bearing load to transfer from beam saddle to fasteners, causing splitting of beam.

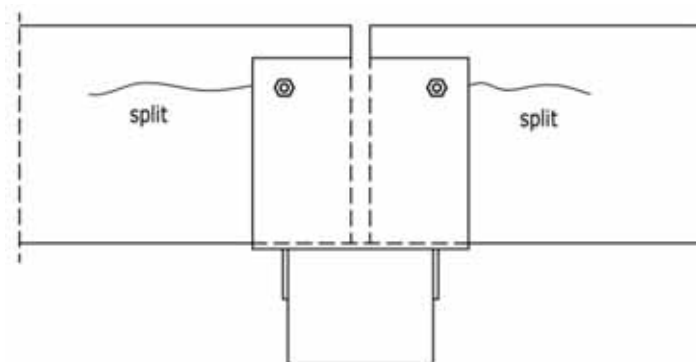


Fig.3. Splice steel plates applied to both sides of members may cause splitting if members shrink. Plates resist this shrinkage and may induce tensile stresses perpendicular to grain which may lead in return to splitting.

Cross Laminated Timber – New technology in timber engineering wood

Cross Laminated Timber – CLT, a modern concept to build with wood

The cross laminated timber as a new wood technology – may soon open up the construction sector to wood building. Wood is an excellent structural material because it is strong, lightweight, easy to work with, inexpensive and environmentally friendly (Schickhofer 2011-2). The wood-framed construction, where dimension lumber in LWF in Poland (45x150 mm for studs and 60x222mm for joists and rafters, etc), are used to create the building's structure in small residential houses in many countries. This use in larger buildings above 3 stories is limited by building codes for structural and fire-resistance reasons. Cross laminated timber (CLT) refers to large panels that are created by laminating dimensional lumber. The panels can be very large – 15 m long, 3,00 m high and 0,30 m thick or larger – depending on the structure requirements. Because they are very thick, they have the excellent fire properties of big section timber elements. For example, for a CLT building in Britain, a four-person crew was able to assemble an entire floor of the nine-storey building in three days. CLT is now being manufactured and used in Europe, USA and Canada. Building with wood is good because it allows us to use an affordable and renewable material for one of our most important needs. CLT may now allow to build even more things with wood.

Cross-Laminated Timber Panels (Schickhofer 2011-1)

Cross-Laminated Timber Panels are formed using boards from 25mm thick x 120 – 170mm wide, laid and glued using formaldehyde-free, glue in a vacuum press in alternate layers, at 90 degrees to each other, creating panels that are from 3 to 11 layers thick. Quality control is optimized with the pre-fabrication of the structural panels in an atmospherically controlled facility using computer controlled cutting equipment. The primary benefits of the CLT system are the components' superior performance characteristics and the speed of the building process. When compared to traditional building materials and

technology, the CLT system has a number of significant advantages (Finch et al. 2011), (Karacabeyli, Desjardins 2011), (Mohammad 2011), (Pirvu et al 2011), (Schickhofer 2011-1), (Sorensen et al 2005), (Zurkov 1957), (EN 1992), including:

- Thermal efficiency: CLT buildings can double the energy efficiency of conventional buildings. The ‘thermal mass’ characteristics of the CLT building system allows to retain with less energy the ambient temperature of the internal environment of any building, ensuring minimum expenditures of heating and cooling costs.
- Acoustic protection: The mass of the wood in the CLT panels and specialized wood fiber insulation materials combine to achieve increased acoustic protection compared with other systems.
- Seismic strength: Buildings with similar components have been shown to exhibit superior performance to conventional buildings under earthquake hazards.
- Structurally better behavior under fire performance: CLT materials are highly fire-resistant and maintain extraordinary structural integrity under fire attack. Low carbon footprint: CLT materials are exceptionally ‘green’ when compared to competitively performing structural systems in consideration of the embodied energy in the building materials, the high energy efficiency of the CLT thermal envelope, and what will evolve into a carbon-neutral manufacturing process.
- Life cycle and future value: The long life time of CLT components ensures that the future value of any structure remains high; buildings are easily altered and remodeled and are also fully recyclable once they reach the end of their useful life.
- Flexibility of design: Cross-laminated timber panels have a high load bearing capacity and required serviceability limit state considering deflection and modulus of elasticity, providing designers with beautiful structural element for creating exciting new building designs.
- Speed and predictability of construction, where CLT structural systems is arrived on-site ready to assemble, saving time and giving an accurate building process. The raw materials for the CLT system are sourced exclusively from small and medium diameter timber thinned from the forest, as well as fire and insect killed salvage timber. This responsible cultivation practice maintains and even enhances the long-term productivity and health of the forest.
- Superior use of low-grade timber resources: CLT components can be manufactured from low-grade timber resources that otherwise would likely be converted to or consumed as fuel. Using this lumber as the primary raw material for its products is the most environmentally-friendly way to use this resource, which needs to be harvested in order to maintain the health and vitality of the source forests.

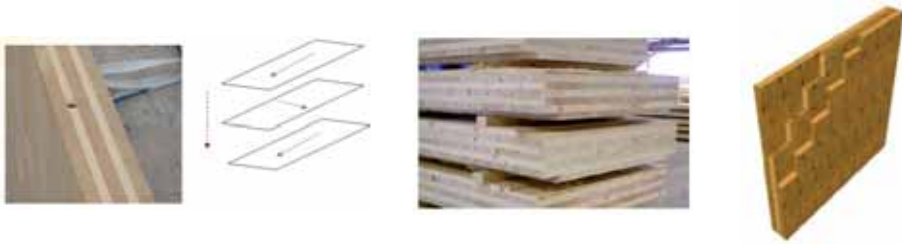


Fig.4. CLT panel formed of n-number of boards

CLT characteristics

There are the main factors affecting creep of wood (Pirvu et al. 2011):

- magnitude, type and duration of continuing application of load or a series of periods of the same type of load application. Creep rupture is attributed to the load duration effect,
- moisture content (service conditions)
- type of material (grain orientation, etc), hence the same conditions like in EN 1995-1-1 (EN 1992).

Canadian Standard on timber structure indicate the load duration factors in the function of duration of load like in the Table 1 , while the strength modification factors and the deformation modification factors are given in Table 2.

Table 1. Load duration factor K_D , according to CSA O86-09

Duration of load	K_D
Short term	1,15
Standard term	1,00
Long term	0,65

Table 2. Strength modification factor, according to EN 1995-1-1 (Zurkov 1957)

Load Duration Class	SC 1	SC 2	SC 3
k_{mod} for GLULAM/PLYWOOD			
Permanent	0,60	0,60	0,50
Long term	0,70	0,70	0,55
Medium term	0,80	0,80	0,65
Short term	0,90	0,90	0,70
Instantaneous	1,10	1,10	0,90

For CLT under 1 year constant load and 9%/25% ultimate load and SC1/SC2; 30-40% higher creep of CLT compared to glulam.

CLT behave more like plywood than like glulam.

Table 3. Deformation Modification Factor, Table 3.2, EN 1995-1-1 (EN 1992)

k_{def}	SC 1	SC 2	SC 3
LUMBER (EN 14081-1)	0,60	0,80	2,00
GLULAM (EN 14080)	0,60	0,80	2,00
PLYWOOD (EN 636)	0,80	1,00	2,50

Larger creep of CLT versus glulam is resulted from significant deformations of the cross plies in shear perpendicular to grain as it is presented in figure 5



Fig.5. Deformation due to rolling shear and higher creep in result.

For CLT under 1 year constant load and 9%/25% ultimate load and SC1/SC2 ; 30-40% higher creep of CLT compared to glulam.

Table 4 presents deformation modification facto for CLT.

Table 4. Factor k_{def} for CLT

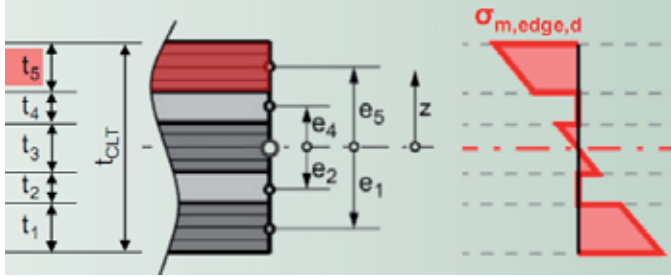
Proposed Deformation Modification Factor, k_{def}	SC 1	SC 2
CLT (less than 7-layer)	0,90	1,10
CLT (more than 9-layer)	0,80	1,00

CLT behave more like plywood than like glulam. Serviceability Limit State – deflection due to total load using $0,75 G_{90}$ with elastic deflection less than $L/180$ (according to CSA 086-09), and permanent deformation due to long term load using $0,5 G_{90}$ is not exceeding $L/360$ (Pirvu et al 2011).

CLT does not change basic wood characteristics and it does not change basic durability principles (Zurkov 1957) in case of wood kept dry wherever possible, minimizing wetting during transportation and construction, preventing wetting in service and allowing drying in case wetting occurs.

Stiffness characteristics of CLT (Schickhofer 2011-1)

BENDING



Calculation of the design value for E_{dg} -bending-stress $\sigma_{m,edge,d}$

$$\sigma_{m,l=5,edge,d} = \frac{M_{max,d}}{K_{CLT}} \cdot \frac{t_{CLT}}{2} \cdot E_{l=5}$$

Bending stiffness of a layered cross section area

$$K_{CLT} = \sum_{i=1}^n (J_i \cdot E_i) + \sum_{i=1}^n (A_i \cdot e_i^2 \cdot E_i)$$

Calculation of the design value for bending strength $f_{m,clt,d}$ according to the load-bearing-model for CLT (TU Graz)

$$f_{m,clt,k} = a_{clt} \cdot f_{t,0,l,k}^{0,8} \Rightarrow f_{m,clt,d} = \frac{k_{mod} \cdot f_{m,clt,k}}{\gamma_M}$$

with:

$f_{t,0,l,k}$ - characteristic tension strength of boards (raw material)

a_{clt} - pre-factor to take into consideration

- the coefficient of variation (COV) of the raw material
- the laminating effect
- the system effect
- the size effect
- the structure | assembling effect

load bearing model for CLT in bending according to technical approvals:

- ETA-09/xxx

with:

$$f_{m,clt,k} = \text{minimum} \begin{cases} a_{clt} \cdot f_{t,0,k}^{0,8} \\ 1,2 \cdot f_{m,k} \end{cases}$$

$f_{m,k}$ - characteristic bending strength acc. to EN 338

$f_{t,0,k}$ - characteristic tension strength acc. to EN 338

$a_{clt} = 3,5$ - for visually graded timber

- DIBt Z-9.1-xxx

$f_{m,clt,k} = k_l \cdot f_{m,gl,k} \rightarrow$ reference depth $d_{ref,cit}$ not defined

need for research suggestion: $d_{ref,cit} = 150\text{ mm}$

with:

$f_{m,gl,k}$ - characteristic bending strength for GLT $d_{ref,gl} = 600\text{ mm}$

k_l - pre-factor to take in consideration the system effects ($k_l = 1,1$ if $n \geq 4$)

Load bearing models for CLT in bending – a comparison:

example | strength-class C24 according to EN 338 or GL24h acc. to DIN 1052

- Load bearing model in bending
- $f_{m,clt,k} = a_{clt} \cdot f_{t,0,l,k}^{0,8} = 3,5 \cdot 14,0^{0,8} = 28,9\text{ N/mm}^2$
- ETA-09/xxx

$$f_{m,clt,k} = \min \left(\begin{array}{l} a_{clt} \cdot f_{t,0,l,k}^{0,8} = 3,5 \cdot 14,0^{0,8} = 28,9\text{ N/mm}^2 \\ 1,2 \cdot f_{m,k} = 1,1 \cdot 24,0 = 26,4\text{ N/mm}^2 \end{array} \right)$$

- DIBt Z-9.1.-xxx

$$f_{m,clt,k} = k_l \cdot f_{m,gl,k} = 1,1 \cdot 24,0 = 26,4\text{ N/mm}^2$$

Note: system factor k_l conservative | no depth correction, $d_{ref,cit}$ not defined

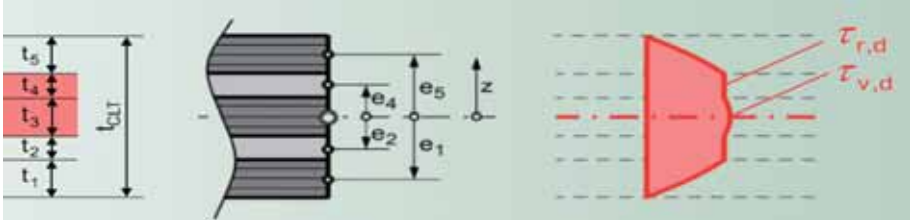
$$f_{m,clt,d=150,k} = k_h \cdot k_l \cdot f_{m,gl,k} = 1,1 \cdot 1,1 \cdot 24,0 = 29,0\text{ N/mm}^2$$

design

$$\frac{\sigma_{m,edge,d}}{f_{m,clt,d}} \leq 1,0 \quad \text{normally very low utilization ratio} \rightarrow \text{seldom relevant}$$

SHEAR | longitudinal | transverse (rolling shear)

calculation of the design value for shear stress



$$\tau(z_0)_d = \frac{V_{z,d} \cdot \int_{A_0} E(z) \cdot z \cdot dA}{K_{clt} \cdot b(z_0)}$$

→ $\tau_{v,d}$ (longitudinal) und $\tau_{r,d}$ (transverse)

Calculation of the design values of shear strength $f_{v,clt,d}$ and rolling shear strength $f_{r,clt,d}$

$f_{v,clt,k} = 3,0 \text{ N/mm}^2$, based on $f_{v,k}$ of GLT (approximate)

Considering the system effect, a 25% higher value for $f_{r,clt,k}$ compared to GLT is proposed (e.g. “BSP Handbuch” | TU Graz).

$f_{r,clt,k} = 1,25 \text{ N/mm}^2$, based on ‘BSP handbuch’ | TU Graz, design:

$$\frac{\tau_{v,d}}{f_{v,clt,d}} \leq 1,0 \quad \frac{\tau_{r,d}}{f_{r,clt,d}} \leq 1,0 \quad \text{Both verifications normally result in a low utilization level.}$$

Important role in CLT construction play connections. They maintain structural integrity, provide ductility for lateral load like wind and seismic, affect the serviceability limit state, they may also affect the fire resistance, facilitate a quick assembly of structure and interior and exterior finishes (Mohammad 2011).

Lateral performance of CLT wall panels is governed by connections as it is indicated in figure

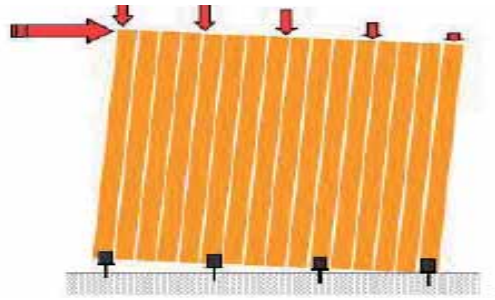


Fig.6. Lateral behavior of wall panel connected to the bottom structure.

Connections in CLT structures

Except traditional fasteners used in timber construction some special fasteners are used in TLC construction. There are self-tapping screws and dowels, glued in roads, bearing type systems and metal hooks. Diameters from 4 to 12 mm, length up to 600mm and they do not require predrilling like in traditional lag screws.

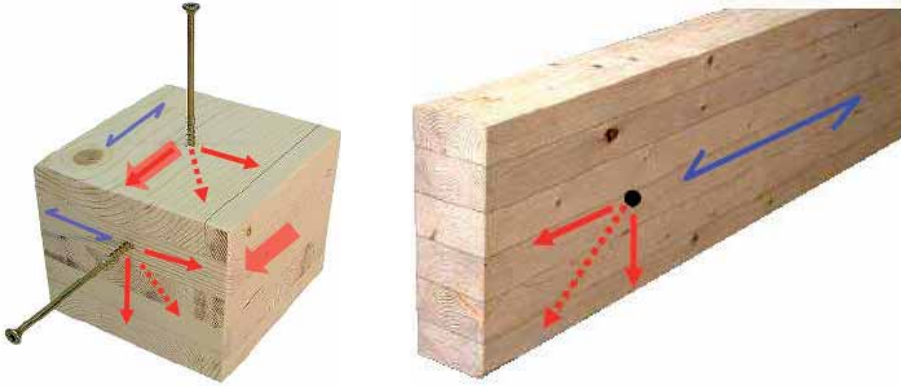


Fig. 7. Different way of loading in case of CLT, while in glulam all laminates are aligned and loaded in similar way (Orłowicz 1989-1).

Except this gaps in unglued cross laminates and artificially sawn grooves to relieve drying stresses in CLT are influencing load bearing capacity of connection. Despite this CLT has a more favorable ability to resist splitting due to X-lamination.

Nails & Screws – Generalized Approach

Perpendicular to plane

$$f_{h,k} = 0,112 \cdot d^{-0,5} \rho_k^{1,05} (N/mm^2)$$

In case of bolts and dowels formulae are described in the form as given below:

Bolts & Dowels

Perpendicular to plane

$$f_{h,k} = \frac{0,031 \cdot (1 - 0,015d) \cdot \rho_k^{1,16}}{1,1 \cdot \sin^2 \alpha + \cos^2 \alpha} (N/mm^2)$$

Panel-to panel connections in CLT panel construction is presented in figure and typical connections details:

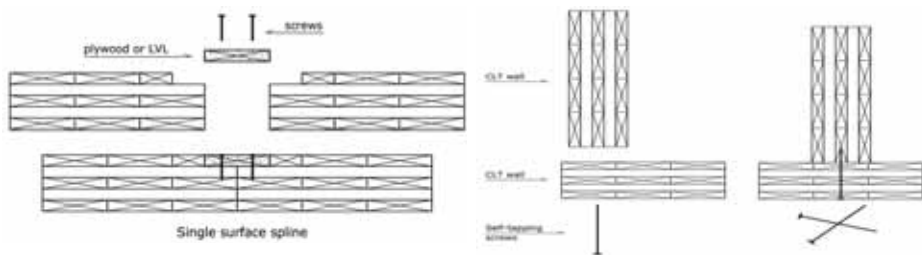


Fig. 8. Innovative connection systems [14]

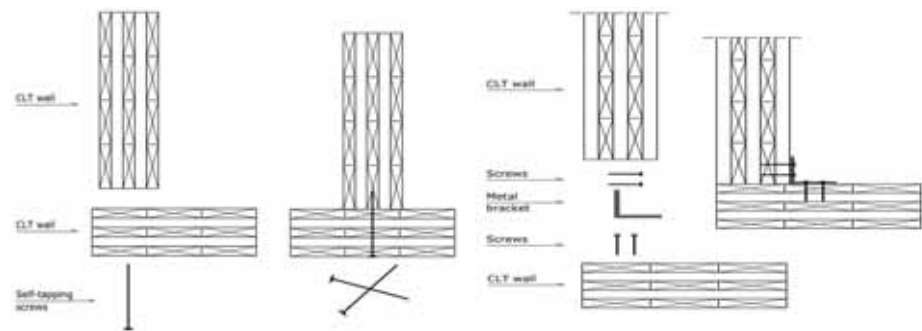
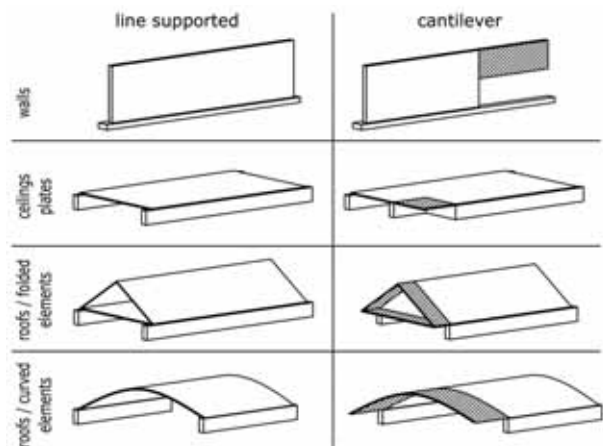


Fig. 9. Wall to wall connections [14].

Different types of elements

Use of CLT as 2D Elements



The diagram presents different static schemes of the supported along the wall and cantilever elements of CLT structure.

References:

1. Barrett JD, Foschi RO. (1978), *Duration of load and probability of failure in wood*. Part 1: modelling creep rupture. Can J Civil Eng; 5(40):505–14.
2. Серов Е.Н., Санников Ю.Д., Серов А.Е. (2010), Проектирование деревянных конструкций: учеб. пособие. – М. Ассоциация строительных вузов, 534 с.
3. Finch G., et al (2011), *Design for durability: Cross-laminated Timber Construction*. Vancouver. BC, Symposium on CLT, February 8-9.
4. Foschi R., Folz B., Yao F. (1989), *Reliability-based design of wood structures*. Structural research series, Rep. no. 34, Dep. of Civil Eng., Univ. of British Columbia, Vancouver, Canada.
5. Fruhval E., et al (2007), *Design of safe timber structures – how can we learn from structural failure*. Report TVBK-3053 Division of Structural Engineering Lund Institute of Technology, Lund University.
6. Gagnon S. (2011), *CLT-Structural Design*. Vancouver. BC, Symposium on CLT, February 8-9.
7. Gerhards CC (1979), *Time-related effects on wood strength: a linear cumulative damage theory*. Wood Sci; 11(3):139–44.
8. Иванов Ю.М., Славик Ю.Ю. (1986), Длительная прочность древесины при растяжении поперек волокон // Изв. высш. учеб. заведений. Строительство и архитектура. №10. С. 22 – 26.
9. Иванов Ю.М. (1981). О длительной прочности древесины // Изв. высш. учеб. заведений. Лесной журнал. №5. С. 71 – 75.
10. Jasieńko J. (2003), *Połączenia klejone i inżynierskie w naprawie, konserwacji i wzmacnianiu zabytkowych konstrukcji drewnianych*. Dolnośląskie Wydawnictwa Edukacyjne, Wrocław.
11. Karacabeyli E., Desjardins R. (2011), *Cross Laminated Timber (CLT) in the Context of Wood Building Systems*. Vancouver. BC, Symposium on CLT, February 8-9.
12. Kotwica E., Gil Z., Orłowicz R. (2011), *Konstrukcje z drewna klejonego - analiza przyczyn awarii i katastrof* - Inżynier Budownictwa №5 , с 76-80
13. Miedziałowski Cz., Malesza M. (2006): *Budynki o szkieletie drewnianym z poszyciem*. PAN, KILIW IPPT Warszawa, Białystok.
14. Mohammad M. (2011), *Connections in CLT Assemblies*. Vancouver. BC, Symposium on CLT, February 8-9.
15. Орлович Р.Б., Найчук А.Я. (1989), О применении критериев длительной прочности в расчетах деревянных конструкций // Изв. высш. учеб. заведений. Строительство и архитектура. №5. С. 15 – 19.
16. Орлович Р.Б., Найчук А.Я. (1989), О достоверности критерия Бейли при оценке длительной прочности древесины // Изв. высш. учеб. заведений. Лесной журнал. №2. С. 124 – 126.
17. Pirvu C., Karacabeyli E., Schickhofer G. (2011), *Preliminary Duration of Load and Creep Factors for Cross Laminated Timber*. Vancouver. BC, Symposium on CLT, February 8-9.

18. Schickhofer G., CLT European experiences. Vancouver. BC, Symposium on CLT, February 8-9, 2011.
19. Schickhofer G., Thiel A. (2011), *CLT – Research and Testing at TU Graz*. Vancouver. BC, Symposium on CLT, February 8-9.
20. Sørensen John Dalsgaard , Staffan Svensson , Stang Birgitte Dela (2005), *Reliability-based calibration of load duration factors for timber structures*. Structural Safety 27, p. 153-169
21. Журков С.Н. (1957), Проблема прочности твердых тел //Вестн. АН СССР. Вып. 11. С. 78 – 82.
22. EN 1995-1-1. (1992), CEN, Eurocode 5 – Design of timber structures – Part 1-1[^] General – Common rules and rules for buildings
23. APA (2007), *Glulam Connection Details*, Tacoma, Washington.

ANALYSIS OF DEFORMATION STATES IN HIGH PERFORMANCE FIBRE REINFORCED CONCRETE BENT PLATES

Piotr Smarzewski

Lublin University of Technology, Faculty of Civil Engineering and Architecture,
Department of Civil Engineering, Nadbystrzycka Street 40, 20-618 Lublin, Poland
e-mail: p.smarzewski@pollub.pl

Summary:

The article presents the results of bending tests on reinforced concrete made of high strength concrete with water/cement ratio of 0.2 with addition steel and polypropylene fibres obtained with the non-contact three-dimensional displacement measuring system – ARAMIS. The plates were reinforced with mesh and the variable was the content of fibres in concrete. The results of strains and vertical displacements for characteristic sections in plates P1-P3 were analysed. Examples of the relationship major strains and vertical displacement along section length for P1 were presented. The experiments proved significant influence structural reinforcement combinations on load capacity of plates. The use of polypropylene fibres is effective and increases the performance of the deformed steel fibres in concrete. The cracks in reinforced concrete plates with fibres were much smaller width across than the cracks in the plate reinforced with the reinforcing mesh.

Keywords: reinforced concrete elements, high performance concrete, steel fibres, polypropylene fibres, plates. ARAMIS system.

Introduction

High strength concrete is an increasingly common building material. Its technology has been developed over the years. By adding various additives and admixtures different concrete properties were improved. The addition of fibres allowed to obtain a new composite with a high tensile strength, high resistance to fracture, increased impact resistance and fatigue strength (Brandt 1996, 2008, 2009, Glinicki et al. 2002, Domański, Czekwianianc 2006). Despite the fact that the research on this material last half century, new developments are determined (Walraven 2009, Prisco et al. 2009, Glinicki 2010). The idea that has been recently in the focus is fibre hybridisation. In high strength concrete a few types of fibres are combined in order to define its optimal qualitative and quantitative composition (Banthia, Gupta 2004). Typically, microfibers combine with macrofibres, or similar-sized fibres but different elasticity module. An example is the use of steel or carbon fibres with high elasticity module with polypropylene fibres with low elasticity module. Correctly anchored fibre with high module gains optimal ability strengthen when there are small or medium cracks. On the other hand, fibres with low module obtain full ability strengthen the large cracks. Such a combination of fibres makes a high strength composite with a high range of crack opening.

The experimental tests concern reinforced concrete plates made of high performance concrete reinforced with steel and propylene fibres. Such a concept of a modern composite has a number of enthusiasts (Cucchiara et al. 2004, Chiaia et al. 2009, Fairbairn et al. 2012). The article presents the results and analyses of non-contact, three-dimensional measurements of deformation states of elements obtained using the ARAMIS system.

Preparing HPFRC plates and research using ARAMIS system

Three reinforced concrete plates P1-P3 sized 1000 x 800 x 60 mm were prepared according to recipes M1, M2, and M3 (Table 1). More detailed information concerning element preparation and curing are provided in articles (Smarzewski et al. 2012, Smarzewski 2013).

Table 1. Recipe concrete mixtures

Component	M1 [kg/m ³]	M2 [kg/m ³]	M3 [kg/m ³]
Cement CEM I 52.5R	596	596	596
Granodiorite 2-8 mm	990	990	990
Quartz sand	500	500	500
Condensed microsilica	59.6	59.6	59.6
Superplasticiser	20	20	20
Water	196	196	196
Steel fibres	–	39	78
Polypropylene fibres	–	0.5	0.5

Ready elements covered with random patterns and the laboratory stand with ARAMIS system digital cameras are presented in Fig. 1. The laboratory test were conducted in Zwick/Roell hydraulic press. Prior to the tests the cameras were mounted onto stands and calibrated with a control cross.



Fig. 1. Laboratory stand for testing reinforced concrete plates.

ARAMIS is a system for three-dimensional measuring the states of strains and displacements, analysing, computing and drafting graphical documentation of the results. Its basic element is a measuring sensor with two digital cameras, a stable base for attaching them, release and driving device for cameras, recording device and a high performance computer with software. Clear visuals of the measuring give full understanding of objects' behaviour. The system takes pictures with digital camera and recognises the structure of the measured surfaces. The state of zero displacement is illustrated in the first photography. All pictures are recorded until the element is completely destroyed. The combination of pictures may allow comparing them and calculating the level of displacement and strain. ARAMIS

compares the pictures with one another and attributed characteristic area with rectangular plains (with side size of a few pixels) called facets. Then it identifies the areas in the pictures. The measuring range of the sensor is broad and covers the area from 1 mm to 2000 mm. Relative strains are registered in the range from 0.01% up to a few hundred percent. Most functions of the measuring system are controlled by software. ARAMIS system can be used in the following types of tests: defining the strength, nonlinear behaviour tests, creeping, checking verifiable models, e.g. in Finite Elements Method, defining material characteristics, deformation processes and strain calculations (ARAMIS 2011).

Reinforced concrete plates were locally loaded with a centrally located steel plate at constant dislocation of the hydraulic press piston. The research was conducted until the layers in the loaded area of concrete were completely crashed and the cracks in the tensed area were over 5 mm. The recording speed and measurement area were defined for the calculations (Fig. 2).



Fig. 2. The measurement area for plate P1 in ARAMIS system

With optical measurement techniques coordinates, displacements and strains will be determined only on the surface of objects. This means that the calculation is limited to local strains, which are tangential to the surface. As additional information perpendicular to the surface is missing, it is not possible to calculate a complete 3D strain tensor. In this case, the calculation of the thickness change is based on the assumption of volume constancy of the material during loading.

Strain is the measure for the deformation of a line element and can be defined as follows:

$$\lambda = \lim_{l \rightarrow 0} \left(\frac{l + \Delta l}{l} \right) \quad (1)$$

A strain value can be defined as the function of the stretch ratio λ . The following known functions are frequently used strain measures: technical strain as $\varepsilon^T = f(\lambda) = \lambda - 1$, logarithmic strain as $\varepsilon^L = \varphi = f(\lambda) = \ln(\lambda)$, Green's strain as $\varepsilon^G = f(\lambda) = 1/2(\lambda^2 - 1)$.

In order to quantitatively display the deformation of a surface element, the deformation gradient tensor \mathbf{F} is introduced. The deformation gradient tensor transforms a line element $d\mathbf{X}$ into the line element $d\mathbf{x}$. In both cases, the line element connects the same material coordinates. Theoretically, it must be an infinitesimal line element. Thus, the deformation gradient tensor is defined as:

$$d\mathbf{x} = \mathbf{F}d\mathbf{X} \quad (2)$$

A disadvantage of the deformation gradient tensor is that rotation and stretch are modeled using one matrix only. This can be compensated by splitting the deformation gradient tensor into two tensors: a pure rotation matrix and a pure stretch tensor. The matrix can be decomposed in two different ways. First way is decomposition into rotation \mathbf{R} and right stretch tensor \mathbf{U} . Mathematically, the deformation gradient tensor is decomposed as follows:

$$\mathbf{F} = \mathbf{R}\mathbf{U} \quad (3)$$

Second way is decomposition into left stretch tensor and rotation. Mathematically, the deformation gradient tensor is decomposed as follows:

$$\mathbf{F} = \mathbf{V}\mathbf{R} \quad (4)$$

With the orthogonal rotation matrix the stretch tensor can be computed from the Cauchy Strain tensor:

$$\begin{aligned} \mathbf{C} &= \mathbf{F}^T \mathbf{F} = \mathbf{U}^T \mathbf{R}^T \mathbf{R} \mathbf{U} \\ \mathbf{R}^T \mathbf{R} &= \mathbf{I} \\ \mathbf{U} &= \sqrt{\mathbf{C}} \end{aligned} \quad (5)$$

Values ε_x , ε_y and ε_{xy} can directly be read from the symmetric stretch tensor \mathbf{U} with the following form:

$$\mathbf{U} = \begin{pmatrix} U_{11} & U_{12} \\ U_{21} & U_{22} \end{pmatrix} = \begin{pmatrix} 1 + \varepsilon_x & \varepsilon_{xy} \\ \varepsilon_{xy} & 1 + \varepsilon_y \end{pmatrix} \quad (6)$$

The strain measures ε_x , ε_y have the disadvantage of being defined as dependent on the coordinate system. This disadvantage can be eliminated by calculating major and minor strain values. The symmetrical matrix \mathbf{U} can be transformed to the main diagonal form. The two eigenvalues λ_1 and λ_2 can be calculated as follows:

$$\lambda_{1,2} = 1 + \frac{\varepsilon_x + \varepsilon_y}{2} \pm \sqrt{\left(\frac{\varepsilon_x - \varepsilon_y}{2}\right)^2 + \varepsilon_{xy}^2} \quad (7)$$

Frequently, the effective strains are needed. The effective strains according to von Mises and von Tresca are available. The effective strain according to von Mises results from the following formula:

$$\varphi_v = \sqrt{\frac{2}{3}(\varphi_1^2 + \varphi_2^2 + \varphi_3^2)} \quad (8)$$

As φ_3 is included in the formula, the effective strain is only valid if the volume constancy is valid.

Analysis of tests' results

ARAMIS system has the functionality of drawing graphs of plates response at any point or along a selected section. Fig. 3 illustrates a scheme of plate P1 with characteristic points and sections.

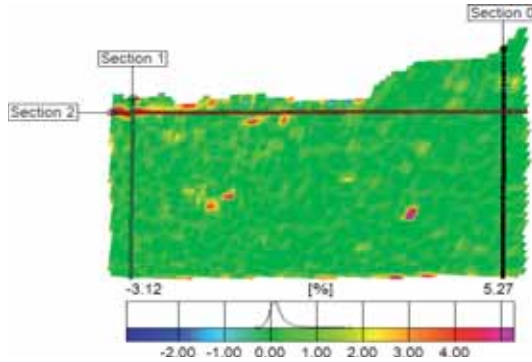
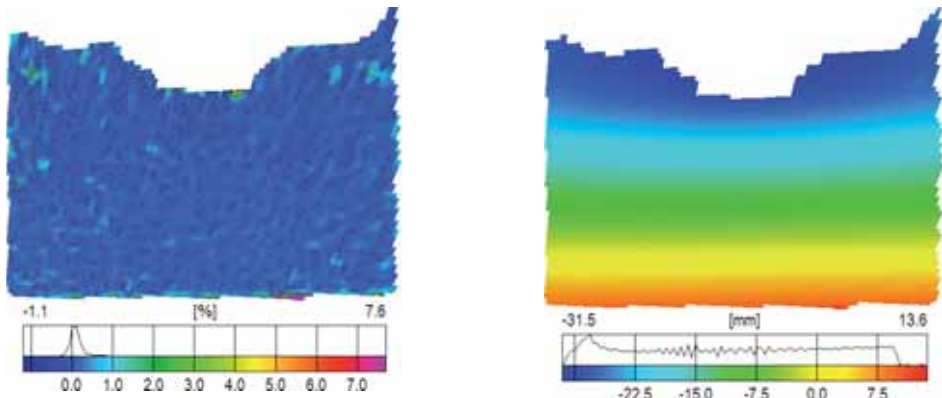


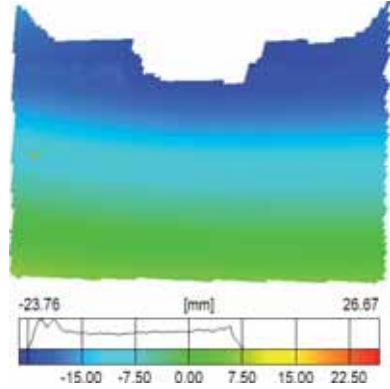
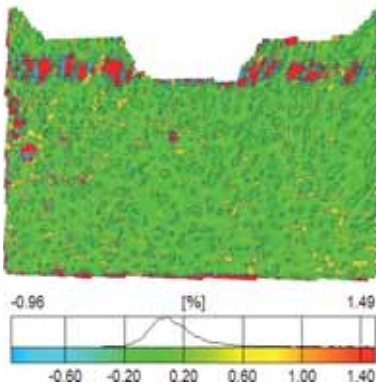
Fig. 3. Example sections selected for plate P1 analysis in ARAMIS

The results of strains and vertical displacements for characteristic sections in the analysed area in plates P1-P3 were presented in a form of images. The images presented in Fig. 4 concern deformation states of plates corresponding to the highest applied load.

$$\mathbf{P1} - F_{\max} = 66.1 \text{ kN}$$



$$P2 - F_{\max} = 72.4 \text{ kN}$$



$$P3 - F_{\max} = 72.2 \text{ kN}$$

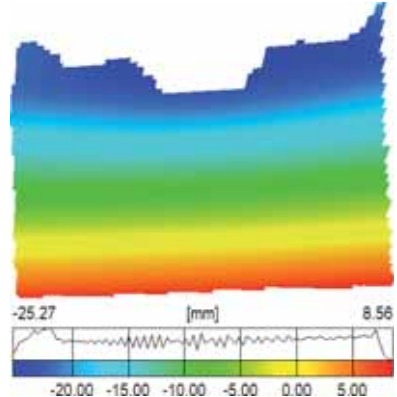
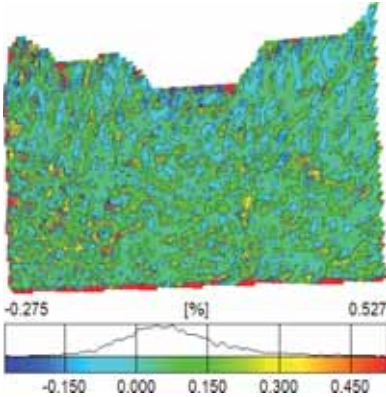


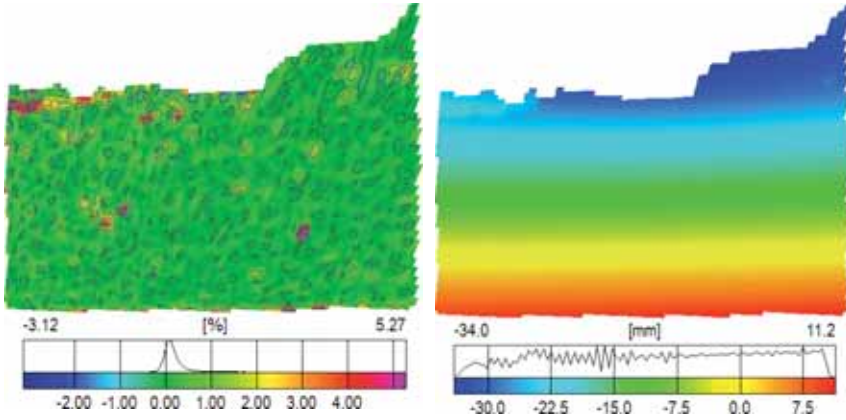
Fig. 4. Images of strains and horizontal displacements of plates at maximum load

Plate P1, without any fibres, was damaged the soonest. Its vertical displacement for maximum strength of 66.1 kN reached the value 31.2 mm. The layer of largest horizontal displacements of 25 to 31.2 mm was 200 mm wide and run centrally across the plate. Maximum values of strains, which appeared at midspan of section 3, were significant and exceeded 3%. They were related to local concrete crushing in the area.

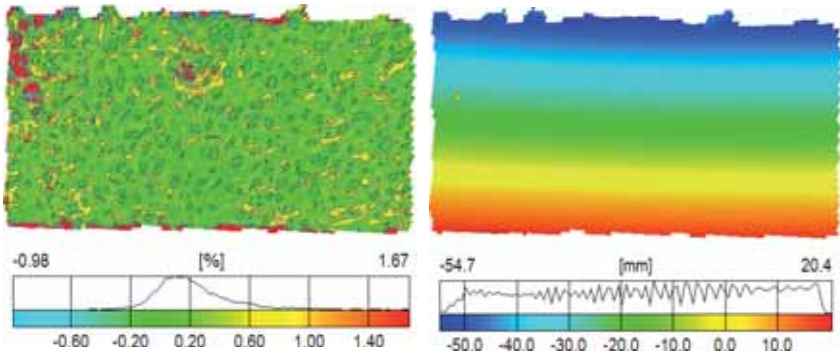
The displacement of plate P2 for maximum load of 72.4 kN reached the value of 32.7 mm. The layer of largest horizontal displacements of 25 to 32.7 mm was reduced to 100 mm. Much smaller strains (1.2%) of elements were observed along all analysed sections. The deformations of 2.8% appeared locally along section 1 in the areas of concrete spalls.

Displacement of plate P3 for maximum value of load equal to 72.2 kN reached the value of 16.2 mm. At the strength value similar to plate P2, local crushing of concrete with fibres appeared. The strains in these areas were the largest, yet they did not exceed 1.2%. Maximum vertical displacements appeared in central layer of 70 mm and reached the value of 12-16.2 mm for the load higher by 18.2% than maximum load for plate P1.

P1 – $F_u = 45.4$ kN



P2 – $F_u = 40.8$ kN



P3 – $F_u = 42.1$ kN

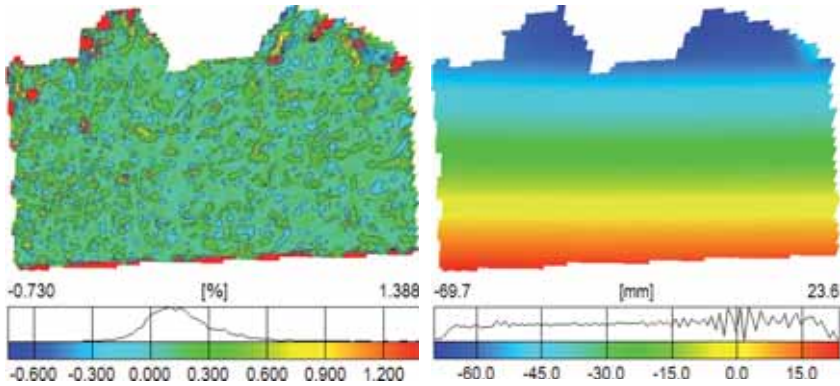


Fig. 5. Images of strains and horizontal displacements of plates at final stage of loading

In the final stage of loading plate P1, the highest strains were recorded along the whole section 2 for the values over 2%. Maximum displacements reached as much as 33.6 mm. In plate P2 strains were usually up to 2% in small fragments. The largest vertical displacements were over twice larger than the displacements in plate P1 and reached 69.8 mm. In P3 with larger share of hybrid fibre reinforcement the strains the compressive fibre concrete layers were larger than in P2 and in longer sections the effects of matrix crushing were observed. The displacements in this case were also significant and reached 56 mm in section 1.

Examples of the relationship major strains and vertical displacement along section length for P1 were presented in Fig. 6.

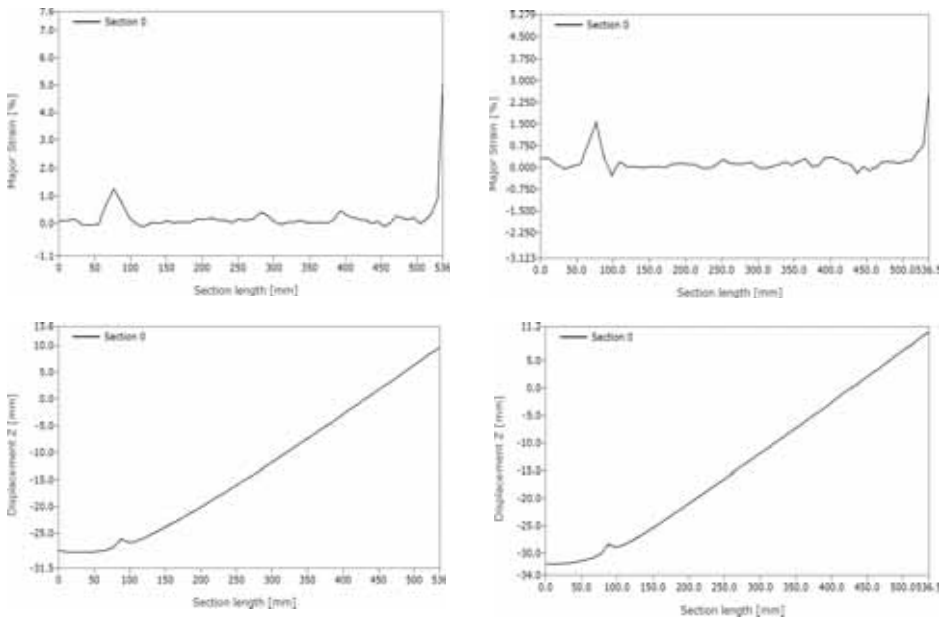


Fig. 6. Sample graphs major strains and vertical displacement along section length for plate P1 at maximum load and final stage of loading

Conclusions

Experimental research proved the correctness of using steel and polypropylene fibres in order to improve the tensile strength of high performance concrete in plate elements. On the basis of the obtained analyses it was stated that 0.5% addition of steel fibres increases the tensile strength of the HPC and stiffness. Moreover, the use of polypropylene fibres, even in small amounts, is effective and increases the performance of the deformed steel fibres in concrete. The cracks in reinforced concrete plates with fibres were much smaller width across than the cracks in the plate reinforced with the reinforcing mesh only. Abrupt energy release was registered in the reinforced concrete plate only. In the plates with fibres instant cracks were observed as a result of bridging fibres. Flexural strength were over 18% for plates with fibres. The failure of reinforced HPC plate with steel fibres in the amount of 1% and polypropylene fibres in the amount of 0.06% was of plastic, gradual and gentle character.

In the most nearest future numerical simulations of failure mechanisms of HPC elements with two kinds of fibres and optimisation of composites are planned.

References:

1. ARAMIS v6.3 (2011), *User Manual - Software*. GOM Optical Measuring Techniques, Germany.
2. Banthia N., Gupta R. (2004), *Hybrid fiber reinforced concrete (HyFRC): fiber synergy in high strength matrices*. Materials and Structures, Vol. 37, 707-716.
3. Brandt A.M. (1996), *Toughness of fibre reinforced cement based materials*. Archives of Civil Engineering, XLII, 4.
4. Brandt A.M. (2008), *Fibre reinforced cement-based (FRC) composites after over 40 years of development in building and civil engineering*. Composite Structures 86, 3-9.
5. Brandt A.M. (2009) *Cement Based Composites: Materials, Mechanical Properties and Performance*. Taylor and Francis. London and New York.
6. Chiaia B., Fantilli A.P., Vallini P. (2009), *Combining fiber-reinforced concrete with traditional reinforcement in tunnel linings*. Engineering Structures 31 1600-1606.
7. Cucchiara C., La Mendola L., Papia M. (2004), *Effectiveness of stirrups and steel fibres as shear reinforcement*. Cement & Concrete Composites 26, 777-786.
8. Domański T., Czekwianianc A. (2006), *Influence of fibre reinforcement on the mechanical parameters of the concrete*. Building Review 6 (in Polish).
9. Fairbairn E.M.R., Toledo Filho R.D., Formagini S., Rosa J.I., Battista R.C. (2012), *Experimental analysis and modeling of ultra high performance fiber reinforced concrete plates*. 1-8.
10. Foster S.J. (2009), *The application of steel-fibres as concrete reinforcement in Australia: from material to structure*. Materials and Structures 42: 1209-1220.
11. Glinicki M.A. (2010), *Concrete with the structural reinforcement*. XXV the Polish Workshops of Work of the Structural Designer, Szczyrk (in Polish).
12. Glinicki M.A., Litorowicz A., Zieliński M. (2002), *Experimental analysis of fracture mode I behaviour of fibre concrete*. Building Materials, No 3, 74-76 (in Polish).
13. Prisco M., Plizzari G., Vandewalle L. (2009), *Fibre reinforced concrete: new design perspectives*. Materials and Structures 42: 1261-1281.
14. Smarzewski P. (2013), *Experimental analysis of high performance fibre reinforced concrete plates*. 1-11 (in press).
15. Smarzewski P., Szwaj M., Szewczak A. (2012), *The analysis of deformation states high strength fibre-reinforced concrete plates in flexural*. Building and Architecture 10, 37-52 (in Polish).
16. Walraven J.C. (2009), *High performance fiber reinforced concrete: progress in knowledge and design codes*. Materials and Structures 42: 1247-1260.

Acknowledgment

This work was financially supported by Ministry of Science and Higher Education within the statutory research number S/15/2013

CALCULATION OF THE THIN PLATES WITH THE LARGE DEFLECTIONS

Aliaksei Tarasevich, Victor Tur

Pope John Paul II State School Higher Education in Biala Podlaska,
Department of Engineering Sciences, Department of Civil Engineering
Sidorska Street 95/97, 21-500 Biala Podlaska, Poland
e-mail: vvtur@bstu.by

Summary:

Very large displacement but small strain of very thin plates is studied using Kirchhoff theory.

When plates are deflected beyond a certain magnitude, the linear theory loses its validity and produces incorrect results. In order for an accurate large deflection solution, one needs to include the coupling between axial and transverse motion, which is geometric non-linearity.

Keywords: thin plates; displacement; deflection.

Introduction

Elasticity theory treats typically linear theory of «rigid» plates. Theory of elasticity in linear version can be used for calculation of plates with small deflection, no more than $1/4 \dots 1/5$ plate thickness.

In these plates, deflections normal to the mid surface of the plate are so small that they do not affect the deformation of the element (Samul 1982).

However, thin plates are widely used in various fields (construction, shipbuilding, aircraft manufacturing).

For thin flexible slabs «load-deflection» relationship is non-linear and hypothesis about non-deformability of mid-surface is unfair, because it appears tensile, compression and shear strains.

For large deflection of plates and the appropriate boundary conditions, axial forces in mid-surface appear independently of the effect of horizontal in-plane loads (Umanski 1973).

Usually in the classic theory of elastic thin slabs used Kirchhoff's (Volmir 1956) it is assumed a mid-surface plane can be used to represent the three-dimensional plate (slab) in two-dimensional form. The following main kinematic assumptions that are made in this theory (Volmir 1956):

1. Straight lines normal to mid-surface remain straight after deformation (shear strains are absent $\gamma_{yz} = 0; \gamma_{xz} = 0$).
2. Straight lines normal to mid-surface remain normal to the mid-surface after deformation ($\varepsilon_z = 0$; linear strain in z-direction is absent).
3. Thickness of the plate does not change during deformation ($\sigma_z = 0$) and in mid-surface of plate tensile, compression and shear strains are absent ($U_o = V_o = 0$).

When the thin plates are deflected beyond a certain magnitude, the linear theory loses its validity and produces incorrect results. Linear theory can predict that the deflection of the member may exceed the length of the member, which is unrealistic. In order for an accurate large deflection solution, one needs to include the coupling between axial and transverse motion (deflection), which is geometric nonlinearity. If the edges of plate are allowed to move freely within the plane of undeformed member, this boundary condition is called «stress-free».

If the edges are restricted from moving, the edges require an equivalent axial load to prevent motion, which is called «immovable» boundary condition.

Nonlinear deflection theories also couple axial loads and transverse deflections.

In the mid-surface of thin-plate there are tensile, compressive and shear forces.

From the hypothesis 2:

$$\varepsilon_z = \frac{\partial W}{\partial z} = 0, \quad (1)$$

and deflections of the thin plate does not depend on the coordinates z :

$$W = W(x, y) \quad (2)$$

Thus, all points lying on a vertical line have the same displacement W . Consequently, to determine the vertical displacements of all point of the plate, sufficient to determine the displacements of its mid-surface.

Strains and curvatures of mid-surface

Using conditions:

$$\left. \begin{aligned} \gamma_{yz} &= 0 \\ \gamma_{xz} &= 0 \end{aligned} \right\} \quad (3)$$

we get:

$$\left. \begin{aligned} \gamma_{yz} &= \frac{\partial W}{\partial z} + \frac{\partial W}{\partial y} = 0 \\ \gamma_{xz} &= \frac{\partial W}{\partial x} + \frac{\partial W}{\partial z} = 0 \end{aligned} \right\} \quad (4)$$

and integrating over z , we get the expressions for calculating the displacement of the mid-surface of a deflections:

$$\begin{aligned} U &= U_0 - Z \frac{\partial W}{\partial x}, \\ V &= V_0 - Z \frac{\partial W}{\partial y} \end{aligned} \quad (5)$$

U_0, V_0 – displacement along X and Y coordinates axis respectively.
Strains of the points on the mid-surface of plate:

$$\begin{aligned}\varepsilon_x &= \frac{\partial U_0}{\partial x} + \frac{1}{2} \left(\frac{\partial W}{\partial x} \right)^2 - Z \frac{\partial^2 W}{\partial x^2} \\ \varepsilon_y &= \frac{\partial V_0}{\partial y} + \frac{1}{2} \left(\frac{\partial W}{\partial y} \right)^2 - Z \frac{\partial^2 W}{\partial y^2} \\ \gamma_{xy} &= \frac{\partial U_0}{\partial y} + \frac{\partial V_0}{\partial x} + \frac{\partial W^2}{\partial x \partial y} - 2Z \frac{\partial^2 W}{\partial x \partial y}\end{aligned}\quad (6)$$

Curvatures of mid-surface:

$$\begin{aligned}\chi_x &= -\frac{\partial^2 W}{\partial x^2}; \\ \chi_y &= -\frac{\partial^2 W}{\partial y^2}; \\ \chi &= -\frac{\partial^2 W}{\partial x \partial y}.\end{aligned}\quad (7)$$

Expression for strains compatibility:

$$\frac{\partial^2 \varepsilon_x}{\partial y^2} + \frac{\partial^2 \varepsilon_y}{\partial x^2} - \frac{\partial^2 \gamma_{xy}}{\partial x \partial y} = \left(\frac{\partial^2 W}{\partial x \partial y} \right)^2 - \frac{\partial^2 W}{\partial x^2} \frac{\partial^2 W}{\partial y^2}.\quad (8)$$

Stress in thin slabs (plates). Stress-strain relationship.

Stress in the thin plates can be considered as the result of superposition of two states: 1) normal uniformly distributed over the plate thickness; 2) bending stress. Consequently, equations must be written for deformed state of thin plate.

Force projection equation on X and Y axis give expressions:

$$\begin{aligned}\frac{\partial \sigma_x}{\partial x} + \frac{\partial \tau}{\partial y} &= 0; \\ \frac{\partial \tau}{\partial x} + \frac{\partial \sigma_y}{\partial y} &= 0.\end{aligned}\quad (9)$$

The equations of moment about the axes X and Y give expressions:

$$\begin{aligned}\frac{\partial M_x}{\partial x} + \frac{\partial H}{\partial y} &= 0; \\ \frac{\partial H}{\partial x} + \frac{\partial M_y}{\partial y} &= 0.\end{aligned}\quad (10)$$

After summing the projections of all forces on the Z-axis for element of plate with sizes dx , dy and vision by $dx dy$ we obtain the following expression:

$$\frac{\partial Q_x}{\partial x} + \frac{\partial Q_y}{\partial y} + \sigma_x h \frac{\partial^2 W}{\partial x^2} + \sigma_y h \frac{\partial^2 W}{\partial y^2} + 2\tau h \frac{\partial^2 W}{\partial x \partial y} + q(x, y) = 0. \quad (11)$$

Assuming, that the strains of plate are elastic, and normal stress in the direction Z are very small in comparison with the normal stress parallel to the mid-surface of the plate. Following «strain-stress» relationships can be written:

$$\begin{aligned} \varepsilon_x &= \frac{\sigma_x}{E} - \mu \frac{\sigma_y}{E}; & \sigma_x &= \frac{E}{1-\mu^2} (\varepsilon_x + \mu \varepsilon_y); \\ \varepsilon_y &= \frac{\sigma_y}{E} - \mu \frac{\sigma_x}{E}; & \sigma_y &= \frac{E}{1-\mu^2} (\varepsilon_y + \mu \varepsilon_x); \\ \gamma &= \frac{2(1+\mu)}{E} \tau; & \tau &= \frac{E}{2(1+\mu)} \gamma. \end{aligned} \quad (12)$$

Expression for calculation of bending, torsion moments and shear forces can be written:

$$\begin{aligned} M_x &= -D \left(\frac{\partial^2 W}{\partial x^2} + \mu \frac{\partial^2 W}{\partial y^2} \right) = -D(\chi_x + \chi_y); \\ M_y &= -D \left(\frac{\partial^2 W}{\partial y^2} + \mu \frac{\partial^2 W}{\partial x^2} \right) = -D(\chi_y + \chi_x); \\ H &= -D(1-\mu) \frac{\partial^2 W}{\partial x \partial y} = -D(1-\mu)\chi; \\ Q_x &= -D \left(\frac{\partial^3 W}{\partial x^3} + \frac{\partial^3 W}{\partial x \partial y^2} \right) = -D \frac{\partial}{\partial x} (\chi_x + \chi_y); \\ Q_y &= -D \left(\frac{\partial^3 W}{\partial y^3} + \frac{\partial^3 W}{\partial y \partial x^2} \right) = -D \frac{\partial}{\partial y} (\chi_y + \chi_x) \end{aligned} \quad (13)$$

Basic differential equations

Substituting the expression (13) for the shear forces in the equation of equilibrium (11) and get the following expression:

$$D \nabla^4 W = h \sigma_x \frac{\partial^2 W}{\partial x^2} + h \sigma_y \frac{\partial^2 W}{\partial y^2} + 2h \tau \frac{\partial^2 W}{\partial x \partial y} + q. \quad (14)$$

Equation (14) relates the deflection of slab and vertically applied load, but contains additional unknown σ_x, σ_y, τ .

To solve the problem use equations (8) and (12):

$$\frac{\partial^2 \sigma_x}{\partial y^2} - 2 \frac{\partial^2 \tau}{\partial x \partial y} + \frac{\partial^2 \sigma_y}{\partial x^2} - \mu \left(\frac{\partial^2 \sigma_x}{\partial y^2} + 2 \frac{\partial^2 \tau}{\partial x \partial y} + \frac{\partial^2 \sigma_y}{\partial x^2} \right) = E \left[\left(\frac{\partial^2 W}{\partial x \partial y} \right)^2 - \frac{\partial^2 W}{\partial x^2} \frac{\partial^2 W}{\partial y^2} \right] \quad (15)$$

The introduction of the stress function (Eri-function) equations (14) and (15) form a system of non-linear differential equations from theory of flexible plates (Karman-equations) (Konchakovskiy 1984):

$$\begin{aligned} \frac{D}{h} \nabla^4 W &= \frac{\partial^2 F}{\partial y^2} \frac{\partial^2 W}{\partial x^2} + \frac{\partial^2 F}{\partial x^2} \frac{\partial^2 W}{\partial y^2} - 2 \frac{\partial^2 F}{\partial y \partial x} \frac{\partial^2 W}{\partial x \partial y} + \frac{1}{h} q; \\ \nabla^4 F &= E \left[\left(\frac{\partial^2 W}{\partial x \partial y} \right)^2 - \frac{\partial^2 W}{\partial y^2} \frac{\partial^2 W}{\partial x^2} \right] \end{aligned} \quad (16)$$

System of non-linear differential equations (16) together boundary conditions are basic system of non-linear differential equations flexible plates theory. The solution of system (16) is not obtained in general form, but received a number partial solutions.

Boundary conditions depend on the restricting conditions on the contour of plate.

For example for conditions:

$$\begin{aligned} U_{x=a} - U_{x=0} &= 0; \\ V_{y=b} - V_{y=0} &= 0. \end{aligned} \quad (17)$$

boundary conditions may be written in the form:

$$\begin{aligned} \left[\frac{\partial^2 F}{\partial y^2} - \mu \frac{\partial^2 F}{\partial x^2} - E \left(\frac{\partial W}{\partial x} \right)^2 \right] dx &= 0; \\ \left[\frac{\partial^2 F}{\partial x^2} - \mu \frac{\partial^2 F}{\partial y^2} - E \left(\frac{\partial W}{\partial y} \right)^2 \right] dy &= 0. \end{aligned} \quad (18)$$

Special computer program was developed for the calculation of the thin plates under various boundary conditions using the package «MATEMATICA».

Consider the example of calculating the square and rectangular (side ratio 1:2) supported on four corner columns and loaded with concentrate loads in the middle of each finite element (see fig. 1).

Calculations results in the form of diagrams of deflections are shown on the fig. 1 and 2. Using a system of non-linear differential equations linking load and deflection, can be constructed diagrams bending and torsion moments, shear forces and stress.

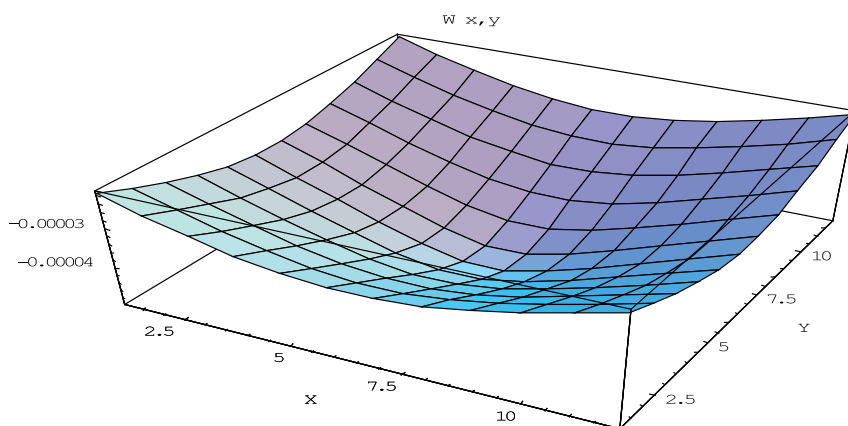


Fig. 1. Deflection of square plate

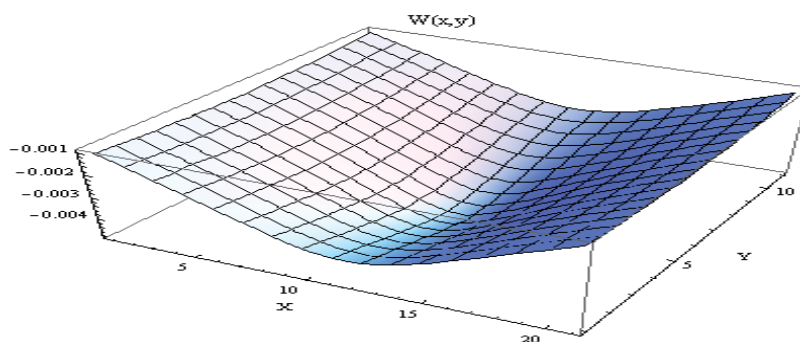


Fig. 2 Deflection of rectangular plate

Conclusion

Analysis of the values of the bending moments and axial forces in thin plate can determine the ratio of bending and membrane stress as a function of deflection. The solutions obtained are in satisfactory agreement with the results of calculating using the formulas of (Umanski 1973).

References:

1. Samul V. (1982), *Principles theory of elasticity and plasticity*. Vyshaja skola, Moscow.
2. Volmir A. (1956), *Flexible plates and membranes*. Gosizdat, Moscow.
3. Konchakovskiy Z (1984), *Slabs. Static design*. Stroyizdat, Moscow.
4. Umanski A. (1973), *Guide of designer*. Stroyizdat, Moscow.

RECENT RESEARCH AND DEVELOPMENT IN COMPOSITE STRUCTURES

Agnieszka Jabłońska-Krysiewicz, Barbara Sadowska-Buraczewska

Białystok University of Technology, Wiejska Street 45E, 15-351 Białystok, Poland
e-mail: a.krysiewicz@pb.edu.pl, bsadowska@pb.edu.pl

Summary:

Composite steel–concrete and concrete–concrete structures represent an efficient and economical form of construction for building and bridge applications. Composite structures, exploring advantages of concrete and structural steel, have been increasingly applied in commercial and parking buildings. This paper presents state of art, achievements and new experimental works of concrete–concrete and steel–concrete structures. There are described experimental studies on composite beams with partial use fibre reinforced concrete. The researches on composite joints and steel–concrete beams are presented and additionally new method of FE modelling of such structures are shown.

Keywords: composite structures, concrete, steel, experiment, numerical modelling

Introduction

Composite steel–concrete and concrete–concrete structures represent an efficient and economical form of construction for building and bridge applications. Composite structures, exploring advantages of concrete and structural steel, have been increasingly applied in commercial and parking buildings.

In the first part of this article the new approaches in concrete–concrete beams are presented. The second part is voted to steel–concrete beams and joints.

The composite concrete – concrete beams

In concrete–concrete structures many researches are investigated experimentally and theoretically behaviour of HSC and HSC using fibre. In the last decade HPC (or HSC) are more widely used in practice parallel with growing interest of researchers to precisely describe mechanical properties and methods of design of structural members (Bae et al, 2003; Lessard et al 1992).

As reported by (Yamada et al. 1997, 1999), the structural reinforced concrete and prestressed composite beams with the HSC layer tested in Japan under short-time load, may have improved sectional parameters, eg a higher flexural stiffness and greater bending capacity in comparison to homogenous members, made of normal strength concrete. Composite reinforced concrete beams presented intermediate behaviour between reinforced concrete beams made of HSC and beams of normal strength concrete.

Experimental analysis of flexural composite beams.

This chapter presented experimental studies presented the selected results of composite beams with partial use fibre reinforced concrete with the cross section of 80 x 120 mm and the effective span of 1100mm , using the above describe concept of strengthening, preparing top concrete layer 40 mm thick (Sadowska-Buraczewska 2012, 2013).

The FRC was elaborated (Sadowska-Buraczewska 2012,2013) based on the cement type CEM I-52,5 with reactive powder and steel- fibre. The static scheme and cross sections of tested beams and also load conditions are shown in Fig.1. Fig. 2 presents the view of the beam under testing.

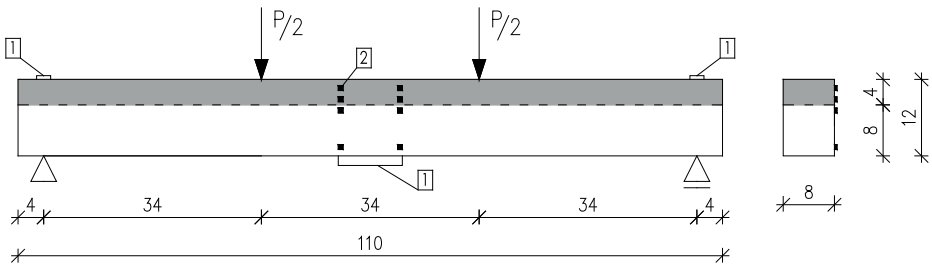


Fig.1. Loading scheme and cross section in tested beams.(Sadowska-Buraczewska,2012)

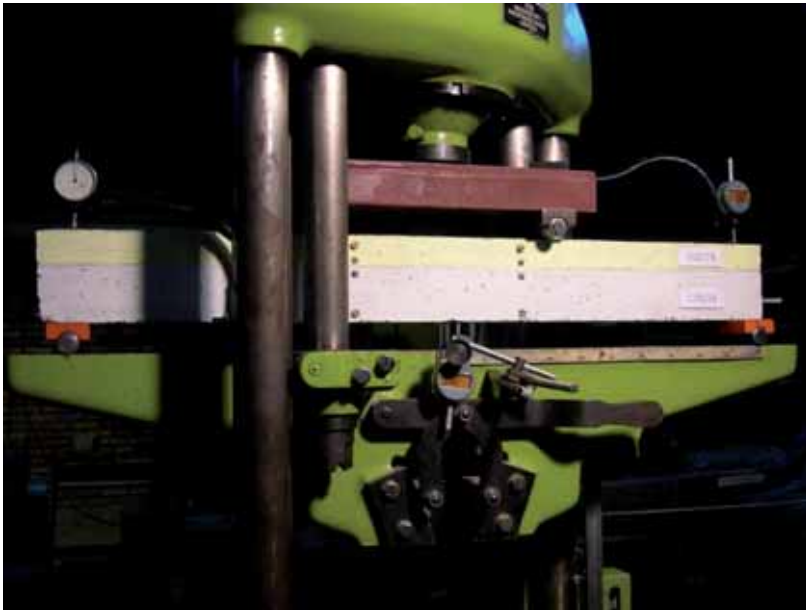


Fig. 2. The beam on the test stand in the testing machine.(Sadowska-Buraczewska,2012)

Analysis of short-time effects under bending

The selected values of deflections are presented in Table 1. The diagram showing experimental relationships between loading force F and compressive strains for FRC beams and also for homogenous control beams HSC and N are presented in Fig.3.

Table 1. Experimental values of deflections [mm] for composite beams made with use of FRC and beams totally made of HSC(Sadowska-Buraczewska,2012)

Force [kN]	Experimental values of deflections [mm] for composite beams made with use of FRC and beams totally made of HSC.	
	FRC	HSC
5	0,36	0,45
10	0,54	0,65
15	1,31	1,50
20	1,74	2,13
25	2,97	3,02
30	3,54	3,73
35	4,02	4,34

The diagram showing experimental relationships between loading force F and compressive strains for FRC (blue) beams and also for homogenous control beams HSC (red) and N (green) are presented in Fig. 3.

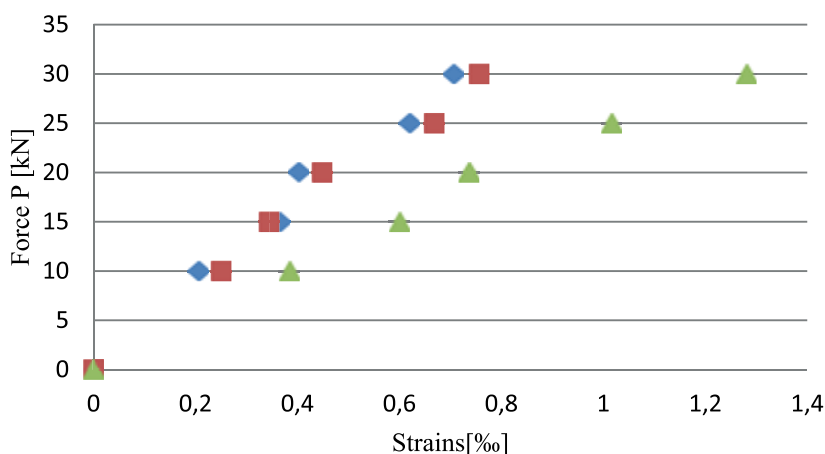


Fig. 3. Experimental relationships between concentrated force and strains for tested beams under short time load (Sadowska-Buraczewska,2012,2013)

The experimental test conducted on reinforced concrete composite beams made of normal concrete and FRC layer in compressive zone tested under short time load show the positive effects of strengthening of such beams in comparison of homogenous normal strength concrete and totally made of HSC. The future studies and efforts will be concentrated on short time and long-term deformations of reinforced concrete beams prepared in natural scale. The results of these investigations proved the effectiveness of composite structures with the partial use of FRC in the compressive zone as a way of strengthening of the structural members wanted a rehabilitation or reconstruction.

Steel-concrete structures

The effective application of steel and concrete leads to the increased strength and stiffness if compared with traditional solutions such as bare steel or reinforced concrete structural elements. Due to advantages of composite construction, the scope of application of composite actions in steel frameworks have been widened, finally involving not only the composite actions between the structural floor beams and the reinforced concrete slab, but also taking advantage of composite joints.

The nonlinear analysis of composite structures, carried out up to the failure of limit, is rather difficult due to the complexity of physical phenomena accompanying the structure deterioration process under increasing actions, bond interaction between concrete and steel parts, stress redistribution between the concrete and steel reinforcement after cracking, interaction of the behaviour of steel beam shear studs and concrete, the presence of any profiled metal decking, occurrence of slip between the steel parts and reinforced concrete slab, and due to a variety of all other possible local effects existing in the structure composed of such different materials like steel and concrete, with regard to the overall ductility behaviour (Gizejowski et al., 2010).

Composite joints

Researches

Design rules for steel-concrete structures were developed on basis of worldwide researches efforts since there had been rather limited guidance and lack of expertise in this field (Simoes da Silva et al, 2001). Existing design rules of Eurocode 4 (Eurocode 4, 2005) are not however since they do not cover all possible solutions, especially in design of composite joints (Gizejowski et al., 2010). Recently, the research on the behaviour of composite joints has been done by Kozłowski (Kozłowski, 2000). Gizejowski, Barcewicz and Salah (Gizejowski et al. 2010) have conducted laboratory tests in order to investigate the behaviour of steel and steel-concrete composite end-plate beam-to-column joints under bending. The eight tests were carried out. The general arrangement of composite joint specimen is presented in Fig. 4.

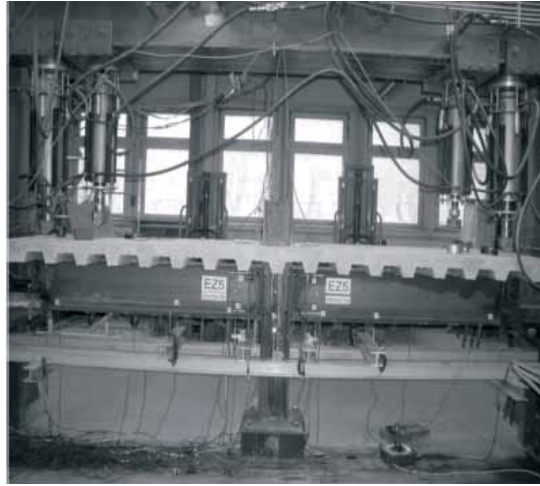


Fig.4. General setup of the test rig (Gizejowski et al, 2010)

Beams elements of all the specimens were made of IPE 300 and columns of HEB 200. All the steel elements were made of steel grade S235JR. The bolt connectors were M20 of class 10.9. The concrete slab was cast on the dip-profiled sheeting, using the Cofraplus 60 composite flooring. The ribs of the sheeting were arranged in the transverse direction to the supporting beams. The composite action was partially provided by the sheeting and the headed studs $SD\phi 19 \times 100$ mm, that were friction welded to the upper flange of the beam.

The results for the bare steel joint with extended end -plate proved that the existence of the concrete slab had a positive influence on the initial stiffness and the ultimate moment capacity.

Design method

According to Eurocode 4 (Eurocode 4, 2005) Eurocode 3, part 1-8 (Eurocode 3) may be used as a basis for the design of composite beam-to-column joints and splices provided that the steel part of the joint is within the scope of that section. The structural properties of components assumed in design should be based on tests or on analytical or numerical methods supported by test. In determining the structural properties of a composite joint, a row of reinforcing bars in tension may be treated in a manner similar to a bolt-row in tension in a steel joint, provided that the structural properties are those of the reinforcement. Composite joints should be design to resist vertical shear in accordance with relevant provisions of Eurocode 3. The design resistance moment of a composite joint with full shear connection should be determined by analogy to provisions for steel joints given in Eurocode 3, taking account of the contribution of reinforcement.

The basic joint components for composite beam-to-column connections are:

- Longitudinal steel reinforcement in tension,
- Steel contact plate in compression,
- Column web in transverse compression,
- Column web panel in shear,
- Column web in transverse compression,

The rotational stiffness of a joint should be determined by analogy to provisions for steel joints, taking account of contribution of reinforcement. The rotation capacity of composite joint may be demonstrated by experimental evidence. Account should be taken of possible variations of the properties of materials from specified characteristic values. Experimental demonstration is not required when using details which experience has proved have adequate properties. Alternatively, calculation methods may be used, provided that they are supported by tests.

Composite beams and slabs

Composite steel-concrete beams are formed typically from rolled sections and reinforced concrete slab of a constant thickness or a variable thickness when slab is cast in-situ on profiled sheeting (Johnson, 2004). In case of profiled sheeting used for in-situ casting, it is treated as a lost decking (Type 1) or it is assumed to play the role of additional reinforcement of composite beam subjected to service loads (Type 2).

The system Cofrasolfloor (Floor systems guide, ARVAL, 2013) is the example of Type 1 of profiled sheeting. It is made up of steel decks used to provide formwork for the reinforced concrete when it is poured (Fig.5). For slabs on self supporting permanent formwork, the deck is only stressed during the construction stage and is not taken into account in the final floor resistance.

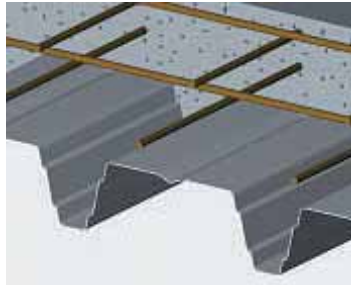


Fig.5. Cofrasol floor (Floor systems guide, ARVAL, 2013)

Composite floor systems combine the beneficial features of steel and concrete. Cofraplus (Floor systems guide, ARVAL, 2013) is open-rib composite floor decks (Fig.6). These are made up of two open-rib trapezoidal and nestable decks with embossments for easy storage and transportation.

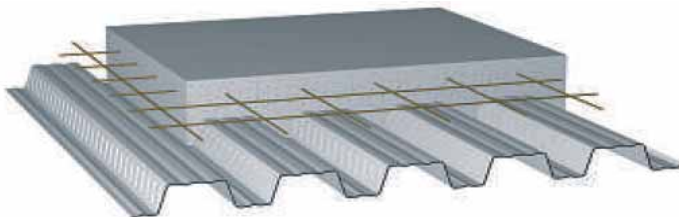


Fig.6. Cofraplus floor (Floor systems guide, ARVAL, 2013)

According to Eurocode 4 (Eurocode 4,2005) composite behaviour between profiled sheeting and concrete shall be ensured by one or more of the following means:

- a) mechanical interlock provided by deformations in the profile (indentations or embossments);
- b) frictional interlock for profiles shaped in a re-entrant form;
- c) end anchorage provided by welded studs or another type of local connection between the concrete and the steel sheet, only in combination with (a) or (b);
- d) end anchorage by deformation of ribs at the end of the sheeting, only in combination with (b).

A composite floor is designed in two different stages: the assembly and concrete-pouring stage, and then the composite stage. During the assembly and concrete-pouring stage, the deck is used as self-supporting formwork and provides a working platform. In composite stage, the deck is structurally combined with hardened concrete (composite action) and completely or partially replaces the tensile reinforcement of the slab. The design of the profiled steel sheeting as shuttering should be in accordance with Eurocode 3. In composite stage the following methods of analysis may be used for ultimate limit state:

- a) linear plastic analysis with or without redistribution;
- b) rigid plastic global analysis provided that it is shown that sections where plastic rotations are required have sufficient rotation capacity;
- c) elastic-plastic, taking into account the non-linear material properties.

Numerical methods in composite steel-concrete structures

During last years, different FE software packages were used to study the nonlinear behaviour of composite structures. Oven et al. (Oven et al.,1997) developed a two dimensional nonlinear FE model for analysis of composite beams with partial interaction. Baskar and Shanmugam (Baskar and Shanmugam, 2003) proposed 3D FE model to analyse four simply supported composite plate girders. They used 8-node doubly curved thin shell elements to model steel parts and rebar layer to model reinforcement (Fig.7).

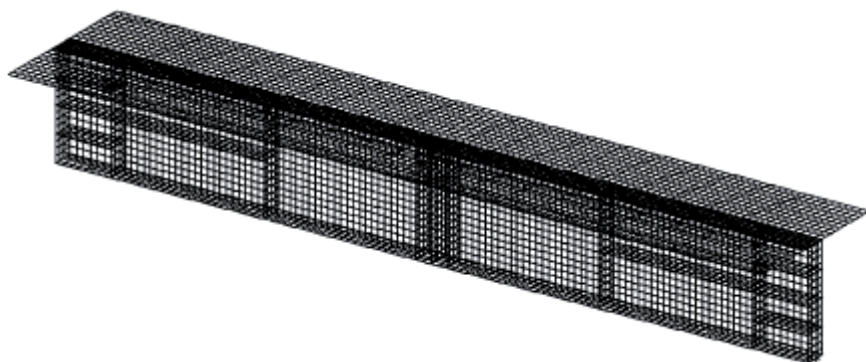


Fig.7. Finite element model of composite girders (Baskar and Shanmugam, 2003)

Lang et al. (Lang et al., 2004) developed a 3D FE model to consider the geometric and material nonlinear behaviour of continuous composite beams. The four- node doubly curved general shell elements were employed to model the concrete slab, the flanges and the web of the steel beam. The stud shear connectors were modelled using 3D beam elements (Fig.8.)

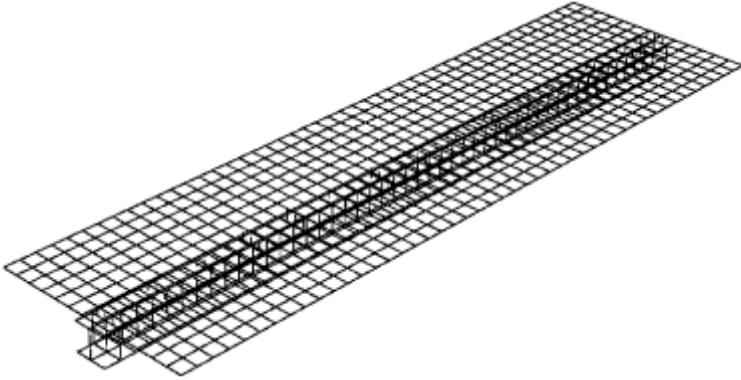


Fig.8. Finite element mesh for composite beam (Lang et al., 2004)

Barth and Wu (Barth and Wu,2006) used a four-node general purpose shell elements S4R to model the steel girder, concrete slab and stiffeners. The steel reinforcement in concrete was modelled by means of REBAR LAYER available in ABAQUS code.Full composite action between the concrete slab and the top flange of the steel girder was considered using beam type multi-point constraints (Fig.9)

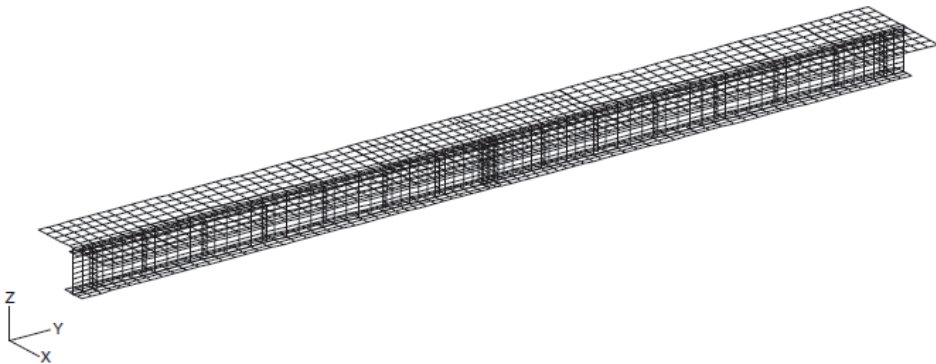


Fig.9. Typical FEA mesh for composite girder elevation (Barth and Wu,2006)

Fu et al. (Fu et al, 2008) developed the continuum elements available in the ABAQUS code to model semi-rigid composite joints with precast hollow core slabs. 3D continuum elements were used to model all parts of the composite joints and the contact was applied between all the joint components (Fig.10)

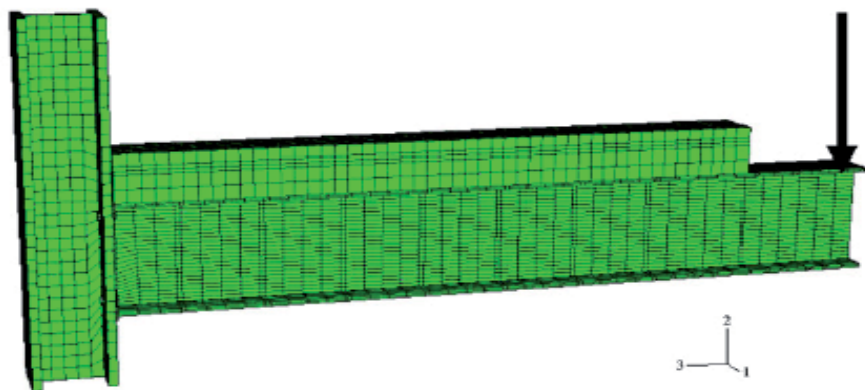


Fig.10. 3-D finite element model of composite connection (Fu et al.,2008)

Gizejowski et al.(Gizejowski et al.,2010) used 4-node shell elements to model steel parts of joint and special REBAR LAYER for modelling of reinforcing bars in the reinforced concrete section. The beam element type B31 were employed to model shear studs. A general 3D view of modelled steel-concrete composite joints is depicted in Fig.11.

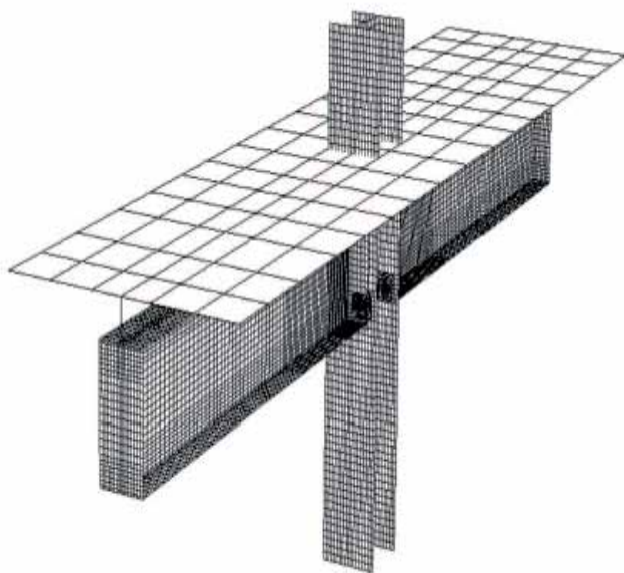


Fig. 11. 3D FE mesh for composite joint (Gizejowski et al.,2010)

Lam (Lam, 2008) used 3D solid elements to build FE model of semi-rigid composite connection with precast hollowcore slabs (Fig.12). Material nonlinearity was included by specifying the stress-strain curves of the material taken from the test specimen.

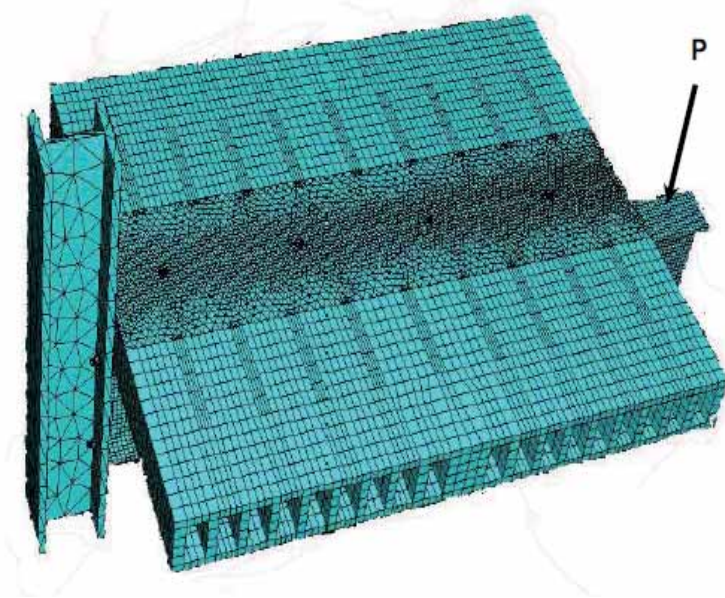


Fig.12. Finite element model of semi-rigid composite joint. (Lam, 2008)

Zeng and Makelamen (Zeng and Makelamen, 2009) conducted a numerical study on semi-rigid composite joint in slim floor frame (Fig.13).

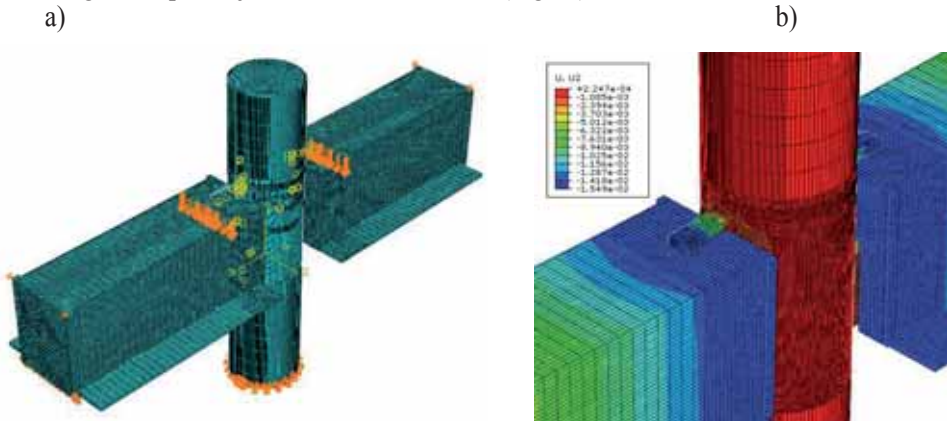


Fig.13. a) Overview of mesh and boundary condition for 3D model of semi-rigid composite joint with composite column; b) Maps of deformations of FE model(Zeng and Makelamen, 2009)

Some main components, such as structural steel and concrete filled in the column, eight-node, first-order solid continuum element (C3D8I) were selected for the modelling. A solid element with incompatible modes has a better performance for such types of problem, including large plasticity calculations, bending, and contact interaction, though these elements take more time, which is expensive. The longitudinal reinforcing bars were modelled via a two-node, first-order truss element (T3D2).

The presented numerical investigations confirm the use of FE model as a potential tool in current design approaches in order to improve the characterization of the real behaviour of composite structures.

Conclusions

This paper has presented state of art, achievements and new experimental works of concrete-concrete and steel-concrete structures. There were described experimental studies on composite beams with partial use fibre reinforced concrete. The researches on composite joints and steel-concrete beams were presented and additionally new method of FE modelling of such structures was shown.

References:

1. Bae S. and Bayrak O. *Stress block parameters for high-strength concrete members*, ACI Structural, Vol 100, Issue 5, Sept/Oct 2003, p. 626-636.
2. Barth K.E., Wu H., *Efficient nonlinear finite element modelling of slab on steel stringer bridges*, Finite Elements in Analysis and Design, 42, 2006, p.1304-1313.
3. Baskar K., Shanmugam N.E., *Steel-concrete composite plate girders subject to combined shear and bending*. Journal of Constructional Steel Research, 59, 2003, p.531-557.
4. Eurocode 3 ENV 1993-1-8::, Design of Steel Structures, Part 1-8 Design of Joints, 2005.
5. Eurocode 4: ENV 1994 Design of composite steel and concrete structures, Part 1-1: general rules and rules for buildings, 2005.
6. *Floor systems guide*, ARVAL by Arcelor Mittal, 2013.
7. Fu F., Lam D., Ye J, *Modelling semi-rigid composite joints with precast hollowcore slabs in hogging moment region*, Journal of Constructional Steel Research, 64, 2008, p.1408-1419.
8. Gizejowski M., Salah W., Barcewicz (2010), *Finite element modelling of the behaviour of certain class of composite steel-concrete beam-to-column joints*, Archives of Civil Engineering, LVI,1,2010.
9. Kozłowski A. *Shaping of the steel and composite skeletal structures with semi-rigid joints [in Polish]*, Oficyna Wydawnicza Politechniki Rzeszowskiej, Rzeszów, 2000.
10. Lam D., *Recent research and development in semi-rigid composite joints with precast hollowcore slabs*. Connections in Steel Structures VI. Proceedings of the Sixth International workshop, Chicago, 2008, p.265-276.
11. Lessard M. and Aitcin P.C. *Testing high performance concrete*. In: *High performance concrete-from material to structure*. Ed by Y. Malier, Van Nostrand Reinhold Inc, New York 1992.

12. Liang Q.Q, Uy B., Bradford M.A., Ronagh H.R., *Ultimate strength of continuous composite beams in combined bending and shear*, Journal of Constructional Steel Research, 60, 2004, p.1109-1128.
13. Sadowska-Buraczewska B. *HSC and steel-fibre concrete in structures*, Przegląd Budowlany 1/2013, p. 32-34.
14. Sadowska-Buraczewska B. *The concrete new generation with steel-fibre with the partial use in structures.*, Energy-saving and ecological materials, installations and technology in construction, Ed Fic St, PSW JP II, p. 142-149.
15. Simoes da Silva L., Simoes R.D., Cruz P.J.S. *Experimental behaviour of end-plane beam-to-composite joints under monotonic loading*, Engineering Structures, 23, 11, 2001, p.1383-1409.
16. Yamada M. and Matsuura H. *High-strength concrete for prestressed concrete*, In: Proceedings of International Conference on high-strength concrete, Kona, Hawaii, US. Engineering Foundation Conference, July 13-18 1997.
17. Zeng J., Makelamen P., *Finite element modelling of semi-rigid composite joint in a slim floor frame*, Nordic Steel 2009 Construction Conference, Malmo, Sweden, p.335-342.

RESISTANCE OF NON-WELDED RHS CONNECTIONS

Piotr Oponowicz, Martyna Michalska

University of Technology, Department of Civil & Environmental Engineering,
Wiejska Street 45E, 15-351 Białystok, Poland
email: oponowicz@aioni.pl

Summary:

Aim of the study: These days creation a new type of connection such as non-welded joints can be useful. It allows save money and time. Idea of push-pull type joints in application to steel truss made with RHS is the base to this research.

Research methods: Experimental evidence of such joint behavior tested in natural scale is described. Geometry and material properties of the tested connections are given. Axial-deflection curves are presented. Yield line local push mechanism on front wall and as the alternative front and bottom wall chord section is used to the theoretical estimation of the failure load. Numerical model of “plug & play” type T and N joints for calculation and a prediction of joints resistance is proposed.

Results: Theoretical and experimental results of joints resistance are shown. Eleven T RHS laser made joints in natural scale were tested here up to failure. Typical joint failure was the inelastic deformation of the loaded top & bottom flange of chord..

Eight joints of N-type grid of a natural scale were tested. Two selected joints of the chord thickness 3.0 mm (WTLN5 and WTLN6) were selected. The numerical model mapped the load method used during experimental studies.

In both case(T RHS joints and N-type joints) computation model to a large extent reflects the real work of a joint, assuming reasonable time of numerical calculations.

Keywords: non-welded joints, RHS T joints, numerical model of “plug & play” type T and N joints

Introduction

Welding is extensively used in modern production of steel. Above-mentioned technique of merging steel elements is not complicated, but requires a highly qualified staff to make the whole process done accurately. Because of the variety of construction designs it is not possible to fully robotisethe automatic welding machines at the current stage of its development.

Due to the rising cost of steel structures welding, it is expected to search for new methods of connecting sections, which will involve a small labour input, as well as eliminate the need to pursue professional certification.

The new idea RHS made of joints uses the internal forces in the bars to make them merged (uses share and friction forces). This can be achieved by using a specific type of connections without welding employment.

Joints made of RHS selections review

Shaping RHS joints made of RHS sections significantly differs from other hot-rolled sections. A closed hollow intersection causes a number of handicaps, both at the design and manufacturing stages. Compared to traditional solutions (joints made of open profile - (such as H-shape, T-shape, L-shape, C-shape) closed hollow structure shave much lower stiffness due to their thinner walls (causing susceptibility of the designed joints). They have a lower carrying capacity for pressure and shear as well. Popularisation of welding technique let the pipes to be widely used in steel structures.

Welded connections aren't demountable. They occur in the following forms: joints without shear plate, with shear plate and with spacers. The most commonly used joints solution of T RHS truss joints are joints without shear plates (Bródka, Broniewicz 2001).

Forming of the joints, computation methods and models of damage of classic welded connections have been thoroughly discussed in the paper 'Hollow sections in structural applications' (Wardnier i in., 2010). The model proposed by the standard EN 1993-1-8 (Eurocode 3) is based on yield line theory. Carrying capacity calculation of RHS joints can also be done by applying other models. These models are often more accurate in describing the work of the joint, but because of the fact they are time-consuming, they are not widely used (Szlendak 2007).

Brief history of RHS joints

The first calculation formulas (joints K and N) were published by W. Estwood and A.A. Wood in the late 60 and 70 (United Kingdom). Calculation formulas were later developed by J. Davies and T. W. Giddings.

In the 60's, to estimate the carrying capacity of the welded type T joint, R.G. Redwood and J. E. Jubbs used a yield line model. This method, developed by Johansen (1962) was used in the construction of reinforced concrete to determine the bearing capacity of the plates.

In 1973, the research team was formed in the Netherlands, which took up the issue of carrying capacity of welded RHS joints. The leading role was played by prof. J. Wardnier.

In Canada, in the 80's A. Packer and S. S. Haalem were engaged in the joints made of steel RHS topic.

In Poland, behavior of welded RHS joints was taken by a research team at COBPKM "Mostostal" under the guidance of prof. J. Bródka in the 80's. A. Czechowski, J. Życiński, J.K. Szlendak, J. Kordjak were the members of a team.

Classification of the links

Links in steel structures can be divided into several types:

1) Depending on the type of connector

- a) Welded
- b) Screw

2) Manufacturing venue

- a) Workshop
- b) Assembly plant

3) Type

- a) fixed
- b) demountable

4) Stiffness

- a) Rigid
- b) articulated
- c) susceptible

The new type connection in the form of push-pull joint should be classified depending on the type of connector as the innovative joint with adopted screws. Nevertheless the screw parts should be considered secondary and the primary feature is the possibility to transfer the forces with the employment of pressure. The joint is fully demountable and susceptible. It can be made either in the workshop or on the construction site (during assembly).

Modern technologies of steel cutting

Using modern methods for cutting the steel components like the industrial laser, you can make desired types and shapes of slots with high accuracy. Similar methods of steel processing were used only in the machinery industry.



Fig. 1. Laser cut of lock.

Laser cutting technology is used for the metal processing. Laser cutting processing can be used for all types of metals such as carbon steel, structural steel, stainless steel, nonferrous metal. Laser technology can achieve precise cut of 0.1 mm. Adequate process control of cutting and shaping the slots and the ends of the profiles are fully automated. Thereby it allows to avoid the need to prepare the templates used in older technologies. Machines are responsible for proper cutting of the parts. They collect cutting data (nc files) from the files included in the drawings .dwg in electronic form .dstv. Until recently a steel was cut only in one plane (2D). Along with a development of technology, lasers can cut profiles in 3D (cut in one plane, but they can freely rotate the workpiece, without human intervention). Technology mentioned above eliminates the considerable investment of human labour who don't have to merge the structure by means of welding anymore.

Concept of non-welded joint

Extended rods of truss are attached with a single bolt, and compressed parts will carry the load by means of local shear and pressure. For this purpose, the chord rods were suitably prepared (in the form of locking slots), and the ends of the truss branches (in the form of keys). Inserting the key (branch) in the lock (chord) creates a non-welded connection of plug & play / push-pull capable of transferring shear and compression (by pressure).

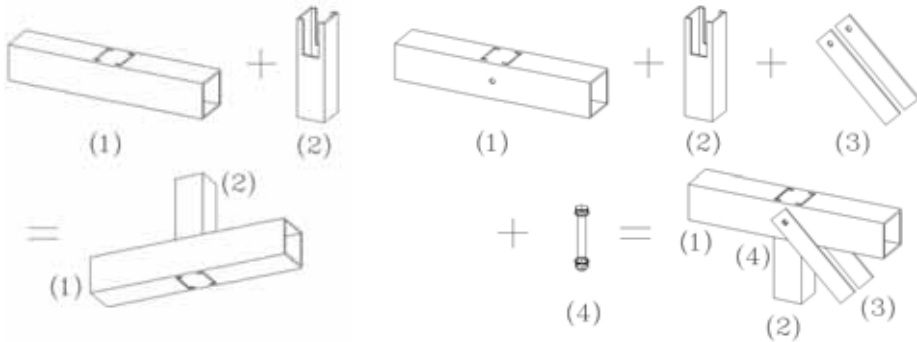


Fig. 2. The type T joint, and type N joint

Non-welded joint application

Structures made in technology that does not require welding can be successfully used in the construction industry e.g. for manufacturing facilities, warehouses, sheds, etc. This type of construction is easy to carry in separate parts and don't have to be fixed with the ground so that it can be built as temporary or permanent hall. There are demountable connections between the construction parts so it can be removed and re-building elsewhere.

Advantages and disadvantages of non-welded joint

Advantages of using the non-welded joint:

- Little experience required
- Possibility to assembly directly on the construction site
- Full demountability of the structure
- The possibility of typification of the parts
- Full automation in the production of the structure

Disadvantages of non-welded joint:

- Production of the construction requires sophisticated cutting machines
- High precision in manufacturing required
- Branch does not carry the tensile force

The T joints

The proposed non-welded joints in the form of a “plug & play” can only transfer a force through the pressure of the branch to the chord. This joint can be designed in the way the external load is carried by the top chord. With the proper design of cut the bottom chord can also be employed. In this case, the clamping force is distributed on the top and bottom chord of the RHS.

The computation model

Based on the theory of yield line the model of this type of joint destruction was developed. In the paper (Oponowicz 2011) the issues of T joint using only the top chord were discussed. In the joint being discussed, both chords were used. Model I describes the joint plastic failure of the upper wall of chord, model II describes the plastic failure of the bottom wall of chord.

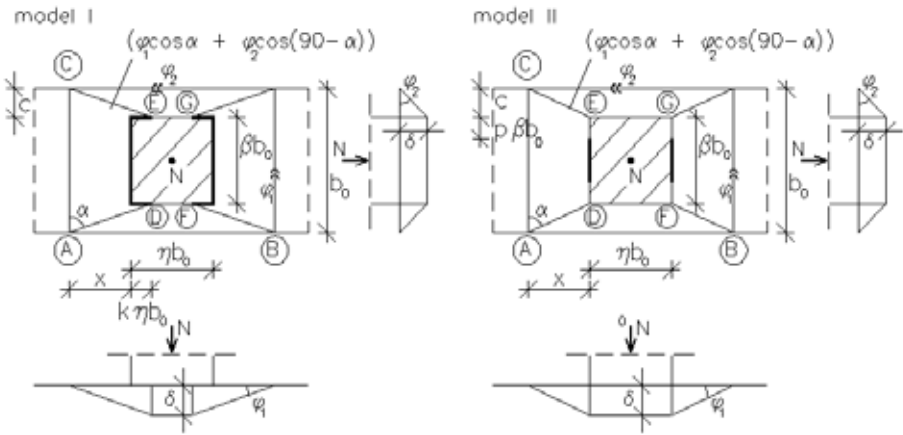


Fig. 3. One & double side yield line model of T THS joint plastic failure.

The energy of external force N:

$$Z = N \cdot \delta \quad (1)$$

Non-welded joints -upper wall of chord [only Model I]

From geometry of mechanism occurs:

$$AD = \sqrt{(x + k\eta b_0)^2 + c^2}; \quad c = \left(\frac{1-\beta}{2}\right)b_0; \quad \varphi_1 = \frac{\delta}{x + k\eta b_0}; \quad \varphi_2 = \frac{\delta}{c}$$

The energy dissipated in the yield lines is as follows, [3]:

$$D = \sum D_{ij} = \left[4\eta b_0 \cdot (1-2k) \cdot \frac{\delta}{c} + 8 \cdot (x + k\eta b_0) \cdot \frac{\delta}{c} + 2 \cdot (b_0 + 2c) \cdot \frac{\delta}{x + k\eta b_0} \right] \cdot m_{pl} \quad (2)$$

After assumption that a shape of the laser cut hole on the face of chord is constant the coefficient $k = \text{const}$. When and because (1) could be equal to (2) so

$$\frac{N}{m_{pl}} = 4\eta b_0 \cdot (1 - 2k) \cdot \frac{1}{c} + 8 \cdot z \cdot \frac{1}{c} + 2 \cdot (b_0 + 2c) \cdot \frac{1}{z} \quad (3)$$

For the minimum

$$\frac{\partial N}{\partial z} = 0 = 0 + 8 \cdot \frac{1}{c} - \frac{2}{z^2} \cdot (b_0 + 2c) \left| \cdot \frac{cz^2}{8} \right. \quad (4)$$

$$z^2 = \frac{c(b_0 + 2c)}{4} \quad (5)$$

Because and after substituting value of c :

$$x + k\eta b_0 = \frac{b_0}{2} \sqrt{10 \frac{3}{2} \beta + \frac{\beta^2}{2}} \Rightarrow x = \frac{b_0}{2} \sqrt{10 \frac{3}{2} \beta + \frac{\beta^2}{2}} - k\eta b_0 \quad (6)$$

Finally, when values x , c and m_{pl} are given, formula (3) is given as:

$$N = f_0 \cdot t_0^2 \cdot \left[\frac{2 \cdot \eta \cdot (1 - 2k) + 2 \cdot \sqrt{1 - \frac{3}{2} \beta + \frac{\beta^2}{2}}}{1 - \beta} + \frac{2 - \beta}{\sqrt{1 - \frac{3}{2} \beta + \frac{\beta^2}{2}}} \right] \quad (7)$$

Non-welded joints-bottom wall chord [only Model II]

From geometry of mechanism occurs:

$$AD = \sqrt{x^2 + c^2}; \quad c = \left(\frac{1 - \beta}{2} \right) b_0; \quad \varphi_1 = \frac{\delta}{x}; \quad \varphi_2 = \frac{\delta}{c}$$

The energy dissipated in the yield lines is as follows, [3]:

$$D = \sum D_{ij} = \left[4\eta b_0 \cdot \frac{\delta}{c} + 8 \cdot \frac{\delta x}{c} + 2 \cdot b_0 (1 + 2p\beta) \cdot \frac{\delta}{x} + 4 \cdot \frac{c}{x} \right] \cdot m_{pl} \quad (8)$$

After assumption that a shape of the laser cut hole on the face of chord is constant the coefficient $k = \text{const}$ and because (1) could be equal to (8) so:

$$\frac{N}{m_{pl}} = 4\eta b_0 \cdot \frac{1}{c} + 8 \cdot \frac{x}{c} + 2 \cdot b_0 (1 + 2p\beta) \cdot \frac{1}{x} + 4 \cdot \frac{c}{x} \quad (9)$$

For the minimum

$$\frac{\partial N}{\partial z} = 0 = 0 + 8 \cdot \frac{1}{c} - 2 \cdot b_0 \cdot (1 - 2p\beta) \frac{1}{x^2} - 4 \cdot \frac{c}{x^2} \left| \cdot \frac{cx^2}{8} \right. \quad (10)$$

After substituting value of c:

$$\ddot{u} = \frac{b_0}{\ddot{u}} \sqrt{1 - \beta \left(-\frac{3}{2} \right) + \beta^2 \left(-\frac{1}{2} \right)} \quad (11)$$

Finally, when values x, c and m_{pl} are given, formula (9) is given as:

$$N = f_0 \cdot t_0^2 \cdot \left[\frac{\eta + \sqrt{1 - \beta \left(p - \frac{3}{2} \right) + \beta^2 \left(p - \frac{1}{2} \right)}}{1 - \beta} + \frac{2 + 2p\beta - \beta}{\sqrt{1 - \beta \left(p - \frac{3}{2} \right) + \beta^2 \left(p - \frac{1}{2} \right)}} \right] \quad (12)$$

Non-welded joints-the upper and bottom wall of chord work [Model I + Model II]

To compute the carrying capacity of the joint with the upper and bottom wall of chord work you should add up calculations for the bottom and top chord.

Final formula (7+12):

$$N = f_0 \cdot t_0^2 \cdot \left[\frac{2 \cdot \eta \cdot (1 - 2k) + 2 \cdot \sqrt{1 - \frac{3}{2}\beta + \frac{\beta^2}{2}}}{1 - \beta} + \frac{2 - \beta}{\sqrt{1 - \frac{3}{2}\beta + \frac{\beta^2}{2}}} \right] + f_0 \cdot t_0^2 \cdot \left[\frac{\eta + \sqrt{1 - \beta \left(p - \frac{3}{2} \right) + \beta^2 \left(p - \frac{1}{2} \right)}}{1 - \beta} + \frac{2 + 2p\beta - \beta}{\sqrt{1 - \beta \left(p - \frac{3}{2} \right) + \beta^2 \left(p - \frac{1}{2} \right)}} \right] \quad (13)$$

The experimental joints “plug&play” type T

Eleven T RHS laser made joints in natural scale were tested here up to failure. Three of them have been one side joints, where only face wall of RHS chord has been loaded - WTL (i), the remaining eight joints utilized top and bottom wall of chord of T RHS to carry the force - WT2L (i). In several steps the branch was loaded up to reach the failure load. After each loading step, the joint was unloaded to measure the permanent deformations of the tested specimen. Typical joint failure was the inelastic deformation of the loaded top & bottom flange of chord. LVDT gauges were used to measure the displacements. Registrations of the results were made permanently during the full loading and unloading process, up to failure. In Table 1 and 2 the geometric parameters were showed along with the mechanical features of investigated joints.

Tab.1. Geometrical dimensions and mechanical properties WTL joints

Geometrical dimensions					Yield stress	Parameters		
No specimen	Profile RHS chord $b_o \times h_o$	RHS branch $b_n \times h_n$	Chord wall thickness t_o	Branch wall thickness t_n	Chord f_{y0}	β	η	$\lambda_o = b_o/t_o$
	mm	mm	mm	mm	MPa			
WTL1	100x100	40x40	3,0	3,0	334	0,40	0,40	33,3
WTL2	100x100	60x60	3,0	3,0	343	0,60	0,60	33,3
WTL3	100x100	80x80	3,0	3,0	335	0,80	0,80	33,3

Tab.2. Geometrical dimensions and mechanical properties WT2L joints

Geometrical dimensions					Yield stress	Parameters		
No specimen	Profile RHS chord $b_o \times h_o$	RHS branch $b_n \times h_n$	Chord wall thickness t_o	Branch wall thickness t_n	Chord f_{y0}	b	h	$\lambda_o = b_o/t_o$
	mm	mm	mm	mm	MPa			
WT2L1	100x100	40x40	3.0	3.0	335	0.40	0.40	33.3
WT2L2	100x100	60x60	3.0	3.0	335	0.60	0.60	33.3
WT2L3	100x100	80x80	3.0	3.0	335	0.80	0.80	33.3
WT2L4	100x100	40x40	4.0	3.0	335	0.40	0.40	25.0
WT2L5	100x100	60x60	4.0	3.0	335	0.60	0.60	25.0
WT2L6	100x100	80x80	4.0	3.0	335	0.80	0.80	25.0
WT2L7	100x100	40x40	5.0	3.0	335	0.40	0.40	20.0
WT2L8	100x100	60x60	5.0	3.0	335	0.60	0.60	20.0

where:

b_o, h_o, t_o - width, height, thickness wall of chord

b_n, h_n, t_n - width, height, thickness wall of RHS branch

f_{y0} - yield stress chord

$\beta = b_n/b_o, \eta = h_n/b_o$ - dimensionless width, height of RHS branch

$\lambda_o = b_o/t_o$ - slenderness wall of chord.

Numerical model of “plug & play” type T joints

The numerical model mapped the load method used during experimental studies. Nets with a mesh size of 16mm were used in secondary zones, and in the areas with a threat of maximum deformation the grid was concentrated to 4mm. The model uses finite element of ‘tetrahedrons’ type with the intermediate joints. The backlash offset (0.3 mm), inaccuracies in the production of steel profiles, (including stitches on RHS) were not included.

Using the dual symmetry the joint quadrant was modeled. In the computation model carried in ANSYS system, base of RHS branch- modeld as one-way contact of preasure force (without extension), additionallyin some joints used offset size 0,05mm to included imperfections production specimen.

This computation model to a large extent reflects the real work of a joint, assuming reasonable time of numerical calculations.

Results and numerical calculations for the T RHS joints

To compute joints carrying capacity with the work of the upper and bottom wall of chords we have to add up.

Tab.3. Theoretical and experimental resistance of joints WTL(i)

Specimen No	Theoretical resistance (7+12)* N_{teo} [kN]	Experimental resistance (elastic) N_{exp} [kN]	MES software resistance (elastic) N_{num} [kN]	N_{teo} / N_{exp}
WTL1	15,88	10,03	21,18	1,58
WTL2	20,96	18,01	31,49	1,16
WTL3	32,94	28,01	35,31	1,18

*Theoretical resistance has been calculated from formula (7) for joints, where parameter $k=0.25$, $p=0.25$ was used.

Tab.4. Theoretical, experimental and analytical resistance of joints WT2L(i)

Specimen No	Theoretical resistance (7+12)* N_{teo} [kN]	Experimental resistance (elastic) N_{exp} [kN]	MES software resistance (elastic) N_{num} [kN]	N_{teo} / N_{exp}	N_{num} / N_{exp}
WT2L1	34.7	30	25	1.16	0.83
WT2L2	48.7	37.4	37.4	1.30	1.00
WT2L3	82.7	64	64	1.29	1.00
WT2L4	61.8	45	45	1.37	1.00
WT2L5	86.5	70	70	1.24	1.00
WT2L6	146.9	110	93	1.34	0.85
WT2L7	96.5	75	75	1.29	1.00
WT2L8	135.2	112	96	1.21	0.86

*Theoretical resistance has been calculated from formula (7+12) for joints, where parameter $k=0.25$, $p=0.25$ was used.

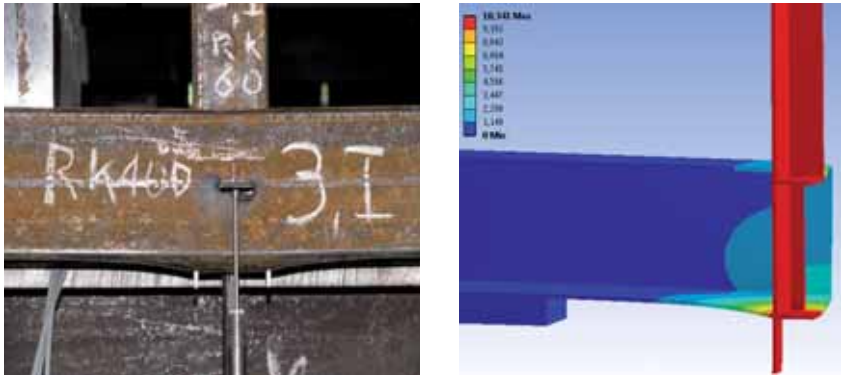


Fig. 4. Joint WT2L2 ($\beta=0,6$) during test with numerical model



Fig. 5. Joint WT2L4 after test (detail of face wall failure in right corner).

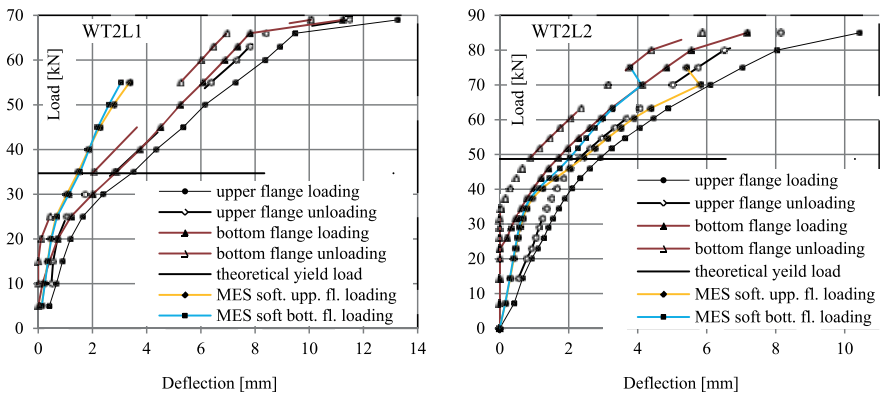


Fig. 6. Load-deflection diagram for joint WT2L1 ($\beta=0,4$) & WT2L2 ($\beta=0,6$)

N-type joints

In the N type joints two forces are involved, compressive force that influences the branch and the tensile force carried by the diagonal strut. Non-welded the N type joints plug & play connections work only by pressure and shear contact of key parts (grid) and lock (the hole in the chord truss).

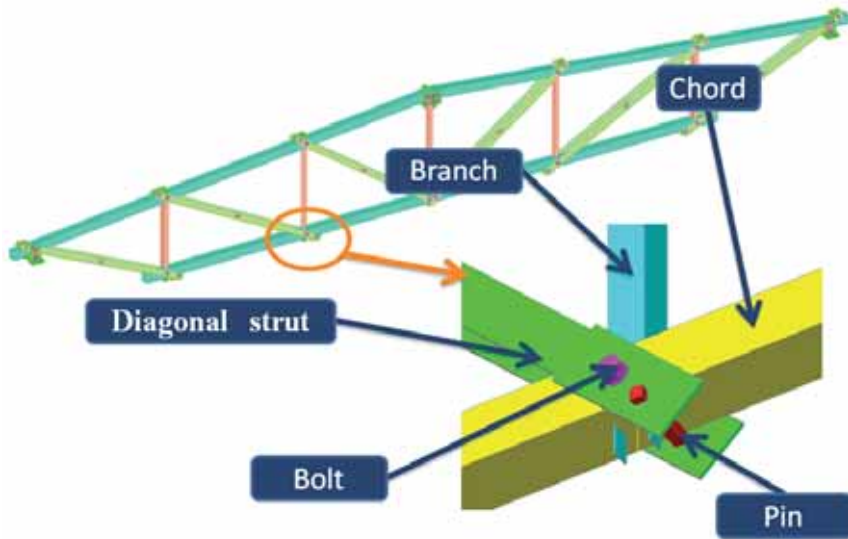


Fig. 7. View one selected joint (with pin) type N from non-welded truss.

In order to transfer the load of the internal forces in the chord of truss the “lock” (slot) is made, which allows the insertion of a “key” branch. Dual diagonal strut (it is possible to use plates, L-shapes or C-shapes) comprising the chord, is attached to the chord via a pin inserted through the openings in the rods of the diagonal strut and side walls of the chord. Diagram of the grid and N type joints are shown in Figure 6. Chord and branch are made of RHS. As diagonal strut used plate, which include mutually chord, in the middle of the dual diagonal strut we put C-shape profile to reduce buckling. Because in extended diagonal strut are considerable forces, which contribute to the ovalisation hole of RHS chord in fast way, additionally introduced stiffening pin. This pin to a large degree limit ovalisation hole in side walls of the chord, cause pin carries part of load from the bolt to walls. The connection of this type eliminates the need to use seams in the joint. In previous publications and in the last chapter the results of experimental and theoretical estimation of carrying capacity of T RHS truss joints, made in non-welded technology, in the form of plug & play (Szlednak, Oponowicz 2011) were presented. The theoretical carrying capacity calculated using the yield line model was compared to the experimental studies (Szlednak, Oponowicz 2013).

The experimental joints “plug & play” N

The study was carried out at the Technical University of Białystok in 2009-2012 under a grant PR/WBiIŚ/1/09/NCBR on designed for this purpose bench.

Eight joints of N-type grid of a natural scale were tested. Two selected joints of the chord thickness 3.0 mm (WTLN5 and WTLN6) were selected. For those numerical models were developed. In Table 5 the joints geometry and mechanical properties of the steel are shown.

Tab.5. Geometrical dimensions and mechanical properties of joints

Geometrical dimensions RHS members					Yield stress	Parameters		
No specimen	Chord b_o, h_o mm	Branch b_n, h_n mm	Chord wall thick t_o mm	Branch wall thick t_n mm	Chord f_{y0} MPa	β	η	$\lambda_o = b_o/t_o$
WTLN5	100x100	60x60	3.0	3.0	335	0.60	0.60	33.3
WTLN6	100x100	40x40	3.0	3.0	335	0.40	0.40	33.3

where:

b_o, h_o, t_o - width, height, thickness wall of chord

b_n, h_n, t_n - width, height, thickness wall of RHS branch

f_{y0} - yield stress chord

$\beta = b_n/b_o, \eta = h_n/b_o$ - dimensionless width, height of RHS branch

$\lambda_o = b_o/t_o$ - slenderness wall of chord .

A numerical model for “plug & play” type N joints.

The numerical model mapped the load method used during experimental studies. Nets with a mesh size of 20mm were used in secondary zones, and in the areas with a threat of maximum deformation the grid was concentrated to 5mm. The model uses finite element of “tetrahedrons” type with the intermediate joints. The backlash offset (0.3 mm), inaccuracies in the production of steel profiles, (including stitches on pipes) were not included. Using the symmetry the joint half was modeled.

In the computation model carried in ANSYS system the following assumptions were made:

- branch base on walls of chord- one-way contact of preasure force (no extension), additionally in some joints used offset size 0,05mm to included imperfections production specimen was modeled
- contact between the diagonal strut and the chord- only one-way contact of pressure force (no extension) was modeled
- contact between the screw (bolt) and the chord- only one-way contact of pressure force (no extension) was modeled
- contact between the screw (bolt) and the diagonal strut - only one-way contact of pressure force (no extension) was modeled
- contact between the pin and the bottom wall of chord - modeled as a frictional contact with a coefficient of 0.3

- contact between the diagonal strut and the nut - modeled as a frictional contact with a coefficient of 0.3
- contact between the diagonal strut and the pin - modeled as a frictional contact with a coefficient of 0.3

This computation model to a large extent reflects the real work of a joint, assuming reasonable time of numerical calculations.

Results and numerical calculations for the N type joints

For the graphs following abbreviation were used: PD -bottom chord, PG-top chord;

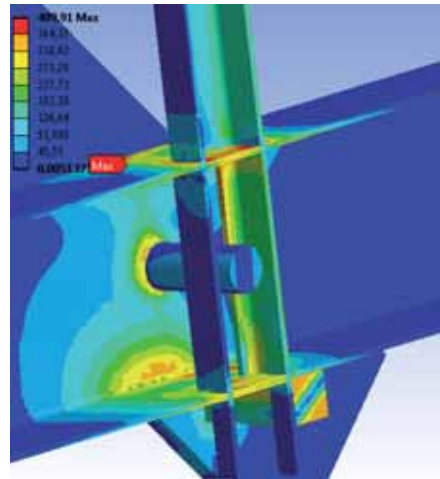
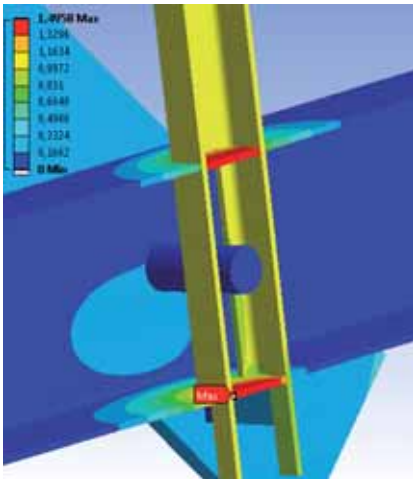
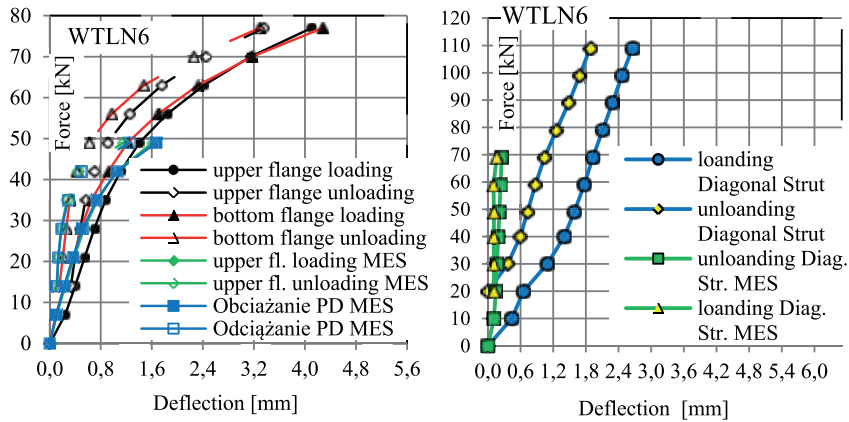


Fig. 8. Charts force – displacement of the WTLN 6 joint (beta = 0.4) respectively: branch, diagonal strut and deformation and stress for the WTLN 6 joint (beta = 0.4)

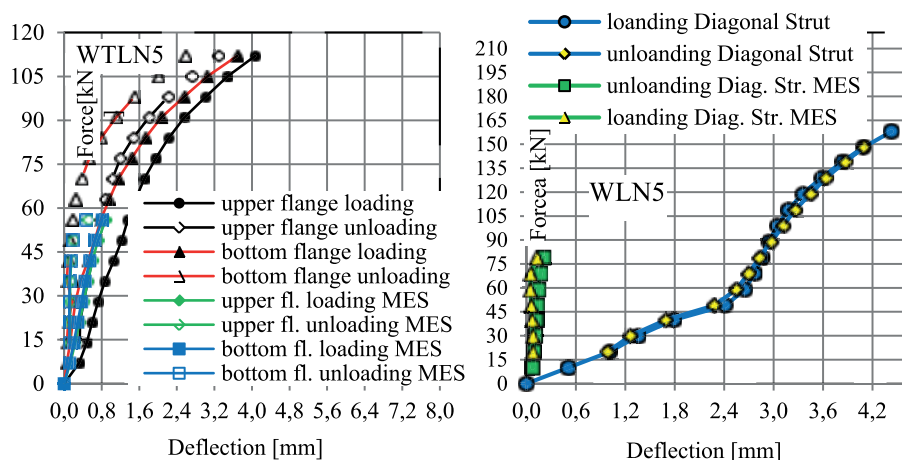


Fig. 9. Charts force - displacement WTLN 5 joint ($\beta = 0.6$), respectively: branch, diagonal strut

The results with the numerical analysis for the rest of the N type joints (with different thicknesses) are currently being developed and will be presented at a scientific conference Krynica 2013 (Szlendak, Oponowicz 2013)

References:

1. Bródka J., Broniewicz M. (2001), *Tubular steel structures*. Arkady, Warsaw (in Polish).
2. EN 1993-1-8:2006, Eurocode 3 (2006), Design of Steel Structures *Part 1-8: Design of Joints*.
3. Oponowicz P.L. (2011), Nośność węzłów typu T z rur prostokątnych obciążonych siłą normalną w formie klucz-zamek niewymagających spawania, *Badania i analiza wybranych zagadnień z budownictwa*, Wydawnictwo Politechniki Śląskiej, Gliwice, s. 339-347.
4. Szlendak J. K. (2007), Design models of beam-column welded joints in steel structures made with rectangular hollow sections. „*Rozprawy Naukowe*” nr 148, *Politechnika Białostocka*, Białystok, s. 1-212 (in Polish).
5. Szlendak J.K. (2009-2012), Kratownice i ramownice stalowe o węzłach kształtowanych laserowo w formie klucz-zamek nie wymagających spawania. Grant NCBR N R04 0008 06, *Politechnika Białostocka*.
6. Szlendak J.K., P.L. Oponowicz P.L. (2011), Behaviour of one and double side non-welded T RHS compression truss joints, 7th International Conference on Steel & Aluminium Structures, Kuching, Sarawak, Malaysia, 13th –15th July 2011.

7. Szlendak J.K., P.L. Oponowicz P.L. (2013), Experimental tests and numerical models of one and double side non-welded T RHS truss joints, 11th International Conference "Modern Building Materials, Structures and Technique, Vilnius, 16-17 May 2013.
8. Szlendak J.K., P.L. Oponowicz P.L. (2013), Nośność węzłów kratownicowych typu N z rur prostokątnych o połączeniach w formie klucz-zamek, Krynica, 15-20 Wrzesień 2013
9. Wardnier J., Packer J.A., X.-L. Zhao van der Vegte G.J. (2010), Hollow sections in structural applications CIDECT

NUMERICAL PREDICTION OF WAVE REACTION OF THE LAYERED ELASTIC HALF-SPACE

¹Grzegorz Bąk, ²Wojciech Gosk

¹Military University of Technology

²Białystok University of Technology, Faculty of Civil and Environmental Engineering,
Institute of Geotechnics, Wiejska Street 45E, 15-351 Białystok, Poland
e-mail: w.gosk@pb.edu.pl

Summary:

This paper presents the results of numerical analysis obtained for layered elastic half-space loaded dynamically. The main problem was to study the dynamic response of the medium in conditions of multiple reflections and refractions of waves on the borders of layers.

The subject of this study was the dynamic behaviour of heterogeneous, isotropic, horizontally – layered, elastic half-space. The numerical calculations program included variations of the foundation. The foundation was composed of two layers, wherein the first layer's thickness was 2, 4 or 6 m. Wave propagation modelling was performed using the method of finite differences.

The decline of the amplitude of vertical vibrations along with the distance in uniform media generally is supported by the standardized prediction. The standardized prediction for the decline of amplitudes of the horizontal vibration along with the distance may lead to understating. Local fading and strengthening of amplitude of vertical and horizontal displacements occur. This effect should not necessarily be connected with ground medium stratification, even though such effects in case of stratified medium have increased. If a vulnerable layer is on top of the rigid one, larger amplitude of vertical displacement is obtained at the surface rather than in a uniform, weak medium. In the case of inverse layout of the layers, i.e. if the rigid layer is lying on top of a thick, vulnerable layer, the amplitude of vertical displacements on the surface are smaller compared to the amplitude obtained in a uniform, rigid medium.

Keywords: wave mechanics, vibrations, layered ground medium

Introduction

Determination of dynamic influences, which may affect a construction designed in the vicinity of the source of vibration, requires forecasting of wave propagation in the ground medium. Prediction can be based on a theoretical analysis, experimental studies or by using models that estimate the amplitude of vibration that may occur at the location of the object. Unquestionably the greatest confidence should be put in the results of experimental studies. The correctness of the theoretical predictions depends on simplifying assumptions about the geometric and physical modelling of the ground medium, as well as on the accuracy of the methods used, which almost always are numeric or numerical - analytical. Ready analytical formulas should be taken with some caution due to their unspecified conditions of accuracy and limitations of the scope of applicability. Formulas for estimating the amplitudes of vertical and horizontal

displacements are discussed in the monograph by (Lipinski 1985). One of them is called Barkan curves. They were verified by experiments widely recounted in the work of (Ciesielski et alia (1996, 1997, 1999, Kwiecien 1997). They are also used in the standard PN-80/B-03040.

This paper presents the results obtained from the numerical analysis carried out for the ground medium treated as an isotropic elastic half-space with the heterogeneity of the layer type. Stratification is a natural feature of the ground medium and the corresponding geometric schematization model creates a heterogeneous medium. The medium layers may be positioned horizontally or tilted down, be in regular arrangements, or be folded in varying degrees. The so called „wedging” of the layers has also been observed. The occurrence of ground water also requires a separation of different geotechnical layers in the ground. In addition, a significant problem is the modelling of the building structure in terms of its interaction with the subsoil (example diagram in Figure 1). It is important here to apply appropriate contact zone at the interface between two media with significantly different mechanical properties. The elements of this interaction, however, are not the subject of analysis presented in the work.

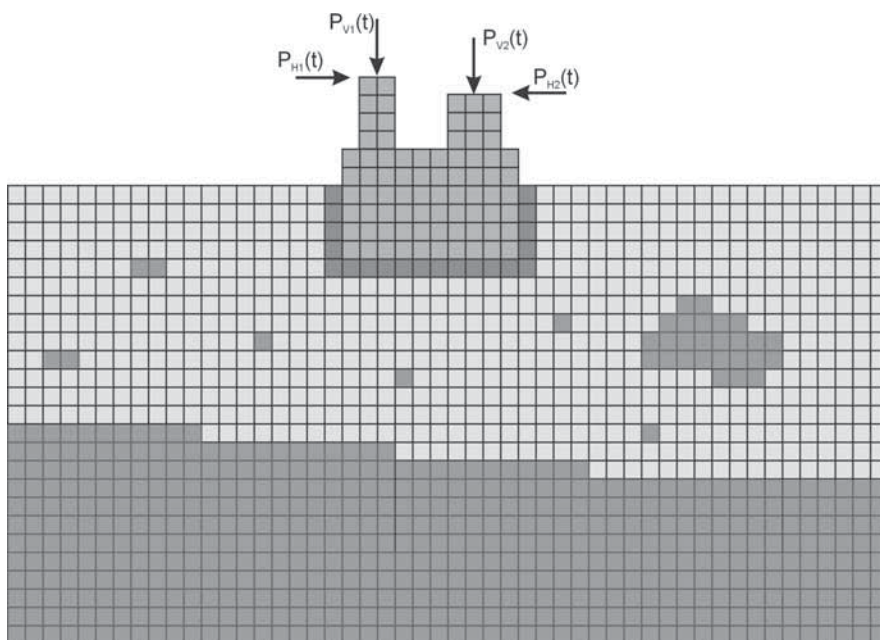


Fig. 1. Block foundation in diversified ground (cross section of spatial task)

Inclusion of stratification in geometric modelling of ground medium allows for a theoretical approach to characteristic effects of reflection and refraction of stress waves at the border of layers, testing whether any of the layers does not become a waveguide. These effects cause the instantaneous stress distributions to become highly unstable and significantly alter the stress – deflection response of the layered medium in relation to the uniform medium.

The results presented in the paper were discussed at the 2nd Geotechnical Conference “Soil-Structure Interaction”, Białystok - Białowieża 2004 (Bąk, Gosk 2004). Extended analysis based on that work are presented in this article.

Assumptions and basics of numerical analysis

The subject of this study was the dynamic behaviour of heterogeneous, isotropic, horizontally – layered, elastic half-space. The analysis covered a quarter of the half-space, which was approximated by a cuboids’ area of a considerable size: $L_x = L_y = 100$ m, $L_z = 50$ m and the vertical planes of symmetry $(x, 0, z)$, $(0, y, z)$. The planes separating the area out of half-space included supports „transmitting” both, longitudinal and transverse waves. Also, harmonic, uniformly distributed load acting on a limited area of a rectangle with dimensions l_x and l_y , located as coordinates: $(\langle 0, l_x \rangle, \langle 0, l_y \rangle, z = 0)$ was taken into consideration. Numerical analysis was carried out on the basis of author’s own calculation program which uses a differential algorithm proposed in a book by (Szczesniak 1999) for the spatial task of wave mechanics. This algorithm can automatically model the effects of multiple reflections and refractions of stress waves. There is no need of a separate tracking of forming of wave fronts. In the case of one-dimensional spatial tasks an error-free approximation of the problem of reflection and refraction of waves can be achieved, as in (Bak, Szczesniak, 1987).

Numerical analysis program

The numerical calculations program included variations of the foundation. Homogeneous areas and horizontally layered areas were studied. The foundation was composed of two layers, wherein the first layer’s thickness was 2, 4 or 6 m. Analyzed variants of stratification are shown in Figure 2. The material constants reflect the dynamic characteristics of the soil. Applying harmonic load acting on a limited area of the medium is being considered.

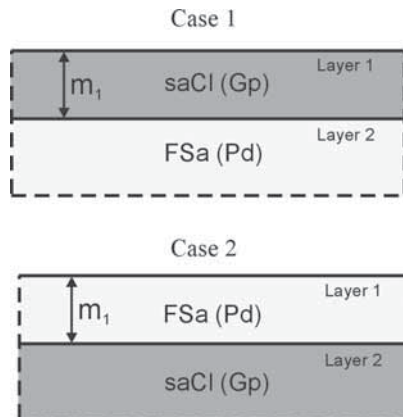


Fig. 2. Analysed ground variants

Sandy clay – saCl (Gp):

$$\rho = 2050 \text{ kg/m}^3 \quad E = 320 \text{ MPa} \quad \nu = 0.30 \quad a_1 = 458 \frac{\text{m}}{\text{s}} \quad a_2 = 245 \frac{\text{m}}{\text{s}}$$

Fine sand – FSa (Pd):

$$\rho = 1800 \text{ kg/m}^3 \quad E = 120 \text{ MPa} \quad \nu = 0.25 \quad a_1 = 283 \frac{\text{m}}{\text{s}} \quad a_2 = 163 \frac{\text{m}}{\text{s}}$$

$$m_1 = 2 \text{ m} \quad m_1 = 4 \text{ m} \quad m_1 = 6 \text{ m}$$

Studying of effects of reflections and refractions on the borders of layers

In general, in the case of the effects of reflection and refraction of a monochrome wave - angles, the amplitudes of the waves and shearing can be designated as an extended solution of algebraic equations. This system is created by the conditions for compatibility of displacements and stresses on the boundary of layers and Snell's law. In the case of a plane wave of amplitude A , incident perpendicularly to the plane of the boundary layers of a medium with varying impedance ($\rho_1 \neq \rho_2$), and according to the work edited by (Kaliski 1966) the following results obtained:

$$A_0 = \frac{(\rho)_2 - (\rho)_1}{(\rho)_1 + (\rho)_2} A, \quad A_z = \frac{2(\rho)_1}{(\rho)_1 + (\rho)_2} A \quad (1)$$

The correctness of numerical analyses of the effects of reflection and refraction of a plane wave with a strong discontinuity at the front, was verified by authors - developed calculation program. The results for both cases of stratification of the ground are shown in Figure 3.

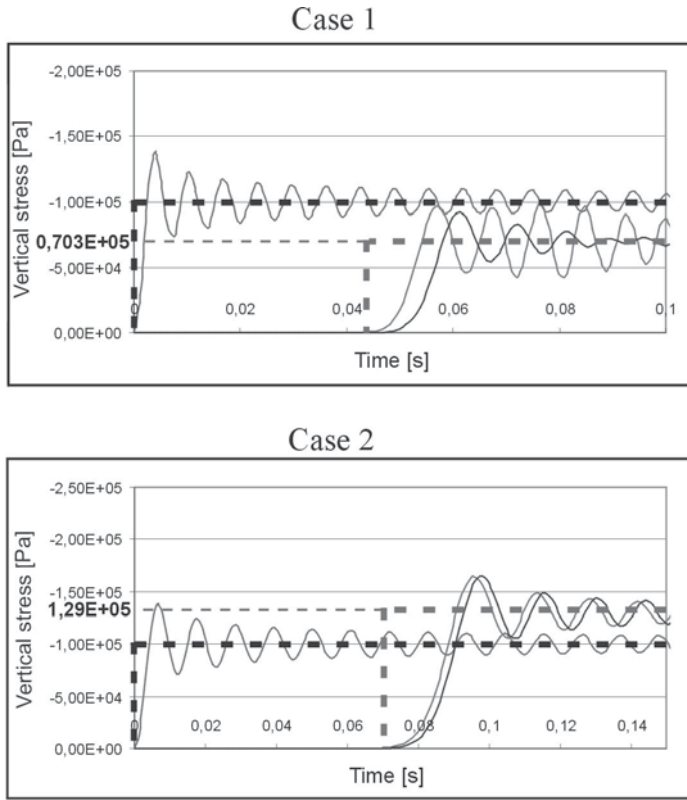


Fig. 3. Comparison of numerical results and theoretical solution

They are generally consistent with the theoretical prediction (1). A strong front of the stress wave, however, “vanishes in time”, because of its inability to meet the condition of an error-free differential approximation.

Selected results of numerical analysis

The following are some of the results of the numerical analyses of the stratified and uniform ground displacement amplitudes.

Figures 4 and 5 show the boundaries of vertical and horizontal displacements on the surface of the ground with different stratification, but in the system: the upper layer, vulnerable – FSa (Pd) - lower, rigid – saCl (Gp). Highlighted, solid line matches the estimate of the amplitude of vibration with distance according to PN-80/B-03040. It is confirmed that it is correct in the uniform medium. Decline of amplitudes in layered media is monotonic. Another quantitative conclusion, constituting a direct consequence of the effects of reflection and refraction, is that the rigid, bottom layer of the foundation – saCl (Gp), increases the value of the amplitude, which is a result opposite to the experience from the static effects.

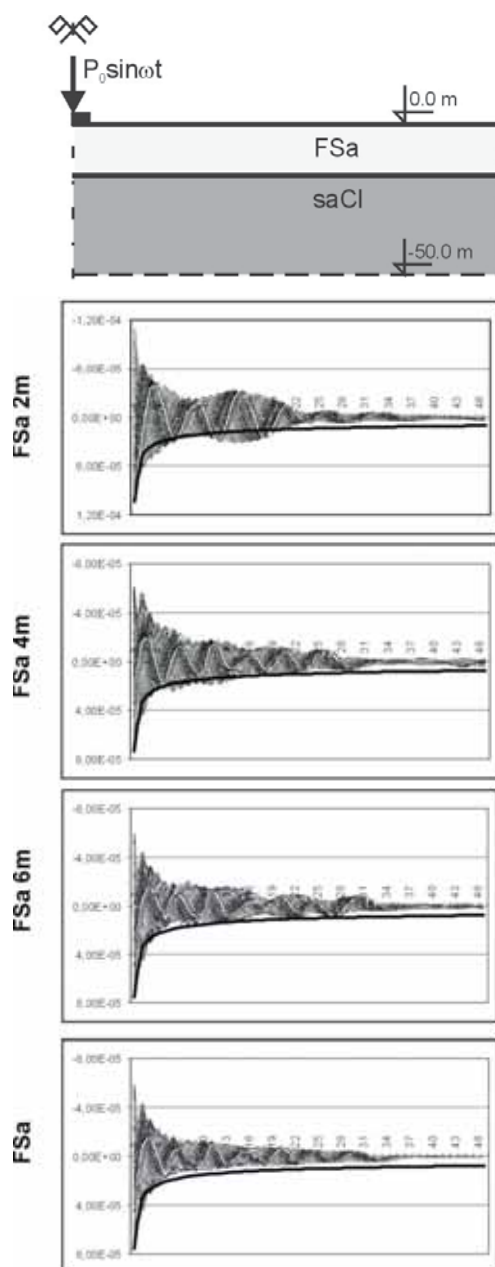


Fig.4. Vertical displacements boundaries [m] on the ground surface for various layers of ground medium
($n = 30\text{Hz}$, thick line – prediction in accordance with the norm: PN-80/B-03040)

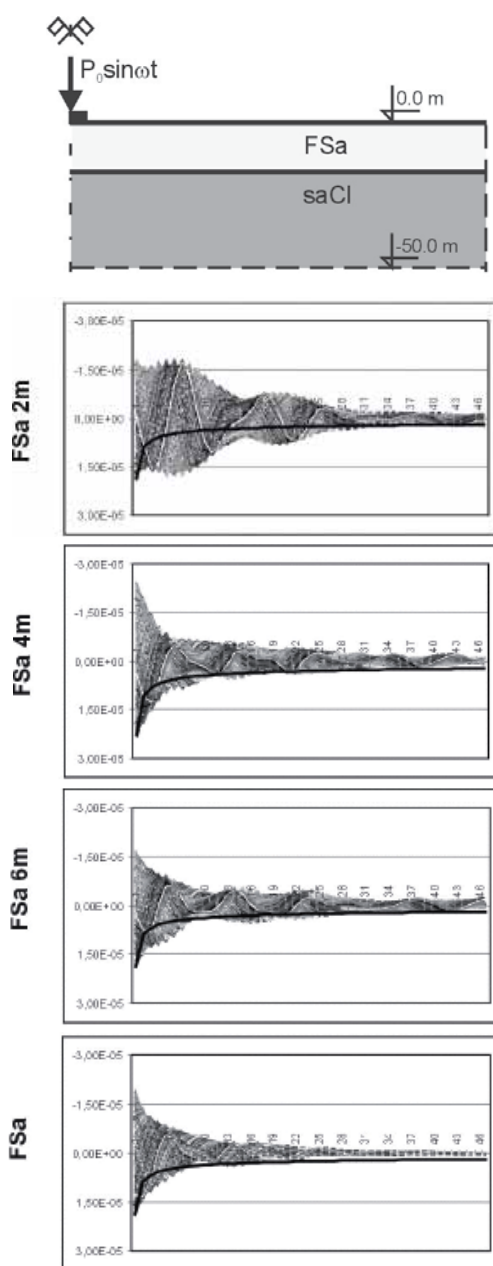


Fig.5. Horizontal displacements boundaries [m] on the ground surface for various layers of ground medium
($n = 30\text{Hz}$, thick line – prediction in accordance with the norm: PN-80/B-03040)

Figure 6 shows the boundaries of horizontal displacement along the depth set out in points distant from the source by 12.5 m. Appropriate prediction of amplitude decline of these oscillations, which are considered as a result of the dominance of Rayleigh waves in deforming reaction of subsurface zone of the medium, taken from the work by (Lipinski 1985), can be represented as follows:

$$A_H(z) = A_H(0) e^{-\frac{2\pi z}{\lambda} \beta}, \quad (2)$$

and: z - ordinate along the depth, λ - wavelength, β - a correction factor introduced for the purposes of satisfying comparisons made in this study, see Figure 6. The research recounted in the work by (Ciesielski et al 1997) showed that β should also cover the impact of dynamic load frequency.

Formula (2) proves that it can be observed that the correct prediction of decline of horizontal vibrations is only possible in subsurface ground medium, i.e. in the depth of shallow foundations. In the case of deep foundations one must take into consideration extremely different values of the amplitudes of horizontal displacement, which is a forced kinematic displacement of the erected object.

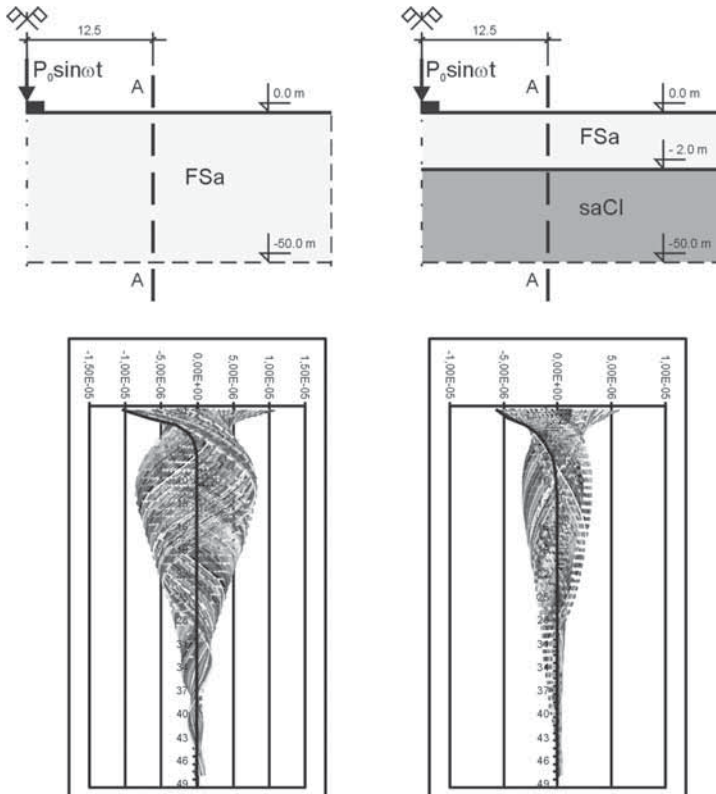


Fig.6. Influence of layered structure of the medium on horizontal displacements in central point of external impacts activity ($n = 10\text{Hz}$, thick line –Barkan's prediction)

Shapes of maximum amplitudes of horizontal boundaries indicate that the range of relatively extensive horizontal vibration along the depth is significant, even in a uniform medium. It is not, however, in agreement with the conclusion relating to fast decline and depth of these vibrations. These conclusions are generally formulated on the basis of Rayleigh solution applied to a single wave. Only the prediction relating to the occurrence of a significant weakening of these vibrations right under the ground surface is applicable. However, at greater depths strong reinforcement covering a large area occurs. The rigid layer – saCl (Gp) under a vulnerable layer – FSa (Pd), significantly reduces the amplitude of horizontal displacement.

Conclusions

From the presented numerical results the following conclusions can be drawn:

- The decline of the amplitude of vertical vibrations along with the distance in uniform media generally is supported by the standardized prediction.
- The standardized prediction for the decline of amplitudes of the horizontal vibration along with the distance may lead to understating.
- Local fading and strengthening of amplitude of vertical and horizontal displacements occur. This effect should not necessarily be connected with ground medium stratification, even though such effects in case of stratified medium have increased.
- If a vulnerable layer is on top of the rigid one, larger amplitude of vertical displacement is obtained at the surface rather than in a uniform, weak medium - the effect of a weak layer being intensively compressed by stress interfering waves, incident and reflected. This was clearly observed in case of the FSa (Pd) layer with a thickness of 2 m.
- In the case of inverse layout of the layers, i.e. if the rigid layer is lying on top of a thick, vulnerable layer, the amplitude of vertical displacements on the surface are smaller compared to the amplitude obtained in a uniform, rigid medium - reflection effect - the amplitude of the reflected wave is negative, $(1)_1$.

This article was created as part of statutory study conducted at the Faculty of Civil and Environmental Engineering of Białystok University of Technology

References:

1. Bąk G., Gosk W. (2004), Numerical forecast of the wave response of the layered halfspace. *Proceedings of the 2nd Geotechnical Conference "Soil-Structure Interaction"*, Białystok - Białowieża 2004, 1, p. 13-22 (in Polish).
2. Bąk G., Szcześniak Z. (1987), The method of discrete one-dimensional modelling of wave processes in elastic, non-prismatic layered bars. *Engineering Transactions*. No 35, 2, p. 309-325 (in Polish).
3. Ciesielski R., Kwiecień A., Stypuła K. (1996), Experimental attempt to determine the course of changes in vibration propagation in subsurface layers of the site. *Research Bulletins of Rzeszow University of Technology, Mechanics*, issue 48, Problems construction dynamics, vol. III, Rzeszów, pgs. 153-164 (In Polish).

4. Ciesielski R., Kwiecień A., Stypuła K. (1997), The possibility of supplementing Barkan curve of the propagation of vibrations near the surface of the earth. Materials at the VIIIth Symposium: "Seismic and paraseismic influences on buildings" Kraków, pgs 133-140 (in Polish).
5. Ciesielski R., Kwiecień A., Stypuła K. (1999), The propagation of vibration in subsurface layers of the ground. The in situ study – the monograph 263, Kraków (in Polish).
6. Lipiński J. (1985), Foundations for machines. Arkady, Warszawa (in Polish).
7. Kaliski S. (1966), Vibrations and waves. PWN, Warszawa (in Polish).
8. Kwiecień A. (1997), Boundaries of harmonic acceleration peaks near the surface of the area. Materials at the VIII Symposium "Seismic and paraseismic influences on buildings" Kraków, pgs. 141-147 (in Polish).
9. Szcześniak Z. (1999), Modelling of the dynamic behaviour of underground structures when subjected to air blast. Military University of Technology Publishing House, Warszawa, 1999 (in Polish).
10. PN-80/B-03040. Machine foundations and supporting structures. Calculation and design (in Polish).

EFFORT ANALYSIS OF STRUCTURAL ELEMENTS OF THE HIGH BUILDING SUBJECTED TO LARGE DISPLACEMENTS

Sandra Matulewicz, Tadeusz Chyży

Białystok University of Technology, Faculty of Civil and Environmental Engineering,
45E, Wiejska Street, 15-351 Białystok, Poland
e-mail: s.matulewicz@pb.edu.

Summary:

The following material was analyzed by structural effort of so much contemporary ubiquitous high-rise buildings. In one of the chapters presents the dynamic development of urban areas and thus increased demand for building high. The team also closer to the „silhouette” of several of the world’s tallest buildings. The next section shows the differences between the most commonly used first-order analysis, and the analysis of the second order. In large buildings, high-impact forces occurring on the structural members has a deflection which occurs under the action of the horizontal external load. The standard design of such buildings is quite adequate analysis of small displacements, while there may be instances such as analysis pokrytyczna where you should take into account the displacement of the load-induced deformation of the structure. The comparative analysis presented in the paper were modeled in the calculation Robot Structural Analysis Profesional high building (Matulewicz, 2012), which was increased horizontal thrust. So pay structure were analyzed by standard methods of calculation available in the form of a linear analysis. The results obtained from these calculations have been compared with the results obtained after analysis of non-linear, which takes into account the effects of P-Δ. Results of the comparison are shown in the following figures article also selected several nodes whose effort was well described in the tables. Based on these results it can be concluded that in some stages of the design work is very important to the application of advanced computational techniques.

Keywords: high building, first order, second order

Introduction

The construction components in the majority of cases are subjected to static analysis of the first order, which is based on the theory of small displacements and does not reflect the actual structural response to an applied external load. In the analysis of the first order, the principle of stiffness is applied, i.e. the undeformed, original geometry of the structure is considered, regardless of the load. In most cases, it is sufficient, as the impact of displacements of the structure on the value of passive forces (the reaction of supports) and internal forces (cross-sectional) is negligibly small. This means that at the calculation of these forces we do not distinguish between the current configuration and the initial one. Whereas, the analysis of the structure responses in advanced stages of work, especially during the phase of its destruction and post-critical phase, as well as in modern high-rise buildings, which in the operation phase also experience large displacements and rotations, requires the use of special finite elements and complex algorithms, including the calculation that take into account the state of large displacements and rotations. This analysis is called second-order analysis. In the theory of structure, the effects of second order are distinguished as:

- P- Δ effects relating to taking into account the shifts of structure nodes in the calculation,
- P- δ effects concerning taking into account bending of rods between nodes in the local calculations.

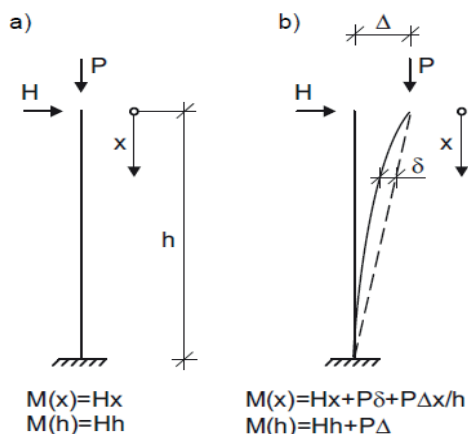


Fig. 1. Static calculations of the support rod: a) of the first order, b) of the second order

Figure 2 shows the cases of a standard solution and the expected (actual) one, which we hope to obtain by using the algorithms of the second-order theory. The beams presented in Figure 1.a) experience large deflections and in 1.b) are shown with the damaged support, which falls off in a gravitational field.

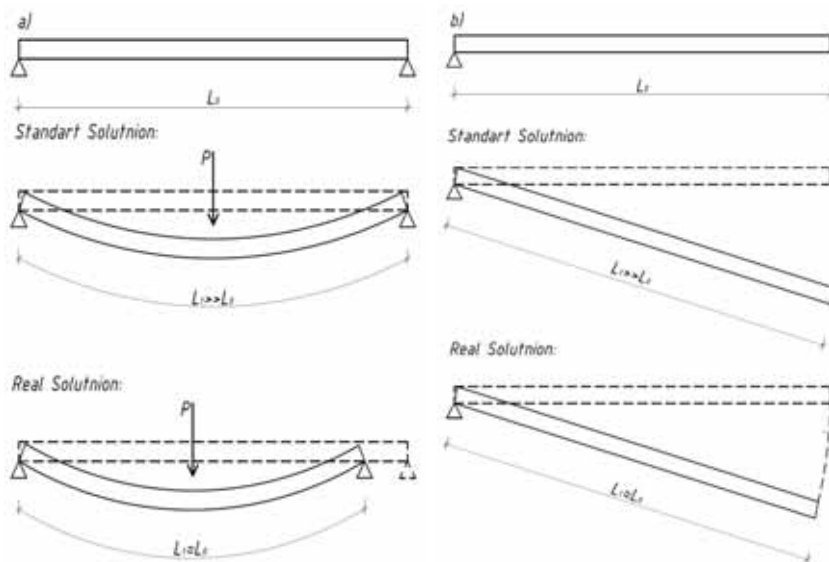


Fig. 2. Standard and real solutions for specific problems

The following material presents an analysis of a high-rise building, experiencing large displacements under the operating load. The analysis was carried out according to the theory of small displacements (first order) what in the computing programs is defined as the linear analysis of a computational model, while trying to take into account the effects of the second order one should use non-linear analysis, as the calculation algorithms require the use of iterative methods for solving the systems of nonlinear equations.

High-rise buildings

The most common structures in the modern times that are exposed to large displacements, e.g. by the action of wind or seismic vibrations are modern high-rise buildings. High-rise buildings are used as offices or residential buildings, thus the operational loads occurring in them are not great. Despite of this, one of the main problems is to maintain adequate stiffness of the system and to protect it from the effects of horizontal loads (from wind pressure and seismic and paraseismic impacts). This stiffness is achieved by an adequate design of the building, the use of vertical and horizontal diaphragms - discs created by walls, shafts, pillars, and ceilings. There are many original solutions to the construction of high-rise buildings, but a monolithic frame with a stiff body should be considered as the most commonly in the corridors and installations.

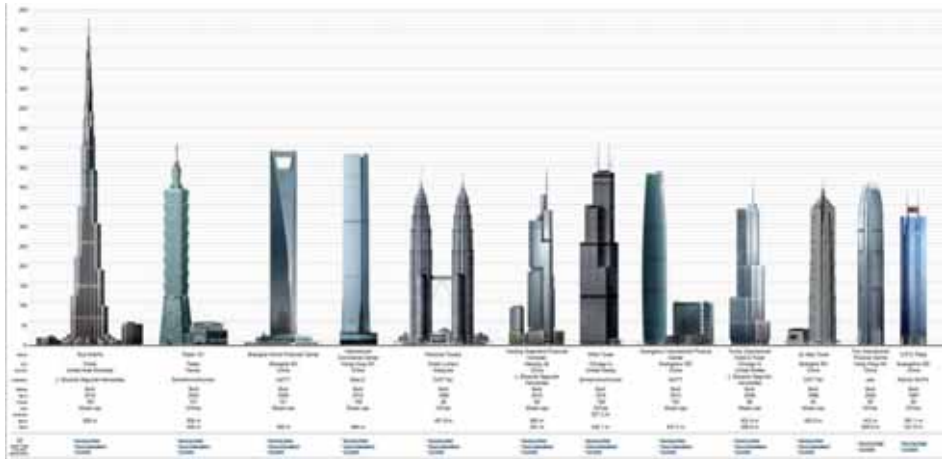


Fig. 2. The classification of the tallest buildings in the world

Examples of high-rise buildings can easily be found in any major city. The highest building in the world is Burj Khalifa located in the United Arab Emirates in Dubai. The building reached a height of 829m and has 163 utility floors. The overall design and plan of the tower refers to the flower of the desert and the architecture of Islam (ornaments, decorations, etc.). The tower consists of a central body and three “arms” - with the increase of the high-rise building the individual “arms” are getting smaller, which gives it slenderness and necessary aerodynamics. At the top, the central core emerges at the spire crowning the building. Second place is given to Abraj Al Bait, situated in Mecca,

Saudi Arabia. This building complex completed in 2012 is as high as 601m. It achieved several world records: it is the highest hotel in the world; there is the highest clock tower here on the planet, which has the largest clock face in the world. The third place is the famous Taipei 101, i.e. the skyscraper with a height of 509.2 meters and 101 floors, located in Taiwan.

It is the first building in the world to exceed the height of half a kilometre. It was opened in 2004 taking the title of the tallest building from Petronas Towers in Kuala Lumpur. The biggest challenge was to secure the Taipei 101 from earthquakes. This was difficult because only 200 meters from the building there is a 10-metre wide tectonic fault. In order to make Taipei 101 withstand earthquakes, the engineers who designed it, designed a powerful structure. The inner core of the building is connected to eight external columns by a horizontal truss network. The columns serve as a backbone of the structure, allowing it to bend as needed, but not break. Each of the sections of the building remains independent of the other, transferring the weight of the building from external structures towards the centre. This idea has been used before, but never before the supporting columns have reached such proportions. The “competition” for the world’s tallest building is still ongoing. Currently, in Saudi Arabia there are preparations for building the Kingdom Tower, the height of which is expected to exceed one kilometre, and in the United Arab Emirates there are plans to build a one mile giant building. The interesting thing is the limit of human capabilities.



Fig. 3. The highest buildings in the world a) Burj Khalifa b) The Empire State Building

Example of calculations

As has already been said, mostly high-rise buildings undergo such states. In order to see how the values of the internal forces are affected by the displacements in the construction of such a building, a computational model of a high-rise building taken from the elaboration (Matulewicz, 2012) was analysed. The analysed facility is a high-rise 36-storey building, 124.44 m high, designed in a monolithic technology with a composite construction consisting of pillars and slabs with a core. In the lower part of the building there are service-office premises, while in the upper part the building becomes narrower as the successive floors contain living quarters. The first floor is a basement located under the entire surface of the facility. In the central part of the building there is the core with 30-cm thick walls, which serves as a communication link. The building is finished with green flat roof, which is a terrace. On the perimeter of each floor there is an edge beam with a rectangular cross-section 35cm x 60cm operating in a continuous system. Floor slabs are designed as monolithic with a thickness of 20 cm, based on the pillars with a square cross-section 60cm x60cm. The thickness of a flat roof slab was increased to 25 cm due to the higher operating loads. The foundation is a monolithic reinforced concrete slab with a height equal to 1.00 m Figure 4 shows the projection of the analysed building.

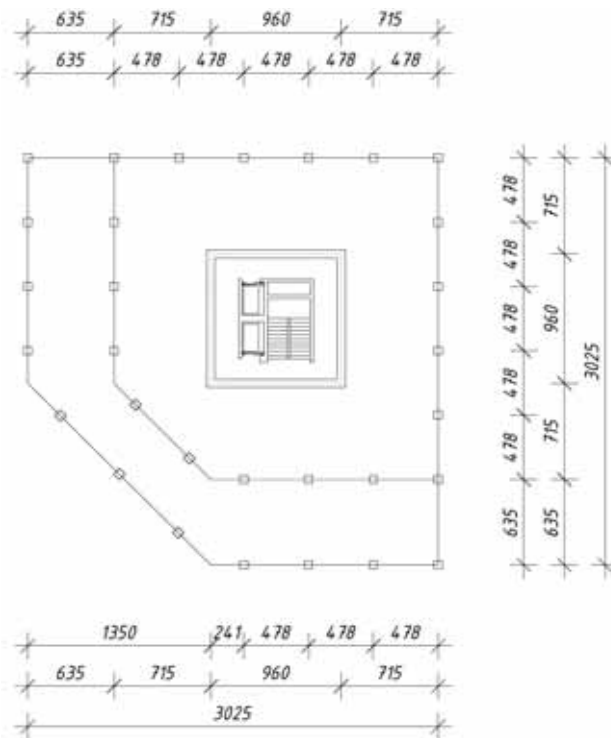


Fig. 4. A plan of the analysed high-rise building (lower tier)

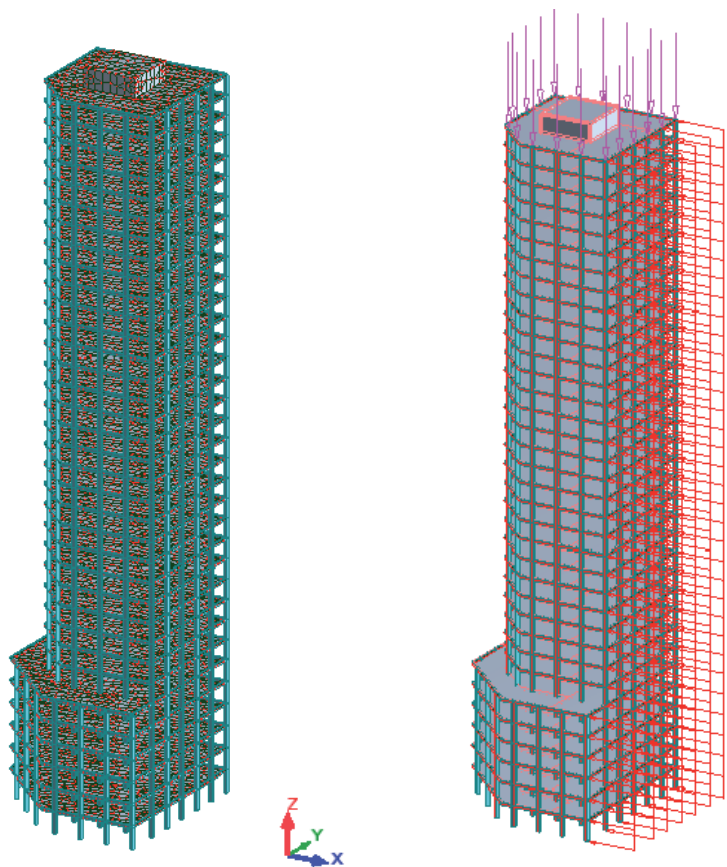


Fig. 5. The computational model with the discretisation grid and load in axonometry

Fig. 5 presents the model used for the computations with the load. The building was loaded with 50 kN vertical point applied forces operating on the axis of pillars of the top floor and a uniform load operating horizontally on the building with the value 4000kN/m.

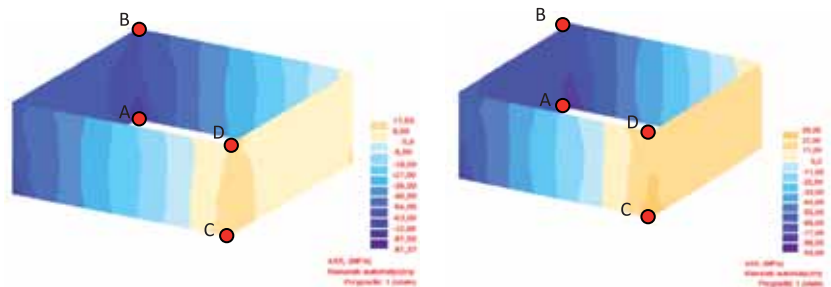


Fig. 6. Tension maps according to a) linear b) nonlinear analysis.

Table 1. The comparison of the obtained tension values in the lowest floor of the building at the points indicated in Figure 5.

Type of Analisys	Point A [MPa]	Point B [MPa]	Point C [MPa]	Point D [MPa]
Linear (first order)	-80,29	-65,00	16,75	9,36
Non-linear (secondo order)	-91,75	-75,28	28,18	19,66

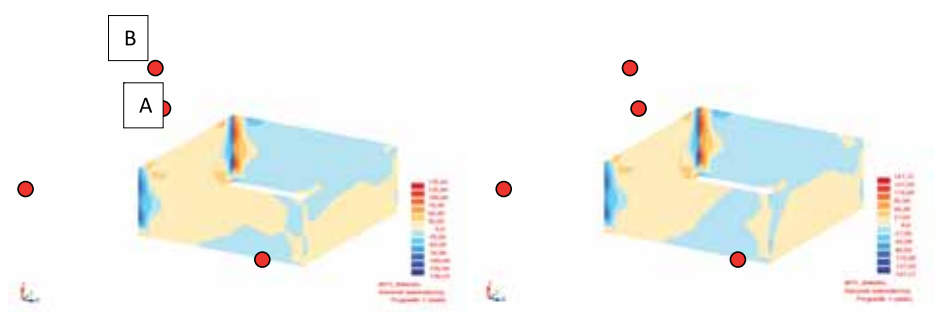


Fig. 7. Maps of the bending moments according to a) linear b) nonlinear analysis.

Table 2. The comparison of the obtained values of bending moments at the lowest floor of the building at the points indicated in Figure 5.

Type of analysis	Point A [MPa]	Point B [MPa]	Point C [MPa]	Point D [MPa]
Linear (First order)	117,90	67,32	-108,94	24,58
Non-linear (Second order)	133,86	81,07	-121,63	30,31

Figures 6 and 7 present maps of tensions and bending moments in the walls of the core of the lowermost floor of the building analysed. It was noted that in the non-linear analysis, the values of internal forces occurring in the elements of construction are greatly increased in relation to the linear analysis, which assumes the theory of small displacements without taking into account the displacement of force with the node that is displaced under the influence of the same load.

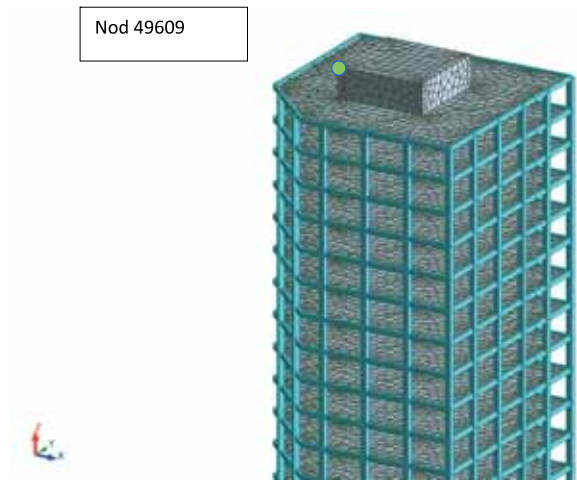


Fig. 8. The node which undergoes largest displacements

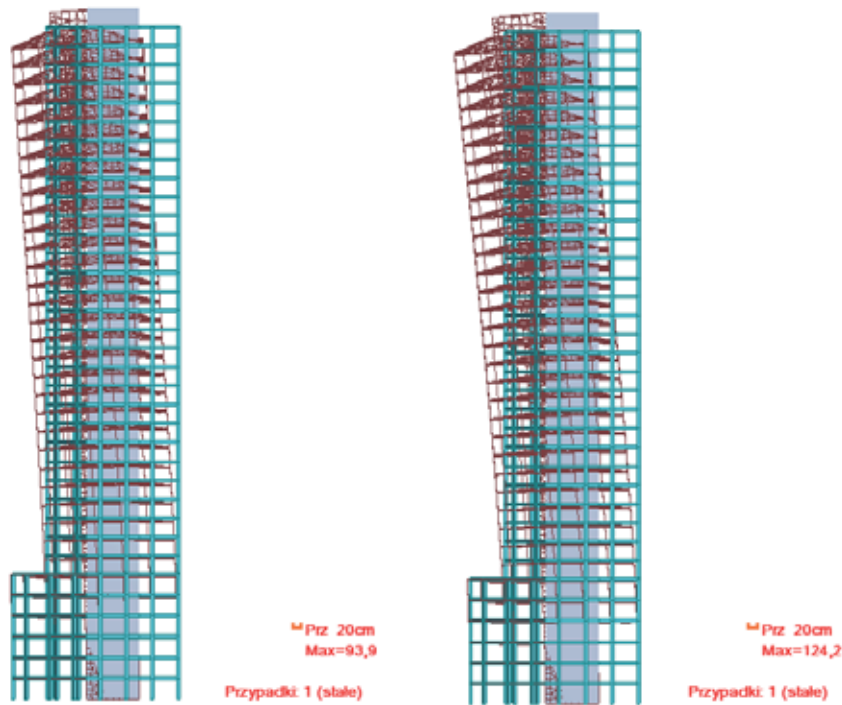


Fig. 9. Results of the a) linear b) nonlinear analysis of a high-rise building

Figure 9.a) shown below presents a comparison of the analysis of the deflection of a high-rise building according to the theory of the first order with the results of the analysis taking into account the effects of the second order (Figure 9.b)). As shown in the Figure, in the nonlinear analysis the building deflects about 30 cm more than in the linear analysis. If we consider this difference, the axial force on such an arm will give us a much bigger bending moment in the elements of the structure. It was found that high-rise buildings must be analysed taking into account the effects of $P-\Delta$, as they have great influence on the values of the internal forces in the structure and its subsequent operation during use. Maximum displacements occur in the node number 49609 marked in Figure 8.

Final conclusions

In most computational analyses of building structures, with which we face the designer's work, we will obtain a sufficiently accurate solution using standard calculation procedures and commercially available software. However, it should be remembered that standard solutions use model and computing simplifications, called the theory of the first order. The article particularly draws attention to the fact that there are structural situations and types of loads for which more sophisticated computational techniques should be used, such as the theory of second order. One such structural situation is the design of high-rise buildings, which may be affected by high wind pressure load. The article proves and shows a calculation example of how big difference there can be between the standard solution and the solution that considers the actual deformation of the structure. It has been shown that in specific design situations it is necessary to use more advanced computational techniques.

References:

1. Zienkiewicz O.C., Taylor R.L., Zhu J.Z. (2005), *The finite element method: its basis and fundamentals*. Amsterdam: Elsevier, Butterworth-Heinemann.
2. Kleiber M., Woźniak Cz. (1991), *Nonlinear mechanics of structures*. PWN-Polish Scientific Publishers, Warszawa.
3. Chyży, T. (2009), *Metoda analizy budynków mieszkalnych obciążonych nadciśnieniem w strefie wewnętrznego wybuchu gazu*. Oficyna Wydawnicza Politechniki Białostockiej, Białystok.
4. Foti F., Martinelli L. (2012), *Dynamics of corotational beam elements in large displacements and rotations. Some aspects on the kinetic energy and the integration of the equations of motion*. Vienna: ECCOMAS.
5. Autodesk Robot Structural Analysis 2010 – Podręcznik użytkownika.
6. Kapela M., Sieczkowski J. (2003), *Projektowanie konstrukcji budynków wielokondygnacyjnych*. Oficyna Wydawnicza PW, Warszawa .
7. Pawłowski A.Z., Cała I. (2006), *Budynki wysokie*. Oficyna Wydawnicza PW, Warszawa.
8. Matulewicz S. (2012), *Praca dyplomowa magisterska.: Projekt budynku wysokiego mieszkało-usługowego*. Białystok.

A NEW SUBSOIL MODEL FOR THE ANALYSIS SOIL-STRUCTURE INTERACTION

Joanna Krętowska

Faculty of Civil Engineering and Environmental Engineering, Białystok Technical University
Wiejska Street 45E, 15-351 Białystok, Poland
e-mail: J.Kretowska@kmb.pb.edu.pl

Summary:

Three-dimensional description of building structure taking into consideration soil-structure interaction is a very complex problem and solution of this problem is often obtained by using finite element method. However, this method takes a significant amount of computational time and memory. Therefore, an efficient semi-analytical description procedure of subsoil, that could provide accurate results with significantly reduced computational time is proposed in this study for the analysis soil-structure-interaction. The model allows the description to be made in three dimensional scheme and takes into account the complicated characteristic of subsoil strata. Because of the small number of unknowns the computation can be carried out easily on commonly used hardware of PC class. The examples prove the efficiency and the computing possibilities of the model.

Keywords: subsoil model, soil-structure interaction, finite element method, three dimensional analysis

Introduction

Soil-structure interaction is a very complex problem and the solution of this problem needs not only the suitable choice of structure model (Chyzy et al. 2006, Choi et al. 1996, 1998, 1999) but also the suitable choice of subsoil model. Much work describing the structure and subsoil contribution indicates wide application of finite element method (FEM) in the domain (Wang and Cheung 2001, Kundu et al. 1991, Miedzialowski 1996, Viladkar et al. 1995). Three-dimensional classical finite element analysis of building structure-subsoil system incorporates substantial disadvantages as a result of high time-consuming computations (high number of degrees of freedom) and extended data processing. Elaboration of the subsoil model significantly delimiting number degree of system freedom seems to be sensible.

This paper deals with three dimensional model of subsoil via finite element method, applicable in scientific research and engineering practice in the static analysis of the spatial building structures. The prismatic elements separated from soil space under the footing or strip foundation interconnected through spatial coupling elements are the roots of the model. The displacement far field around the foundation is simulated by using infinite elements.

Presented model of subsoil is compatible with many models (based on FEM) of the structure but especially by semi-analytical model (MQDES) of building structure presented by (Chyzy et al. 2006).

The soil-structure interaction model

Fig.1. shows the soil-structure interaction model which takes into account the building structure model, contact area and subsoil model.

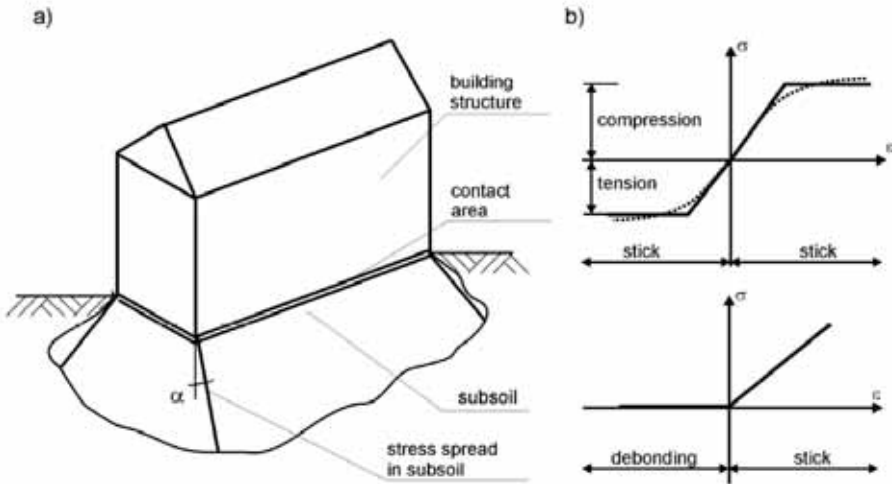


Fig. 1. a) soil-structure system, b) contact area behavior.

Building structure model

The model is constructed using the subdivision of the structure into building elements such as wall and floor slab elements, plane and three-dimensional joints (vertical and horizontal) and lintels. Wall and floor elements, which are treated as vertical and horizontal strips, are described by deep beam scheme taking into account compression and twisting. Transverse section deformation is assumed as in Timoshenko-type beam (Chyzy et al. 2006).

Subsoil model

The subsoil solid elements have the shape of prism (Fig.1., Fig.2., Fig.3) and are separated from the soil space under the footings or foundations strips. Generating lines are coming from the footings edges being in contact with the soil.

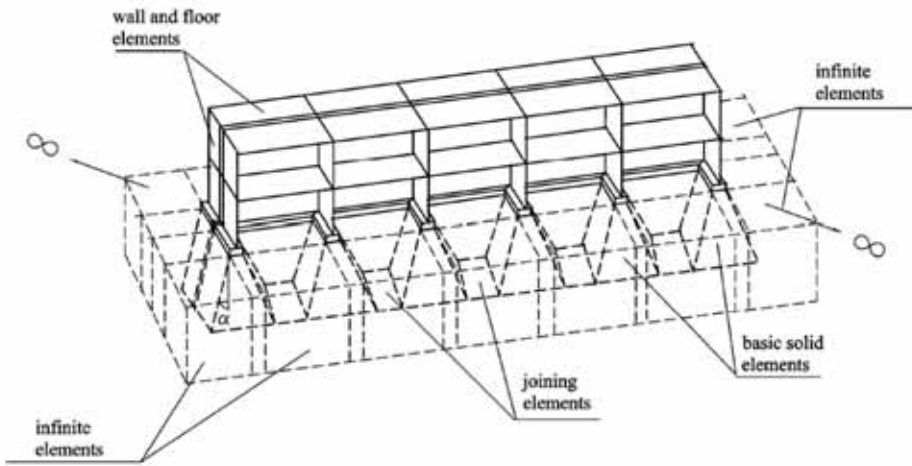


Fig. 2. View of the subsoil solids under the building.

The idea of the prism-shaped element rises from the observation, that the computation of the vertical stresses in the subsoil at any depth below a foundation is based on the assumption that the load is spread uniformly at an angle of $(90^\circ - \alpha)$ with the horizontal; but the area considered as supporting the load shall not extend beyond the intersection of $(90^\circ - \alpha)$ planes of adjacent foundations. Following the work of Andersen (1956), the angle α depends on the type of soil.

The special spatial elements are introduced to interconnect the soil solids separated under the footings. The infinite elements have been used to model far field domains (Fig.2).

The state of displacement inside the prism is assumed in three dimensional scheme as a short prismatic bar. The bar is subjected to bending and compression in the planes of building walls and is twisted and compressed as a result of the surrounding soil interaction. The displacements of horizontal sections are assumed as linear, such as in Timoshenko's beam.

The properties of the half-space determined by the soil solids and far field domains, at a given moment of time and loading, are presumed to be linear elastic.

Interface model

The importance of the interface behavior in the soil-structure interaction problems have been recognized for a long time. In the finite element analysis the introduction of interface (and joint) elements has proved to be very useful. There are various modes of deformation that an interface element can undergo: stick or no-slip, sliding or slip, separation or debonding and redbonding (Fig.1b.) So far, various interface/joint elements have been presented. These include zero thickness interface elements reported by (Goodman et al. 1968), Day and Potts 1994), Coutinho et al. 2003) , isoparametric

joint element presented by (Zienkiewicz et al 1970), simple interface elements for two and three dimensional problems described by (Beer 1985) and thin-layer element presented by (Desai et al. 1984,1988).

In the presented paper 8-node thin-layer element for interface behavior, such as that of (Desai et al. 1984) is used to describe this problem.

The subsoil computational model

The model formulation.

Let us consider the solid element shown in Fig.3.

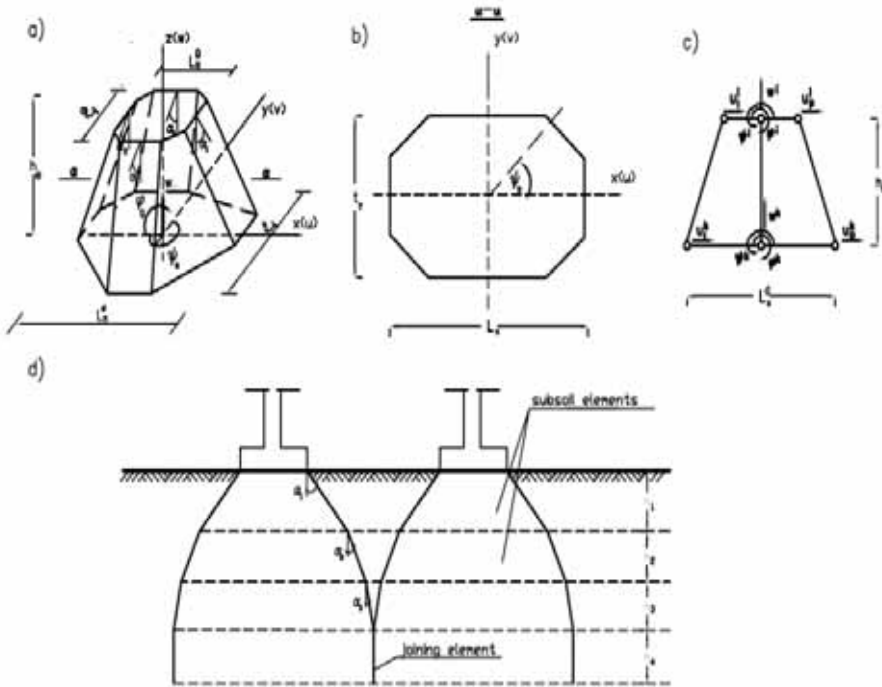


Fig. 3. The basic solid element.

The state of displacement is defined by three displacement components u , v and w in directions of the three coordinates x , y and z .

$$\text{Thus } \mathbf{q} = \begin{Bmatrix} u \\ v \\ w \end{Bmatrix} = \begin{Bmatrix} u \\ 0 \\ w_0 \end{Bmatrix} + \begin{Bmatrix} 0 \\ x\psi_s \\ -x\phi_g \end{Bmatrix}, \quad (1)$$

where: ϕ_g - angle of the rotation of the cross-section in x - z plane,
 ψ_s - angle of the element twist in x - y plane.'

The strain field can be expressed as

$$\boldsymbol{\varepsilon} = \begin{Bmatrix} \varepsilon_x \\ \varepsilon_y \\ \varepsilon_z \\ \gamma_{xz} \\ \gamma_{zx}^s \end{Bmatrix} = \begin{Bmatrix} \frac{u_l - u_p}{L_x} \\ \frac{x\psi_s}{2t_y} \\ \frac{\partial w_0}{\partial z} - x \frac{\partial \varphi_g}{\partial z} \\ -\varphi_g + \frac{\partial(u_l + u_p)}{2\partial z} \\ 2y \frac{\partial \psi_s}{\partial z} \end{Bmatrix}, \quad (2)$$

where: l, p - two neighboring points between which the stresses are averaged,
 L_x - length of element,
 t_y - width of element.

The strain $\boldsymbol{\varepsilon}_z$ has been divided into $\boldsymbol{\varepsilon}_z^w$ and $\boldsymbol{\varepsilon}_z^\varphi$.
Hence

$$\boldsymbol{\varepsilon} = \begin{Bmatrix} \varepsilon_x \\ \varepsilon_y \\ \varepsilon_z^w \\ \gamma_{xz} \\ \varepsilon_z^\varphi \\ \gamma_{zx}^s \end{Bmatrix} = \mathbf{L}\bar{\mathbf{u}} = \begin{bmatrix} \frac{1}{L_x} & -\frac{1}{L_x} & 0 & 0 & 0 \\ 0 & 0 & 0 & 0 & \frac{x}{2t_y} \\ 0 & 0 & \frac{\partial}{\partial z} & 0 & 0 \\ \frac{\partial}{2\partial z} & \frac{\partial}{2\partial z} & 0 & -1 & 0 \\ 0 & 0 & 0 & -x \frac{\partial}{\partial z} & 0 \\ 0 & 0 & 0 & 0 & 2y \frac{\partial}{\partial z} \end{bmatrix} \begin{Bmatrix} u_l \\ u_p \\ w_0 \\ \varphi_g \\ \psi_s \end{Bmatrix} \quad (3)$$

The stress field has a form

$$\bar{u}$$

$$s = \mathbf{D} e = \mathbf{D} \mathbf{L} \quad , \quad (4)$$

where \mathbf{D} - the constitutive relationship matrix in which the compression has been taken into account by introducing the shear coefficient k .

$$D = \frac{E_0}{(1 + \nu)(1 - 2\nu)} (D_{\text{diag}} + D_{12}) \quad , \quad (5)$$

$$D_{\text{diag}} = \begin{bmatrix} 1 - \nu, & 1 - \nu, & 1 - \nu, & \frac{1 - 2\nu}{2} k, & 1 - \nu, & \frac{1 - 2\nu}{2} \end{bmatrix} \quad , \quad (6)$$

\mathbf{D}_{12} - six by six matrix, in which $d_{12} = d_{13} = d_{21} = d_{23} = d_{31} = d_{32} = \nu$, and the others elements are equal 0,

ν - Poisson's ratio.

In the joined elements and in the elements which describe the far field domains the state of displacement has the form

$$\mathbf{q} = \begin{Bmatrix} u \\ v \\ w \end{Bmatrix} = \begin{Bmatrix} u(x, y, z) \\ v(x, y, z) \\ w(x, y, z) \end{Bmatrix} \quad (7)$$

The Finite Element Method application

The discrete model is formulated within the Finite Element Method in agreement with Zienkiewicz (1986). The global scheme is created by prism-shaped finite elements, joined finite elements and infinite elements.

The basic prism-shaped finite element.

The basic element is presented in Fig.4a.

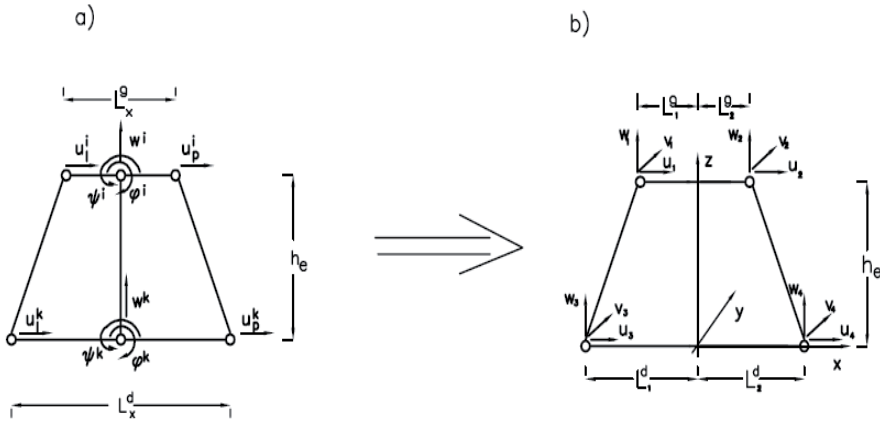


Fig. 4. The unknown displacements at corners of the element.

The displacements of an arbitrary point can be written as

$$\bar{u} = \mathbf{N} \mathbf{d}_e \quad (8)$$

where \mathbf{N} - shape function matrix,

\mathbf{d}_e - unknown displacements to be determined.

Components of the unknown displacement vector of the nodes “i” and “k” of a basic subsoil finite element are given by

$$\mathbf{d}_e = \{u_l^i, u_p^i, w_0^i, j^i, y^i, u_l^k, u_p^k, w_o^k, j^k, y^k\}^T \quad (9)$$

The principle of virtual work has been used to establish FEM relations

$$\iiint_V (\mathbf{de})^T s dV - \iiint_V (\mathbf{d}\bar{u})^T p dV = 0 \quad (10)$$

Hence

$$\mathbf{K}_e \mathbf{d}_e = \mathbf{P}_e \quad (11)$$

where \mathbf{K} - element stiffness matrix,

$$\mathbf{K}_e = \iiint_V \mathbf{B}^T \mathbf{D} \mathbf{B} dV \quad (12)$$

\mathbf{B} - matrix of relations between strains and nodal displacements in an element,

\mathbf{P} - vector of nodal forces,

$$\mathbf{B} = \begin{bmatrix} \frac{N_i}{L_x} & -\frac{N_i}{L_x} & 0 & 0 & 0 & \frac{N_k}{L_x} & -\frac{N_k}{L_x} & 0 & 0 & 0 \\ 0 & 0 & 0 & 0 & \frac{x}{2t_y} \frac{N}{t_y} & 0 & 0 & 0 & 0 & \frac{x}{2t_y} \frac{N}{t_y} \\ 0 & 0 & \frac{\partial N_i}{\partial z} & 0 & 0 & 0 & 0 & \frac{\partial N_k}{\partial z} & 0 & 0 \\ \frac{\partial N_i}{2\partial z} & \frac{\partial N_i}{2\partial z} & 0 & -N_i & 0 & \frac{\partial N_k}{2\partial z} & \frac{\partial N_k}{2\partial z} & 0 & -N_k & 0 \\ 0 & 0 & 0 & -\frac{x\partial N_i}{\partial z} & 0 & 0 & 0 & 0 & -\frac{x\partial N_k}{\partial z} & 0 \\ 0 & 0 & 0 & 0 & 2y\frac{\partial N_i}{\partial z} & 0 & 0 & 0 & 0 & 2y\frac{\partial N_k}{\partial z} \end{bmatrix} \quad (13)$$

$$P_e = \iiint_V N^T p dV \quad (14)$$

In order to obtain more convenient computer implementation the unknown displacements are defined at corners of elements (Fig.4.).

Hence, the stiffness matrix has to be transformed according to the formula

$$\bar{K} = A^T K' A \quad (15)$$

where A - transformation matrix.

$$A = \begin{bmatrix} A_{11} & 0 \\ 0 & A_{22} \end{bmatrix} \quad (16)$$

$$\mathbf{A}_{11} = \begin{bmatrix} 1 & 0 & 0 & 0 & 0 & 0 \\ 0 & 0 & 0 & 1 & 0 & 0 \\ 0 & 0 & \frac{L_2^g}{L_x^g} & 0 & 0 & \frac{L_1^g}{L_x^g} \\ 0 & 0 & \frac{1}{L_x^g} & 0 & 0 & -\frac{1}{L_x^g} \\ 0 & -\frac{1}{L_1^g} & 0 & 0 & 0 & 0 \\ 0 & 0 & 0 & 0 & \frac{1}{L_2^g} & 0 \end{bmatrix} \quad \mathbf{A}_{22} = \begin{bmatrix} 1 & 0 & 0 & 0 & 0 & 0 \\ 0 & 0 & 0 & 1 & 0 & 0 \\ 0 & 0 & \frac{L_2^d}{L_x^d} & 0 & 0 & \frac{L_1^d}{L_x^d} \\ 0 & 0 & \frac{1}{L_x^d} & 0 & 0 & -\frac{1}{L_x^d} \\ 0 & -\frac{1}{L_1^d} & 0 & 0 & 0 & 0 \\ 0 & 0 & 0 & 0 & \frac{1}{L_2^d} & 0 \end{bmatrix} \quad (17)$$

The new vector of unknown has the form

$$d_e = \{u_1, v_1, w_1, u_2, v_2, w_2, u_3, v_3, w_3, u_4, v_4, w_4\}^T \quad (18)$$

Joining finite elements and infinite elements.

Joining finite elements which are used in presenting subsoil model are shown in Fig.5. The unknown displacements of the discrete model are the same as in the case of the three dimensional finite elements.

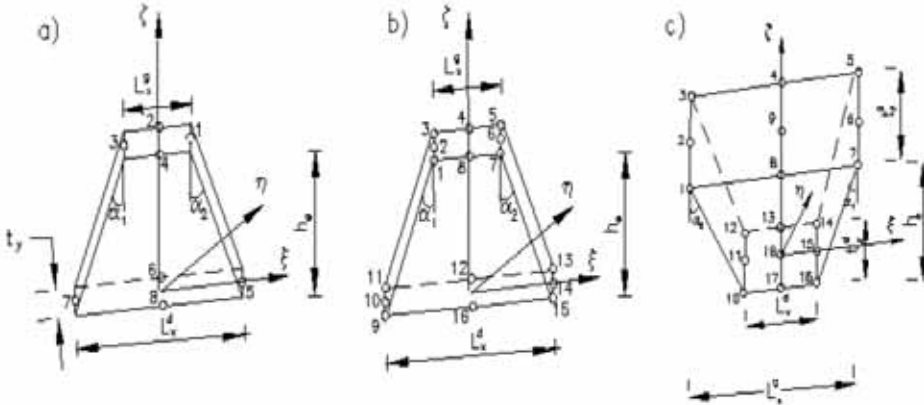


Fig.5. Joining elements.

The stiffness matrices of those elements are created by using classical finite elements (8-node, 16-node and 18-node).

Infinite elements are used to model far field domains. These help in reducing the total number of elements and model the domain at infinity in a better way.

Various procedures exist to model the unbounded region in the far field. These include Bettles (1984,1992) who reported 2D and 3D mapped element with exponential decay, where a finite element is stretched to an infinite element, (Beer & Meek 1981) presented how the infinite boundary can be accommodated within the finite element analysis by developing special elements which extend to infinity in one direction and (Viladkar et al. 1990) presented some new 3D mapped infinite elements with $(1/r)$ and $(1/\sqrt{r})$ type of decay.

The infinite elements used in the model are presented in Fig.6. The displacement vector is defined by three displacement components u , v and w . In agreement with (Bettles (1984, 1992) the infinite elements stiffness matrices are based on the finite element method, but the element shape functions have to be modified.

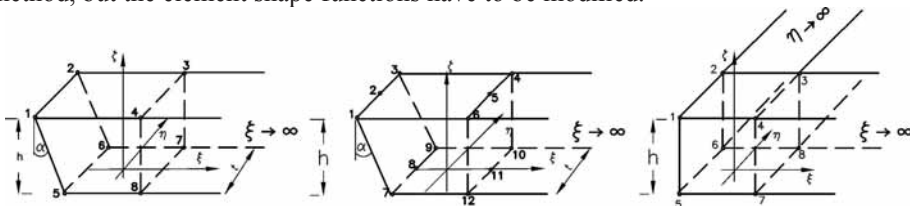


Fig. 6. Infinite elements.

In this case the shape function , such as that of Bettles (1992) formulation, has been used.

$$N_i(\xi, \eta, \varsigma) = f_i(\xi, \eta, \varsigma) M_i(\xi, \eta, \varsigma) \quad (19)$$

where N_i - infinite element shape function,

M_i - finite element shape function,

f_i - decay function.

The decay functions used for the elements presented in Fig.6. have the form

$$f_i(\xi, \eta, \varsigma) = \exp\left(\frac{\xi_i - \xi}{L}\right) \quad \xi \rightarrow \infty ,$$

$$f_i(\xi, \eta, \varsigma) = \exp\left(\frac{\xi_i + \eta_i - \xi - \eta}{L}\right) \quad \xi \rightarrow \infty , \eta \rightarrow \infty , \quad (20)$$

$$f_i(\xi, \eta, \varsigma) = \exp\left(\frac{\xi - \xi_i}{L}\right) \quad \xi \rightarrow -\infty .$$

where

L - the severity of the decay described by Bettles (1992).

Soil - structure interaction model.

The soil - structure interaction FEM model has the form

$$\begin{bmatrix} K_{kk} & K_{kkt} & 0 & 0 \\ K_{ktk} & K_{ktkt} & K_{ktg} & 0 \\ 0 & K_{gkt} & K_{gg} & K_{gn} \\ 0 & 0 & K_{ng} & K_{nn} \end{bmatrix} \begin{bmatrix} u_k \\ u_{kt} \\ u_g \\ u_n \end{bmatrix} = \begin{bmatrix} P_k \\ 0 \\ 0 \\ 0 \end{bmatrix} \quad (21)$$

where k - degrees of freedom of the structure,

g - degrees of freedom of the subsoil,

n - degrees of freedom of the surrounding ground,

kt - degrees of freedom of the interface elements

\mathbf{K} - submatrices,

\mathbf{u} - displacement vector,

\mathbf{P} - nodal forces vector.

In the presented paper 8-node thin-layer element (Fig.7) is used to describe the interface behavior in the soil-structure interaction problems

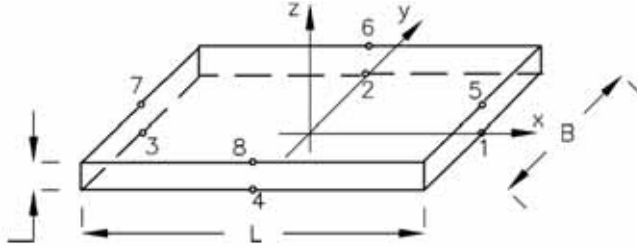


Fig. 7. The interface element.

The interface element is assumed to have a finite thickness t . The value of t can be chosen such that the ratio t/B is in the range of 0.001-0.100 in which B – width of adjoining solid element. For further details of this interface element see Desai et al. (1984).

Numerical examples

Several numerical tests have been solved to verify the correctness, accuracy and efficiency of the presented subsoil model.

Numerical test No.1.

The horizontal displacements u , caused by force $P=10\text{kN}$, have been determined in the system presented in Fig.8. The system consists of four basic subsoil elements and joining element. The verification of displacements convergence of the proposed subsoil model by the comparison with the results obtained by using commercial software MSC/NASTRAN have been done. Material and geometrical data: $E_0 = 80 \text{ MPa}$, $\nu = 0.3$, $t = 1 \text{ m}$, $L=4.0 \text{ m}$, $h = 6 \text{ m}$. Table 1 shows the horizontal displacements u (Fig.8). Fig.9. shows the displacements values determined in point 2 in comparison to the height of elements and number of nodes.

Error has been expressed by relative Euclidean norm of displacements obtained by proposed model and comparative method. The obtained results show that error value is equal 3.5% but the number of unknowns has been significantly reduced (10.5 times).

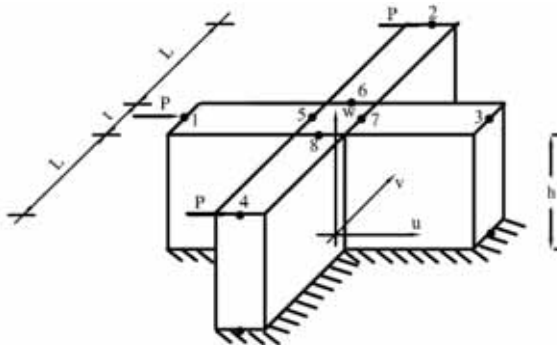


Fig. 8. Tested system.

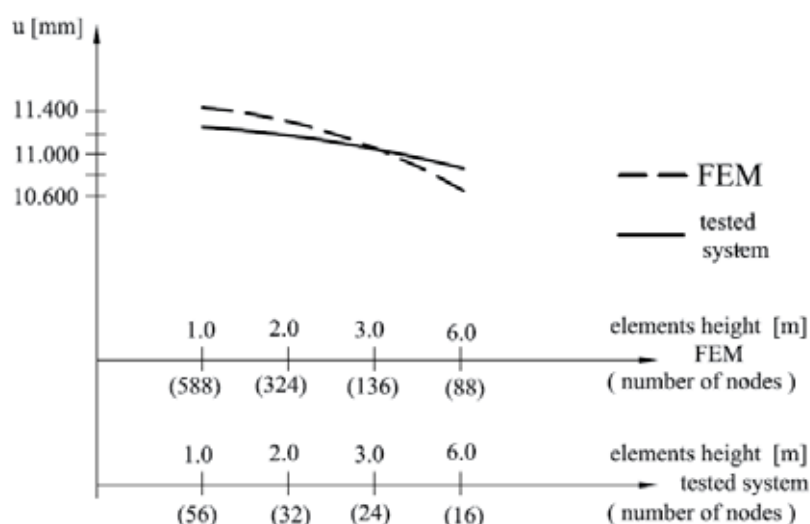


Fig. 9 Displacements values determined in point 2 in comparison to the height of elements and number of nodes.

Tab. 1. The horizontal displacements u (Fig.8)

method \ displacement		u [mm]							
		1	2	3	4	5	6	7	8
	2.0x1.0x1.0	1.689	11.456	0.842	11.456	0.952	0.906	0.892	0.906
FEM	2.0x1.0x2.0	1.580	11.320	0.831	11.320	0.945	0.888	0.883	0.888
20-node	4.0x1.0x3.0	1.476	11.070	0.825	11.070	0.939	0.880	0.871	0.880
	4.0x1.0x6.0	1.312	10.631	0.813	10.631	0.923	0.876	0.858	0.876
	$h_i=1.0\text{m}$	1.521	11.234	0.832	11.234	0.946	0.891	0.883	0.891
proposed	$h_i=2.0\text{m}$	1.496	11.157	0.828	11.157	0.943	0.886	0.879	0.886
elements	$h_i=3.0\text{m}$	1.483	11.002	0.826	11.002	0.941	0.884	0.874	0.884
	$h_i=6.0\text{m}$	1.392	10.826	0.822	10.826	0.934	0.881	0.861	0.881

The test proved that proposed elements give good accuracy of the results with significantly reduced number of unknowns.

Numerical test No.2.

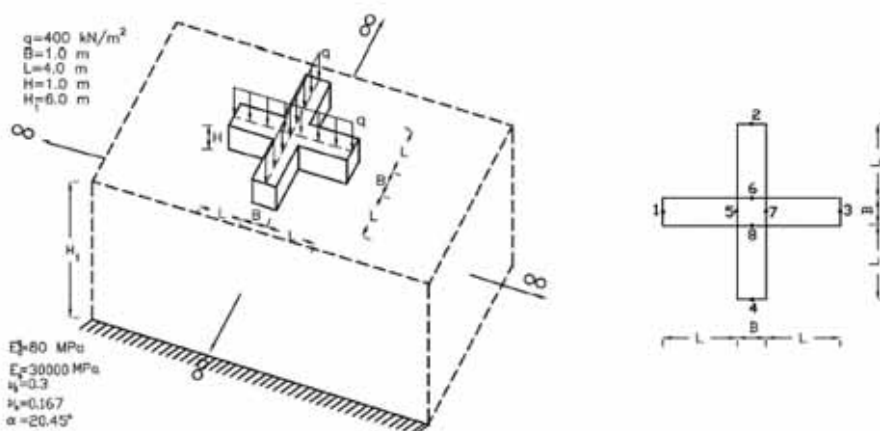


Fig. 10. Analyzed foundations system.

For the foundations system presented in Fig.10. the settlement analysis has been done. The results have been compared with the settlements received by using classic finite elements and commercial software MSC/NASTRAN. Material and geometrical data are shown in Fig.10.

Using proposed elements the subsoil has been divided into 6 layers of 1.0 m thickness.

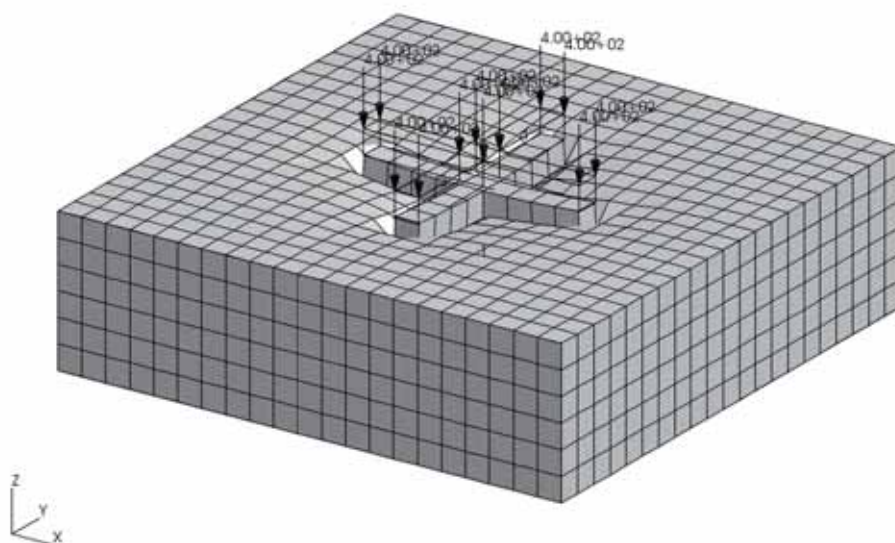


Fig. 11. The discretization of the system by using MSC/NASTRAN and the subsoil deformation caused by existing load.

Tab. 2. The settlement results (Fig. 10).

Points, where settlements has been determined	Proposed model [mm]	MSC/NASTRAN [mm]
1	5.56	5.40
2	5.56	5.40
3	5.56	5.40
4	5.56	5.40
5	6.63	6.24
6	6.63	6.24
7	6.63	6.24
8	6.63	6.24

The foundations have been described 4 finite elements proposed by Chyzy et al. (2006). The subsoil and foundations system gives 532 nodes. In classic FEM analysis (by using MSC/NASTRAN) the three dimensional 8-node elements $1.0 \times 1.0 \times 1.0\text{m}$ have been used to discretize the subsoil of $21.0 \times 21.0 \times 6.0\text{m}$ dimensions and the foundations. This system gives 3432 nodes. Fig.11 shows the discretization of the system by using MSC/NASTRAN and the subsoil deformation caused by existing load. Table 2 shows the settlement results.

Error has been expressed by relative Euclidean norm of settlements obtained by proposed model and comparative method. The obtained results show that error value is equal 5%.

Summary and conclusion

The semi-analytic description of subsoil for static analysis building structures loads has been presented. The model, which is formulated on the basis of the finite element method, takes into account the complicated characteristic of subsoil strata and allows the description to be made in three - dimensional scheme. The method formulation allows in a quickly way to obtain results convergence. The accuracy of the described model depends (like in classic FEM) on the division of the subsoil into constituent elements. Good accuracy (about 5%) has been obtained, what is acceptable in engineering practice. The infinite elements, which are used to model far field domain, help in reducing the total number of elements. The number of unknowns is small in comparison with the number of unknowns used for structure and subsoil description in classic FEM (from several to a dozens times less for the real structures) so the analysis of large building structures in three-dimensional scheme taking into account soil-structure interaction can be carried out easily in relative short time on commonly used hardware of PC class (the computational time is from dozens to several-hundreds times less in comparison with the commercial software).

References:

1. Andersen P. (1956), *Substructure analysis and design*, The Ronald Press Company.
2. Beer G., Meek J. L. (1981), *Infinite domain elements*, International Journal for Numerical Methods in Engineering, 17, 43-52.
3. Beer G. (1985), *An isoparametric joint/interface element for finite element analysis* International Journal for Numerical Methods in Engineering, 21, 293-300.
4. Bettess P. (1992), *Infinite elements*, Penshaw Press.
5. Bettess P., Bettess J.A. (1984), *Infinite elements for static problems*, Engineering Computations, 1, 4-16.
6. Choi C. K., Cheung K.Y. (1996), *Three-dimensional non-conforming 8-node finite elements with rotational degrees of freedom*, Structural Engineering and Mechanics, 4(5), 41-61.
7. Choi C. K., Kim S.H., Park Y. M., Cheun K.Y. (1998), *Two-dimensional nonconforming finite elements: A state-of-art*. Structural Engineering and Mechanics, 6(1), 41-61.
8. Choi C. K., Lee P. S., Park Y. M (1999), *Defect-free 4-node flat shell element: NMS-4F element*, Structural Engineering and Mechanics, 8(2), 207-231.
9. Chyzy T., Kretowska J., Miedzialowski Cz. (2006), *Analysis of 3D building structures dynamic response*, Structural Engineering and Mechanics, 22(1),
10. Coutinho A.L.G.A., Martins M.A.D., and Sydenstricker R.M. (2003), *Simple zero thickness kinematically consistent interface elements*, Computers and Geotechnics, 30, 347-374.
11. Day R. A., Potts D.M. (1994), *Zero thickness interface elements - numerical stability and application*, International Journal for Numerical and Analytical Methods in Geomechanics, 18, 689-708.
12. Desai C. S., Zamann M. M., Lightner J. G., Siriwardane H.J. (1984), *Thin-layer elements for interfaces and joints*, International Journal for Numerical and Analytical Methods in Geomechanics, 8(11), 19-43.
13. Desai C.S., Nagaraj B.K. (1988), *Modeling for cyclic normal and shear behavior of interfaces*, Journal of Engineering Mechanics, 114, 1198-217.
14. Goodman R.E., Taylor R.L., Brekke T.L. (1968), *A model for the mechanics of joined rock*, J Soil Mech Foundations Div, ASCE, 94(3), 637-659.
15. Kundu T., Mathur R.P., Desai C.S. (1991), *Three-dimensional soil-structure interaction analysis: deformable structures in multilayered soil mass*, Engineering Computations, 8, 153-180.
16. Miedzialowski Cz. (1995), *Three dimensional modelling wall structures for buildings*, Archives of Civil Engineering, XLI(2), 195-212.
17. Miedzialowski Cz. (1996), *Modeling of subsoil flexibility in computations of complex three-dimensional structural schemes of buildings*, Archives of Civil Engineering, XLII(1), 83-102.
18. Viladkar M.N., Godbole P.N., Noorzaeei J. (1990), *Some new 3-D infinite element*, Computers & Structures, 34, 455-467.

19. Viladkar M.N., Godbole P.N., Noorzaei J. (1995), *Elasto-plastic analysis for soil-structure interaction in framed structures* Computers & Structures, 55(5), 797-807.
20. Wang Y.H., Cheung Y.K. (2001), *Plate on cross-anisotropic foundation analyzed by the finite element method*, Computers and Geotechnics, 28, 37-54.
21. Zienkiewicz O.C., Best B., Dullage C. (1970), *Analysis of nonlinear problem in rock mechanics with particular reference to joined rock systems* .. Proc. 2nd Congress of the International Society for rock mechanics, 501-509.
22. Zienkiewicz O. C. (1986). *The finite element method*, McGraw-Hill .

EXPERIMENTAL STUDIES OF CONCRETE BEAMS REINFORCED LONGITUDINALLY WITH STEEL AND GFRP BARS

Victor Tur, Uladzimir Malykha

Pope John Paul II State School Higher Education in Biala Podlaska,
Department of Engineering Sciences, Department of Civil Engineering
Sidorska Street 95/97, 21-500 Biala Podlaska, Poland
e-mail: vvtur@bstu.by

Summary:

The present article is part of research work aiming to contribute to the development of hybrid reinforcement system what combines GFRP (Glass Fiber Reinforced Polymer) and steel bars in an optimized arrangement of the bars, using potentialities that each material can provide. The special experimental studies of concrete beams reinforced with steel-GFRP bars were carried out. Results of the experimental studies indicate that presence of the steel bars contributes considerably to ductility and stiffness, reduces crack width and crack spacing values.

Keywords: flexural steel and GFRP reinforcement; deflection; crack width.

Introduction

The present article is part of research work aiming to contribute to the development of reinforcement system what combines GFRP (Glass Fiber Reinforced Polymer) and steel bars in an optimized arrangement of the bars, using potentialities that each material can provide.

The replacement of conventional steel reinforcement by GFRP bars has been investigated (Toutanji, Saafi 2000; Abdalla 2002) to prevent the corrosion problem and to improve the durability of concrete structures near marine environments, near the ground, in chemical and other industrial plants, in places where good quality concrete cannot be achieved, and in the thin structural elements. Was shown (Taheri et al 2009) in comparison with steel, GFRP materials have higher resistance to corrosion, and higher strength-to-weight ratio. Furthermore GFRP materials are non-electrical conductive and non-magnetic material (ACI440R-07). However, how it was shown in (Aiello, Ombres 2002) the major obstacles of the application of GFRP bars as a reinforcing material for concrete structures are relatively high initial costs, low modulus of elasticity, lack of ductility (linear stress-strain relationship up to rupture with no discernible yield point), and absence of well-consolidated design guidelines. Concrete members reinforced with GFRP and subjected to bending moments behave linearly up to cracking, and almost linearly after cracking with significant lower stiffness (Taheri et al 2009).

Deflections of concrete members reinforced with GFRP bars are generally large than the members reinforced exclusively with steel reinforcement. This is due to the low modulus of elasticity and different bond characteristics of GFRP reinforcement (Taheri et al 2009). In addition, as a result of a larger crack width and smaller compressive stress blocks when using GFRP bar for the flexural reinforcement, the shear capacity of GFRP-reinforced concrete beams is smaller than in the case of steel-reinforced concrete beams of the same reinforcement ratio (Taheri et al 2009).

In an attempt to overcome these drawback, actual studies proposed a combination of GFRP and steel reinforcement for concrete beams. As was shown by Aiello and Ombres (Aiello, Ombres 2002) with this combination of the reinforcement materials, and considering the minor (minimum required for bond) concrete cover required for GFRP, an effective solution in term of durability is obtained by placing GFRP bars near the outer surface of the tensile zone and steel bars at the inner level of the tensile zone. The presence of the steel bars in the above mentoned hybrid reinforcement systems contributes significantly to ductility and stiffnes.

Experimental studies of hybrid reinforced beams

The special experimental study of concrete beams reinforced hybrid (steel and GFRP bars) reinforcement were carried out. Two series of concrete beams of rectangular cross-section, of width $b = 120$ mm, height $h = 190$ mm and length $l = 2070$ mm, reinforced with different percentage of tensile longitudinal steel and GFRP bars were tested in four point loading configuration (see fig. 1). This figure also represent the geometry of the beams, the reinforcement arrangement, as well ass the loading and support condition. In table 1 are indicated the values of geometrical and material parameters of beams. Figure 2 shown a perspective view of the test setup.

The test program has been drawn up in such a way that the total amount of reinforcement, what is estimated mechanical reinforcement index ω

$$\left(\omega = \frac{f_{yk} \cdot \rho_l + f_{yk(f)} \cdot \rho_{l(f)}}{f_{cm}} \right) \text{ that achieve approximately equal values of the ultimate}$$

bending moment (M_u) and tensile reinforcement failure mode.

Up to near the failure of the control beam I-B1 reinforced exclusively with steel bars tensile strains in reinforcement exceeded the yielding value $\epsilon_{sy} = 2,5$ ‰ and tensile strain $\epsilon_{s,exp} = 9,8$ ‰ nave bin attained. Concrete compressive strain was near ultimate value $\epsilon_{cu} \cong 3,5$ ‰. Beam I-B1 failure occurred as a result of the achievement of yield strains of the steel reinforcement.

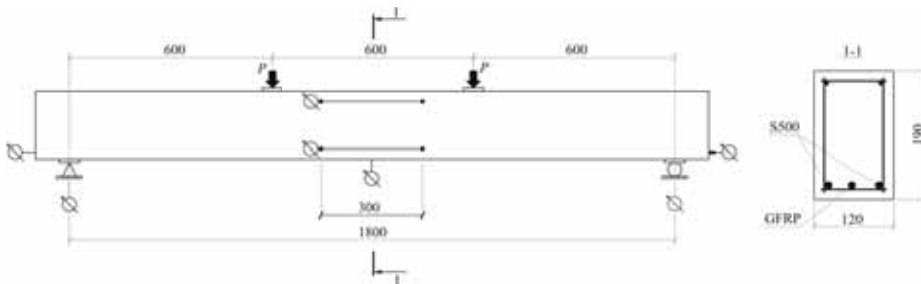


Fig. 1. Geometry and reinforcement arrangement of tested beams

Tab. 1. Program of experimental research

Serie	Beam	Cross-section size, mm	Mean concrete compressive strength f_{cm} , MPa ²⁾	number	Reinforcement				
					area, mm ²		reinforcement ratio, %		
					A _s	A _{s(t)}	ρ _{st}	ρ _p	w
I	I-B1(t) ¹⁾	120×190	37,6	2Ø12S500	226,2	–	0,99	–	19,8
	I-B2(t)			2Ø10S500 + Ø8GFRP	157,1	50,3	0,69	0,22	22,6
	I-B3(t)			2Ø8S500 + Ø10 GFRP	100,5	78,5	0,44	0,34	22,6
	I-B4(t)			2Ø6S500 + Ø12 GFRP	56,5	113,1	0,25	0,50	24,8
	I-B5(t)			2Ø4S500 + 2Ø10 GFRP	25,1	157,1	0,11	0,69	29,8
II	II-B2		29,2	2Ø10S500 + Ø8 GFRP	157,1	50,3	0,69	0,22	22,6
	II-B3			2Ø8S500 + Ø10 GFRP	100,5	78,5	0,44	0,34	22,6
	II-B4			2Ø6S500 + Ø12 GFRP	56,5	113,1	0,25	0,50	24,8
	II-B5			2Ø4S500 + 2Ø10 GFRP	25,1	157,1	0,11	0,69	29,8

Notes:
¹⁾ index (t) means that the manufacture of the tested beams heat treatment was applied (e.g. by system);
²⁾ the mean compressive strength of concrete was tested on cube specimen.

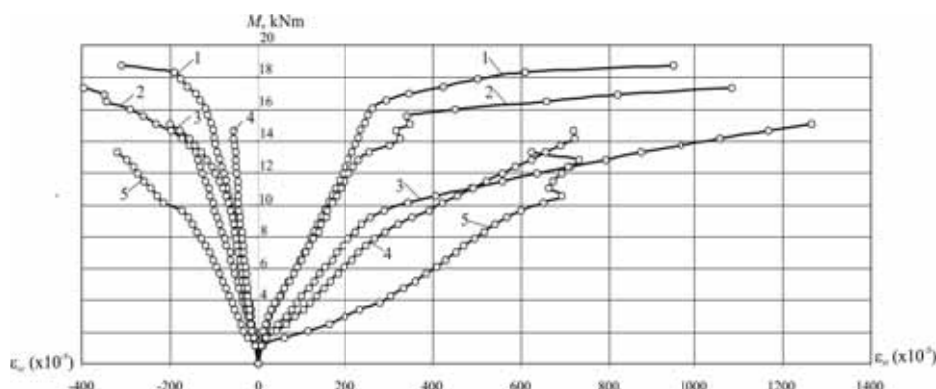


Fig. 2. General view of the test setup

Figure 3 represent the “load – strain” and “moment – deflection” diagrams respectively.

The ductility ratio which represents a ratio between the ultimate and yielding deflections of the beam I-B1 at midspan point ($\eta = a_u / a_y$), was equal to $\eta = 2,44$ (see table 2). The same ductility behavior showed concrete beams I-B2 and I-B3 reinforced with steel and GFRP bars ($2\text{Æ}10 \text{ S500} + \text{Æ}8 \text{ GFRP}$, $\omega = 0,226$).

The failure of the beams I-B2 and I-B3 occurred as a result of reaching the yield strains in the steel reinforcement and then the crushing of concrete in compression zone of the section (loading process ended due to the failing of concrete in compression zone of section, where the ultimate compression strains was attained).



1 – I-B1; 2 – I-B2; 3 – I-B3; 4 – I-B4; 5 – I-B5

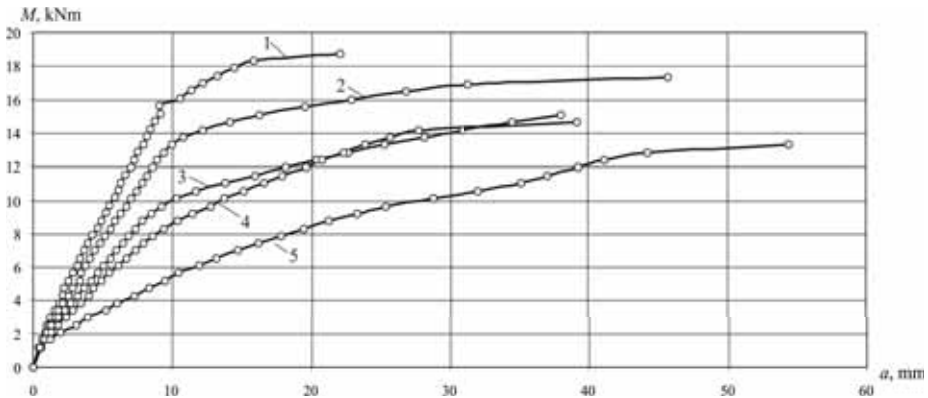
Fig. 3. Load-strains response for tested beams

Tab. 2. Results of experimental studies

Serie	Beam	Cracking parameters			Deflection, mm				M_{Ru} , kN×m
		M_{crc} , kN×m	w_{max} , mm	w_m , mm	$a_{0,6}$	a_y	a_u	$\eta = a_u / a_y$	
I	I-B1	6,53	0,20	0,17	6,47	9,05	22,05	2,44	18,76
	I-B2	4,27	0,25	0,20	7,42	9,93	45,76	4,61	17,35
	I-B3	2,05	0,75	0,63	8,19	8,51	38,06	4,47	15,05
	I-B4	2,05	0,70	0,62	10,40	7,90	39,23	4,97	14,60
	I-B5	1,60	1,00	0,79	17,81	6,09	54,42	8,94	13,25

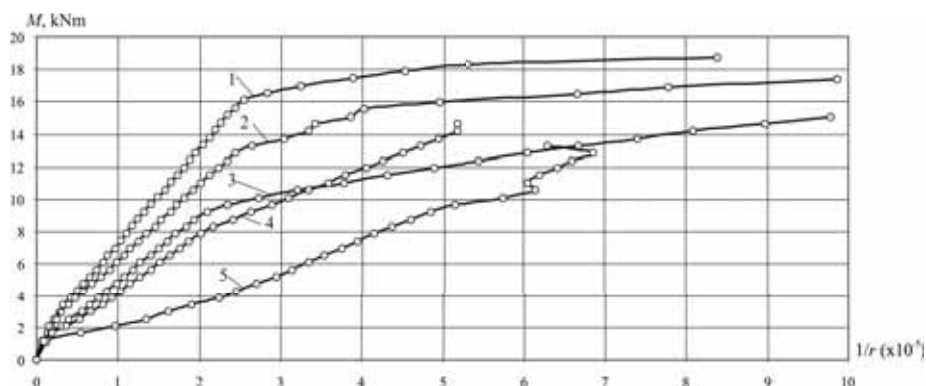
w_{max} , w_m – maximum and mean (average) crack width at loading level $M / M_{Ru} = 0,6$;
 $a_{0,6}$, a_y , a_u – midspan deflection for different loading level: $0,6 M_u$, M_y and M_u , respectively;
 M_{crc} – cracking moment; M_{Ru} – ultimate moment.

For beams I-B2 and I-B3 value of ductility ratio was $\eta = 4,61$ (see figures 4, 5, table 2) and ultimate deflections were twice more that the deflection of the control beam I-B1. Up to near the failure tensile strain in steel reinforcement was equal to $\varepsilon_{s,exp} = 11 \text{ ‰}$, and strain in compression concrete was $\varepsilon_{cu} \cong 4 \text{ ‰}$.



1 – I-B1; 2 – I-B2; 3 – I-B3; 4 – I-B4; 5 – I-B5

Fig. 4 – Moment-deflection response for the tested beams



1 – I-B1; 2 – I-B2; 3 – I-B3; 4 – I-B4; 5 – I-B5

Fig. 5. Moment-curvature response for the tested beams

As shown in figure 6 the bulk of the total tensile force in reinforcement is perceived by steel bars (78 kN) and only 28 % of the total force takes GFRP bars.

Ultimate bending moment ($M_u = 15,05 \text{ kN}\cdot\text{m}$) was smaller for the concrete beams I-B3 ($2\text{A}8 \text{ S500} + \text{A}10 \text{ GFRP}$) and I-B4 ($2\text{A}6 \text{ S500} + \text{A}12 \text{ GFRP}$) than for the reference beam I-B1, but the ductility ratio was almost the same (see figures 4, 5) (experimental value of tensile strain in steel reinforcement was equal to $\varepsilon_{su,exp} = 12 \text{ ‰}$ and $\varepsilon_{su,exp} = 9 \text{ ‰}$ for beams I-B3 and I-B4 respectively).

In table 2 are indicated the values of cracking and ultimate bending moments, deflections and ductility ratios for tested beams.

As figures 4, 5 illustrates, the yield strains in steel reinforcement was achieved at comparatively low loading rate ($M_y / M_u \cong 0,3$). After yielding of steel reinforcement as the bending moment increases, as the tensile force in GFRP bars is increased practically linearly (see figure 7). The tensile force in the steel bars and GFRP bars at ultimate stage was almost equal for beam I-B3, but for beam I-B4 tensile force in GFRP bars was near 45 % greater than tensile force in steel bars. For beam I-B2 yield strain in steel reinforcement was achieved at loading rate ($M_y / M_u \cong 0,6$).

Figures 4, 5 is illustrated relationships “ $M - 1/r$ ” and “ $M - a$ ” for tested beams. As shown in figures 4, 5 relationships “ $M - 1/r$ ” and “ $M - a$ ” can be idealized trilinear diagram. The first range of curves is characterized elastic behavior of concrete beams before cracking. The second branch with different slope is characterized post-cracking behavior, and third branch with smallest slope is characterized behavior of concrete element after yielding of steel reinforcement.

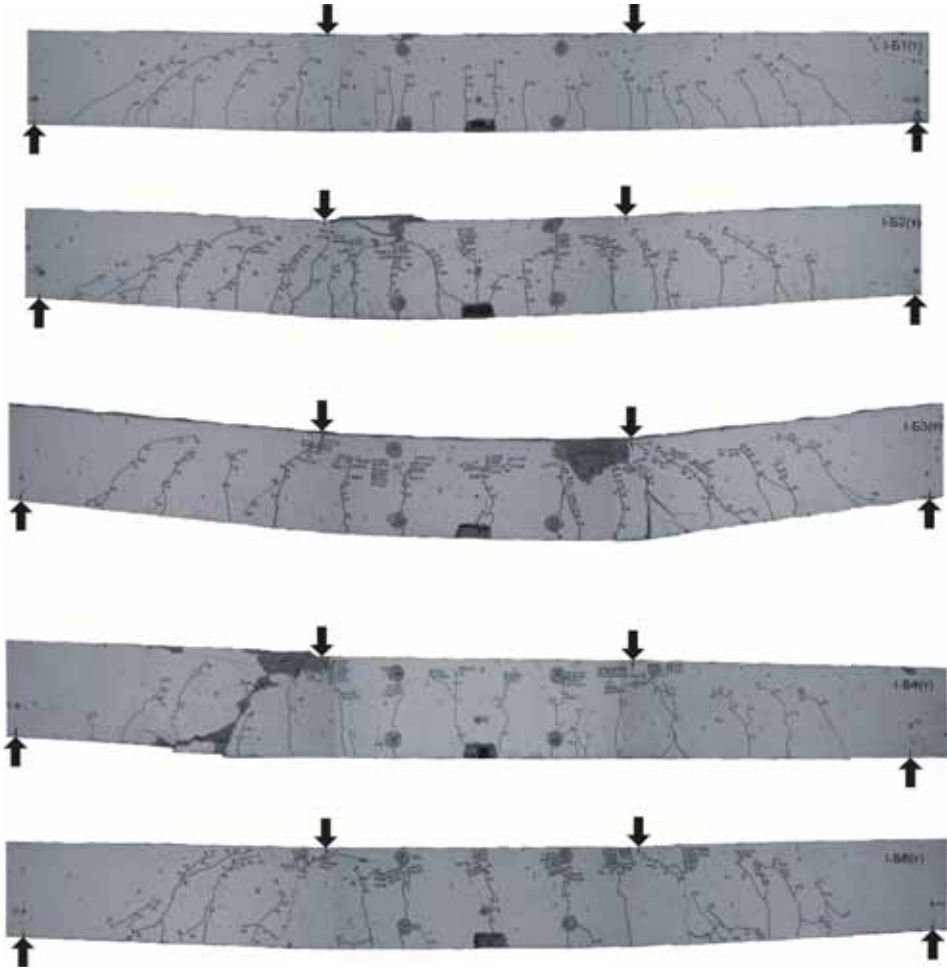
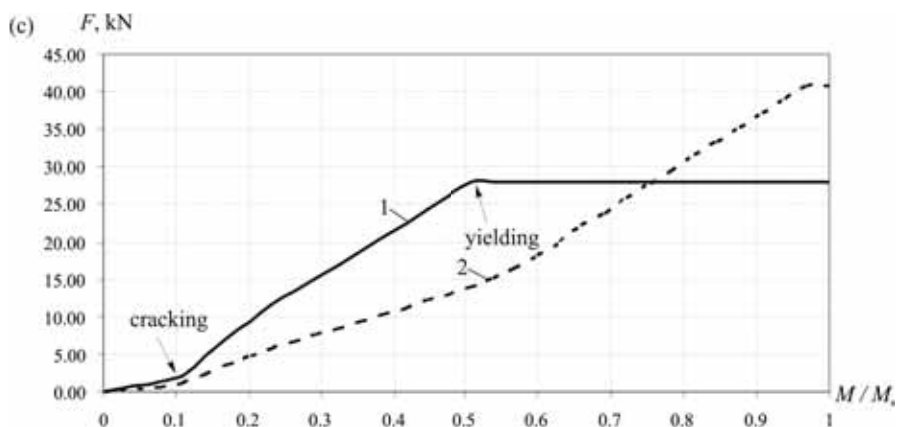
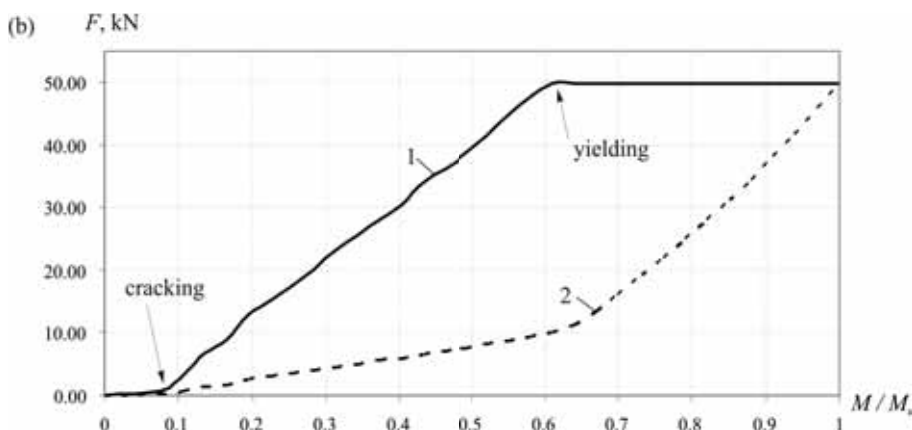
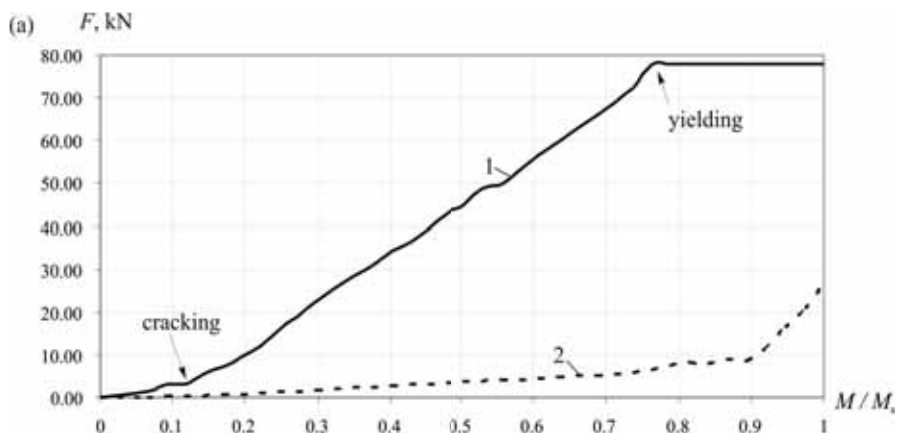
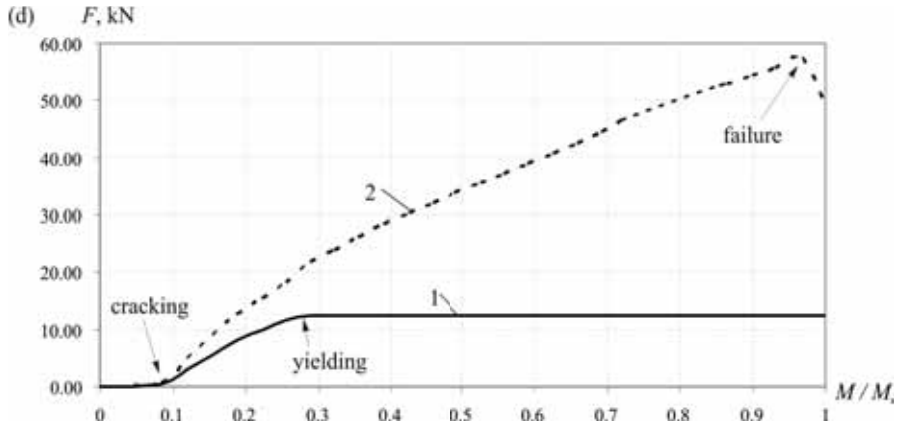


Fig. 6. Crack pattern for the tested beams

The different slopes are explained by crack width grown (see figure 10), increasing of deflections and as a result decreasing of bending (flexural) stiffness (see table 2). Figure 10 represent the crack distribution on the length of concrete beams after failure. As shown in diagram (figure 8) which represents ratios between mean and maximum cracking width, for all tested beams, except of beam I-B2, maximum crack width exceeded a limit value $w_{lim} = 0,3 \text{ mm}$ in accordance with EN 1992-1. For tested beams I-B3 and I-B4 it can be explained by early achievement of yielding strains in steel bars. But in comparison with the beam I-B4 reinforced mainly with GFRP bars, maximum crack width for beams I-B3 and I-B4 was from 24 % to 26 % lower at the same loading condition.





(a) I-B2; (b) I-B3; (c) I-B4; (d) I-B5

Fig. 7. Redistribution of the tensile force between steel (1) and GFRP (2) bars as the load increases

In fact, it can be concluded that the deflection of concrete beams reinforced with GFRP and steel bars was smaller than that of beams reinforced exclusively with GFRP. In comparison with beam exclusively reinforced with GFRP bars, the presence of steel bars reduces crack width and crack spacing value (see figures 7, 8).

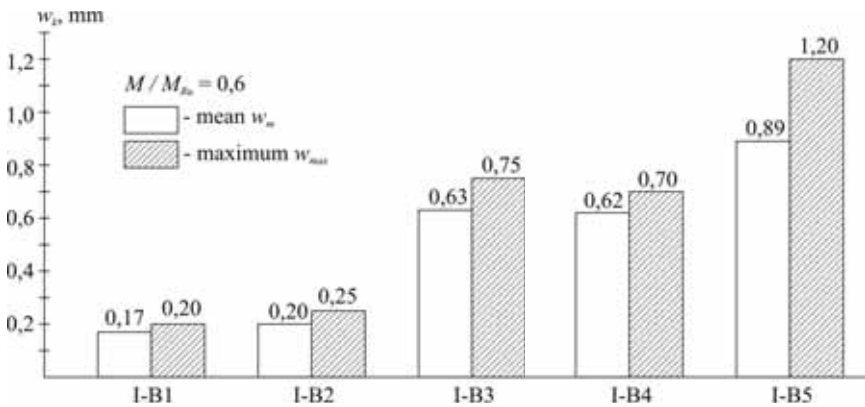


Fig. 8. The experimental values of the mean (average) and maximum crack width for the tested beams (loading level $M / M_u = 0,6$)

It should be noted that all the tested beams reinforcement bars are located equidistant one from the top fiber. In-fact non-corrodible GFRP bars with height tensile strength, but with brittle behavior and low modulus of elasticity are near bottom fiber, while ductile steel bars have a concrete cover thickness that assures a high protection from the effects of corrosive agents (Taheri et al 2009). Reinforcement ratio of steel reinforcement and

its location in the cross-section should be designed in such a way that requirements were provided restrict deflection, width of cracks and structural safety, even in case of a fire occurrence and the consequent loss of GFRP reinforcing capacity. For the optimization of the reinforcing systems for given type of beams (the location of the steel and GFRP bars in the cross-section) a currently running a special parametric studies, based on analytical model (Aiello, Ombers 2002).

Conclusions

Results of experimental studies indicate that presence of the steel bars in the above mentioned hybrid reinforcement system (steel bars + GFRP bars) contributes significantly to ductility and stiffness. It was shown that the deflection of concrete beams reinforced with steel and GFRP bars was smaller than that of beams reinforced with GFRP, and the presence of steel bars reduces crack width and crack spacing values.

The hybrid reinforcement system (steel + GFRP bars) is a competitive solution whn the long term costs with repairing activities are also taken into account (Taheri et al 2009).

References:

1. Toutanji H., Saafi M. (2000). Flexural behavior of concrete beams reinforced with glass fiber-reinforced polymer (GFRP) bars. *ACI Structural Journal*; 9715: p. 712–719.
2. Abdalla H.A. (2002). Evaluation of deflection in concrete members reinforced with fiber reinforced polymer (FRP) bars. *Journal of Composite Structures*; 56: p. 63–71.
3. ACI440R-07 (2007). Report on fiber-reinforced polymer (FRP) reinforcement for concrete structures. American Concrete Institute, Reported by ACI Committee 440.
4. Aiello M.A., Ombres L. (2002). Structural performance of concrete beams with hybrid (fiber-reinforced polymer – steel) reinforcements. *Journal of Composites for Construction*, 6(2): p. 133–140.
5. Taheri M., Barros J., Salehian H. (2009). A design model for strain-softening and strain-hardening fiber reinforced elements reinforced longitudinally with steel and FRP bars. Researching programs “DURCOST”, PTDC/ECM/105700/2008.

MODELLING BEHAVIOUR OF HIGH-STRENGTH CONCRETE BEAMS

Piotr Smarzewski

Pope John Paul II State School of Higher Education in Biała Podlaska,
Faculty of Economic and Technical Sciences, Department of Technical Sciences,
Sidorska Street 95/97, 21-500 Biała Podlaska, Poland
e-mail: p.smarzewski@pollub.pl

Summary:

The comparative analysis of the own numerical results with experimental results was presented for the examples of the reinforced high-strength concrete beams under static load. The arc-length method was used in combination with Newton-Raphson method to trace the complete response in load-deformation space. The comparison of the obtained results indicates on the correctness of the assumptions and constitutive models of the high-strength concrete and reinforcement steel, and the effectiveness of the solution method. Numerical results of smeared crack patterns are qualitatively agreeable, for the localization, the direction and the concentration with experimental results. The development of strain in outer concrete layer of the compression zone and the development of strain for longitudinal reinforcement have excellent agreement in the most presented cases. The full nonlinear load-deformation at midspan response of the model produced compares well with the experimental response taken from literature. In the presented paper the usefulness of the arc-length method was verified on a spatial numerical model of the reinforced concrete beams with consideration of the concrete softening during compression and tension. The numerical solutions obtained for the reinforced concrete beams are coherent with the experimentally obtained results.

Keywords: Finite Element Method, beams, reinforced high-strength concrete.

Introduction

Improved performance computing systems and the possibility of their use in the design of engineering structures enforces intensive development of numerical methods for the calculation of static and dynamic analysis of structural behavior. Numerical methods are the only way to achieve practically useful solutions to complex spatial members with materials not subjected to the laws of linear elasticity.

A high performance concrete, the concrete of high strength and also high tightness, includes all the components previously applied to the concrete, but in different proportions dosed. Detailed information regarding the classification and characteristics of the composite cement-based materials have been presented in the works (Aitcin 1998, Calderon 2009).

The subject of work is the reinforced high-strength concrete beams considered as composition of materials consisting of reinforced concrete steel rods distributed discretely in the concrete matrix. The purpose of the work is modelling the mechanisms of destruction of reinforced concrete beams loaded statically, the static deformation processes reinforced high-strength concrete beams, taking into account the physical nonlinearity of structural materials.

Modelling of concrete

The equations of the limit surfaces for concrete are described in the papers of (Willam, Warnke 1975, Ottosen 1977, Klisiński 1984, Stolarski 2004). The proposed equations depend on the limit surfaces of the first invariant of the stress tensor and the second and third invariant of the stress deviator. Such a description allows the most faithful approximation of concrete experimental results in complex stress states. In this paper, limit surface equation depending on five stress invariants in accordance with the theory of (Willam, Warnke 1975) and its proposal of the surface evolution law as a function of strain.

The failure criterion of concrete in a complex state of stress is described in the following expression:

$$F / f_c - S \geq 0, \quad (1)$$

in which: F - the function of stresses conditions $\sigma_{xp}, \sigma_{yp}, \sigma_{zp}$ in the direction of the Cartesian coordinate system x, y, z , S - failure surface dependant on the principal stresses $\sigma_1, \sigma_2, \sigma_3$, where: $\sigma_1 = \max(\sigma_{xp}, \sigma_{yp}, \sigma_{zp})$, $\sigma_3 = \min(\sigma_{xp}, \sigma_{yp}, \sigma_{zp})$ and $\sigma_1 \geq \sigma_2 \geq \sigma_3$ and five strength parameters: f_c - uniaxial compressive strength causing crushing, f_t - uniaxial tension strength causing cracking, f_{cb} - ultimate biaxial compressive strength causing crushing, f_1 - ultimate compressive strength for a state of biaxial compression superimposed on hydrostatic stress state σ_h^a and f_2 - ultimate compressive strength for a state of uniaxial compression superimposed on hydrostatic stress state σ_h^a .

The description failure of concrete is defined in four domains of stresses: compression – compression – compression, when $0 \geq \sigma_1 \geq \sigma_2 \geq \sigma_3$, tension – compression – compression, as $\sigma_1 \geq 0 \geq \sigma_2 \geq \sigma_3$, tension – tension – compression, when $\sigma_1 \geq \sigma_2 \geq 0 \geq \sigma_3$ and tension – tension – tension, as $\sigma_1 \geq \sigma_2 \geq \sigma_3 \geq 0$.

In each range of strain, independent functions F_1, F_2, F_3, F_4 and S_1, S_2, S_3, S_4 describe the function state of stresses F and the failure surface S . These functions in each of the state of stress are presented by (Smarzewski 2011).

Concrete limit surface with evolution laws is used as a criterion of destruction according to the following interpretation. The material is destroyed if the Eq. (1) is fulfilled. The state of failure can be distinguished as the state of cracking, if any principal stress is tensile, or the state of crushing, if all principal stresses are compressive. Safe working conditions describe the stress state interpreted as the elastic state inside the surface. Evolution of the limit surface is determined by the fallowing proposition of hardening or softening laws.

The essence of this proposition is shown in Figure 1. The stress-strain function for the uniaxial compressive phase of elastic-plastic strengthening and softening is confirmed in the experimental observations, indicating much larger the limit strains in the structural member than in the control plain concrete samples.

Interpreting the numerical results of the high-strength reinforced concrete beams, it was observed that the use of the equations describing relationships between strains and stresses proposed in (Model Code 90 1995) leads to a significant decrease in structural deflection. On the basis of numerical experiments in comparison with experimental results (Kamińska 1999, 2002) the concept of the behavior of high-strength concrete with uniaxial compression and tension in reinforced concrete was included in proposed model of concrete behaviour.

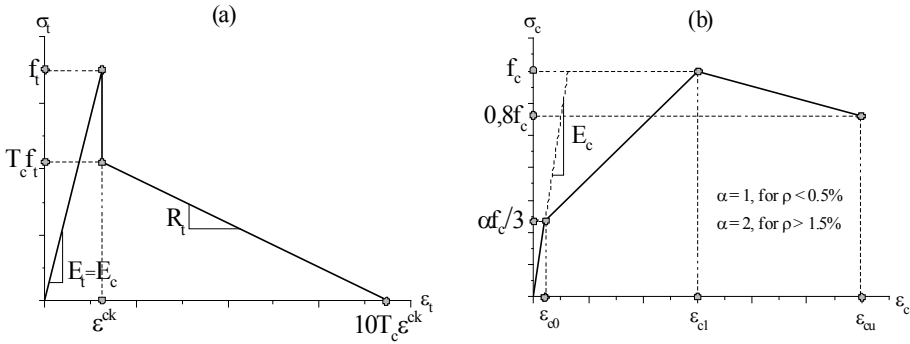


Figure 1. Assumed stress-strain relationship for concrete for uniaxial tension (a) and compression (b)

Stress-strain curve for tensile concrete (Fig. 2a) is linear up to the tensile strength f_t . It is assumed that the tensile deformation modulus is equal to the compressive one. After reaching f_t the cracks begin to develop. The brittle fracturing suddenly decrease the stress to a value greater or equal than $T_c f_t$. Value of parameter T_c should be chosen from the range $0.6 \leq T_c \leq 1$. The stiffening effect, included by founding a gradual, soft decrease of tensile strength to zero is described by strains equal to 0.8 ‰ if $T_c = 0.6$ and to 1.4 ‰ if $T_c = 1$.

The limit of elastic phase in the compressive concrete in relation to the reinforcement ratio was determined (Fig. 2b). For a reinforcement ratio greater than 1.5 ‰ it was assumed linear stress-strain diagram to the level of $0.7 f_c$. Then begins the phase of elastic-plastic strengthening with linear increase in stress up to the uniaxial compressive strength f_c , and after then the stresses in concrete are decrease to $0.80 f_c$ at the limit strain ε_{cu} . For the proposed model strain $\varepsilon_{c1} = 6$ ‰ at the uniaxial compressive strength f_c and the limit compression strains $\varepsilon_{cu} = 12$ ‰ were assumed.

More slanted $\sigma - \varepsilon$ curve for the high-strength concrete is not always reflected in the behaviour of reinforced concrete elements. Experimental results (Lambrotte et al. 1990, Taerwe 1991, Bernardi 1999, Kamińska 1999) showed that low ductility concerns high-strength concrete in the structural elements is not justified. In such members, which were damaged by the crushing of concrete compression zone, the strains of concrete reached up to 6-12 ‰, and were appropriately twice the damaging strains registered on the plain concrete samples.

In the numerical analysis the hexahedral elements were applied for the concrete. Finite element is defined by the isotropic properties of the material, and eight nodes with three degrees of freedom in each of them, as the displacements of nodes in three-dimensional orthogonal local coordinate system. In each finite element at all points of the numerical integration the strains and stresses are calculate. Smeared crack model provides a description of the cracking at any point numerical integration in three directions perpendicular to the principal stresses. Crack formation is described by proposed model of concrete. In the graphical representation the results are presented in cracking outline form of a circle shape in the direction perpendicular to the principal stress. In the state of cracking or crushing concrete for the numerical balance in the finite element is added a small value of stiffness.

The matrix of elasticity for an isotropic material \mathbf{D}_c is represented in the form:

$$\mathbf{D}_c = \frac{E_c}{(1+\nu_c)(1-2\nu_c)} \begin{bmatrix} 1-\nu_c & \nu_c & \nu_c & 0 & 0 & 0 \\ \nu_c & 1-\nu_c & \nu_c & 0 & 0 & 0 \\ \nu_c & \nu_c & 1-\nu_c & 0 & 0 & 0 \\ 0 & 0 & 0 & 0,5-\nu_c & 0 & 0 \\ 0 & 0 & 0 & 0 & 0,5-\nu_c & 0 \\ 0 & 0 & 0 & 0 & 0 & 0,5-\nu_c \end{bmatrix} \quad (2)$$

where: E_c - modulus of elasticity of concrete, ν_c - Poisson's ratio.

In the state of cracking and crushing the matrix is adapted to the state of the damage. In numerical modeling, it is necessary to take account of the characteristics of concrete description after they have formed. The parameter β_t is introduced as a multiplier for reducing shear transfer causing slip in the plane perpendicular to the cracks surface. The relationship between stress and strain of the cracked material in one plane is written in the form of a matrix:

$$\mathbf{D}_c^{\text{ck}} = \frac{E_c}{1+\nu_c} \begin{bmatrix} R_t(1+\nu_c)/E_c & 0 & 0 & 0 & 0 & 0 \\ 0 & 1/(1-\nu_c) & \nu_c/(1-\nu_c) & 0 & 0 & 0 \\ 0 & \nu_c/(1-\nu_c) & 1/(1-\nu_c) & 0 & 0 & 0 \\ 0 & 0 & 0 & 0,5\beta_t & 0 & 0 \\ 0 & 0 & 0 & 0 & 0,5 & 0 \\ 0 & 0 & 0 & 0 & 0 & 0,5\beta_t \end{bmatrix} \quad (3)$$

Graphical interpretation of the module weakness R_t and the multiplier for amount of tensile stress relaxation T_c is shown in Figure 2a. When cracks closing in the matrix \mathbf{D}_c^{ck} , shear parameter β_c is introduced:

$$\mathbf{D}_c^{\text{ck}} = \frac{E_c}{(1+\nu_c)(1-2\nu_c)} \begin{bmatrix} 1-\nu_c & \nu_c & \nu_c & 0 & 0 & 0 \\ \nu_c & 1-\nu_c & \nu_c & 0 & 0 & 0 \\ \nu_c & \nu_c & 1-\nu_c & 0 & 0 & 0 \\ 0 & 0 & 0 & \beta_c(0,5-\nu_c) & 0 & 0 \\ 0 & 0 & 0 & 0 & 0,5-\nu_c & 0 \\ 0 & 0 & 0 & 0 & 0 & \beta_c(0,5-\nu_c) \end{bmatrix} \quad (4)$$

Stiffness matrix for concrete cracked in two and three dimensions is written in the form:

$$\mathbf{D}_c^{ck} = E_c \begin{bmatrix} R_i / E_c & 0 & 0 & 0 & 0 & 0 \\ 0 & R_i / E_c & 0 & 0 & 0 & 0 \\ 0 & 0 & 1 & 0 & 0 & 0 \\ 0 & 0 & 0 & 0,5\beta_i / (1+\nu_c) & 0 & 0 \\ 0 & 0 & 0 & 0 & 0,5\beta_i / (1+\nu_c) & 0 \\ 0 & 0 & 0 & 0 & 0 & 0,5\beta_i / (1+\nu_c) \end{bmatrix} \quad (5)$$

and if the cracks are closed in two or three planes, the relationship is expressed in a matrix form Eq. (4). Opening or closing of cracks at the point of numerical integration depends on the sign of the cracking strains.

Modelling of steel

The simplified uniaxial model of steel for the reinforcing bars is used. The elastic-plastic material model with linear hardening, of identical stress-strain characteristics for the tension and compression. Spatial spar element, with two nodes with three degrees of freedom, was applied in the modeling of steel bars. Moreover, linear elastic model was assumed for the steel plates located in support and concentrated external force areas. To modeling of steel plates the hexahedral elements were applied.

Modelling of high-strength concrete beams

Spatial mesh steel rebar finite element was associated with the mesh of the concrete finite element by modeling the compatibility of displacements at common nodes. For such a mesh system the stiffness matrix is the sum of the finite element stiffness matrices for concrete and for reinforcement steel. In support areas steel plates were modeled as nodal imparting forces on steel rollers allow free rotation of the beam in the plane of bending. External concentrated force is also applied through the steel plate. Uniform distribution of forces at the nodes in the direction of the transverse symmetry axis of the steel plate was assumed.

The numerical model of spatial beams used dimensions and properties of the material as rectangular beams BP-1b and BP-2b investigated by (Kamińska 1999). Dimensions of beams with reinforcement and loading arrangements are shown in Fig. 2.

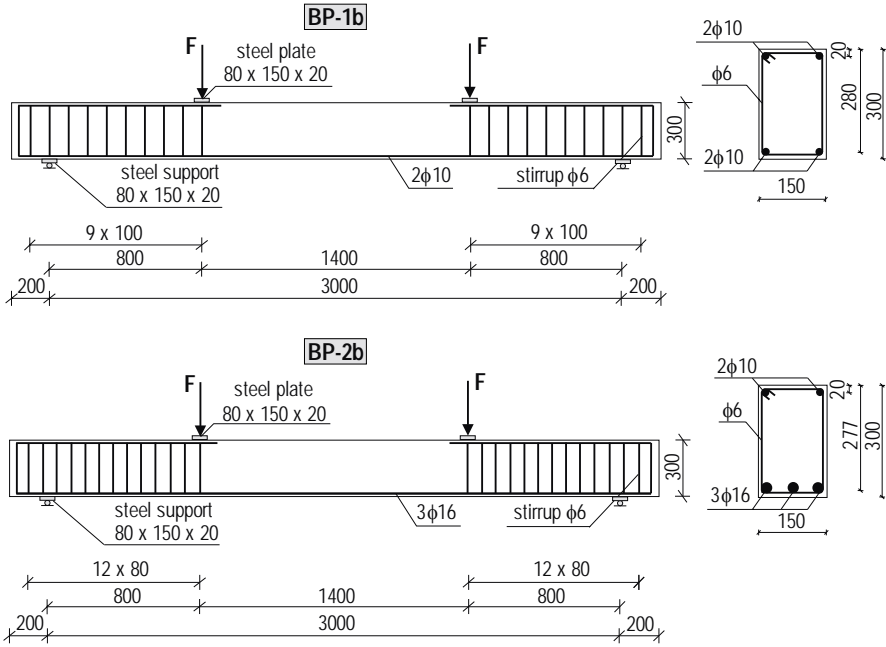


Fig. 2. Dimensions and cross-section of BP beams with reinforcement and loading arrangements

The parameters of constitutive concrete model are given for the beams BP-1b / BP-2b, respectively. High-strength concrete is defined by the uniaxial compressive strength $f_c = 72.8 / 73.3$ MPa, modulus of elasticity $E_c = 34 / 35.8$ GPa, tensile uniaxial strength $f_t = 4.73 / 5.06$ MPa, Poisson's ratio $\nu_c = 0.15$, density $\rho_c = 2600$ kg/m³, compressive strain at the strength stress level $\epsilon_{cl} = 6$ ‰, ultimate compressive strain $\epsilon_{cu} = 12$ ‰, shear transfer coefficients for an open crack $\beta_t = 0.5$ and shear transfer coefficients for the closed crack $\beta_c = 0.99$.

The appropriate material parameters for the steel bars of $\phi 16 / \phi 10 / \phi 6$ mm diameters are as follows: modulus of elasticity $E_s = 196 / 194 / 201$ GPa, yield stress $f_y = 437 / 420 / 353$ MPa, tensile uniaxial strength $f_{st} = 713 / 624 / 466$ MPa, limit strain at the yield stress $\epsilon_{su} = 106 / 116 / 75$ ‰, modulus of plastic deformation $E_T = 2659.7 / 1792.1 / 1542.8$ MPa, Poisson's ratio $\nu_s = 0.3$ and density $\rho_s = 7800$ kg/m³.

Supporting and load transferring steel plate are defined by modulus of elasticity $E_s = 210$ GPa, Poisson's ratio $\nu_s = 0.3$ and density $\rho_s = 7800$ kg/m³. Having regard the longitudinal symmetry elements one half of the beams was modeled.

Methods of numerical solutions of the equilibrium equations

Newton-Raphson method with adaptive descent

Newton-Raphson method, shown graphically in Figure 3, is an iterative process of solving nonlinear equations

$$\mathbf{K}_i^T \Delta \mathbf{u}_i = \mathbf{F}^a - \mathbf{F}_i^{nr}, \quad (6)$$

$$\mathbf{u}_{i+1} = \mathbf{u}_i + \Delta \mathbf{u}_i, \quad (7)$$

where: \mathbf{K}_i^T - tangent stiffness matrix, i - index corresponding to the number of the incremental step, \mathbf{F}^a - generalized load vector, \mathbf{F}_i^{nr} - vector of restoring loads representing the element internal loads in the discretised system.

Matrix \mathbf{K}_i^T and vector \mathbf{F}_i^{nr} are calculated on the basis of the displacement vector \mathbf{u}_i .

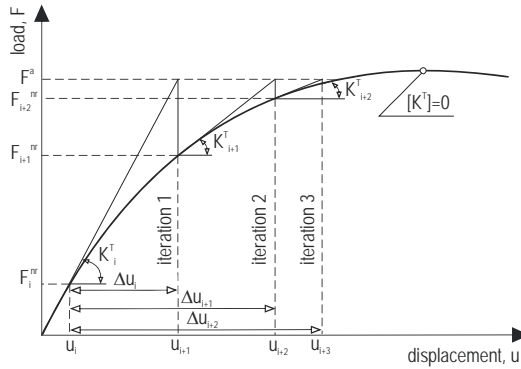


Fig. 3. Newton-Raphson method

Adaptive descent method presented in the work by (Eggert et al. 1991) is based on the change of solution path approximating the limit point and reversing along the secant until obtaining the convergence of numerical solution.

The stiffness matrix in Newton-Raphson equation Eq. (6) is described as a sum of two matrixes:

$$\mathbf{K}_i^T = \xi \mathbf{K}^S + (1 - \xi) \mathbf{K}^T, \quad (8)$$

\mathbf{K}^S - secant stiffness matrix, \mathbf{K}^T - tangent stiffness matrix, ξ - adaptive descent parameter.

The method is based on the agreement adaptive descent parameter ξ in equilibrium iteration. The secant stiffness matrix is generated in the numerical method as a result of solving nonlinear tasks concerning material plastification, construction stiffness with large deformations or concrete crushing.

Arc-length method

In the method of numerical Crisfield's arc-length (Crisfield 1983), presented in Fig. 3 equation Eq. (6) is dependent on load parameter λ :

$$\mathbf{K}_i^T \Delta \mathbf{u}_i = \lambda \mathbf{F}^a - \mathbf{F}_i^{nr} \quad (9)$$

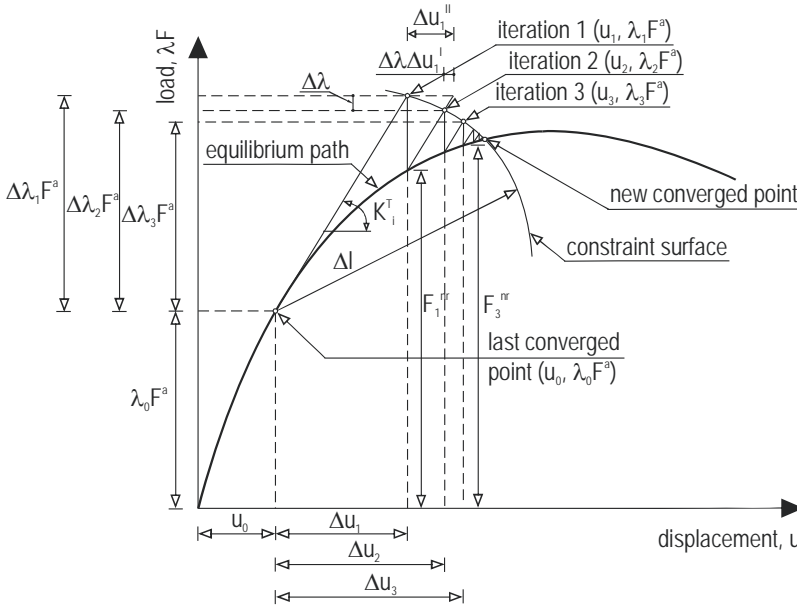


Fig. 3. Crisfield's arc-length method

In this procedure the variable load parameter λ is searched in the range $-1 \leq \lambda \leq 1$. In the incremental substep the equation has the following form:

$$\mathbf{K}_i^T \Delta \mathbf{u}_i - \Delta \lambda \mathbf{F}^a = (\lambda_0 + \Delta \lambda) \mathbf{F}^a - \mathbf{F}_i^{nr} \quad (10)$$

$\Delta \lambda$ - incremental load parameter.

On the basis of equation Eq. (10) the vector of incremental displacement $\Delta \mathbf{u}_i$ consists of two components described as follows

$$\Delta \mathbf{u}_i = \Delta \lambda \Delta \mathbf{u}_i^I + \Delta \mathbf{u}_i^{II} \quad (11)$$

$\Delta \mathbf{u}_i^I$ - vector of displacement increment caused by a unit load parameter, $\Delta \mathbf{u}_i^{II}$ - vector of displacement increment in the Newton-Raphson method.

Displacement vectors are defined as

$$\Delta \mathbf{u}_i^I = \mathbf{K}_i^{T-1} \mathbf{F}^a \quad (12)$$

$$\Delta \mathbf{u}_i'' = \mathbf{K}^{-1} \left[(\lambda_0 + \Delta \lambda_i) \mathbf{F}^a - \mathbf{F}^{nr} \right], \quad (13)$$

The incremental load parameter $\Delta \lambda$ is defined from the arc length equation:

$$l_i^2 = \Delta \lambda_i^2 + \beta^2 \Delta \mathbf{u}_n^T \Delta \mathbf{u}_n, \quad (14)$$

β -scaling factor, n - current step number, $\Delta \mathbf{u}_n$ - the sum of all displacement increments $\Delta \mathbf{u}_i$ in the current iteration step.

The work (Forte, Stierner 1987) presents a general procedure of calculating the parameter $\Delta \lambda$ based on ensure orthogonality:

$$\Delta \lambda = \frac{r_i - \Delta \mathbf{u}_n^T \Delta \mathbf{u}_i''}{\beta^2 \Delta \lambda_i + \Delta \mathbf{u}_n^T \Delta \mathbf{u}_i'}, \quad (15)$$

r_i - unbalanced parameter obtained by scalar multiplication of normal and tangential vector.

The finale vectors are updated according to:

$$\Delta \mathbf{u}_{i+1} = \Delta \mathbf{u}_0 + \Delta \mathbf{u}_n + \Delta \mathbf{u}_i, \quad (16)$$

$$\lambda_{n+1} = \lambda_0 + \Delta \lambda_i + \Delta \lambda, \quad (17)$$

Iterations stop at the moment of obtaining the desired convergence of the numerical solution.

Numerical analysis high-strength concrete beams

Cracking analysis

The images of real cracks in full BP beams are presented against numerical images of smeared cracks for the left half of the beams with the same values of load in Figure 4.

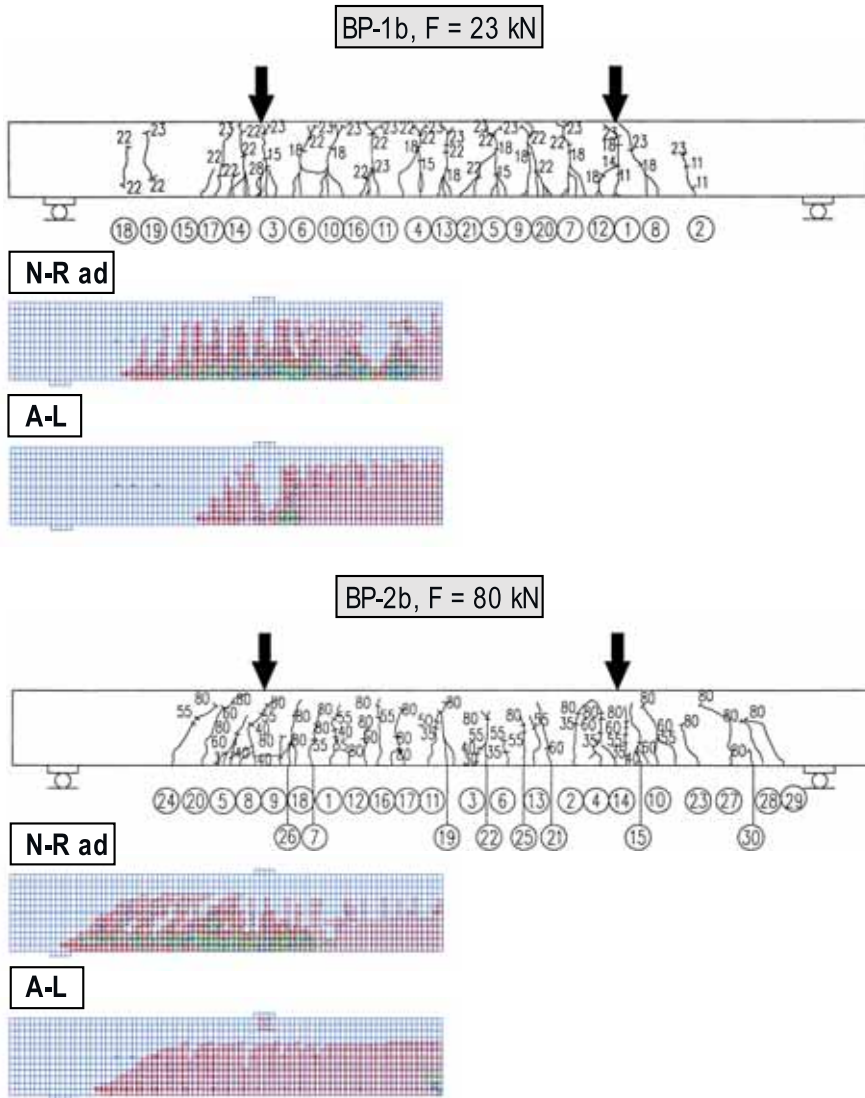


Fig. 4. Experimental and numerical images of cracking BP beams

All the obtained numerical results are in qualitative agreement with experimental results in terms of their location, direction and concentration. In case of Newton-Raphson method with adaptive descent slightly larger zone of smeared cracks was observed. Due to the lack stirrups in the model and experimental BP-1b beams with low reinforcement and BP-2b with a higher degree of reinforcement in the section of pure bending, arrangement of cracks is arbitrary.

Strain analysis

For the observation of strain changes in concrete, depending on the load, is assumed at the upper edge the point of the mid span of beams BP. The development of strain in the outer layer of the concrete compression zone are shown in Figure 5.

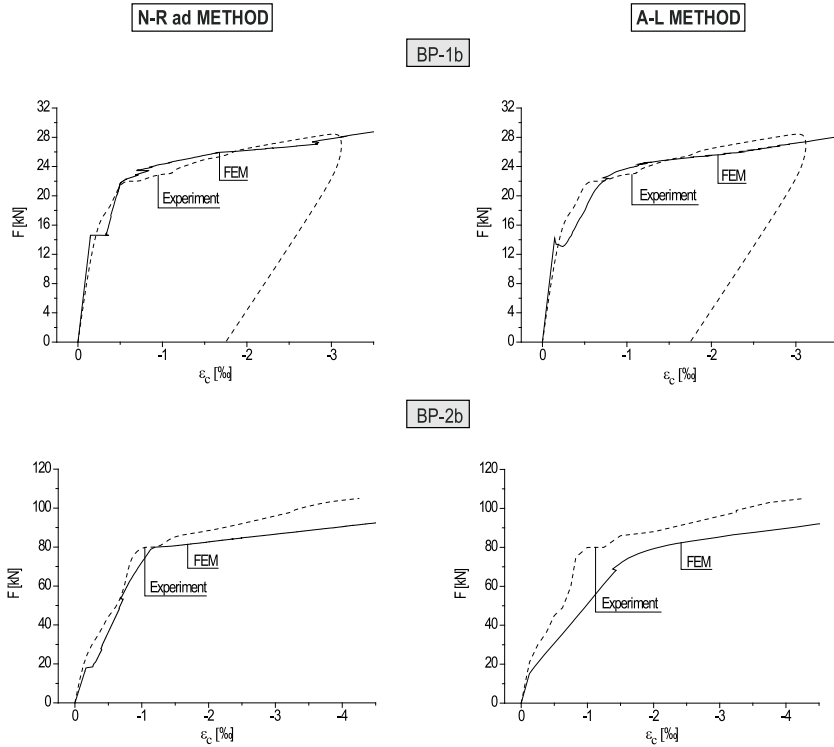


Fig. 5. Comparison of strains in outer layer of concrete in mid span of BP beams

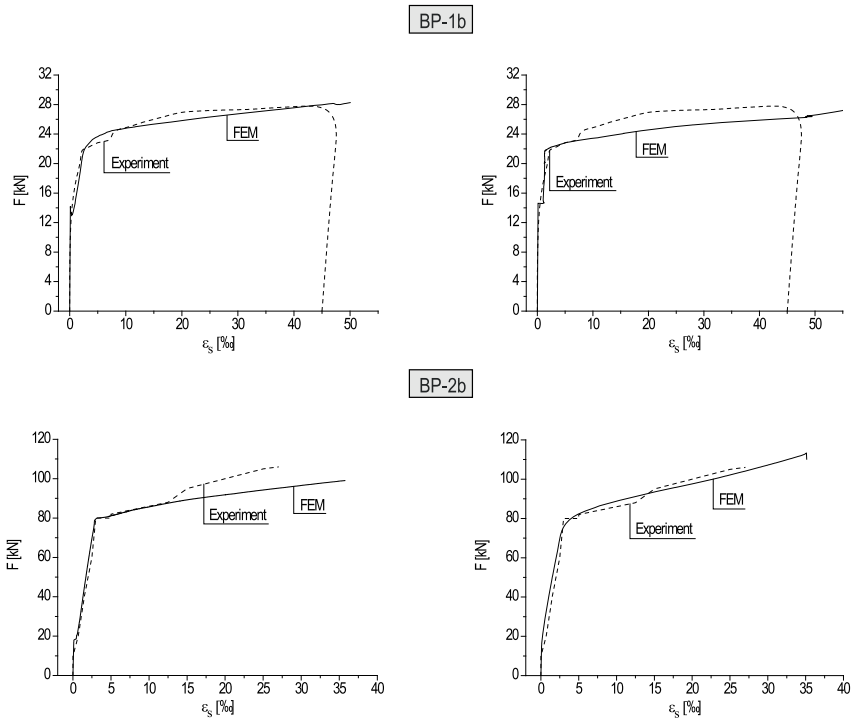


Fig. 6. Comparison of strains in longitudinal bar in mid span of BP beams

The registration of strain changes in tensile reinforcement bar depending on the load level is performed in the mid span cross-section of the beams, Figure 6.

In case of the experimental curve BP-1b also shows the unloading branch member. The numerical results are almost identical in the linear-elastic range as the experimental data.

Load capacity and displacement analysis

Nonlinear load-displacement in the mid span of beams received in numerical analysis in comparison with experimental results are shown in the Figure 7.

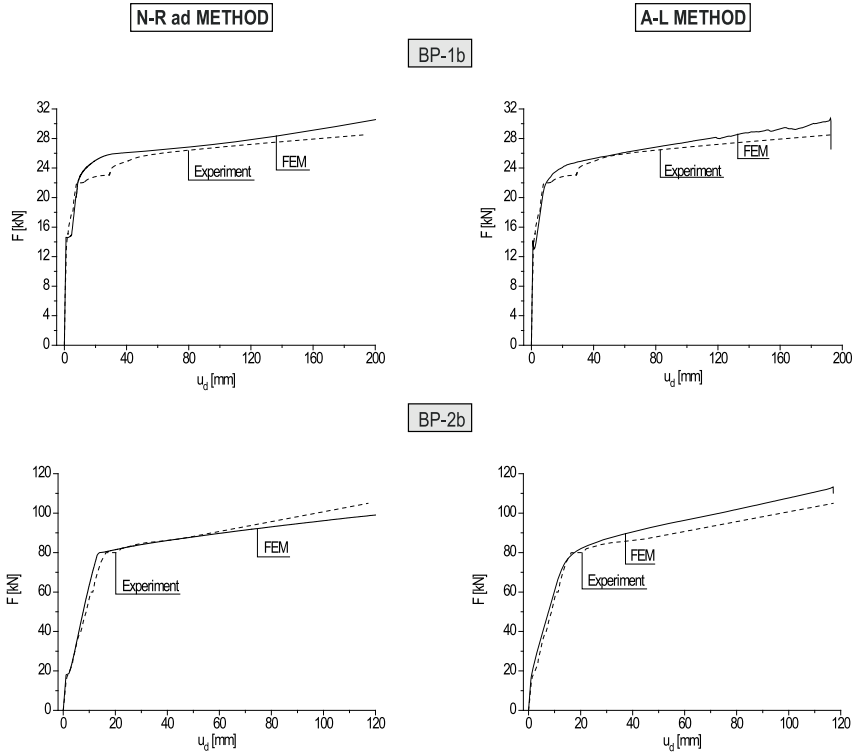


Fig. 7. Comparison of load-displacement at mid span of BP beams

The incremental-iterative methods, both the adaptive descent and the arc-length, give satisfactory numerical results, qualitatively consistent with the experiments. The study on reinforced concrete beams by *e.g.* (Fabbrocino, Pecce 1999, Ashour 2000, Rashid, Mansur 2005), using precise measuring apparatus show that the effects of cracks in the tension zone are not entirely compensated by the elastic properties of steel and plastic properties in the concrete compression zone. Therefore, softening effects are observed on the curve load-displacement as a sudden load capacity drop. These results in presented numerical calculations are possible to obtained using arc-length calculation algorithm which allows to generate a complete load-displacement path with local and global stiffness softening of the structure. In addition, the arc-length method is characterized by high efficiency, because a variable increment step load and properly selected the arc-length parameters provides significant reduction in computation time and makes it possible to obtain very precise numerical solution.

Conclusions

In the modeling of reinforced concrete as simple as possible the finite elements should be used in order to obtain an accurate solution in accepted time. Moreover, especially important is modeling of steel plates in areas of support and load application reflecting the real boundary conditions.

The use of the incremental-iterative arc-length method allows to obtain a complete path of load-deflection with both local and global softening. Moreover, the method is characterized by high efficiency; a variable step of load increments and properly selected arc-length parameters guarantee shortening the time of numerical computing, and additionally very precise solutions. In the presented paper the usefulness of the arc-length method was verified on a spatial numerical model of the reinforced concrete beams with consideration of the concrete softening during compression and tension. The numerical solutions obtained for the reinforced concrete beams are coherent with the experimentally obtained results. This fact indicates the correctness of concrete and reinforcement steel constitutive models and detailed parameters determined these models.

References:

1. Aïtcin P.C. (1998), *High-Performance Concrete*. E & FN SPON.
2. Ashour S.A. (2000), *Effect of Compressive Strength and Tensile Reinforcement Ratio on Flexural Behaviour of High-Strength Concrete Beams*. Engineering Structures, Vol. 22, No 5, 413-423.
3. Bernardi S., Mesureur B., and Rivvilon P.H. (1999), *Cracking of Reinforced High-Strength Concrete Structures*. Proc. 5th International Symposium on Utilization of High Strength / High Performance Concrete, Sandefjord, Norway, Vol. I, 147-153.
4. Calderone M.A. (2009), *High-Strength Concrete. A practical guide*. Taylor & Francis.
5. Comité Euro-Internacional du Béton (1995), *High Performance Concrete. Recommended to the Model Code 90. Research Need*. Bulletin d'Information, Nr 228.
6. Crisfield M.A. (1983). "An arc-length method including line searches and accelerations." *International Journal for Numerical Methods in Engineering*, 19, 1269-1289.
7. Eggert G.M., Dawson P.R., and Mathur K.K. (1991), *An Adaptive Descent Method for Nonlinear Viscoplasticity*. International Journal for Numerical Methods in Engineering, Vol. 31, 1031-1054.
8. Fabbrocino G., Pecce M. (1999), *Experimental Analysis of Influence of Flexure-Shear Interaction on the Rotation Capacity of HPC Beams*. Proc. 5th International Symposium on Utilization of High Strength / High Performance Concrete, Sandefjord, Norway, Vol. I, 243-252.
9. Forde B.W.R., Stiemi S.F. (1987), *Improved arc length orthogonality methods for nonlinear finite element analysis*. Computers and Structures, 27, 625-630.
10. Kamińska M.E. (1999), *Experimental research on HSC one-dimensional members*. Department of Concrete Structures Technical University of Łódź, Poland.

11. Kamińska M.E. (2002), *High-strength Concrete and steel interaction in RC members*. Cement and Concrete Composites, 24, 281-295.
12. Klisiński M. (1984), *Degradation and plastic deformation of concrete*. Institute of Fundamental Technological Research Polish Academy of Sciences Report, Warsaw, Poland, 38, (in Polish).
13. Lambotte H., Taerwe L.R. (1990), *Deflection and Cracking of High Strength Concrete Beams and Slabs*. High-Strength Concrete, Second International Symposium, SP-121, W.T. Hester, ed., American Concrete Institute, Farmington Hills, Michigan, 109-128.
14. Ottosen N.S. (1977), *A failure criterion for concrete*. Journal of the Engineering Mechanics Division, American Society of Civil Engineering, 103, EM 4, 527-535.
15. Pecce M., Fabbrocino G. (1999), *Plastic Rotation Capacity of Beams in Normal and High-Performance Concrete*. ACI Structural Journal, 290-296.
16. Rashid M.A., Mansur M.A. (2005), *Reinforced High-Strength Concrete Beams in Flexure*. ACI Structural Journal, Vol. 102, Nr 3, 462-471.
17. Smarzewski P. (2011), *Modelling of static behaviour of inelastic reinforced high-strength concrete beams*. Monographs – Lublin University of Technology, Lublin, Poland, (in Polish).
18. Stolarski A. (2004), *Dynamic Strength Criterion for Concrete*. Journal of Engineering Mechanics, ASCE, Vol. 130, Nr 12, 1428-1435.
19. Taerwe L.R. (1991), *Brittleness versus Ductility of High Strength Concrete*. Structural Engineering Journal, 4, 40-45.
20. Willam K.J., and Warnke E.P. (1975), *Constitutive Model for the Triaxial Behavior of Concrete*. Proceedings, International Association for Bridge and Structural Engineering, Vol. 19, ISMES, Bergamo, Italy.

MODERN COMPUTER METHODS OF MULTIVARIANT ANALYSIS OF A TALL BUILDING

Sandra Matulewicz, Czesław Miedziałowski

Białystok University of Technology, Faculty of Civil and Environmental Engineering,
Wiejska Street 45E, 15-351 Białystok, Poland
e-mail:s.matulewicz@pb.edu.pl

Summary:

At the beginning of this material to familiarize the reader with the definition of a high building and shows how modern, dynamically developing urban centers and with their growth, increasing the demand for housing high. This is confirmed by the examples presented in the article, the tallest buildings in the world. In this paper we present a variant static analysis of building construction high. It was carried out on the computational model described in point. 2 Calculations were performed in Autodesk Robot Structural Analysis 2012. In the first embodiment focuses on the calculation adopted discretization effects. The analysis was four computational models vary in terms of the finite element shape (square or triangular) and the maximum dimension of the finite element (0.50 m or 1.00 m). We analyzed the behavior of the structure according to the modeled subsoil on which it was set. In this variant, have been studied in two models of the object. In one model was taken into account susceptibility of the ground, while the second vulnerability is omitted and assumed the rigid connection. Another important problem that the stiffness of the building is analyzed, namely the effect of increasing stiffness are located inside the object individual components. Another element that was tested in the calculation of their time and memory occupation. In the last paragraph of articles presents the results of analyzes with figures obtained from the calculation. Selected elements more fully described in the tables. Analysis results were compared with each other and makes appropriate proposals, which were presented in the results of the subsequent variants of the analysis.

Keywords: high building, finite elements, discretization

Introduction

In this work, a multivariate analysis of a tall building, which is more and more common in the urban development, is presented. The definition of a tall building is a controversial issue and generally it is considered to be a building with more than several levels. In accordance with the Order of the Minister of Infrastructure of 12 April 2002 regarding the technical requirements that must be met by the buildings and their location [6], the buildings are classified into the groups in terms of height in order to determine the technical and usage requirements:

- low buildings – up to and including 12 m above the ground level or housing buildings with a height of up to and including 4 above-ground levels;
- mid-low buildings – from above 12 to and including 25 m above the ground level or housing buildings with a height of above 4 up to and including 9 above-ground levels;
- tall buildings – from above 25 up to and including 55 m above the ground level or housing buildings with a height of above 9 up to and including 18 above-ground levels;
- high-rise buildings – from above 55 m over the ground level.

Since tall buildings are used as office or residential blocks, the service loads are not high. However, one of the basic issues is their foundation - the transfer of very high total loads to the ground. As a solution, the foundation is usually a stiffened slab or reinforced concrete box that transfers the pressure to the ground and prevents an uneven foundation of the structure. The other equally important issue is to ensure the appropriate stiffness of the structure, its protection against the effects of operation of horizontal loads (caused by the wind pressure as well as seismic and para-seismic forces). This stiffness is achieved through a proper structure of the building, use of vertical and horizontal membranes – plates formed by walls, cores, pillars and ceilings. There are plenty of unique construction solutions for tall buildings but the most common should be considered the monolithic framework with a stiffened core usually used as a passageway or installation path.

Despite the hardships and costs related to the design and operation of tall buildings, these are erected more and more, with Poland being no exception. Tall buildings ceased to be the pride of rich shopping malls and became the omniscient type of housing and office blocks. Due to the development of conurbations, which entailed the reduction of land for development, the demand for tall buildings has grown. Such buildings have many advantages, such as: housing of a substantial amount of people and large usable area on a relatively small portion of land.

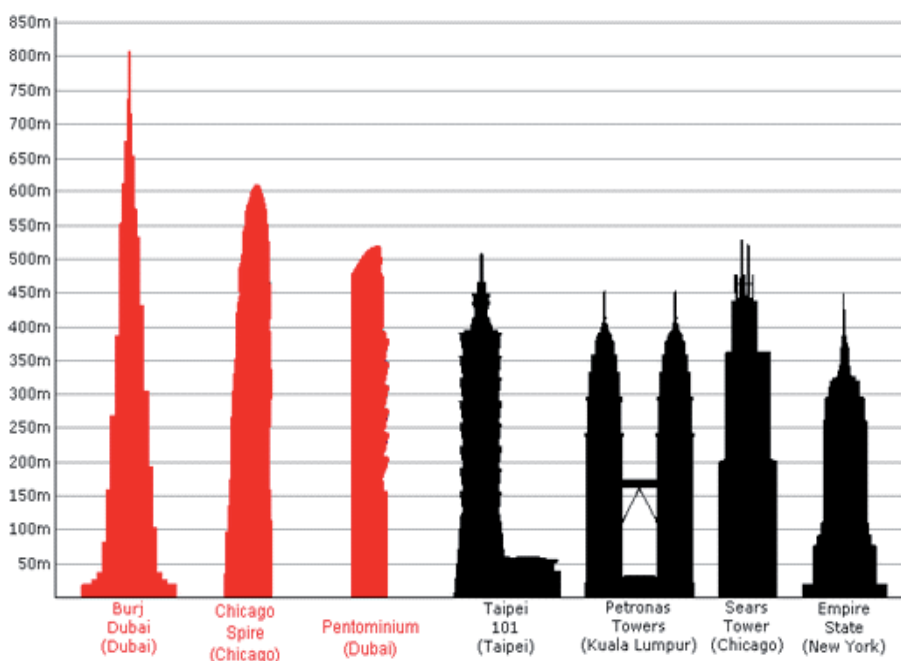


Fig. 1. Classification of the tallest buildings in the world

The examples of tall buildings can be easily found in every larger city. The tallest building in the world is Burj Khalifa in Dubai, the United Arab Emirates. The building has a height of 829 m and boasts 163 service levels. The general appearance and design of the tower reflects the character of the flower of desert and the Islamic architecture (ornaments, decorations, etc.). This tower block consists of the central core and 3 “arms” –the higher the height of the block, its “arms” get smaller, making the block slender and having necessary aerodynamics. On the very top, the central core goes into a spire that finishes the building. The second tallest building in the world is Abraj Al Bait, located in Mecca, Saudi Arabia. This complex of buildings, completed in 2012, has a height of 601 m. It holds several world records: it is the tallest hotel in the world and has the tallest clock tower with the largest clock face. The third tallest building is the famous Taipei 101, the skyscraper with a height of 509.2 m and 101 levels, located in Taiwan. It is also the first building in the world to exceed the height of half a kilometre. It was commissioned in 2004, thus, taking away from Petronas Towers in Kuala Lumpur the title of the tallest building. The greatest challenge was to protect Taipei 101 against earthquakes. This was even harder since at the distance of 200 m from the building is a 10-cm wide tectonic offset. For Taipei 101 to be able to sustain the quakes, the engineers designed a massive structure. The internal core of the building is connected with eight external columns through a net of horizontal trusses. The columns are the backbone of the building allowing its inclination as needed but protecting from fracture. Each building section is independent to other, transferring the weight of the building from external portions towards inside. This idea has already been put in practice but the supporting columns have not been so large ever. The “competition” for the tallest building in the world is still underway. Presently, in Saudi Arabia, the construction of Kingdom Tower is being prepared, the height of which is to exceed one kilometre, while in the United Arab Emirates, a giant with a height of up to 1 mile is planned to be constructed. We may wonder how high are the limits of human capability.

The static analysis of buildings of this type uses the method of folded cantilevers, equivalent frame method, coefficient methods or more universal method of finite elements in computer implementation.

Today, we can use multiple software to perform calculations, design, drawing of the structure, which in combination with the efficiency of the modern computer equipment makes that the time needed to calculate and even design of the majority of types of structures that are common in the engineering practice boils down to a few or several minutes of work. Most time consumes the preparation of the calculation model for analysis. This allows for the projection of the actual structure in the calculation model in the manner as accurate as possible and the possibility not to use a series of simplifications, as well as the long-hour solving of mathematic equations. The problem is, however, in the correct formulation of the calculation model of a structure to be able to obtain as reliable results as possible. Even a seemingly small change in the calculation model can give completely different results of the static analysis of the discussed issue.

Description of the analysed building

The analysed object is a tall, 15-level building, designed based on the monolithic technology of the mixed slab and column construction with a core. Each of the nine levels of the housing part has six flats. The building also has five levels for service and office use, on the 5. floor is a café with a viewing terrace, while the first level is the basement located under the whole area of the object. In the central part of the object is the core with the walls having a thickness of 30 cm, which serves as a passageway. The top of the building is finished with a green flat roof, which is to be the viewing terrace. On the circumference of each level is an edge beam with a rectangular cross section of 35cm x 60cm as functioning in a continuous arrangement. The ceiling slabs are designed as monolithic with a thickness of 20 cm, supported by the columns with a square cross section of 60 cm x 60 cm. The thickness of the flat roof slabs was increased to 25 cm due to the higher load operating. The foundation is a monolithic reinforced concrete slab with a height of 1.00 m. Figure 2 shows the view and cross-section of the analysed building.

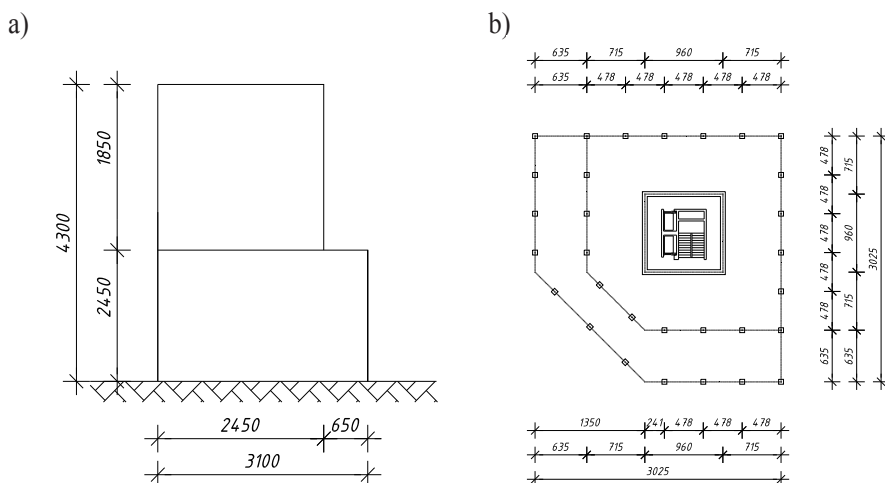


Fig. 2. Analysed tall building a) vertical cross-section b) office level view

Multivariant static analysis of building's structure

In this work, we will present the multivariant static analysis of the structure of the above-described tall building. The calculations were performed in Autodesk Robot Structural Analysis 2012. Robot is an integrated graphic software for modelling, analysis and design of various types of structure. This software allows for modelling of a structure, static calculations, verification of the results, norm calculations of the elements of a structure and creation of a construction documentation.

In the first variant of calculations, the focus is on the impact of the adopted discretisation (shape and size of finite elements). In each of the analysed cases, the complex discretisation in the form of Delaunay + Kang was adopted. The Delaunay triangulation method can be used to form a net of finite elements for any flat surface. If the Kang method is selected, the net will

be generated only near the emitters (user-defined points around which the net is condensed) according to the set parameters. The combination of these two methods means that around these emitters the net will be formed with the Kang method and outside these areas with the Delaunay method. Four calculation models were adopted for analysis, diversified in terms of shape of finite elements (quadrangular or triangular) and maximum size of the finite element (0.50 m or 1.00 m). The net was condensed twice in the points of concentration of stresses, i.e. in edges and support nodes, to the size of a finite element, that is, to 0.25 m or 0.50 m, respectively. Ultimately, in the analysed calculation model the following finite elements were adopted:

- quadrangular with a maximum size of 0.50m;
- triangular with a maximum size of 0.50m;
- quadrangular with a maximum size of 1.00 m;
- triangular with a maximum size of 1.00 m;

Figure 3 below shows the net with quadrangular elements with a maximum size of the element of 1.00 m.

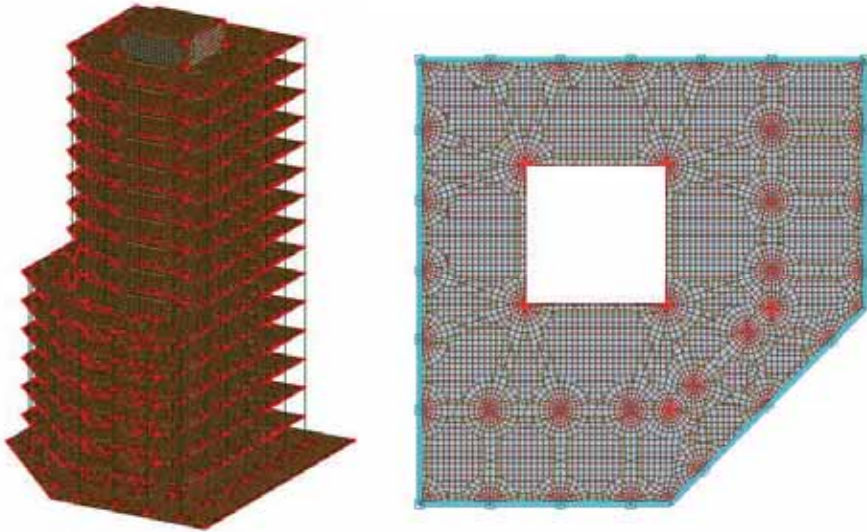


Fig. 3. Adopted discretisation in the calculation software

In the table below the main characteristics is shown for the sizes of the calculation models:

Tab. 1. Characteristics of the calculation models

DISCRETIZATION	quadran. 0,50m	trian. 0,50m	quadran. 1,00m	trian. 1,00m
NUMBER OF NODES	23873	63892	23873	63892
NUMBER OF RODES	732	732	732	732
NUMBER OF AREA	149	149	149	149
NUMBER OF ROD FINITY ELEMENTS	4362	4362	4362	4362
NUMBER OF AREA ES	68227	100575	68227	100575

The behaviour of the structure as a function of the modelled subgrade, on which it was founded, was analysed as well. In this variant, the two models of the above-described object were put to analysis. Both of them were modelled on a square base plate with a length of sides of 10.00 m and a height of cross-section of 1.00 m, with the susceptibility of the subgrade considered in one of them and omitted in the other, where a stiff joint was used. The results of this analysis are shown in the next section of this work.

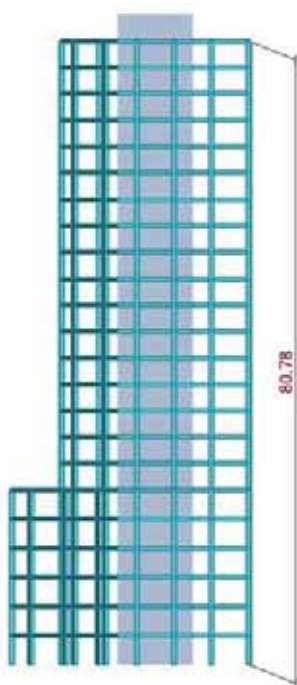


Fig. 4. Analysed building view

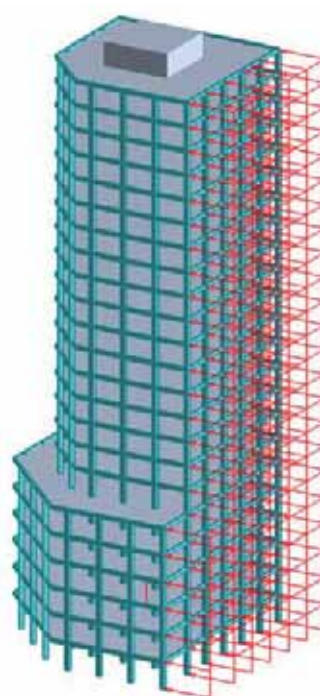


Fig. 5. Wind load on the structure

The next important issue that was analysed is the stiffness of the building. For the purpose of this analysis, the height of the building was increased from 43 m to 80 m (Fig. 4). The building was loaded equally distributed load with a value of 30 kN/m, operating horizontally on the columns and beams situated in the plane of one façade, which is shown on Figure 5.

Initially, the building designed without the walls inside the core was analysed, as shown on Fig. 6 below.

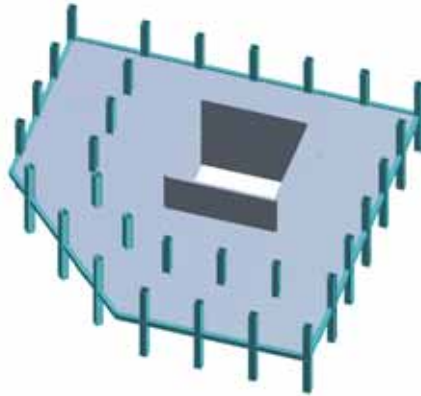


Fig. 6. A level of the analysed building (variant I) with all the structure elements

The second variant of the structure adopted for calculations has an additional stiffening in the form of walls dividing the inside of the core. The purpose of this analysis is to examine how these walls affect the inclination of the building and hence, the stiffness of the structure. The inserted walls are shown on Fig. 7.

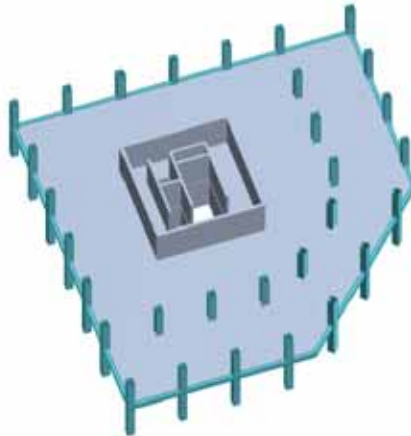
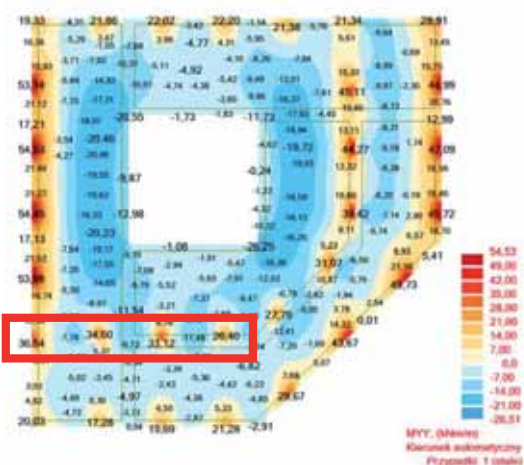
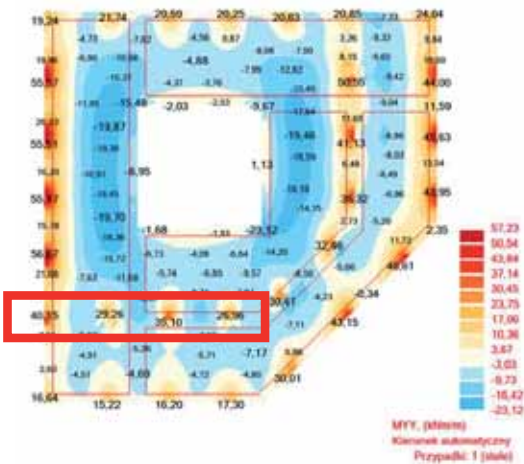


Fig. 7. A level of the analysed building (variant II) with all structure elements

Comparisons and final conclusions

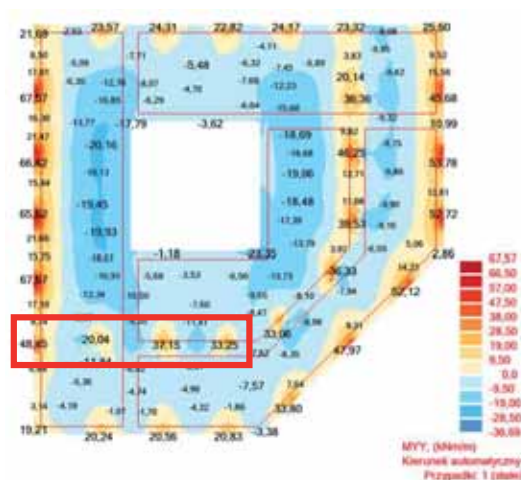
After the static calculations were made, the values of internal forces in the analysed structure with a height of 43 m were obtained. For comparison purposes, the figures below show the maps of bending moments caused by dead loads with various shape and size of finite elements. As can be seen, the description of the structure significantly affects the obtained results. The comparison of the results is shown in Table 2.

a) Quadrangular elements



Triangular elements

b) Quadrangular elements



Triangular elements

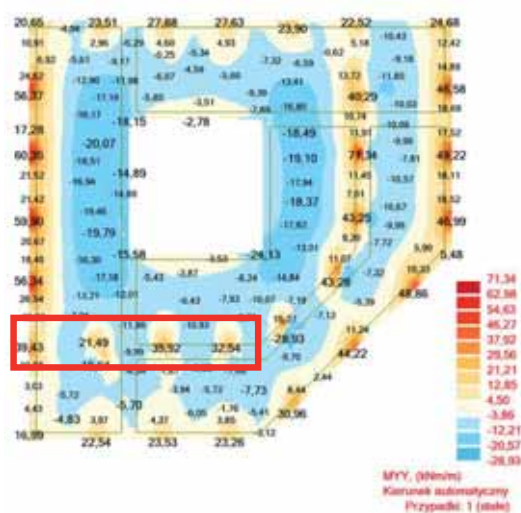


Fig. 8. Maps of bending moments M_y in the analysed ceiling plate; a) dimension of the net element 0.50 m; b) maximum size of the net element 1.00 m.

Tab. 2. Comparison of the obtained values of bending moments in the analysed internal field marked with a frame on Fig. 8.

TYPE FINITY ELEMENTS	support A [kNm]	span 1 [kNm]	support B [kNm]	span 2 [kNm]	support C [kNm]	span 3 [kNm]	support D [kNm]
Quadran. 0,50m	40,15	8,53	29,26	9,67	35,10	9,21	26,96
Trian. 0,50m	36,54	7,78	34,60	9,73	33,12	11,48	26,40
Quadran. 1,00m	48,45	9,56	20,04	9,91	37,15	11,68	33,25
Trian. 1,00m	39,43	9,01	21,49	9,99	35,97	10,93	37,54

The analysis of the structure of a tall building is significantly affected by its deformation due to the vertical and, for the most part, horizontal loads. As it has already been mentioned, the foundation of such a building is of great importance. Below are the results of the analysis of deformation of the structure of a tall building with consideration of the susceptibility of the subgrade, with the full stiff restraint of the base plate. On the figures below marked are the maximum values of the net vector of vertical and horizontal dislocation of nodes, where the dislocations are extreme. The table below shows extreme dislocations towards the axes x, y, z depending on the type of finite elements in a low building.

Tab. 3. Extreme dislocations of nodes in the model with consideration of susceptibility of the subgrade

	UX (cm)	UY (cm)	UZ (cm)	RX (Rad)	RY (Rad)	RZ (Rad)
MAX	0,4	1,6	-0,4	0,003	0,003	0,000
Nod	22132	22140	10234	15062	15140	19253
MIN	-1,7	-1,0	-3,7	-0,003	-0,003	-0,000
Nod	22128	22092	15150	15478	15550	18705

Tab. 4. Extreme dislocations of nodes in the model without consideration of susceptibility of the subgrade

	UX (cm)	UY (cm)	UZ (cm)	RX (Rad)	RY (Rad)	RZ (Rad)
MAX	0,1	0,3	0,0	0,003	0,003	0,000
Nod	21988	22145	310	5889	15400	15057
MIN	-0,3	-0,1	-1,3	-0,003	-0,003	-0,000
Nod	22121	22228	15146	15304	5712	15228

a)



b)



Fig. 9. Deformation of the object a) with consideration of susceptibility of the subgrade b) with a stiff restraint of the base plate

The fig. 9 shows the deformations of the structure due to the susceptibility of the subgrade. As it can be noted, the structure elements of the designed tall building are subject to much greater deformations assuming the susceptibility of the subgrade under the foundation.

As implied by the performed analyses, the size of the finite elements affects the accurate determination of the result of calculations. It is noted that at the greater size of the elements, the moments are greater as well. The size of the calculation elements should be selected not to allow the values of the forces operating in the structure exceed 5% [2]. The greater size of the finite element causes less accurate results and greater deviation, therefore the smaller size of finite elements should be used. Thus, the selection of the correct size of the element depends on the accuracy of the projected results and reasonable condensation of the partition net, which afterwards, affects the calculation time and transparency of results. Based on these results of calculations, we also found that the shape of the element does not affect that much the results of bending moments as obtained here.

Below are the results of two variants of analysis of stiffness of a tall building. Variant I does not consider the walls inside the central core of the building, and variant II was analysed with vertical partitions modelled, located inside the passageway. Table 2 shows the results of maximum dislocations of nodes caused by the applied operational and wind load.

Tab. 5. Maximum dislocation of structure nodes (variant I)

	UX (cm)	UY (cm)	UZ (cm)	RX (Rad)	RY (Rad)	RZ (Rad)
MAX	0,4	0,5	1,9	0,003	0,003	0,000
Nod	49423	49458	44900	26436	38539	241
MIN	-25,4	-0,4	-1,9	-0,003	-0,004	-0,000
Nod	49609	49604	38612	38318	26259	502

Tab. 5. Maximum dislocation of structure nodes (variant II)

	UX (cm)	UY (cm)	UZ (cm)	RX (Rad)	RY (Rad)	RZ (Rad)
MAX	0,4	0,5	1,8	0,003	0,003	0,001
Nod	49423	49458	44900	26436	38539	241
MIN	-24,6	-0,5	-1,8	-0,003	-0,004	-0,001
Nod	49609	49604	38612	38318	26259	502

UX dislocations are horizontal dislocations parallel to the operation of wind pressure, UY – horizontal dislocations perpendicular to the operation of wind pressure, UZ – vertical dislocations. As can be read from Table 2, subject to the greatest horizontal dislocation is the node no 49609, which was marked on Figure 4 below. The dislocation obtained is quite significant and exceeds the permissible standard deviation, however, it is done on purpose through the increase of a height of the building and the value of the horizontal load operating on the structure to make the difference between variant I and II more noticeable.

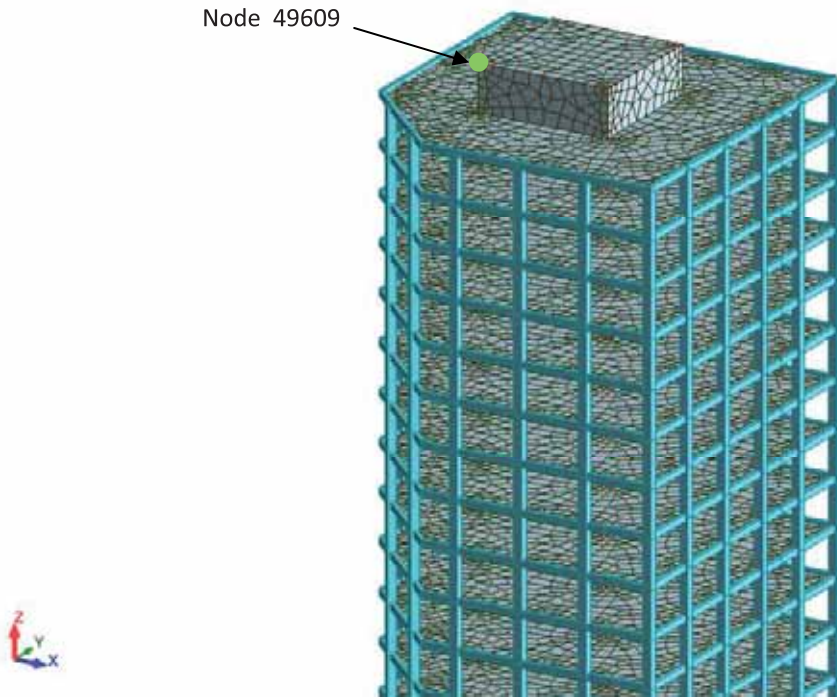


Fig. 10. The node subject to greatest dislocation

By comparison of the results obtained from two variants of analysis of stiffness of the building, it was found that the greatest stiffness in the analysed tall building is achieved by the columns designed on the external circumference of the object, having a significantly greater moment of inertia due to their position against the centre of gravity of the horizontal view of a building's level. Additional stiffness is achieved by the core designed at the centre of the object, while the vertical partitions in the inside of the structure indeed provide extra stiffness but not that much. After the insertion of additional walls to the model, the maximum dislocation of a node decreased by just 0.3 cm.

The additional element tested during the measurements was their duration and usage of memory. As already mentioned, with the today's equipment and software available, the effect of these two factors on the design of the structure is virtually negligible. The time needed to carry out the measurements for the above-described analyses was around 8 minutes, and the usage of memory – around 135000000 B. The recorded time values obviously do not consider the time used for modelling of this structure in the calculation software, where it is as long as from a few to several days depending on the complexity of the structure.

References:

1. Ajdukiewicz A., Starosolski W. (1981), *Żelbetowe ustroje płytowo-słupowe*. Arkady, Warszawa.
2. *Autodesk Robot Structural Analysis 2010 – Podręcznik użytkownika*.
3. Kapela M., Sieczkowski J. (2003), *Projektowanie konstrukcji budynków wielokondygnacyjnych*. Oficyna Wydawnicza PW, Warszawa.
4. Matulewicz S. (2012), *Praca dyplomowa magisterska.: Projekt budynku wysokiego mieszkało-usługowego*. Białystok.
5. Pawłowski A.Z., Cała I. (2006), *Budynki wysokie*. Oficyna Wydawnicza PW, Warszawa.
6. Rozporządzenie Ministra Infrastruktury z dnia 12 marca 2009r. w sprawie warunków technicznych jakim powinny odpowiadać budynki i ich usytuowanie. (Dz. U. nr 56, poz. 461 zmieniające Dz. U. nr 75 poz. 690 z dnia 12 kwietnia 2002r.).
7. Starosolski W. (2012), *Komputerowe modelowanie betonowych ustrojów inżynierskich*. Wydawnictwo Politechniki Śląskiej, Gliwice.

NONLINEAR ELASTIC-PLASTIC 3D-FINITE ELEMENT MODELLING OF SEMI-RIGID STEEL END-PLATE CONNECTIONS

Agnieszka Jabłońska-Krysiewicz, Emilia Waśniewska

Białystok University of Technology
Wiejska Street 45E, 15-351 Białystok, Poland
e-mail: a.krysiewicz@pb.edu.pl

Summary:

Although the effect of semi-rigid steel beam-to-column connections on the behaviour of steel frames and their substantial economical benefits are recognized nowadays, many structural analyses still consider connections as either fixed or pinned. For that reasons, there is need to be able the generate moment-rotation responses of semi-rigid connections that can be used for analysis and design proposes. Numerical elastic-plastic 3D finite models was performed in order to establish a numerical analysis method for evaluating deformation of extended end-plate-beam-to-column joint for varying thickness of end plates. There were used contact elements between bolts and beam and column. This kind of model was generated by using the FEM software package ANSYS version 14. The study were performed the influence of thickness of end plates on moment-rotation curves for analysing joints and proved that the FE technique was capable of prediction connection response to an acceptable degree of accuracy.

Keywords: Steel joints, end plate, FE modeling, nonlinear analysis

Introduction

Cost optimization is one of the most important items in steel construction in order to be competitive in the market of buildings. The joints determine almost 50 % of the total cost of steel structure. The cost of joints can decrease substantially if stiffeners between flanges can be avoided (Bijlaard 2006). The distribution of forces and moments in the structure due to the loading is a result of the strength and stiffness distribution in the structure. So the structural characteristics of the joints such as stiffness, strength and rotation capacity, together with those of the structural components like beams and columns, produce these forces in the joints. This means that the choices made by the designer in designing the joints, including the connecting parts, are of direct influence on the level of forces and moments in these joints. In fact construction is joining components such as column and beams together while designing is making choices for components taking the structural properties such as strength as stiffness into account.

In traditional design it is assumed that the joints are stiff and strong and the forces and moments in the structure can be determined using the linear-elastic theory (Bródka et al., 2011). Because it is assumed that the joints were stiff, it needs to be checked whether the joints are really stiff.

In modern design the joints are considered as structural components such as column and beams with properties as stiffness, strength and deformation capacity. These structural properties of the joints are incorporated into the design on the same level as those of column and beams. The joint layout should only be influenced by fabrication considerations for easy and safe construction on-site.

Eurocode 3 part 1-8 “Design of Joints” (EN 1993-1-8) provides the rules to determine the structural behaviour of joints in terms of strength, stiffness and deformation capacity. If the designed joints are out of scope of Eurocode 3, experiments and FEM modeling have to be carried out to obtain reliable design values for the structural properties.

Aim of studies

The aim of these studies is to develop the FEM model of extended end-plate beam-to-column connections (Fig.1) and obtained moment-rotation curves for varying thickness of end plates, from very small thickness to thicker one.

There were used hot rolled sections IPE240 as a beam, HEB200 as a column and 10.9 grade high strength bolts with a diameter of 16 mm. In testing joints according to EC3 (ENV 1993-1-8) there were involved three thicknesses of end plate: 6 mm, 10 mm and 20 mm. All parts of connection (without bolts) were designed from steel grade S235. Key geometric parameters of specimen are shown in Fig.2

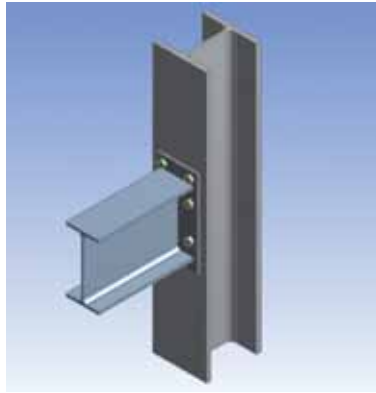


Fig. 1. Extended end-plate beam-to-column connection

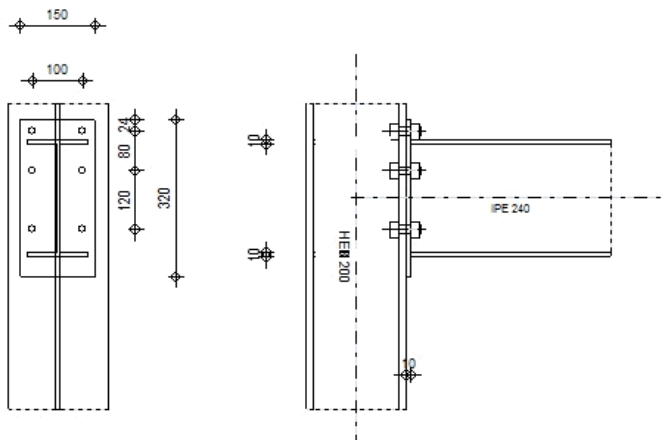


Fig. 2. Geometry of beam-to-column joint.

Modelling of bolted joints is rather complex problem because it involves geometrical and material non linearity, and the contact problem between components of the connections as well as a selection of suitable type of finite elements for modeling joint components. In spite of this difficulties and complexities, a large number of advanced FE studies have been conducted on end plate connections (Giżejowski et al. 2008, 2010, Chen and Du, 2007, Maggi et al., 2005, Abolmali et al., 2005) and other types of connections (Jabłońska-Krysiewicz 2011, Huang et al., 2010, Reinoso et al., 2008, Kim and Oh, 2007, Urbonas and Daniunas 2006, Citipitioglu, 2002) to provides stiffness, strength and ductility estimates for large variety of connection geometries. In general, these detailed studies have attempted to develop global connection behaviour responses, for example moment-rotation curves, that can be readily incorporated into modern structural analysis programs like ADINA, COSMOS, NASTRAN, ANSYS, and ABACUS. This objective was addressed through the using the FEM software package ANSYS version 14 (ANSYS Manual 2013).

FE modeling

General

The numerical tests were carried out by code ANSYS –Workbench version 14 (ANSYS Manual 2013). Solid 186 elements were used to mesh the beam, column, end plate and bolts. Contact surfaces between the flange of column and end plate, the bolt shanks and end plate and flange of column, and nuts and heads of bolts and flange of column and end plate are meshed by Conta174 elements. The description of these elements taken from ANSYS Manual (ANSYS Manual 2013) is listed in the next section. The coefficient of friction of 0.2 is employed for contact surfaces. The meshed FE models of connection and bolt are shown in Fig.3.

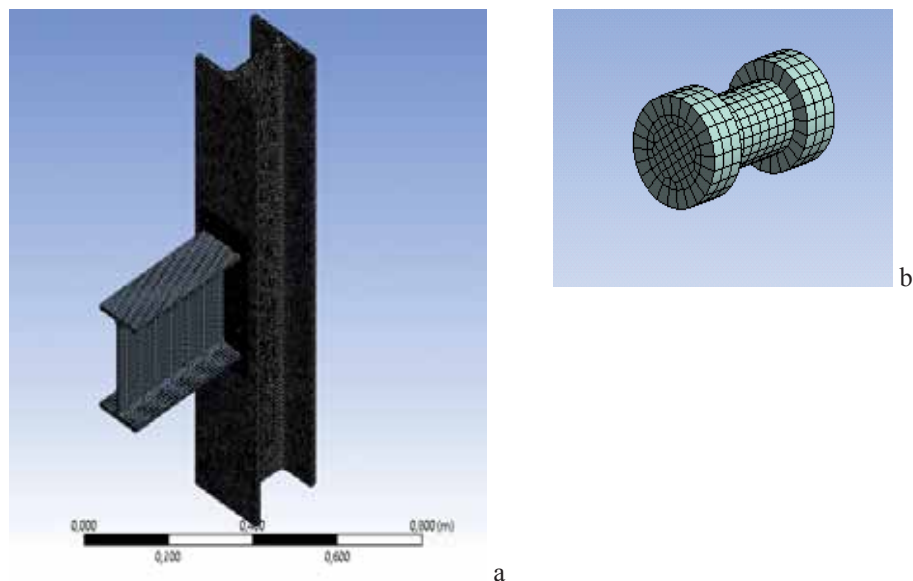


Fig. 3. Finite element models: a) end plate-beam-to-column-connection, b) bolt.

Element description

Solid 186

Solid 186 is used for the 3-D modeling of solid structures. The element is defined by twenty nodes having three of freedom at each node: translation in the nodal x, y and z directions. The element has plasticity, creep, swelling, stress stiffening, large deflection and large strain capabilities. Geometry of the element is shown in Fig.4.

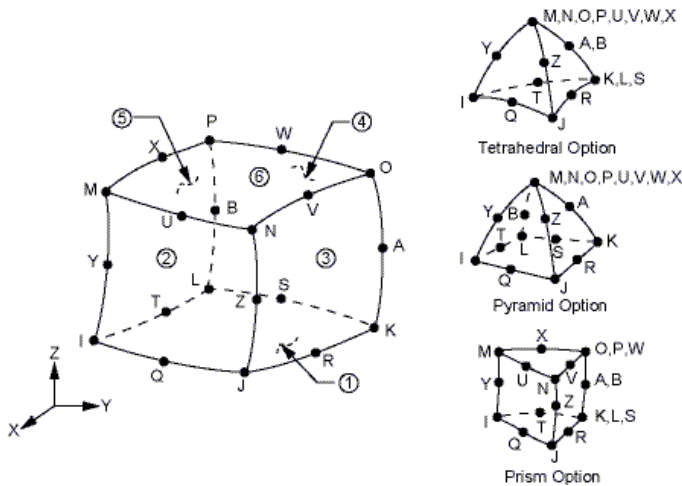


Fig. 4. Geometry of Solid 186 element (ANSYS Manual 2013)

Conta174

Conta174 is used to represent contact and sliding between 3-D “target” surfaces (Target170) and deformable surfaces, defined by this element. The element is applicable to 3-D structural and coupled field contact analyses. This element is located on the surfaces of 3-D solid elements. It has the same geometric characteristics as the solid element face with which it is connected. Contact occurs when element surface penetrates one of the target segment elements (Targe 170) on a specified target surface. Coulomb and shear stress friction is allowed. In Fig.5 there are shown geometry of the element.

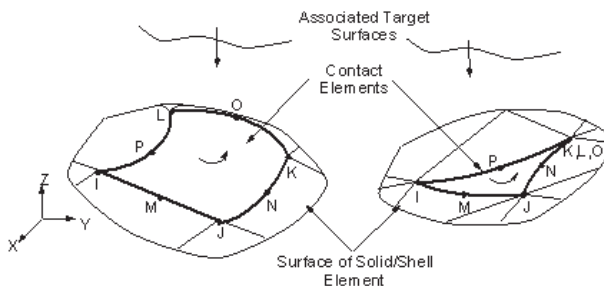


Fig. 5. Geometry of Conta174 element (ANSYS Manual 2013)

Material property

The 3-D model uses the bilinear isotropic hardening option for plate elements of joints. The von Mises yield criteria was employed to define the plasticity. For this option is preferred for large strain analyses. The material behaviour is described by bilinear stress-strain curve. The initial slope of the curve is taken as the elastic modulus of the material. At the yield stress, the curve is continuous along the second slope defined by the tangent modulus (Fig.6). The tangent modulus is defined as about 0.1 % of the initial modulus of elasticity. For bolts there are used linear model of material. The material property of plate components and bolts in joints are listed in Table.1.

Tab.1. Material properties

Elements	Yield stress [MPa]	Ultimate stress [MPa]	Elastic modulus [GPa]	Tangent modulus [MPa]
Beam, column, End plate	235	360	210	360
Bolts	900	1000	210	-

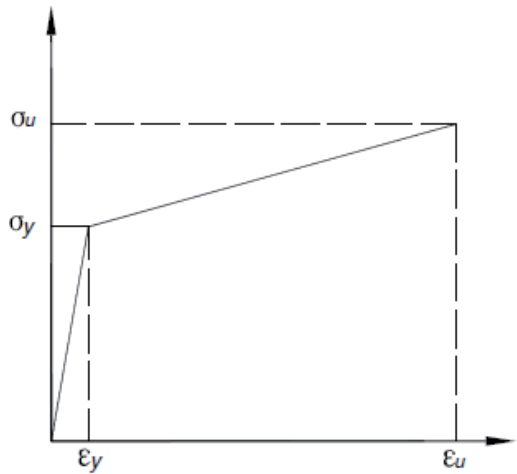


Fig. 6. Stress-strain curves for plate elements of connection

Testing results

Three numerical analyses for vary thicknesses of end plate were made. The bending moment and axial forces were applied to free end of beam section in 10 steps of load to keep respectively value of moment in each connection. The comparison of moment-rotation curves achieved from FE model calculation for thicknesses 6mm,10mm and 20mm was depicted on Fig.7.

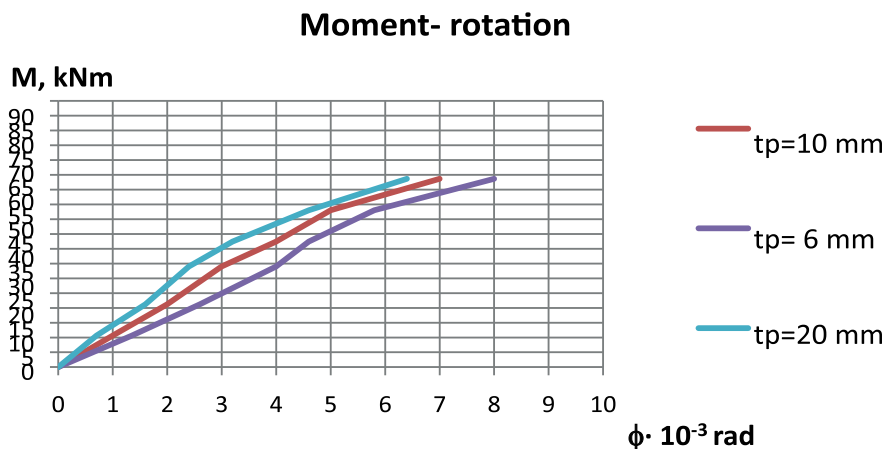


Fig. 7. Moment rotation curves for vary thicknesses of end plate

We can see that initial connection stiffness is affected by end plate thickness what is according to initial stiffness $S_{j,ini}$ obtained from formulas proposed by Pisarek and Kozłowski (Bródka, Kozłowski, 1996) based on component method described in EC3 (EN 1993-1-8) for such kind of joints. In Table 2. there are shown values of $S_{j,ini}$ for each connection.

Tab. 2. Initial stiffness values for connections with end plate thicknesses of 6mm, 10mm and 20mm.

End plate thickness [mm]	Initial stiffness $S_{j,ini}$ [kNm/rad]
6	4980
10	5955
20	7590

For each connection moment-rotation curve from FEM there were compared with curve calculated according EC3 model. For all thickness of end-plate there were obtained good agreement. To show it $M-\phi$ curve from FE and Eurocode 3 were depicted in Fig.8. We can see that the FE results lightly overestimates results achieved from component method from EC3. It was caused probably by using linear model of material for bolts in numerical analysis.

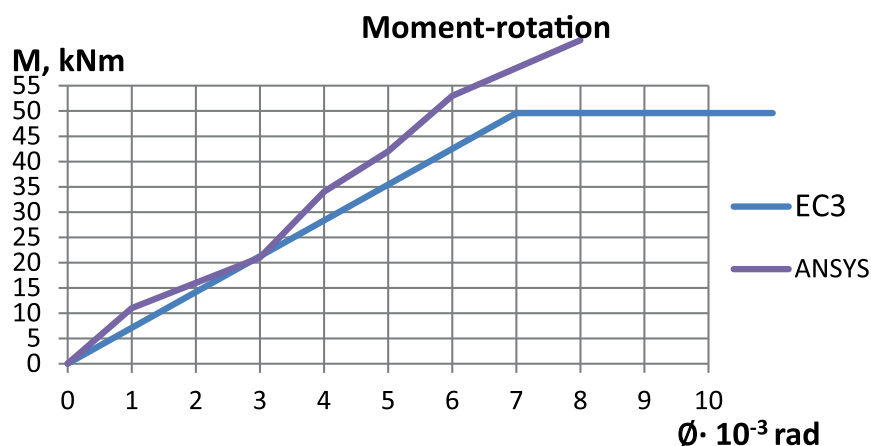


Fig. 8. Moment-rotation curve for connection with end-plate thickness value 20 mm.

The deformation of end plate has important influence on response of the connection, specially on displacement of beam. Using of thicker end plate causes increasing in displacement values of end of IPE section. To notice this effect in connection behaviour there is shown deformation of end plate in each step of load in Fig.9. Based on this results it can be observed 14 % decreasing in deformation value for joint with 10 mm plate and 24% for 20 mm in compare to 6mm end plate thickness. Additionally, to confirm that the joint behaviour is governed by geometry of its components the views of deformed shapes at ultimate state of load are shown in Fig.10.

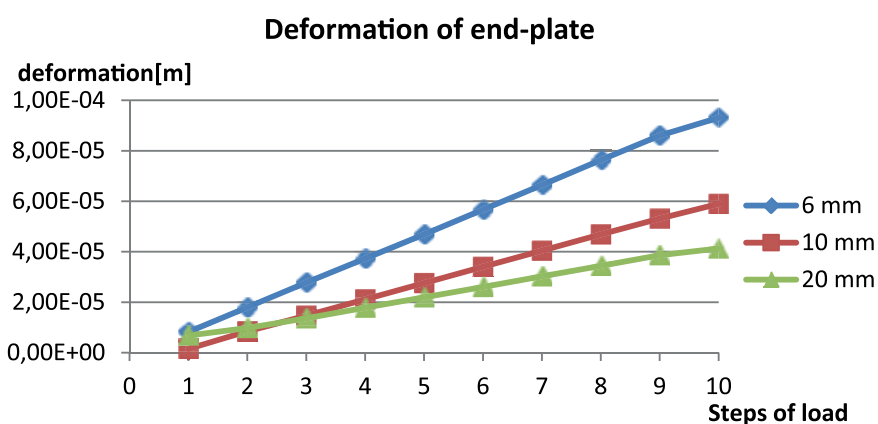


Fig. 9. Curves deformation versus steps of load for different values of end plates.

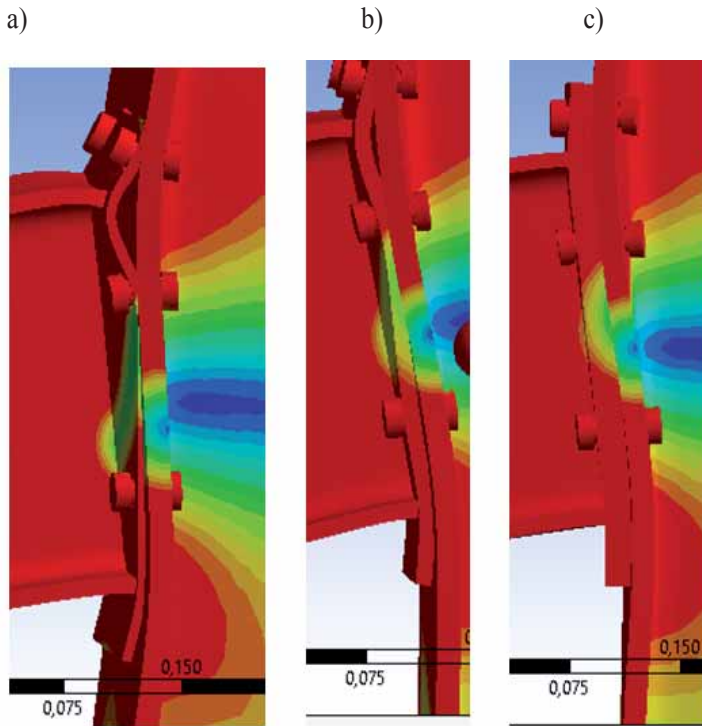


Fig.10. Deformed shapes at ultimate state of load for end plate value: a) 6 mm, b) 10 mm, and c) 20 mm.

These results show that in case of employment of using thicker end plate it does not come to its breaking away from column flange. For thinner end plate the flexural mechanism of its collapse has a much effect on ultimate shape of connection. This phenomena was observed by Maggi (Maggi et al, 2005) in experimental tests and numerical analyses of steel bolted end-plate joints. The mechanisms of destruction of analyzed connections are according to component method which is described in Part 1-8 of Eurocode 3.

Conclusions

In order to establish a numerical analysis method for estimating moment-rotation curves of end-plate-beam-to-column connections 3-D FE analyses have been performed. Finite element models have included material, geometric, and contact nonlinearities and large displacements. The numerical investigation has shown that thickness of end plate is one of most important parameters for representing connection behaviour and its influence on connection response is significant. It was observed that initial stiffness was proportional to increasing of the end-plate thickness, while the free end of beam displacement was inversely proportional. Moment-rotation curves from numerical investigation showed good agreement with curves calculated according to component method from EC3.

Finally, the results of numerical tests has conducted that FE method is a powerful tool to improve the knowledge about connections.

References:

1. Abolmaali A, Matthys J. H., Farooqi M., Choi Y. (2005), *Development of moment – rotation model equations for flush end-plate connections*. Journal of Constructional Steel Research Vol 61, pp. 1595-1612.
2. ANSYS Manual. ANSYS 14.0. On line help.
3. Bijlaard F. (2006), *Eurocode 3, basis for further development in joint design*, Journal of Constructional Steel Research Vol 62, pp.1060-1067.
4. Bródka J., Kozłowski A, Ligocki I, Łaguna J., Ślęczka L. (2013), *Projektowanie i obliczanie połączeń i węzłów konstrukcji stalowych*, Polskie Wydawnictwo Techniczne, Rzeszów .
5. Bródka J., Kozłowski A. (1996), *Sztywność i nośność węzłów podatnych*. Wydawnictwo Politechniki Białostockiej i Oficyna Wydawnicza Politechniki Rzeszowskiej, Białystok-Rzeszów.
6. Chen S., Du G. (2007), *Influence of initial imperfection on the behaviour of extended bolted end-plate connections for portal frames*, Journal of Constructional Steel Research Vol 63, pp.211-220.
7. Citipitioglu A. (2002), *Refined 3D finite element modelling of partially restrained connections including slip*, Journal of Constructional Steel Research Vol. 58 (8) pp. 995-1013.
8. ENV 1993-1-8: Eurocode 3, Design of Steel Structures, Part 1-8 Design of Joints.
9. Gizejowski M., Salah W., Barcewicz (2010), *Finite element modelling of the behaviour of certain class of composite steel-concrete beam-to-column joints*, Archives of Civil Engineering, LVI,1,2010.
10. Gizejowski M., Salah W., Barcewicz W. (2008), *Steel beam-to-column Bolted joint with thin end-plates*, Proceedings of EUROSTEEL 2008, 3-5 September 2008, Graz, pp. 483-488.
11. Huang Y., Wang R., Zou J., Gan Q. (2010), *Finite element analysis and experimental study on high strength bolted friction grip connections in steel bridges*, , Journal of Constructional Steel Research Vol. 66, pp. 803-815.
12. Jabłońska-Krysiewicz (2011), *Analiza numeryczna i eksperymentalna stalowych węzłów ze śrubami sprężonymi*, Zeszyty Naukowe Politechniki Rzeszowskiej, Budownictwo i Inżynieria Środowiska, Z.58, s. 241-248.
13. Kim Y.-J., Oh S.-H. (2007), *Effect of the moment transfer efficiency of a beam web on deformation capacity at box column-to-H beam connections*, Journal of Constructional Steel Research Vol. 63, pp.24-36.
14. Maggi Y.I., Goncalves R.M., Leon R.T., Ribeiro L.F.L. (2005), *Parametric analysis of steel bolted end plate connections using finite element modelling*, Journal of Constructional Steel Research Vol. 61,pp. 689-708.
15. Reinoso J.M., Loureiro A., Gutierrez R., Moreno A., (2008), *Nonlinear elastic-plastic 3D finite element modelling*, Proceedings of EUROSTEEL 2008, 3-5 September 2008, Graz, pp. 501-506.
16. Urbonas K., Daniunas A. (2006), *Behaviour of semi-rigid steel beam-to-beam joints under bending and axial forces*, Journal of Constructional Steel Research Vol. 62, pp. 1244-1249.

METHOD OF EMBANKMENT MODELING USING ONE-DIMENSIONAL LAYERED FINITE ELEMENTS

Tadeusz Chyży, Monika Mackiewicz

Białystok University of Technology, Faculty of Civil and Environmental Engineering,
Wiejska Street 45E, 15-351 Białystok, Poland
e-mail: m.mackiewicz@pb.edu.pl

Summary:

An original method of computer modeling of ground layers in road embankments has been presented in the paper. A particular areas of presented method application are structures with a large distinctions in the stiffness parameters of each layer of the ground. These changes could be done by an emergency situations or simply by the errors made during the realization processes. The issue of the method is the use of a special finite elements, as a springs, for modeling of whole layered cross-section of road embankment. One single special linear finite element, which describes spring in Finite Element Method, is divided into sub-areas. Each sub-area can be separately integrated and the same can have different stiffness and geometric parameters corresponding to the particular layer of subsoil or road embankment. Shape functions in so defined finite element need to be modified. Modification is necessary for matching the strain field distribution to the changes of the ground parameters. An example for subsidence calculation of layered road embankment has been done. Results were obtained from the different calculation methods. Comparison of these obtained results has been presented in the paper. A precise description of a special finite element and example of its application in the modeling of road embankments has been explained in the paper.

Keywords: road embankment, subsoil, FEM, shape functions

Introduction

The buildings and the road constructions have their own specific tasks to fulfill. To ensure durability and safety of construction, the issue of cooperation between construction and the subsoil should be considered. The same what is the foundation for building, the same for road construction is subsoil placed exactly under the pavement. If the walls of buildings cracks, it means the foundation is too weak. For comparison, if the pavement surface cracks it might be a sign that embankment is too weak. Therefore in the pavement surface structure could appear damages, as a result of degradation of the embankment layers. In addition, in this case there is another factor causing the greatest danger. This factor is of course water, which penetrates the pavement surface structure for example through the dilatation. The result of it might be a significant weakening of the subsoil capacity. A dank embankment lose capacity due to sedimentation and subsidence under load. In winter, there is another risk in form of uneven lifting of the ground. As a result of it, pavement surface is lifted, as well. In this case the pavement plate could be easily broken under its own weight or under car load.

Therefore there is a problem with a proper modeling and the same with a calculation of road embankments. Especially embankments, which might have design errors or defects made during the realization process. Very often on the construction site a lot of

errors and mistakes are made. As a reasons of it could be listed for example remissness or simply lack of knowledge and experience of workers. The consequence of not sufficient realization is lack of proper embankment strength. That is why first of all special attention should paid to the mistakes made during the compacting of embankment layers. The process of ground densification is very important for giving a proper load capacity for each layer. Defects of one road embankment layer can influence of stability and capacity of all construction in this range. So it is very important to control the quality and parameters of each embankment layer during the erection process.

The idea of one-dimensional special finite elements application for Finite Elements Method modeling analysis of layered road embankment, has been presented in the paper. In the analysis, one of the simplest ways of computer modeling of ground, which is the Winkler's model, has been used. In this model the subsoil is considered as one-dimensional set of springs. These springs have assigned appropriate stiffness parameters, to describe the characteristic of the subsoil.

In justified cases, the Winkler's method can be used in modeling multilayered subsoil. In this model, subsoil is considered as a set of springs connected in series, where each layer of springs describes a particular layer of embankment (Fig. 1). So the stiffness parameters of springs are corresponded to adequate layer of subsoil. Eventually resultant stiffness is achieved as a result of the relevant summation of stiffness components. Different idea of the resultant stiffness determination with the direct use of Finite Element Method algorithms (Bathe 1996) (Zienkiewicz et al., 2005) is proposed in the paper.

The conception of special finite elements

In the analysis, model of interaction between concrete plate (pavement) and road embankment based on Winkler's hypothesis and application of one-dimensional springs, as a subsoil model, has been used (Fig. 1b). The idea of presented conception is application of special linear finite elements (springs). All layered cross-section of embankment can be modeled by one single element (Fig. 1c). The conception has been presented in the Figure 1.

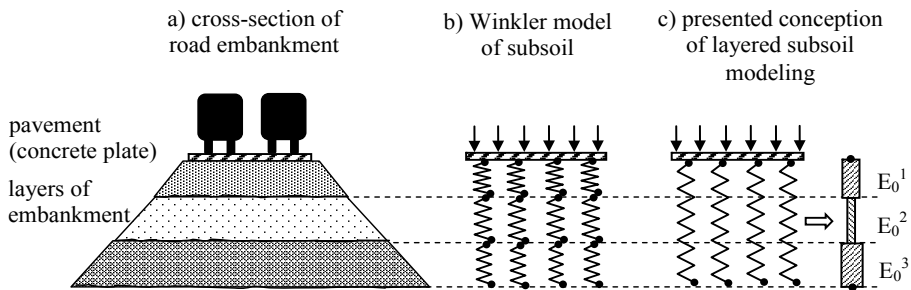


Fig. 1. Conception of one-dimensional layered finite elements in road embankment modeling.

In modeling of layered embankment by one finite element, there is a problem with appropriate description of influence of the individual layer stiffness parameters on the resultant stiffness. The problem is solved by the use of a special finite element (spring)

with variable stiffness in the areas of approximated strain field and with the possibility of controlled changes in stiffness and geometry. Structure of defined finite element requires integration in sub-areas. The conception of elements integrated in sub-areas is based on a division of element e into n parts (sub-areas), Figure 2. The stiffness matrix for one element e is obtained by the aggregation of partial stiffness matrix from each sub-area, which is given by:

$$\mathbf{K}_e = \mathbf{K}_1 + \mathbf{K}_2 + \mathbf{K}_3 + \dots = \int_0^{g_1} \mathbf{K}_e^1(\xi) d\xi + \int_{g_1}^{g_2} \mathbf{K}_e^2(\xi) d\xi + \int_{g_2}^{g_3} \mathbf{K}_e^3(\xi) d\xi + \dots = \sum_{k=1}^n \mathbf{K}_e^k \quad (1)$$

Stiffness matrix for the sub-area k of finite element e (spring) is determined from the equation:

$$\mathbf{K}_e^k = \oint_{V_k} \mathbf{B}_e^{kT} \cdot \mathbf{D}_e^k \cdot \mathbf{B}_e^k \cdot dV_k \quad (2)$$

where: \mathbf{B}_e^k – strain shape matrix of sub-area (layer) k ,
 \mathbf{D}_e^k – elasticity matrix of sub-area (layer) k ,
 V_k – integration volume,
 g_k – the depth of the layer k bottom.

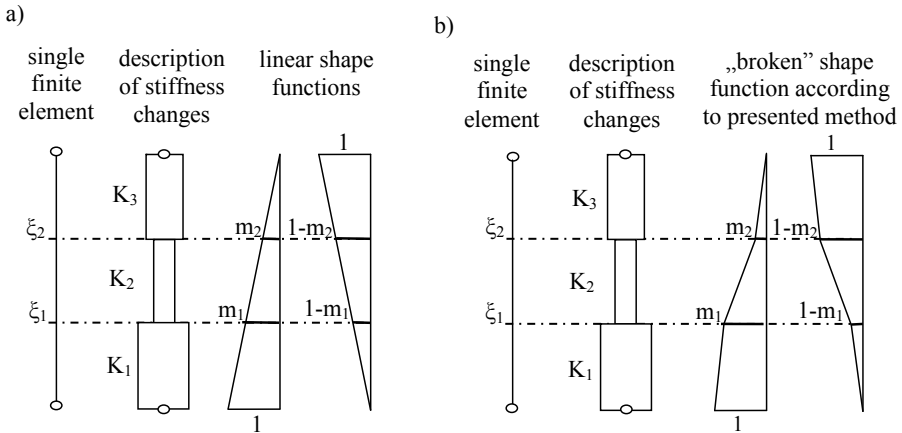


Fig. 2. Division of the finite element into sub-areas.

So defined finite element, shown in Figure 2a, with assumed linear distribution of strain field (standard solution) leads to an erroneous results. It has been illustrated in Figure 3 (Mackiewicz 2012). This is related to the effect of the finite element stiffness increase.

The reason of it, is lack of strain changes adaptability to differences in stiffness parameters inside of the element. To eliminate this effect “broken” shape functions have been used, Figure 2b. Stiffness matrix of so defined finite element is described in the following form:

$$\mathbf{K}_e^k = b^2 \cdot \frac{EA}{L} \cdot \int_{\xi_1}^{\xi_2} \begin{bmatrix} 1 & -1 \\ -1 & 1 \end{bmatrix} d\xi = \begin{bmatrix} b^2(\xi_2 - \xi_1) \cdot \frac{EA}{L} & -b^2(\xi_2 - \xi_1) \cdot \frac{EA}{L} \\ -b^2(\xi_2 - \xi_1) \cdot \frac{EA}{L} & b^2(\xi_2 - \xi_1) \cdot \frac{EA}{L} \end{bmatrix} \quad \text{gdzie } b = \frac{m_2 - m_1}{\xi_2 - \xi_1} \quad (3)$$

The replacement linear distribution of the shape functions by the “broken” shape functions leads to correct results, as illustrated in Figure 3.

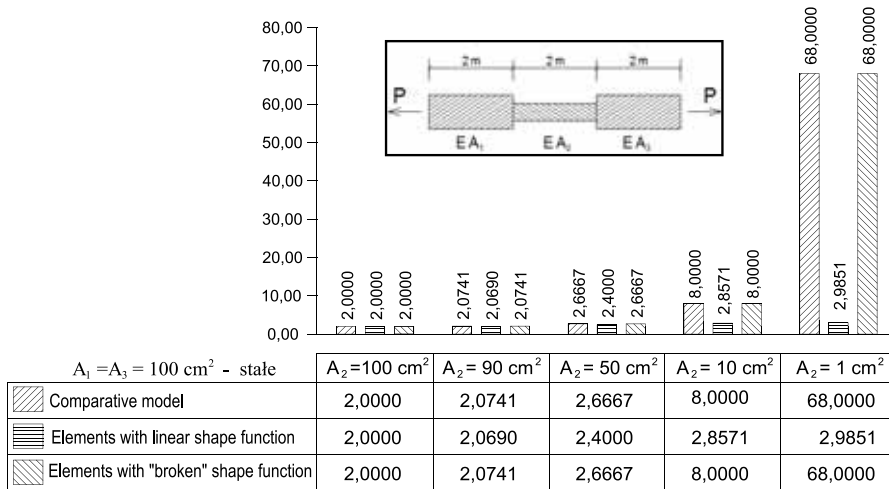


Fig. 3. Comparison of the results obtained from calculations with linear and “broken” shape functions.

The essence of special element conception is the method of estimation of the “broken” shape function parameters. The shape function values m_1 and m_2 , in general m_i , matching strain field distribution inside the sub-area to stiffness changes, have been determined from the formulas showed below (Chyzy et al., 1996). These formulas have been obtained from the assumption that the sub-areas create system of springs connected in series. The idea of determination of parameters m_i has been shown in Figure 4.

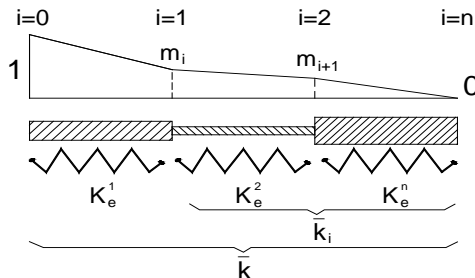


Fig. 4. Determination of parameters m_i .

Adaptation of the formulas for the analysis of layered road embankment is as follows:

$$m_i = \frac{\bar{k}}{k_i} \quad \bar{k} = \frac{1}{\sum_{k=1}^n \frac{1}{k_k}} \quad \bar{k}_i = \frac{1}{\sum_{k=i}^n \frac{1}{k_k}}, \quad i = 1, 2, \dots, n-1 \quad (4)$$

where: \bar{k} – resultant stiffness for total spring system,
 \bar{k}_i – resultant stiffness for part of spring system to the point where value m_i is calculated,
 k_k – stiffness of the k -th layer of the embankment,
 n – the number of layers. (Mackiewicz 2012).

Another issue related to the embankments modeling with the linear elastic elements (integrated in sub-areas) is adequate determination of the layer stiffness (spring). One of the solution is to use Winkler's hypothesis. According to Winkler's model, the subsidence s of the elastic subsoil is proportional to the acting load q .

$$q = k_z \cdot s \quad (5)$$

The coefficient of elasticity k_z for a homogeneous subsoil to a depth z can be determined according to the formula (Wilun 2005):

$$k_z = \frac{E_0}{\omega \cdot B \cdot (1 - \nu^2)} \quad (6)$$

The stiffness of the layered subsoil is the sum of the individual layers stiffness. For a single layer i stiffness is determined from the equation:

$$k_z^i = \frac{E_0^i}{\Delta\omega_i \cdot B \cdot (1 - \nu^2)}, \quad \Delta\omega_i = \omega_i - \omega_{i-1} \quad (7)$$

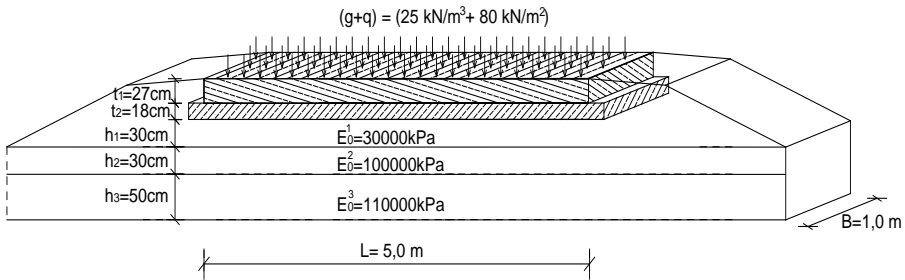
where: q – acting load,
 E_0 – strain modulus of the subsoil,
 B – width of the loaded area,
 ν – coefficient of lateral expansion of the subsoil,
 ω (ω_i) – influence coefficient, depending on the shape of the loaded area, selected according to appropriate tables and nomograms (Wilun 2005).

Calculation example

In a performed calculation test, the values of the road embankment subsidence were compared. In order to obtain distinction between stiffness of the road embankment layers, different parameters for each layer have been established. Based on known traffic categories and the choice of the substructure material, the following arrangement of pavement and embankment structure has been adopted:

1. The concrete slab, thickness 27cm, concrete B50.
2. The substructure, thickness 18cm, concrete B7,5.
3. The top layer of compacted road embankment, thickness $h_1=30\text{cm}$, strain modulus $E_0^1=30000\text{kPa}$.
4. The middle layer of compacted road embankment, thickness $h_2=30\text{cm}$, strain modulus $E_0^2=100000\text{kPa}$.
5. The bottom layer of compacted road embankment, thickness $h_3=50\text{cm}$, strain modulus $E_0^3=110000\text{kPa}$.

In the model, dimensions for a concrete slab and substructure with a corresponding thickness, were adopted equal 5,00 m x 1,0 m. The structure consisted of concrete slab and lean concrete substructure was considered as a construction resting on elastic embankment. The analyzed model and the calculation parameters have been shown in Figure 5.



$g = 25 \text{ kN/m}^3$ – the weight of the concrete,
 $q = 80 \text{ kN/m}^2$ – the load from the cars,
 $\nu = 0.3$ – coefficient of lateral expansion of the soil,
 $\Delta\omega_1 = 0.156 - 0 = 0.156$ – influence coefficient for first layer,
 $\Delta\omega_2 = 0.308 - 0.156 = 0.152$ – influence coefficient for second layer,
 $\Delta\omega_3 = 0.518 - 0.308 = 0.210$ – influence coefficient for third layer.
 Influence coefficients obtained according to (Wilun 2005).

Fig. 5. Parameters of the example of road embankment calculation.

As a constant loads were taken dead weight of concrete slab and dead weight of concrete substructure with following value:

$$g = 25 \text{ kN/m}^3 \cdot (0,27 \text{ m} + 0,18 \text{ m}) = 11,25 \text{ kN/m}^2$$

As a variable loads were taken loads from car transport as a two axes equal 100kN on each roadway. This load was turned into distributed load, by the dividing these forces by the roadway area.

$$q = \frac{2 \cdot 100 \text{ kN}}{2,5 \text{ m} \cdot 1 \text{ m}} = 80 \text{ kN/m}^2$$

Calculations were made in three variants:

1. Variant I – according to the Winkler's hypothesis, using formulas (5), (6), (7) described by (Wilun 2005).

2. Variant II – as a control variant. Flat (two-dimensional) Finite Element Method model was calculated, as shown in Figure 6a. For modeling of subsoil using the flat elements, modulus transformation must be applied to describe susceptibility of subsoil, as in the Winkler's hypothesis:

$$E^i = E_{oi} \cdot \frac{h_i}{\Delta\omega_i} \quad (8)$$

3. Variant III – using special elements presented in this paper. It means layered, one-dimensional finite elements, integrated in sub-areas, and implemented in the computer construction analysis system named "Orcan" (<http://kmb.pb.edu.pl/dydaktyka/tchyzy/orcan.html>), Figure 6b;

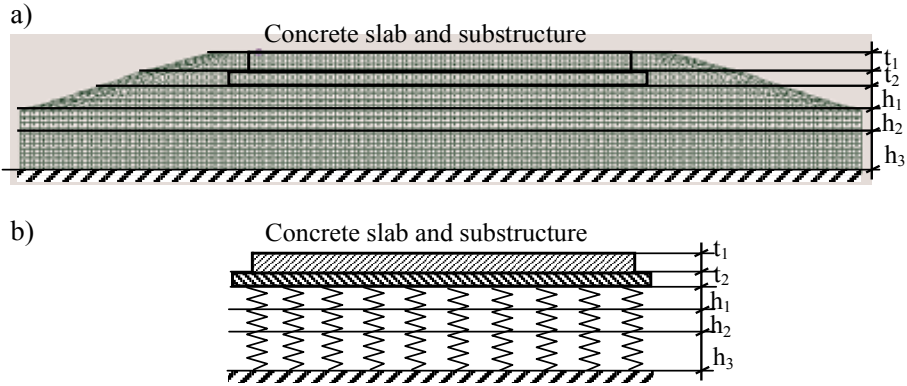


Fig. 6. The computational calculation model: a) two-dimensional Finite Elements Method model with discretisation, b) presented conception of special finite elements.

From the calculations, followed results, as a values of concrete slab subsidence, were obtained:

1. Variant I – the Winkler's hypothesis.

$$s_1 = \frac{q \cdot \Delta\omega_1 \cdot B \cdot (1 - \nu^2)}{E_{o1}} = \frac{91,25 \text{ kN/m}^2 \cdot 0,156 \cdot 1,0 \text{ m} \cdot (1 - 0,3^2)}{30000 \text{ kPa}} = 4,318 \cdot 10^{-4} \text{ m} = 0,4318 \text{ mm}$$

$$s_2 = \frac{q \cdot \Delta\omega_2 \cdot B \cdot (1 - \nu^2)}{E_{o2}} = \frac{91,25 \text{ kN/m}^2 \cdot 0,152 \cdot 1,0 \text{ m} \cdot (1 - 0,3^2)}{100000 \text{ kPa}} = 1,262 \cdot 10^{-4} \text{ m} = 0,1262 \text{ mm}$$

$$s_3 = \frac{q \cdot \Delta\omega_3 \cdot B \cdot (1 - \nu^2)}{E_{o3}} = \frac{91,25 \text{ kN/m}^2 \cdot 0,210 \cdot 1,0 \text{ m} \cdot (1 - 0,3^2)}{110000 \text{ kPa}} = 1,585 \cdot 10^{-4} \text{ m} = 0,1585 \text{ mm}$$

Subsidence: $s = s_1 + s_2 + s_3 = 7,165 \cdot 10^{-5} \text{ m} = 0,7165 \text{ mm}$

2. Variant II – Finite Elements Method model with flat two-dimensional elements.

$$\begin{aligned} \text{– first layer: } E^1 &= E_{0^1} \cdot \frac{h_1}{\Delta\omega_1} & E^1 &= 30000 \text{ kPa} \cdot \frac{0,3 \text{ m}}{0,156} = 57692,31 \text{ kPa} \\ \text{– second layer: } E^2 &= E_{0^2} \cdot \frac{h_2}{\Delta\omega_2} & E^2 &= 100000 \text{ kPa} \cdot \frac{0,3 \text{ m}}{0,152} = 197368,42 \text{ kPa} \\ \text{– third layer: } E^3 &= E_{0^3} \cdot \frac{h_3}{\Delta\omega_3} & E^3 &= 110000 \text{ kPa} \cdot \frac{0,5 \text{ m}}{0,210} = 261904,76 \text{ kPa} \end{aligned}$$

Subsidence: $s = 7,272 \cdot 10^{-5} \text{ m} = 0,7272 \text{ mm}$

3. Variant III – special linear elastic finite elements integrated in sub-areas (presented method).

$$k_{s^1} = \frac{E_{0^1}}{\Delta\omega_1 \cdot B \cdot (1-\nu^2)} \cdot A = \frac{30000 \text{ kPa}}{0,156 \cdot 1 \text{ m} \cdot (1-0,3^2)} \cdot (1 \text{ m} \cdot 0,05 \text{ m}) = 211327,134 \frac{\text{kN}}{\text{m}^3} \cdot 0,05 \text{ m}^2 = 10566,36 \frac{\text{kN}}{\text{m}}$$

$$k_{s^2} = \frac{E_{0^2}}{\Delta\omega_2 \cdot B \cdot (1-\nu^2)} \cdot A = \frac{100000 \text{ kPa}}{0,152 \cdot 1 \text{ m} \cdot (1-0,3^2)} \cdot (1 \text{ m} \cdot 0,05 \text{ m}) = 722961,25 \frac{\text{kN}}{\text{m}^3} \cdot 0,05 \text{ m}^2 = 36148,06 \frac{\text{kN}}{\text{m}}$$

$$k_{s^3} = \frac{E_{0^3}}{\Delta\omega_3 \cdot B \cdot (1-\nu^2)} \cdot A = \frac{110000 \text{ kPa}}{0,210 \cdot 1 \text{ m} \cdot (1-0,3^2)} \cdot (1 \text{ m} \cdot 0,05 \text{ m}) = 575614,86 \frac{\text{kN}}{\text{m}^3} \cdot 0,05 \text{ m}^2 = 28780,74 \frac{\text{kN}}{\text{m}}$$

Resultant stiffness:

$$\bar{k}_s = \frac{1}{\frac{1}{k_{s^1}} + \frac{1}{k_{s^2}} + \frac{1}{k_{s^3}}} = \frac{1}{\frac{1}{10566,36 \frac{\text{kN}}{\text{m}}} + \frac{1}{36148,06 \frac{\text{kN}}{\text{m}}} + \frac{1}{28780,74 \frac{\text{kN}}{\text{m}}}} = 6367,42 \frac{\text{kN}}{\text{m}}$$

Subsidence: $s = 7,290 \cdot 10^{-5} \text{ m} = 0,7290 \text{ mm}$

Conclusions

Using the presented method, for the calculation of the road embankment with large distinctions in the layer parameters, a sufficiently accurate results were achieved. Simultaneously the minimum number of unknowns were provided – it means regardless of the number of subsoil layers, the number of unknowns is the same (3D elastic elements have two nodes, in each node 3 steps of freedom). Thus calculations according to the method presented in the paper lead to correct results with less number of finite elements. It means that in this case the proposed solution is more effective.

The presented method is also an example of a specific application of known solutions – the Winkler's hypothesis. However the prospective application of the presented method is post-critical analysis of the constructions with a large stiffness changes, what is still developed by the authors (Chyzy 2009). Expected advantage of the special finite

elements is also the elimination of the necessity of repeated rearrangement algorithms for Finite Elements Method mesh discretisation. The necessity of computationally expensive discretisation rearrangement could be caused by sudden changes in the parameters of the embankment. Definitely the presented approach can be used in stationary solutions with abrupt and step changes of stiffness, what has been presented in the paper.

References:

1. Bathe, K.J. (1996), *Finite Element Procedures*. Prentice Hall, Englewood Cliffs, NJ.
2. Chyży, T. (2009), *Method of analysis of residential buildings under hypertension gas explosion*. Bialystok University of Technology Publishing House, Bialystok. (in polish)
3. Chyży T., Kazberuk A., Tribillo R. (1996), *Application of self-adapting shape functions to nonlinear analysis plane and solid domains*. Civil and Environmental Engineering, Bialystok University of Technology, no.15, Bialystok, pages 65–72. (in polish)
4. Mackiewicz, M. (2012), *Conception of the linear finite elements for analysis of constructions with large geometrical and stiffness changes*. Scientific Papers of PhD Students, Silesian University of Technology Publishing House, Gliwice, pages 173-180. (in polish)
5. Wilun Z. (2005), *Sketch of Geotechnics*. Transport and Communication Publishing Houses, Warsaw. (in polish)
6. Zienkiewicz O.C., Taylor R.L., Zhu J.Z. (2005), *The finite element method: its basis and fundamentals*. Amsterdam: Elsevier; Butterworth-Heinemann.

ANALYSIS OF LIFE CYCLE ASSESSMENT OF WOODEN CONSTRUCTION

Monika Mackiewicz

Bialystok University of Technology, Faculty of Civil and Environmental Engineering,
Wiejska Street 45E, 15-351 Bialystok, Poland
e-mail: m.mackiewicz@pb.edu.pl

Summary:

Unfortunately, rapid development of new products and manufacturing processes in the modern world, generate more and more negative impact on the natural environment. Therefore, there is a necessity for comprehensive methods of environmental impact assessment, based on the methodology adopted by the international organizations. One of such a methods is Life Cycle Assessment (LCA). This is a relatively new technique of environmental management, which involves particular product assessment in terms of environmental effects, during its entire life cycle. The main goal of this method is a comparative analysis and optimization of production to minimize negative environmental impacts in different phases of product's production, exploitation and elimination. Life Cycle Assessment concerns many areas of human activity, including the civil engineering, which is one of the largest sectors of the economy and of raw materials flow as well.

In this thesis an analysis of life cycle of small wooden construction using the environmental Life Cycle Assessment method has been presented. The scale and type of negative environmental impacts generated during the life cycle of the construction have been analyzed. The analysis has been carried out by using the computer program Sima Pro 7. In this program all particular elements and production processes of wooden construction have been verified. The stages starting from the growth of trees in the forest, treatment of wood, through assembly, till demolition and waste utilization, have been taken into consideration. The processes with the most adverse environmental effects were found. Conclusions concerning the performed analysis have been formulated.

Key words: Life Cycle Assessment (LCA), sustainable development, sustainable civil engineering, wooden construction

Introduction

Sustainable development is a social and economic development, which should satisfy the needs of today's society and simultaneously guarantee the ability to satisfy the needs of future generations. The concept of "sustainable development" – was first defined in the report "Our Common Future" (1987), formulated by the World Commission on Environment and Development, United Nations. Sustainable development was defined as a process, which has been taken in order to meet developmental aspirations of present and future generations as well.

Sustainable development is a necessity of technological and civilization development. This is the effect of taking care of future generations, which someday will manage the environmental resources. The main requirement for sustainable development, the necessity for care of the environment is also a constitutional requirement. Moreover general principles of sustainable development are following:

- renewable resources should not be consumed faster than they can be regenerated,
- non-renewable resources should not be consumed faster than it could be replaced by renewable substitutes,
- pollution and waste should not be formed faster than the nature can absorb and neutralize it (Czarnecki, Kapron 2010).

From the beginning of the seventies of the last century, a significant increase of interest in issues related to environmental protection, natural resources and in particular material and energy consumption of individual manufacturing processes, has appeared. From that time research and studies in this area have been started. Obtained results has been taken into account for creating environment-friendly policies of countries and regions.

One of the methods, which allows to estimate the potential impact on the environment is a Life Cycle Assessment (LCA). This name was introduced in 1990 at a conference in Vermont, where it was found, that for each product subjected to analysis, it is necessary to quantify the materials and energy consumption used during each of product stage (Fig. 1). Only on the basis on such a collected data would be possible to assess the product impact on the environment.

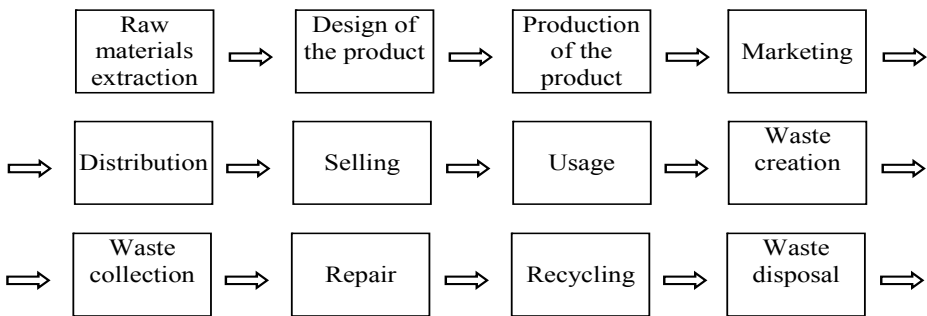


Fig. 1. The main phases of product life cycle (Gorzynski 2007).

General issues for sustainable development in civil engineering

Civil engineering industry consumes more than 40% of produced energy, about 50% of processed materials and emits 35% of greenhouse gases. This is the reason that civil engineering is one of the most important sectors of the economy, where sustainable development is required. The increase in social awareness of the civil engineering impact on the environmental protection and the energy saving, makes more important necessity to fulfill certain conditions and criteria for buildings. Therefore it is necessary to harmonize the European requirements in this scope. The basic rules for harmonization process are going to be standards, developed by the European CEN Technical Committee, which deals with:

- impact assessment of buildings on the environment,
- environmental declaration of building products,
- entire life cycle assessment of buildings and building constructions (Czarnecki, Kapron 2010).

The concept of “sustainable civil engineering” has gained a reputation as one of the most promoted ideas. Described earlier, principles of sustainable development are the basis for this new idea. It could be clearly concluded that sustainable civil engineering for the keynote has the motto “satisfy present needs with thinking about the future”. In other words, sustainable development in civil engineering industry need to take into account future generations especially concerning consumption of raw materials (Karbowski 2010).

Meaning of wood as a raw material

Wood is a material obtained from fallen trees and formed into various assortments. It is necessary to distinguish a tree as a living plant and wood as a material made from tree. Wood is a material used for fuel, constructions, people daily life and also in the arts. From other building materials wood has fundamentally different structure. In fact, it is a band of cells that were part of the living body wood. The technical characteristics and the possibility of the use of wood depends on the arrangement and structure of these cells.

Wood next to coal, iron and oil is the raw material which has a large effect on economic development. A very wide range of applications makes that this material does not leave a man over a lifetime, even despite the increasingly rapid development of technology. It is proved by the continuous increase of consumption and the rising price of wood. Nowadays there is a necessity to replace wood by other materials. The reason of it, is the increasing scarcity and the need for efficient management of this scarce resource. On the other hand, compared with fossil fuels, the advantage of wood is the ability to be produced in a continuous manner, without running out of resources. This is achieved by proper acquisition of timber without disturbing the production potential. All these mentioned issues are the reasons why wooden elements have been chosen as an object of LCA analysis (Krzysik 1976).

Life cycle analysis of a wooden construction in the program SimaPro 7

LCA analysis has been carried out using the computer program SimaPro 7, delivered by Pre Consultants (Dutch company). This program is based on modeling the various components of the product, in order to create the entire product life cycle. As a component may be treated a single element or whole product, consisting of several components. The program allows to analyze and assess the environmental impact of factors common to all the successive stages of a product's life, beginning from its production, through the use until to waste disposal. Analysis using the SimaPro 7 is performed according to methodological assumptions of LCA. Therefore includes four successive stages:

1. Goal and scope,
2. Inventory,
3. Impact assessment,
4. Interpretation (Nowak 2008).

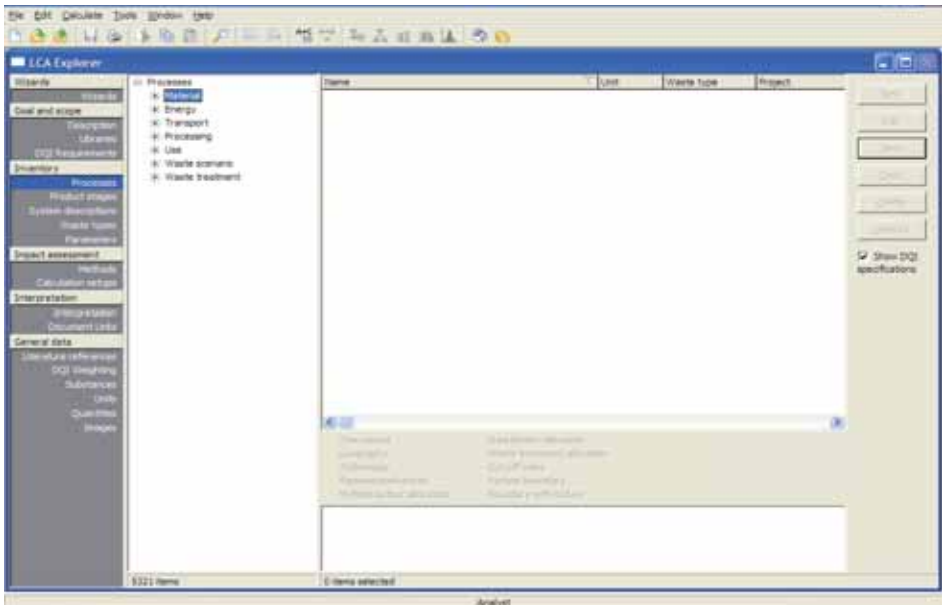


Fig. 2. SimaPro 7 – main menu (LCA Explorer).

Assumption of the life cycle analysis in the program SimaPro 7

According to an example (<http://www.pre.nl> – “SimaPro 7 Tutorial”) as a subject of the environmental analysis was taken a wooden construction in form of bower with a very simple design, which could be placed in a private garden. It is made of wooden planks and a small amount of metal fasteners. Wood is not impregnated and painted. The bower does not have windows and doors. There is no heating and electricity connection. The view and dimensions of bower have been presented in the Figure 3 and Figure 4. For analysis it has been taken 150 kg, as a needed amount of wooden elements.

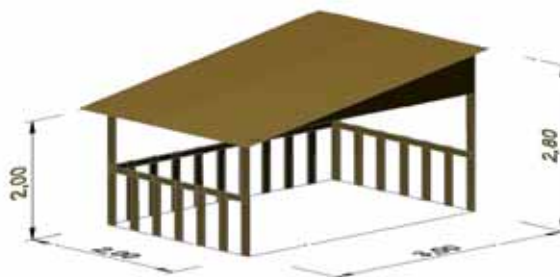


Fig. 3. View of analyzed wooden construction (bower).

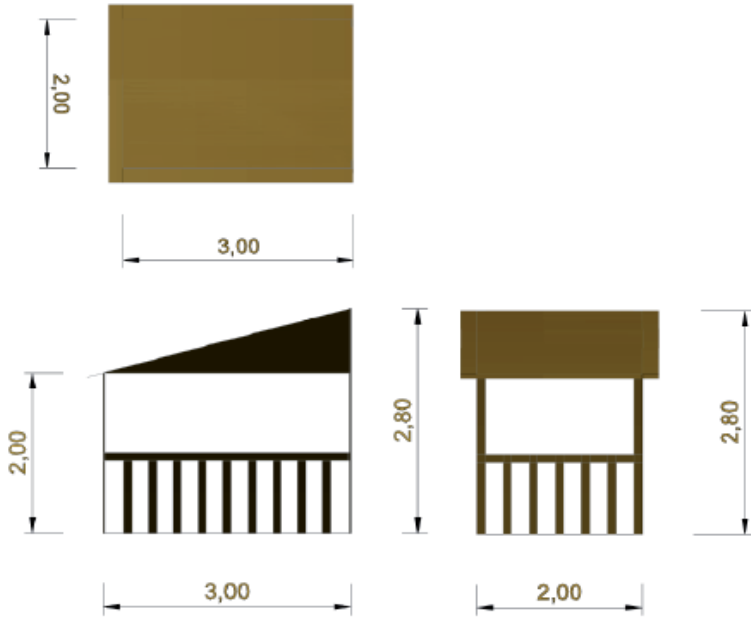


Fig. 4. The dimensions of analyzed wooden construction (bower).

Life cycle of a typical wooden construction consists of the following steps, shown in the Figure 5 (Strykowski et al. 2006).

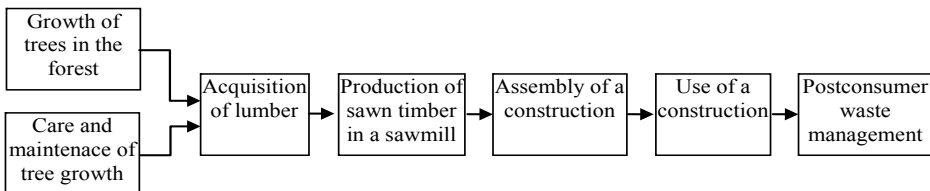


Fig. 5. Diagram of life cycle flow of a wooden construction.

Differently from the order of a typical life cycle phases (Fig. 5), the analysis carried out in the SimaPro 7 successively consists of three basic stages (<http://www.pre.nl> – “SimaPro 7 Tutorial”):

1. Entering processes, that describe the growth and care of trees in the forest, cutting trees and cutting sawn timber in a sawmill.
2. Entering the end processes of the life cycle. Several advanced capabilities of the SimaPro 7 in implementation of waste management have been used. It has been assumed that 40% of the wood is burned in home fireplaces and 60% is stored in a specially adapted landfill.

3. After entering all production processes and the final waste management, it has been carried out assembly and then entire life cycle of the bower.

It should be mentioned that LCA analysis of a wooden construction has been done without taking into account stage “use of a construction”. It has been neglected because in the construction there was no electricity and heat consumption. Successive stages of wood preparation have been described below in the article.

Analysis in the program SimaPro 7 – creation of production processes

Growth of trees in the forest

The beginning of the life cycle of the analyzed construction is associated with preparation of the materials. Because the object is made entirely from wooden elements, should be examined various stages of preparation of wood and its treatment. The first stage of the analysis in case of wood as a building material is “Growth of trees in the forest” and is created in the “Processes” – “Material” – “Wood”. In the inventory table, the amount of carbon dioxide absorbed from the air, solar energy necessary for growth and necessary area for forest cultivation have been taken into account.

Care and maintenance of tree growth

This step could be treated as an existing at the same time with the previous process. During creation of the table inventory, attention should be paid to the problem, which is the use of land for timber production. In environmental life cycle assessment there are two kinds of ground usage: “land occupation” and “land transformation”. Transformation means a change in the quality of the forest ecosystem. The measure of this change are two indicators of biodiversity: the accumulation of species and abundance of species. The benchmark of ecosystem quality is the accumulation and abundance of species assigned to the primary forest. Silviculture is a disturbance of the highest quality and means the conversion from primary forest (“Transformation from forest”) to the secondary forest (“Transformation to forest”). This type impacts are expressed in surface units, for example m^2 . It is assumed that the transformation can take place in an extensive way, for example by enlarging the surface of the culture, and intensive way, by increase the efficiency of culture. In case of timber production, it has been assumed that there is both extensive and intensive land transformation. The second form of surface use is land occupation. There is no change in the quality of the ecosystem, as in the case of the transformation, but there is no possibility for a given area to return to its original form. The impact of the land occupation is determined in units of area and time, for example $m^2 \text{year}$.

In the process “Care and maintenance of tree growth”, the participation of man, such as planting and cultivation of seedlings, saplings treatments, cleaning and thinning treatments, has been taken into account. Therefore has been considered the type and time of forest equipment use (e.g. chain saws, transport vehicles), fuel consumption (e.g. diesel) and the use of the area (e.g. forest roads).

Acquisition of timber (Cutting trees)

To create the table of inputs and outputs (the table inventory) for the timber acquisition stage (menu “Processes” – “Material” – “Wood”), two previously created processes have been taken into account. It has provided inputs and described forestry processes both with and without human intervention. An additional input to the process is necessity to use a chainsaw to fell trees. From the process there is about 250 kg of waste, in form of branches left in the forest.

Production of sawn timber in a sawmill

The next process, which must be defined in the life cycle analysis of a wooden construction is a cutting roundwood in a sawmill. Creating this process is similar to the three previous processes, in the menu “Processes” – “Material” – “Wood”. In the outputs to technosphere, instead of process name, finished products should be listed:

- planks – as 50% of the output, that is 500kg,
- sawdust – in the amount of 40% of output, which is 400kg,
- bark – as 10% of the output, that is 100kg.

After a treatment of one ton of timber in a sawmill, three different products have been created. Therefore, there is a problem of so-called allocation, it means distribution of environmental loads, generated by all processes together, between three final products. All adverse impact and energy used during the cultivation of trees in the forest and in the process of cutting, must be allocated between the planks, sawdust and bark. The analysis has been carried out on the basis on allocation according to weight of the output materials. Thus it is assumed that 50% of the environmental impact is addressed for planks, 40% for sawdust and 10% for bark.

The input to the process from the technosphere is the previous process of “Acquisition of timber”, in the amount of 250 kg more than the overall weight of the starting materials (planks, sawdust and bark). This surplus has been used for burning in the sawmill to allow the drying of wood. The results of wood combustion obviously are air emissions. In this process the transportation between place of cutting down trees in the forest and the sawmill, and the electricity needed for mechanical treatment (cutting sawn timber in sawmill) have been also included.

Analysis in the program SimaPro 7 – waste disposal and postconsumer waste management

After creating a production system of the main components of analyzed construction, that is wooden planks, arrangements for the end of the life cycle of wood products need to be considered (<http://www.pre.nl> – “SimaPro 7 Tutorial”). Even though there was not yet analyzed the assembly stage of bower, it is already possible to predict how the waste will be used at the end of its life. Postconsumer waste management has been considered for two main materials:

- Wood products – planks,
- Metal auxiliary elements – nails, screws.

For simplification of the analysis, the following assumptions have been done:

- 40% of wood waste is burned in home furnaces. It is assumed, however, that the heat from the combustion was not spent on heating any room.
- 60% of the waste is stored in a modern landfill. In this case, it is assumed that the storage was equipped with a special system for methane collection. Some collected methane is used as a fuel.

In the analysis of postconsumer waste management it has been necessary to separate waste into different streams for further processing. As the first separation it has been divided on 40% of waste for incineration and 60% for storage. As the second it has been separated the wood from the metal connectors. In fact, it is difficult to assume that all metal items will be carefully removed during dismantling. However, in case of the analysis seems to be justified by the fact that during the combustion, steel behaves differently than wood. In order to perform this separation should be made different types of waste. The SimaPro 7 has the proper tool called “Waste scenario”. It can be used both for overall separation of waste and for separation into properly defined types of waste, such as wood and steel. But before creating a detailed postconsumer waste management system, first must be considered how emissions coming from each waste management will be treated.

Waste management, called “Waste scenario” is used for indicate the main flow of waste, but does not consider the emissions emitted during the removal or waste disposal. For this purpose there is a tool called “Waste treatment”. It includes data about all compounds emitted during the process of waste disposal, such as incineration or storage. Therefore it is necessary to establish:

- Emission of compounds during the combustion of wood products.
- Emission of compounds during the combustion of the metal parts, if necessary.
- Emissions of compounds during waste storage.

Looking at the final waste management for wood products, it should be taken into account that there may be also found a positive phenomenon. As a positive effect in the analysis should be taken the acquisition of emitted methane. Wood components located on the landfill during the first 150 years are slowly degraded. As a result of this process, methane and carbon dioxide is produced. The emitted methane (in an amount of about 56% of all emissions), can significantly affect global warming. The magnitude of this effect could be demonstrated by the fact that the release 1kg of methane into the environment contributes nearly 20 times more to climate change than 1kg of carbon dioxide emission. Therefore it was assumed, that most of emitted methane is collected on the landfill by a special equipment. This gas can be used as a fuel or simply be burnt, because the emission of carbon dioxide has much less impact on the environment than methane emission. Using collected methane as fuel reduces the consumption of natural gas and this is certainly a positive phenomenon. To model the positive benefits of waste management in the SimaPro 7, option called “Avoided products” is used.

Waste treatment – characteristic of waste storage on the landfill

To model the process of wood products storage as the end of their life cycle, must be used the option named “Waste treatment”, which is located in the “Inventory” – “Processes” – “Waste treatment” – “Landfill” (Storage). Entering procedure is similar to the previously created production processes. The table inventory must include the name of the postconsumer process “Storage on the landfill” specify the type of waste, that is “Wood” (Wood) and the amount of 1kg. As the “Avoided products” should be entered “Natural Gas B300” in the amount of 0.007 kg. It means that collected methane will reduce natural gas consumption in other processes. Necessity of waste transport between the place of the municipal waste collection and landfill at a distance 20 km, should be considered as an input to the technosphere in the amount of 0.02 tonne-kilometers. The output is methane emission that have not been completely captured by collection equipment and the total emission of carbon dioxide.

Waste treatment – characteristic of wood incineration

For creation of process “Incineration of wooden elements” shall also be used the tool “Waste treatment” in the “Inventory” – “Processes” – “Waste treatment” – “Incineration” (Burning). In this case, there is no any benefits coming from the process, so there is no “Avoided products”.

Postconsumer waste management

After completing the processes of the waste treatment, should be enter the processes of postconsumer waste management, which define exactly how much waste is addressed to a particular waste disposal. For analysis three following managements need to be created:

1. Storage.
2. Incineration.
3. Separation of waste between landfill (storage) and incineration.

Waste scenario – waste disposal on the landfill

In fact, it can be expected that the materials supplied on the landfill are not sorted. However, in the analysis to separate metal and wood elements, the tool “Waste scenario” has been used. In this case, it is sure that the wood and metal will go separately to the corresponding disposal operations, which is “Waste treatment”. Entering has been done in the “Inventory” – “Processes” – “Waste scenario” – “Landfill” (Storage). A new process called “Management – Storage of wooden elements” should be created with the amount of 1kg. Then in the “Materials and/or waste types separated from waste stream”, earlier created process of waste disposal named “Storage of wooden elements” should be written. The process of waste disposal for storage of steel elements, already existing and just taken from the program SimaPro7 should be written as well. After entering the data into the table inventory, the program automatically separates waste types and directs them to the appropriate disposal processes. Wood and metal parts are sent into separate storage, and all the other materials are sent to an unspecified treatment.

Waste scenario – waste disposal for wood incineration

Entering the characteristic of the process takes place in the “Inventory” – “Processes” – “Waste scenario” – “Incineration” (Burning). It is created a new process “Management – Incineration of wooden elements” for waste incineration, which is similar to the storage process and includes the combustion of elements coming from disassembled bower, including metal parts as well.

Separation of waste between landfill (storage) and incineration

The final stage of waste management is division of waste stream into:

- 60% for storage,
- 40% for incineration.

Entering the characteristics of the process for waste separation takes place in the “Inventory” – “Processes” – “Waste scenario” – “Others”. Should be put the name as “Final waste management” and the amount of 200 kg. In the process, transportation of parts from disassembled bower to the place of municipal waste collection has been taken into consideration. There is no taken into account any remaining waste, because all waste has been properly allocated to specific disposal processes.

Analysis in the program SimaPro 7 – Assembly of a wooden construction

After entering the operation and processes of final waste management for wooden bower, it is impossible to display the schematic tree showing the unit processes and the relationships between them. The program does not know yet, which materials should be put in the right waste stream. Therefore it must be defined the following two stages of product (“Product stages”):

- Assembly (“Assembly”) to define finished construction,
- Life cycle (“Life cycle”) to connect assembly phase (the production of wooden elements) with final waste management.

In the SimaPro 7 it is done by using the tool “Product stages” in the “Inventory”. A characteristic feature for the creation of both assembly and life cycle is the fact that at these stages, there is no entered any environmental data. Only appropriate references to the previously developed processes need to done.

In the “Inventory” – “Product stages” – “Assembly” must be created a new assembly process and named: “Assembly of a wooden construction”. Successively the table with reference to the appropriate materials and processes should be filled in.

Basic assumptions for assembly process have been adopted with some simplifications:

- Wooden bower is made of 150 kg of planks. There is no waste. Package of the products (planks) is not required.
- About 2 kg of metal elements in form of nails and screws have been used.
- The owner of the bower has to transport the planks from the shop by his own car. The shop is located at a distance of 5 km from his home (<http://www.pre.nl> – “SimaPro 7 Tutorial”).

After editing and saving the assembly process it is possible to check the preview of process tree (Nowak 2008). The program will automatically display a tree with the option, that not all partial processes must be shown on it. The so-called limiting function (“cut-

off level”) gives opportunity to not display the partial processes for which contribution is less than the threshold value. However, for the calculation, the contribution of all processes is taken into account. Helpful is also the option of showing the scale of the environmental impact of the processes by using the thickness of the line (“Show flow indicator in line width”).

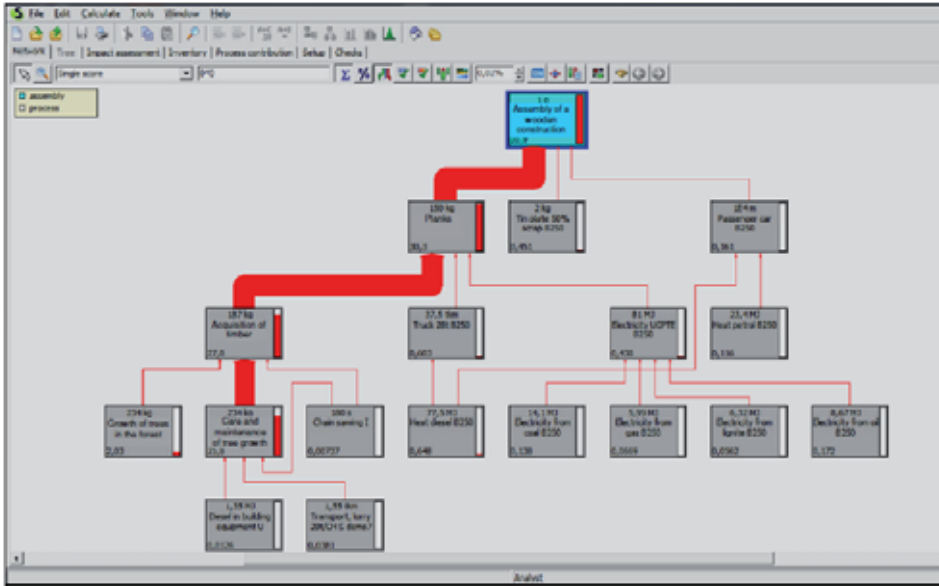


Fig. 6. SimaPro 7 – Network/tree of the process “Assembly of a wooden construction”.

Analysis in the program SimaPro 7 – Life cycle of a wooden construction

The life cycle of the wooden bower is created similar to previously described assembly process. In the “Inventory” – “Product stages” – “Life cycle” must be opened a new process and named “Life cycle of a wooden construction”. Then, must be entered a reference to a previously created assembly process and to the process of postconsumer waste management. On the view of life cycle tree, all the participated processes has not been displayed. Of course, there is possibility to show all processes, but then the scheme gets more unclear. Therefore, the option limiting the number of displayed processes (“cut-off level”) is helpful especially in the visual assessment of analyzed process according to flows tree (Nowak 2008).

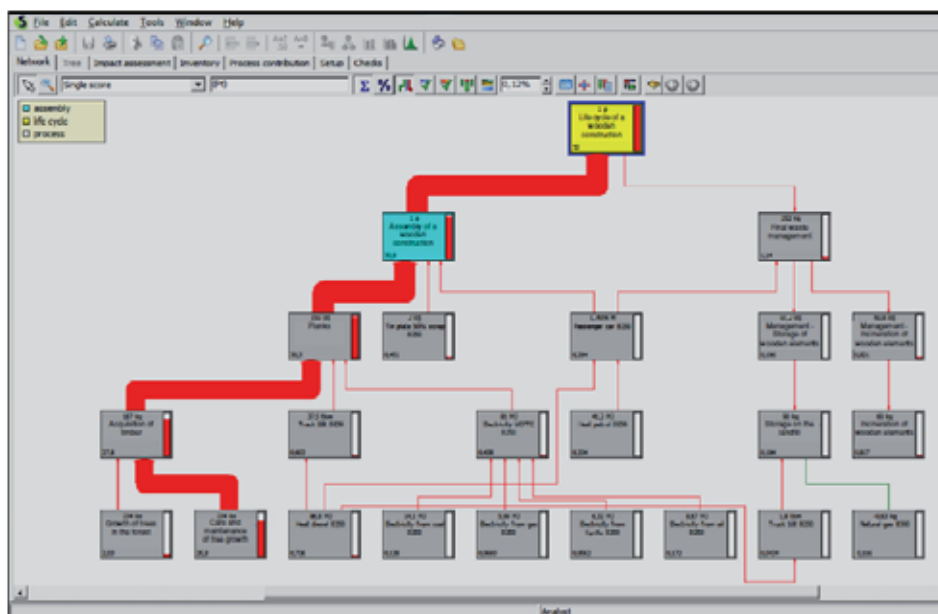


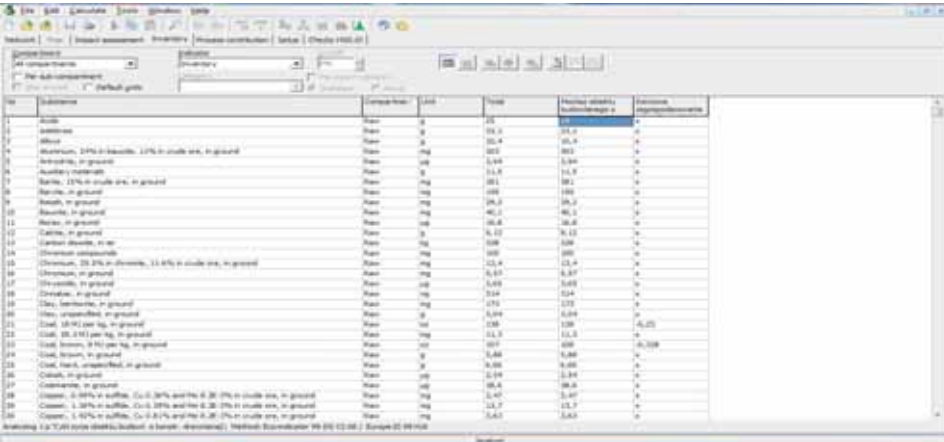
Fig. 7. SimaPro 7 – Network/tree of the life cycle “Life cycle of a wooden construction”

The results of the environmental life cycle analysis in the program SimaPro 7.

The indirect way for checking the results is a view of tree of processes. However in the SimaPro 7, there are many options to display results according to the research needs.

Inventory results

To show the results in a table with a detailed list of all chemical substances and compounds involved in the life cycle should be in the “Product stages” – “Life cycle” opened a previously created life cycle and pressed the “Analyze” button in the top bar menu. Then should be exposed the “Inventory” bookmark. Table with a comprehensive compilation of all the components involved in the analysis is displayed. The data enclosed in the table can be sorted alphabetically according to name or to quantity of given component contents or according to units.



no	substance	Impact class	Unit	Total	Weighting indicator	Indicator
1	Acetic acid	Acid	g	225	1	225
2	Acetic acid	Acid	g	225	1	225
3	Acetic acid	Acid	g	225	1	225
4	Acetic acid, 24% in solution, 11% in crude oil, in ground	Acid	mg	225	1	225
5	Acetic acid, in ground	Acid	mg	225	1	225
6	Acetic acid, in ground	Acid	mg	225	1	225
7	Acetic acid, 15% in crude oil, in ground	Acid	mg	225	1	225
8	Acetic acid, in ground	Acid	mg	225	1	225
9	Acetic acid, in ground	Acid	mg	225	1	225
10	Acetic acid, in ground	Acid	mg	225	1	225
11	Acetic acid, in ground	Acid	mg	225	1	225
12	Acetic acid, in ground	Acid	mg	225	1	225
13	Acetic acid, in ground	Acid	mg	225	1	225
14	Acetic acid, in ground	Acid	mg	225	1	225
15	Acetic acid, in ground	Acid	mg	225	1	225
16	Acetic acid, in ground	Acid	mg	225	1	225
17	Acetic acid, in ground	Acid	mg	225	1	225
18	Acetic acid, in ground	Acid	mg	225	1	225
19	Acetic acid, in ground	Acid	mg	225	1	225
20	Acetic acid, in ground	Acid	mg	225	1	225
21	Acetic acid, in ground	Acid	mg	225	1	225
22	Acetic acid, in ground	Acid	mg	225	1	225
23	Acetic acid, in ground	Acid	mg	225	1	225
24	Acetic acid, in ground	Acid	mg	225	1	225
25	Acetic acid, in ground	Acid	mg	225	1	225
26	Acetic acid, in ground	Acid	mg	225	1	225
27	Acetic acid, in ground	Acid	mg	225	1	225
28	Acetic acid, in ground	Acid	mg	225	1	225
29	Acetic acid, in ground	Acid	mg	225	1	225
30	Acetic acid, in ground	Acid	mg	225	1	225
31	Acetic acid, in ground	Acid	mg	225	1	225
32	Acetic acid, in ground	Acid	mg	225	1	225
33	Acetic acid, in ground	Acid	mg	225	1	225
34	Acetic acid, in ground	Acid	mg	225	1	225
35	Acetic acid, in ground	Acid	mg	225	1	225
36	Acetic acid, in ground	Acid	mg	225	1	225
37	Acetic acid, in ground	Acid	mg	225	1	225
38	Acetic acid, in ground	Acid	mg	225	1	225
39	Acetic acid, in ground	Acid	mg	225	1	225
40	Acetic acid, in ground	Acid	mg	225	1	225
41	Acetic acid, in ground	Acid	mg	225	1	225
42	Acetic acid, in ground	Acid	mg	225	1	225
43	Acetic acid, in ground	Acid	mg	225	1	225
44	Acetic acid, in ground	Acid	mg	225	1	225
45	Acetic acid, in ground	Acid	mg	225	1	225
46	Acetic acid, in ground	Acid	mg	225	1	225
47	Acetic acid, in ground	Acid	mg	225	1	225
48	Acetic acid, in ground	Acid	mg	225	1	225
49	Acetic acid, in ground	Acid	mg	225	1	225
50	Acetic acid, in ground	Acid	mg	225	1	225
51	Acetic acid, in ground	Acid	mg	225	1	225
52	Acetic acid, in ground	Acid	mg	225	1	225
53	Acetic acid, in ground	Acid	mg	225	1	225
54	Acetic acid, in ground	Acid	mg	225	1	225
55	Acetic acid, in ground	Acid	mg	225	1	225
56	Acetic acid, in ground	Acid	mg	225	1	225
57	Acetic acid, in ground	Acid	mg	225	1	225
58	Acetic acid, in ground	Acid	mg	225	1	225
59	Acetic acid, in ground	Acid	mg	225	1	225
60	Acetic acid, in ground	Acid	mg	225	1	225
61	Acetic acid, in ground	Acid	mg	225	1	225
62	Acetic acid, in ground	Acid	mg	225	1	225
63	Acetic acid, in ground	Acid	mg	225	1	225
64	Acetic acid, in ground	Acid	mg	225	1	225
65	Acetic acid, in ground	Acid	mg	225	1	225
66	Acetic acid, in ground	Acid	mg	225	1	225
67	Acetic acid, in ground	Acid	mg	225	1	225
68	Acetic acid, in ground	Acid	mg	225	1	225
69	Acetic acid, in ground	Acid	mg	225	1	225
70	Acetic acid, in ground	Acid	mg	225	1	225
71	Acetic acid, in ground	Acid	mg	225	1	225
72	Acetic acid, in ground	Acid	mg	225	1	225
73	Acetic acid, in ground	Acid	mg	225	1	225
74	Acetic acid, in ground	Acid	mg	225	1	225
75	Acetic acid, in ground	Acid	mg	225	1	225
76	Acetic acid, in ground	Acid	mg	225	1	225
77	Acetic acid, in ground	Acid	mg	225	1	225
78	Acetic acid, in ground	Acid	mg	225	1	225
79	Acetic acid, in ground	Acid	mg	225	1	225
80	Acetic acid, in ground	Acid	mg	225	1	225
81	Acetic acid, in ground	Acid	mg	225	1	225
82	Acetic acid, in ground	Acid	mg	225	1	225
83	Acetic acid, in ground	Acid	mg	225	1	225
84	Acetic acid, in ground	Acid	mg	225	1	225
85	Acetic acid, in ground	Acid	mg	225	1	225
86	Acetic acid, in ground	Acid	mg	225	1	225
87	Acetic acid, in ground	Acid	mg	225	1	225
88	Acetic acid, in ground	Acid	mg	225	1	225
89	Acetic acid, in ground	Acid	mg	225	1	225
90	Acetic acid, in ground	Acid	mg	225	1	225
91	Acetic acid, in ground	Acid	mg	225	1	225
92	Acetic acid, in ground	Acid	mg	225	1	225
93	Acetic acid, in ground	Acid	mg	225	1	225
94	Acetic acid, in ground	Acid	mg	225	1	225
95	Acetic acid, in ground	Acid	mg	225	1	225
96	Acetic acid, in ground	Acid	mg	225	1	225
97	Acetic acid, in ground	Acid	mg	225	1	225
98	Acetic acid, in ground	Acid	mg	225	1	225
99	Acetic acid, in ground	Acid	mg	225	1	225
100	Acetic acid, in ground	Acid	mg	225	1	225

Fig. 8. SimaPro 7 – Results table with a inventory list of all substances and materials involved in the life cycle.

Impact assessment results (LCIA)

The calculation process in the SimaPro 7 is based on the operation defined as a classification. During this process, the values (information) listed in the table inventory are assigned to the corresponding impact categories. After classification results must be converted to comparable values by following processes:

- 1. Characterization,
- 2. Normalization,
- 3. Weighing.

Summary of the results

In the Table 1, the results of Eco Indicators expressed in the unit [Pt] after weighing have been presented. If these data were presented for example for characterization results, it would be expressed in general units of the appropriate impact and damage categories. Presentation of all results in the same unit, the points [Pt], makes the results more transparent and much better described the cross-sectional structure of the whole environmental impact.

Tab.1. The most important results of the life cycle assessment analysis of a wooden construction.

Issue of analysis		Indicator [Pt]	Percentage part in the result of the entire life cycle [%]
1. Environmental impact of the life cycle of a wooden construction			
Final result – Eco Indicator		32,00	100
2. Environmental impact of the life cycle phases			
Assembly of a wooden construction		30,90	96,40
Final waste management		1,14	3,56
3. The processes with the greatest environmental impact			
1. Care and maintenance of tree growth		25,70	80,40
2. Growth of trees in the forest		2,03	6,33
3. Planks (Acquisition of timber)		1,39	4,35
4. Incineration of wooden elements		0,817	2,55
5. Oil for heating (Heat diesel B250)		0,726	2,27
6. Tinned steel (Tin plate 50% strap B250)		0,451	1,41
7. Storage on the landfill		0,267	0,833
8. Heating fuel (Heat petrol B250)		0,204	0,636
8. Electricity from oil (Electricity from oil B250)		0,172	0,538
9. Others		0,214	0,67
4. Damage Categories			
1. Ecosystem Quality		29,80	93,00
2. Human Health		1,31	4,09
3. Resources (Consumption of resources)		0,943	2,95
5. Impact Categories			
1. Land use		29,60	92,30
2. Resp. inorganics		1,79	5,59
3. Fossil fuels		0,628	1,96
4. Minerals		0,315	0,984
5. Acidification / Eutrophication		0,164	0,513
6. Resp. organics		0,0582	0,182
7. Carcinogens		0,0539	0,168
8. Ecotoxicity		0,0332	0,104
9. Ozone layer		0,000316	0,000987
10. Radiation		0,0000193	0,0000602
6. Positive Impact Categories			
11. Climate change		-0,594	-1,86
7. LCI results with the greatest environmental impact			
1. Transformation of forest area, forest road. (Transformation, to traffic area, road embankment.)	13,10 m ²	25,80	80,50
2. Occupation as a forest area. (Occupation, forest, intensive, normal.)	445 m ² rok	3,82	11,90
3. Carbon dioxide. (Carbon dioxide, biogenic.)	185 kg	1,01	3,15

5. Transformation to forest area. (Transformation, to forest, intensive, normal.)	3,18 m ²	0,817	2,55
6. Particulates. (Particulates, <10µm.)	81,10 g	0,792	2,48
7. Petroleum. (Oil, crude, 42.6 MJ per kg, in ground.)	142 oz	0,586	1,83
8. Nitrogen dioxide.	195 g	0,537	1,68
9. Nitrogen oxides.	157 g	0,432	1,35
10. Non-methane volatile organic compounds. (NMVOC, Non-methane volatile organic compounds, unspecified origin.)	60,90 oz	0,313	0,978

Interpretation of the results

Obtaining results from the LCA analysis do not mean the end of the task. There is a problem, if these results are reliable. Taken into account the fact that almost every stage of analysis has specific sources of uncertainty and is affected by them each level of results aggregation, the key role plays the degree of reliability. To finish the task of the analysis, phase of interpretation, which is responsible for statistical determining the uncertainty and sensitivity of the final results, should be done.

Conclusions

In the paper the main phases of LCA analysis of wooden construction using the computer program SimaPro 7 have been presented. The example of creation a production processes and final waste management have been explained. The overall environmental impact from the life cycle of a wooden construction is 32.00 points [Pt]. This impact is the most accumulated in the damage category named as “Ecosystem Quality”, because it represents 93% of total value of Eco Indicator. Analyzing two basic stages of life cycle (assembly and waste management), it is clear that greater environmental impact has an assembly stage equal 30.90 [Pt] (96.40%). This exceeds the stage of final waste management, whose the environmental impact is 1.14 [Pt] (3.56%).

According to the results presented in the Table 1, the main source of environmental impact from the entire life cycle is the process “Care and maintenance of tree growth”, which represents the value of 25.70 [Pt] (80.40%). The second is “Growth of trees in the forest” with a value of 2.03 [Pt] (6.33%). The impact category with the greatest environmental impact is “Land use”. The rate for this category is 29.60 points [Pt], which represents 92.3% of total value of the indicator. The next impact categories are “Resp. Inorganics” (Effects of breathing / inorganic compounds) and “Fossil fuels”. Result as an indicator for the first category is 1.79 points [Pt], which represents 5.59% of the total result. In case of fossil fuels result is 0.628 points [Pt] and covers 1.96% of the Eco Indicator.

According to performed statistical analysis of the obtained results, variability of the data used in the study is quite significant. The standard deviation is 11.50 [Pt], which represents 35.94% of the final result of Eco Indicator. Sensitivity of the obtained results on the changes in value election is much less than sensitivity on the variability of weighing criteria.

For more accurate presentation of the environmental impact scale of a wooden construction, it should be carried out a similar analysis of a similar construction, for example, made of a different material. Then it would be possible to carry out a comparative analysis and draw conclusions about differences in the size of the environmental impact for different materials (e.g. wood and steel).

The presented life cycle analysis of a wooden construction has been modeled without taking into account the phase of use the construction. An important addition to the analysis would be certainly taking into account this phase, expressed as a consumption of electricity, heat, water, etc. It can be expected that stage of use the construction would be an important part of the total environmental impact. However, the purpose of this study is not an evaluation of a different ways of use, so any assumptions related to the phase of use have been omitted. This applies, for example, the assumptions associated with various methods of heating and the power savings.

During carrying out of the analysis, an essential problem has been observed. A significant difficulties in accessing the data, characterizing certain manufacturing processes from the point of view their environmental impact have been found. In particular there is no domestic sources, which would define a detailed quantity of material and energy inputs to individual processes. An even greater problem is with the information about outputs from the processes. This applies in particular difficulties in measuring the emission to the environment.

References:

1. Czarnecki L., Kapron M. (2010), *Defining of the sustainable civil engineering*. Building Materials. Monthly Technical and Economical. Technology, Market, Execution. No. 1/2010. (in polish)
2. Gorzynski J. (2007), *Introduction to environmental analysis of products and objects*. Scientific – Technical Publishing Houses, Warsaw. (in polish)
3. Karbowski A. (2010), *Sustainable civil engineering*. Construction, Technology, Architecture. Polish Cement No. 1/2010. (in polish)
4. Krzysik F. (1975), *The science of wood*. The Polish Scientific Publishers, Warsaw. (in polish)
5. Nowak A. K. (2008), *Ph.D. thesis Environmental and technical aspects of the process of obtaining zinc and lead concentrates*. Krakow. (in polish)
6. Strykowski W., Lewandowska A., Wawrzynkiewicz Z., Noskowiak A, Cichy W. (2006), *Environmental Life Cycle Assessment (LCA) of wood products*. Institute of Wood Technology Publishing House, Poznan. (in polish)

SELECTION OF A CONSTRUCTION TECHNOLOGY FOR A BUILDING OBJECT, ANALYTICAL METHODS

Elżbieta Szafranko

University of Warmia and Mazury in Olsztyn, Faculty of Technical Sciences
Heweliusza Street 4, 10-724 Olsztyn, Poland
e-mail: elasz@uwm.edu.pl

Summary:

Selection of a technology employed to raise a building object is one of the most important decisions to be made while planning an investment project. The problem has been presented using a model of a one-floor, single-span frame with full columns and a mono-pitch spandrel beam with the solid cross-section, made as a steel and monolithic reinforced concrete construction. A series of criteria and analytical methods have been proposed.

Keywords: variant solutions of a building construction, criteria for analysis of building objects, methods for analysis of variant construction solutions

Introduction

When planning to build a construction, we have an opportunity to choose between different technologies of construction works and between different materials. Wishing to achieve economically satisfying solutions while meeting all other requirements that building constructions should fulfill, comprehensive analyses are made, based on different selection criteria. Above all, the structures of a building should be reliable and lasting, needing the least maintenance work during their usable life. Besides, they ought to be raised in a relatively short time, not incurring excessive labour and financial inputs during their construction. While analyzing a construction plan, first we need to identify its specific features, then determine the assessment criteria and finally optimize these criteria. The fundamental requirements most often comprise:

- reliability of the construction and its useful life,
- technological criteria, which depend on the used materials, machines, production processes, availability and the possibility to transport materials and construction elements to the construction site,
- functionality of the building, depending on its size and specific features,
- economic criteria, which define the costs indices, especially the costs of construction works, the maintenance costs once it is erected, consumption of materials, total weight, share of industrialized solutions in the construction process, durability and value of materials recovered once the useful life of a building is over,
- legal considerations, imposed by the law binding in the area where a given building investment is planned and executed,
- formal issues, such as imposed norms and standards,
- ergonomic and esthetic problems, to which investors and future users of the building pay special attention,
- ecological questions, regarding the impact of an erected construction on the surrounding natural environment (Tarnowski W., 1997r.)

Whenever so many criteria have to be considered, a multi-criteria analysis is employed, in which solutions selected from a whole set of options are the ones for which the value of an objective function fulfilling all criteria attains the extreme value. The objectives which should guide our analysis are to minimize costs, an aim which in the recent years has been most often set as a priority, and to reduce the weight and volume of materials, taking into account the proportions of materials, labour and equipment. An optimal construction solution is also attainable in the potential, strain and elastic strain energy by striving to reach the minimum value and the smallest possible frequency of free vibration. While checking off the above criteria, it is important to bear in mind that the reliability and safe use of a building object are two essential objectives. A construction which fails to satisfy these conditions is automatically discarded. Having to fulfill all the above conditions, a designer faces an immense challenge. Apart from knowing the fundamental design rules and principles, they should also be familiar with the current construction market, the latest technological solutions and possible future developments so as to be able to justify the choices they make for a given construction design. This article discusses comparative analytical methods applied to analyze variant construction solutions, using as a case a choice between a steel and ferroconcrete one-story single-span frame with full columns and a mono-pitch spandrel beam.

Description of a model construction

A model of a one-storey, single-span frame with full-walled columns and a mono-pitch spandrel beam with a full and solid cross-section along its entire length, bearing a uniform bracing load of the roof structure and external forces applied to the roof and the walls. For comparison, it was assumed that the construction would be made of steel and of reinforced concrete. In the presented case, for both the steel and the reinforced concrete constructions, it was necessary to assume that all joints are rigid because such is the type of joint made in a monolithic construction. The following basic parameters were assumed:

- a variable span length, that is the centre to centre span between opposite columns,
- a fixed longitudinal span of the frames,
- a fixed slope of the spandrel beam, and consequently variable heights of columns with the variable span and constant height of the construction.

The described construction is composed of the columns and the spandrel beam. With the assumed work of the construction, the horizontal elements are subjected to bending and shearing. In the ferroconcrete construction, the centre to centre span was determined depending on the adopted conditions, with the adequate dimensions typically smaller than 25% of the span of symmetrically reinforced beams; when designing the steel spandrel, HEB I-beams were used. The described structure rests on columns anchored in foundation bases whose height depends on the roof slope angle. The columns are the main elements exposed to compression and transfer all forces to elements of the foundation. Same as in the case of horizontal elements, the dimension of the centre to centre transverse section of a ferroconcrete construction oscillate within a quarter of the span, and the reinforcement is symmetrical; in the steel construction, it is made of I-beams. Figure 1 shows a design of the construction.

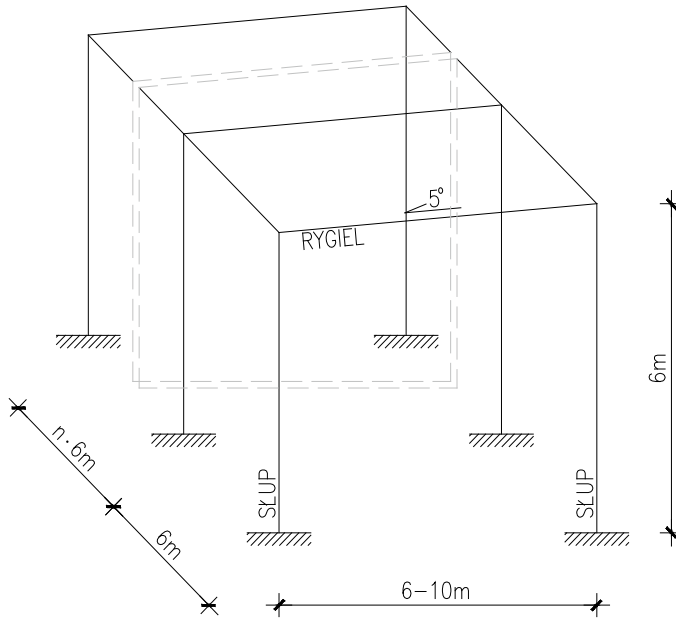


Fig. 1. Computational design of the analyzed construction

Source; the author

The following construction was taken for the calculations: a middle flat frame of a single-span hall with an inclined spandrel beam and a constant slope angle of the roof equal 5° , with the constant height at the highest point of the intersection of the column and spandrel beam equal 6 m and the longitudinal centre to centre span of the frames equal 6 m. The transverse distance between the columns will be variable, from 6 m to 18 m at 2-m intervals. The analyzed building will stand in the IV snow zone and I wind zone according to the Polish standard. The external columns are exposed only to wind, assuming the walls are cased. The length of the hall was assumed to equal $n \times 6$ m, as the analysis comprises only the middle frame and an infinite length of the building affects only the wind load calculation, which simplifies its value to a constant for different widths of the aisle in the particular variants. Below, results of solutions for individual sets of frames are presented in the form of the most optimal – with respect to their strength - steel and reinforced concrete cross-sections for particular elements of the frame, which will serve as a data base for further economic and technical considerations. In the table, depending on the span of the aisle, cross-sections of spandrel beams and columns are divided, but the latter are considered identical in each case, be it the right or the left column.

Tab. 1. Results of the static strength analysis of single-span frames *

No of variant	Span of aisle	Cross-section of left ferroconcrete column	Cross-section of right ferroconcrete column	Cross-section of reinforced spandrel beam	Cross-section of steel column	Cross-section of steel column
1	6m	25x30cm A _{sl} : 4φ12 Binders: φ6 every 20cm	25x30 cm A _{sl} : 4φ12 Binders: φ6 every 20cm	25x40 cm A _{sl} : 4φ12 Binders: φ6 every 27cm	HEB 160	HEB 140
2	8m	30x30cm A _{sl} : 4φ14 Binders: φ6 every 20cm	30x30cm A _{sl} : 4φ14 Binders: φ6 every 20cm	30x45cm A _{sl} : 3φ16 Binders: φ6 every 31cm	HEB 180	HEB 180
3	10m	30x35cm A _{sl} : 4φ16 Binders: φ6 every 27cm	30x35cm A _{sl} : 3φ16 Binders: φ6 every 27cm	30x45cm A _{sl} : 3φ20 Binders: φ6 every 34cm	HEB 200	HEB 200
4	12m	35x40cm A _{sl} : 6φ16 Binders: φ6 every 27cm	35x40cm A _{sl} : 4φ16 Binders: φ6 every 27cm	35x50cm A _{sl} : 4φ20 Binders: φ6 every 34cm	HEB 220	HEB 240
5	14m	35x50cm A _{sl} : 4φ20 Binders: φ6 every 34cm	35x50cm A _{sl} : 3φ20 Binders: φ6 every 34cm	35x55cm A _{sl} : 4φ20 Binders: φ6 every 34cm	HEB 260	HEB 280
6	16m	40x40cm A _{sl} : 6φ20 Binders: φ10 every 17cm	40x40cm A _{sl} : 4φ20 Binders: φ10 every 17cm	40x80cm A _{sl} : 4φ25 Binders: φ10 every 40cm	HEB 280	HEB 300
7	18m	40x70cm A _{sl} : 4φ25 Binders: φ10 every 15cm	40x70cm A _{sl} : 4φ25 Binders: φ10 every 15cm	40x80cm A _{sl} : 4φ25 Binders: φ10 every 40cm	HEB 320	HEB 360

* the results in the above table were calculated for ferroconcrete constructions made of C20/25 cement and A-IIIN RB 500 reinforcement steel, while the steel construction was assumed to be made from S13S steel.

Source: the author.

Foundations of the comparison of constructions with the traditional method

Among the foundations underlying comparative analyses of building constructions are the indices, which can only serve the purpose of making comparisons if possessing the same calculation base. There are several types of indices, and they all depend on the values which we refer them to. The basic parameters, which constitute the most common comparisons are:

- a building object as an entity – total costs of the building object are compared, due to the materials, labour and equipment used to raise it; they enable us to juxtapose buildings constructed by different technologies but performing the same function and used in identical conditions;
- the cubic capacity of a building – rarely used as it can be expanded due to technological requirements or the equipment and appliances used inside a given building;
- the floor area – very often used for comparisons; in the case of constructions, it very faithfully reflects surfaces of cross-sections of the elements which diminish the technological, usable surface of the whole building;
- other parameters, which interfere with the production technology, and are outside the scope of this paper, e.g. a unit that measures production and service outputs (Robakiewicz M. 1969)

The basic parameters include the ones which pertain to costs, that is financial outlays, so that we are able to analyze total costs of the construction undertaking. Other parameters refer to outlays in-kind, that is most often materials used to build the building, and consumption of materials, which helps us to compare same materials with different mechanical properties. This is very important in building objects like the analyzed model construction because the construction material contributes over 50% of the total costs of the building investment.

Other, frequently used parameters refer to weights, are closely connected to transport and assembly costs, and rely on the assumption that the lighter the construction, the more resistant the applied materials. Costs of using a building, including for example heating, repairs and maintenance works, are more often taken into consideration, too. There are some other parameters as well, which handle various spatial and design-specific aspects, e.g. safety and durability of a structure, industrialization rate of the building process, etc.

Traditional methods of analyzing building structures

Among the basic traditional methods is an approach in which parameters of the consumption of materials and unit costs are calculated and juxtaposed. The first is the ratio of the volume of reinforced concrete to steel, in appropriate standard units, used in a given structure,

$$Z = [\text{m}^3] \text{ reinforced concrete} / [\text{t}] \text{ steel} \quad [1]$$

It reflects the ratio of variant consumption of individual materials to erect the same building object, e.g. when a steel structure is chosen, and the used material equals 10 kg per the cubic capacity of the building, or when 0.05 m³ of reinforced concrete is used, the parameter is equal 5. A reverse equivalent would be the quotient of the unit prices of compared materials.

$$N = \frac{\text{unit} - \text{price} - \text{of} - \text{ferroconcrete} - \text{structure}}{\text{unit} - \text{price} - \text{of} - \text{steel} - \text{structure}} \quad [2]$$

The results of this simple analysis is the product of the above parameters. If the $Z \times N$ quotient is more than one, then the steel structure in the analyzed building object is less expensive in terms of used materials. Such comparisons can also be made with respect to other outlays, such as engaged equipment or labour (Górski W., 1970r.) While analyzing potential applicability of the above method, it appears than we can compare structures of a given function built from suitable materials, by comparing weights and strength characteristics of different types of steel or concrete. For example, a compressed element made of steel or concrete, it is possible to derive a formula for Z equivalent:

- assuming that elements achieve maximum strength, we transform the formula for the strength of a section submitted to with concentrated force.

$$\frac{Q}{A} = f_d \quad [3]$$

$$V^b = \frac{Q \cdot L}{f_d^b} \quad \text{- in the case of concrete, we need the volume used in the analyzed element}$$

$$G^s = \frac{Q \cdot L \cdot \gamma^s}{f_d^s} \quad \text{- in the case of steel, we need the used weight}$$

where:

Q - force compressing the element,

A - cross-section of the element,

f_d - calculated compression strength (f_d^b for the concrete and f_d^s for the steel element),

L - length of the element,

V^b - volume of the concrete element,

G^s - weight of the steel element,

γ^s - volumetric density of steel.

- If we assume in the above formulas that the product $Q \times L$ is the same in both cases, we arrive at the final formula to calculate equivalent Z

$$Z = \frac{V^b}{G^s} = \frac{1}{f_d^b} \cdot \frac{f_d^s}{\gamma^s} \quad [4]$$

Below, we present examples of Z equivalents for some classes of concrete and types of steel, which visualize the difference originating from properties of given materials in the analyzed work of a compressed cross-section.

Tab. 2. The comparative index Z of reinforced concrete and steel for a compressed element *

Concrete	Stael	f_d^b [MPa]	S185	S235JR	S275JR	S355J2
f_d^s [MPa]			165	205	225	295
C16/20		11,43	1,84	2,29	2,51	3,29
C25/30		17,86	1,18	1,46	1,61	2,10
C50/60		35,71	0,59	0,73	0,80	1,05
C80/95		57,14	0,37	0,46	0,50	0,66

* results in the table were computed for the steel volumetric density equal 7850kg/m³

Source: the author

Naturally, the results in the table are approximations of actual results. However, although they lack the ideal precision of calculations, this method of comparisons generates reliable results and can serve as a preliminary evaluation of a planned construction, assuming that same load capacity of the structures made from different materials is ensured. Another methods to compare costs of structures built from different materials is the one where the costs ration index is calculated for assembled constructions made from different materials:

$$\psi = \frac{a}{c \cdot S} [n \cdot c + p \cdot c(S - 1)] = \frac{a[n + p(S - 1)]}{S} \quad [5]$$

where:

$$a = \frac{G_i}{G_{i+1}} \text{ - expressed the proportion of weights of structures made from } i^{\text{th}} \text{ material,}$$

$$S = \frac{c + w + m}{c} \text{ - is the ratio of the total costs of a unit quantity of the first material (c),}$$

workshop labour (w) and costs of assembling (m) elements to the costs of material as such

$$p = \frac{w_i + m_i}{w_{i+1} + m_{i+1}} \text{ - expresses the ratio of workshop labour (w) and assembly costs}$$

(m) of the i^{th} material,

$$n = \frac{c_i}{c_{i+1}} \text{ - expresses the proportion of costs of } i^{\text{th}} \text{ materials.}$$

The above method does not include maintenance costs, which may differ from one structure to another, but for the sake of our subsequent considerations, it was assumed that this type of comparison will suffice to describe the set target of the analysis.

Basis of the multi-criteria analysis

In order to perform a multi-criteria analysis, it is necessary to define specifically what requirements the analyzed structure must fulfill and what the significant criteria would be. These criteria have already been mentioned in the introduction to this article.

Consumption of materials and technology

Nowadays, when planning investment projects, much emphasize is laid on the use of materials. This tendency is congruent with the ecological approach to the construction industry, saving raw materials, decreasing the transportation load and ensuring that the investor can attain financial savings.

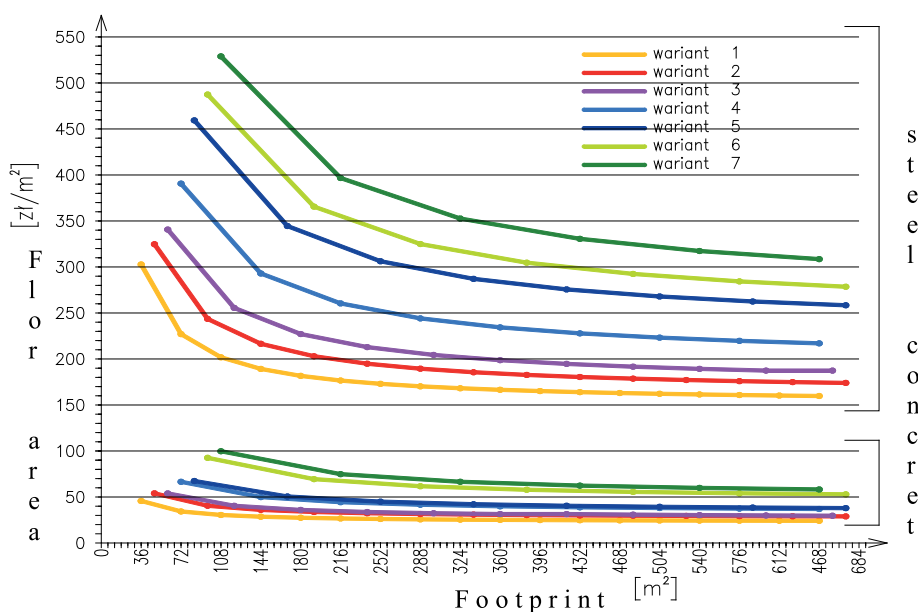


Fig. 2. Cost of used material per 1 m² of the floor area of a building depending on the footprint
Source: the author

The diagram illustrating dependences between costs of materials and footprint has been drafted based on the author's own calculations. The diagram shows an evident advantage of a ferroconcrete structure over a steel one.

It may seem futile to analyze relationships between the consumption of materials and the building's cubic capacity, having examined the its relation to the footprint. And actually many designers will think so. However, we should know that the cubic capacity of a building may change depending on a variety of parameters. The simplest ones,

usually stemming from the applied technology, are the footprint at the constant height of aisles, variable height at the constant floor area and changeable dimensions of a hall only at certain points long- or sidewise.

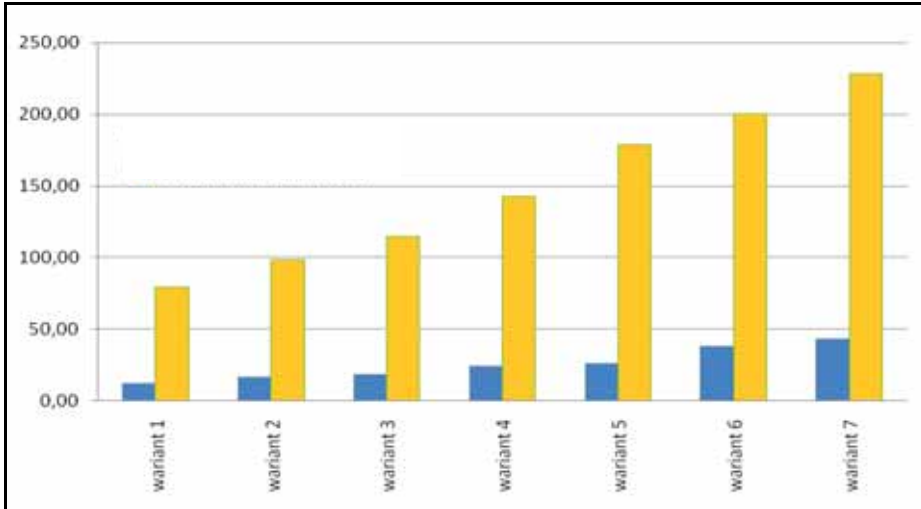


Fig. 3. Comparison of costs of used materials per 1m^2 of the surface of walls in particular variants
Source: the author

The analyzed models are simple halls, which is why the question of the unification of elements will not be considered. We will discuss, however, the effect of the surface of encasement to the costs of used materials per structure, provided the same system of building the walls. All that needs to be done is to compare frames of the spans presented before to the lateral surfaces alone, and owing to their proportional increase as the length of the hall increases, they can be analyzed in the same way as for a single-span hall.

The total costs of encasing the building will decrease proportionally to the decreasing cubic capacity of the hall, which means the decreasing size of vertical surfaces. However, let us focus on the analyzed variants, which we compare with respect to their unit encasement surfaces. It should be added that the total surface is different for each variant due to the changing widths of spans. In such comparison, as in the above point, the reinforced concrete structure is the most economical solution in terms of the consumption of materials. Comparing halls with the same cubic capacity and footprint, and consequently with the same costs of building outside walls, building objects raised from steel will be a more expensive variant with respect to the costs of materials.

Dimensions and shape of a building object

In comparative analyses of different investment project variants, it is sometimes vital to consider their shape and associated consumption of materials, e.g. allocated to the construction of outside walls, which make up the perimeter of the building. It is necessary to consider halls with the same footprint but with different dimensions in their

projections, which will generate the same cubic capacity but may have a significant impact on the costs incurred by making the encasing walls. We can achieve this goal by introducing a certain index:

$$K = \frac{\text{perimeter of the building} - [m]}{\text{the footprint} - [m^2]} \quad [6]$$

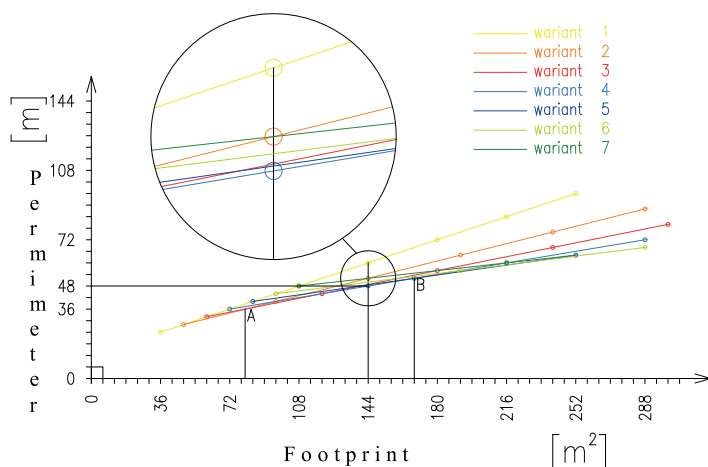


Fig. 4. The k index for particular variants, depending on the footprint and perimeter of the building
Source: the author

Dependence [6], from which the diagram was derived, enables us to demonstrate the effect produced by the shape of the building on the final price of the construction, e.g. in order to secure a set footprint without any specific demands as to dimensions of the building at the lowest possible construction costs. With the illustrated k index for specific variants, which is dependent on two variables, we can select the most optimal option of the span and length of a hall, so that the surface of the external walls should be as small as possible. Above, a certain detail has been marked for a footprint equal 144 m², which indicates that the most economical is the fourth variant, where the perimeter of the building is 48 m, the span is 12 m and the length of the hall is 12 m. For the same floor area, the diagrams drawn from variants two and seven intersect, but they are in the fifth place with respect to the economic aspects. It is worth mentioning that the analyzed hall can be constructed in modules, that is with the constant and set length of each span equal 6 m, the fact marked in the diagram with dots. For the described area of the footprint, only three variants fulfill this criterion. At point A the diagrams of variant two and three intersect, although it might appear that they are both equally optimal solutions for the given surface area of the footprint, they are not modular halls for the set lengths and widths. The situation is similar at point B, where another most optimal intersection appears, but this time it involves variants four and five, but this solution will be the

second optimal because for the footprint of 168m^2 a modular hall will have to have spans measuring 14 m. While analyzing the above diagram more meticulously, we arrive at the conclusion that the most profitable solutions are the ones whose projected shapes are the closest to the figure of a square, e.g. halls measuring 12 x 12 m, 14 x 16m, or 18 x 16 m.

Time of construction works

Another important criterion helping to choose the best solution is the time it will take to construct a given building. Each day at a construction site incurs huge costs, due to the labour done by people and machines. The presented analysis is based on generally accepted time standards determined according to the current behaviour on the market. When conducting such analysis, it is advisable to pay attention technologies employed in order to execute the analyzed variants. As assumed before, the reinforced concrete frames will be made on the site, as monolithic structures, while the steel ones will be raised from prefabricated elements made in a factory. The works required to make ferroconcrete frames include: reinforcement with steel rods (main, transverse and additional reinforcement), making pole scaffold and formwork under the spandrel beam, curing of concrete. We should also add the time needed to make cement, but in the case analyzed herein we assumed that ready-made cement will be delivered from a cement plant.

The works which must be included in an analysis of a steel structure assembled at the beginning are the assembly of elements delivered from a plant and covered with priming paint, and then painting the whole structure on the construction site. A quick look will be enough to see how much the two technologies differ from each other, although they are used to erect seemingly similar building objects. The monolithic structure involves much more complicated works, strongly dependent on numerous external conditions, which has an evident influence on the eventual duration of construction works.

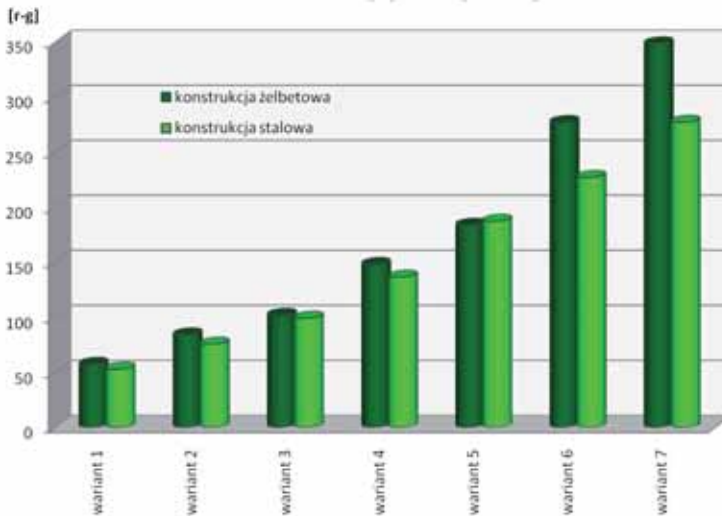


Fig. 5. Comparison of the time needed to build a ferroconcrete and steel structure in particular variants
Source: the author

The diagram illustrates differences in the time it takes to produce one frame in either of the two variants. The numbers corresponding to working hours needed to make elements of the building object oscillate within 53 to 277, which means that the work time extent by 32-50 hours for each 2-meter increase of the frame's span. Eventually, the change of the span between the columns reaching the maximum planned distance causes an increase in the duration of the construction works by as much as 80%. The increasing tendencies are similar in character for both analyzed technologies, and the steel construction is obviously much better than the reinforced concrete one, which takes much longer to make.

Associated costs of construction

When analyzing the structures in terms of the costs incurred by their construction, the costs of labour and materials connected with the major works were presented.

The costs which should be taken into account when delivering and assembling steel constructions covered in priming paint, excluding the cost of the material such as steel itself, are general construction works in respect of labour costs and steel ladders, scaffolds, steel coarse bolts with caps and washers, electrodes for the welding of low carbon steel, compressed technical oxygen, dissolved technical acetylene, grounding anti-corrosive minium phthalic paint, surface phthalic paint, thinner for oil and phthalic paints; the equipment will include: a vehicle crane, a wheeled tractor, a long-load trailer, welding machine, a transportation means.

When describing the works needed to prepare and make ferroconcrete structures, the employed technology should be considered, as it will necessitate using different types of equipment and additional materials. In this case, the costs excluding the costs of basic materials are: general construction works in respect of labour costs; materials such as round timber poles to make pole scaffolds, rough pine boards, round nails, and machines like a wire straightener, scissors for cutting wire, wire bender, a hoist, a vehicle crane, a means of transport, a concrete pump on a motor vehicle.

The diagram below shows the total costs of the above works, materials and equipment, divided into each category.

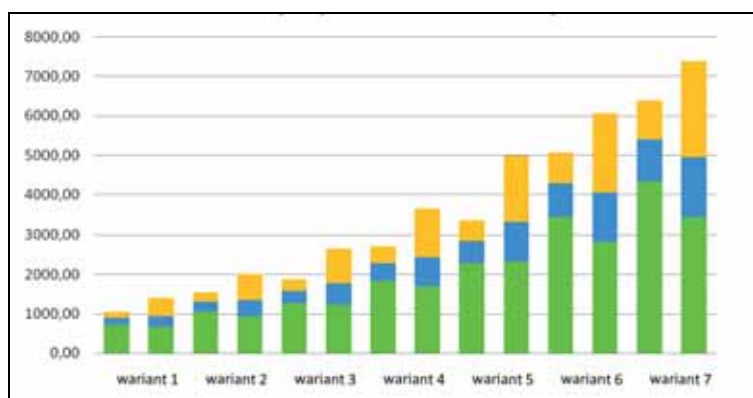


Fig. 6. Comparison of costs of making one ferroconcrete frame and one steel frame in each variant
Source: the author

Safety and durability of constructions

These are the two most important characteristics that all building constructions should possess. According to the Eurocode: ‘A durable should satisfy the set requirements throughout its whole planned life cycle, irrespective of its usability, bearing capacity and stability, without leading to any substantial decrease of its suitability to use or excessive and unpredicted costs of maintenance’ (PN-EN 206-1, 1990). In each applicable book of standards, there are provisions indicating how a structure should be designed to meet the above demands. However, it is important to abide to these norms at each stage of the construction processes, starting from a designer through the contractor to the end user of a building.

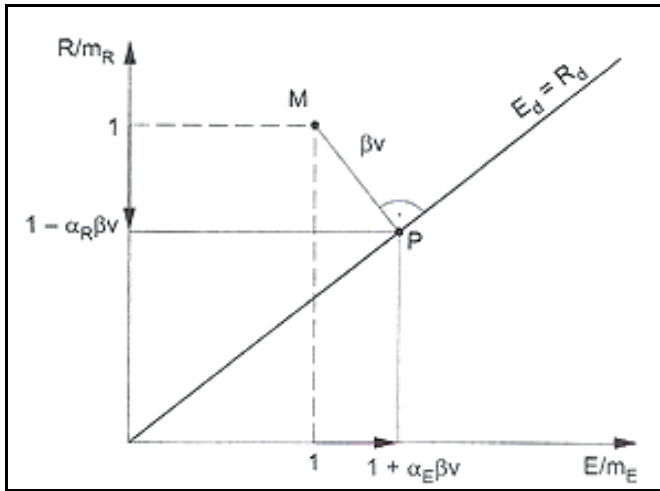


Fig. 7. Safety margin in the area of events *Source: [16]*

The above diagram shows the margin of safety that the analyzed construction has, using the partial safety factors defined in the Eurocode. It illustrates relationships between the bearing capacity and load at the terminal point P , whose coordinates depend on the β reliability index, a sensitivity index and v safety margin changeability index, as well as the margin left with respect to the actual situation of the analyzed construction (point M_0) in the form of the expression βv . This is how the safety of the construction can be defined mathematically, but in reality this aspect also depends on the designer, contractor and final user of the raised building object. The designer, who defines the conditions in which the planned construction will stand, is responsible for any simplifications in calculation procedures, adopted in such a way as to most closely reflect the reality; another task the designer must do is to check the basic reliability conditions and to determine how the construction he will design should be made. The contractor is responsible for ensuring that the building object was erected in compliance with the design and its assumption, and was assembled and prior to that manufactured with the utmost care and accuracy. The last participant of the investment process should use the building according to its designed function, check its technical condition from time to time and, whenever the need arises, perform necessary maintenance work and repairs.

It is somewhat simpler to analyze steel constructions because steel is an isotropic material, owing to which the construction is only slightly divergent from the theoretical computational assumptions. Regarding the aforementioned safety margin factors, the ones which apply to the uncertainty of the dimensions of all cross-sections and resistance specification of steel may not significantly increase the safety margin because there is very little difference between the assumed and actual values, and whenever this gap incidentally grows bigger, it will be levelled by technical checks and controls. The factor which remains highly divergent is load, which - irrespective of the used construction material - is still independent from it, obviously excluding the own weight of the material. Steel elements from a factory go through meticulous controls at each production stage and therefore respond very well to the assumed design conditions. The only element which could raise doubts are the joints. Prefabricated elements are assembled on-site, sometimes in difficult conditions, but if carried out with due care, it should not cause any worries of an unexpected fault. Another advantage of steel elements, arising from their isotropic nature, mentioned previously, is their tolerance to changes in load, either not predicted earlier or caused by some errors made during the construction works. This characteristic feature is also useful during the transport and assembly of steel elements.

Ferroconcrete constructions do not possess most of the above characteristics, especially when made on a construction site. First of all, the material as such is different. In contrast to steel, it is a multi-component material, which makes all the calculation theory more complicated. Apart from ensuring good quality of all components, it is also necessary to guarantee that they will interact with one another properly. The resistance characteristics of such material are therefore varied over a much wider range and attaining a specific strength value is extremely difficult, especially in field conditions. Moreover, it is rarely checked after a given element has been produced. Making the reinforcement exactly according to the design creates many problems and, apart from such mistakes as a wrong diameter of rods or a wrong number of reinforcement rods, practically unverifiable. Common errors are an inadequate thickness of concrete cover or making lengthwise joints between bars, rods or anchors in a way that disagrees with the building art. Other problems are encountered when ready formworks are filled with concrete mix. Irrespective of the quality of formworks, it may happen that when wet concrete whirls the so-called caverns appear, and the builder will not even know about it. All these problems can be compounded by atmospheric conditions, which can alter the whole technological process of making and curing concrete structures. The flaws described above must be alleviated by increasing artificially some of the values taken to calculations, which leads to generating larger cross-sections, reinforced with many steel bars, rods and stirrups, as this is the way to ensure one of the basic characteristics of a good construction, namely its safety.

Looking at both cases, it is safe to claim that both steel and ferroconcrete constructions satisfy all safety conditions. However, when monolithic structures are discussed, there are too many factors which must be looked at to ensure that the construction is almost ideally the same as the design. This, however, results in achieving larger dimensions of cross-sections of elements, thusly the higher own weight of the construction and higher costs involved.

Resistance of constructions to corrosion and fire

Another issue that needs to be considered is the resistance of a construction to unfavourable environmental conditions, substances causing corrosion and high temperature that occurs during a fire. Typically, building standards help us classify individual elements and describe the characteristics they should demonstrate under such circumstances.

All constructions should be as fireproof as possible, which means they should retain their functions during a fire. The recommendations contained in the national guidelines aim at preserving the stability of whole constructions as well as their elements for a set time depending on their class. Another aim is to ensure that further spreading of a fire or smoke, as well as a risk of ignition will be controlled, and the construction will behave in a way that will enable and facilitate fire rescue and escape actions. These conditions are considered in the context of materials used for making whole constructions or their constituent parts, and their interactions during a fire. The two analyzed model constructions belong to non-flammable materials with low smoke emission. Classification of elements depends on two aspects: the criteria and the time during which these criteria must be met. The classification of each element must be determined during the design stage so as to envisage ways of additional, external fire control. The main reason why this is so important to analyze tolerance of constructions to fires is that under high temperatures materials automatically lose resistance. Steel has many advantageous characteristics, but is very sensitive to high temperatures. All steel constructions are typically given fireproof protection, without which they will not last longer than half an hour. The problem is less serious in the case of reinforced concrete structures, but cannot be neglected altogether. Reinforced concrete contains steel elements, which perform an important function in the behaviour of ferroconcrete constructions.

When it comes to protection of ferroconcrete structures, the solution is simple. In order to provide all elements with a desired fireproof class, minimum dimensions of cross-sections and an adequate thickness of concrete cover for the reinforcement are designed. This is usually the only and sufficient method to protect newly raised constructions. Sometimes, however, dimensions of particular elements are limited by technological or architectural demands, which is when other methods must be deployed. These most frequently are: thick-layer covers such as fireclay mortar sprayed directly over the construction, analogously to steel structures. Other systems applied to steel constructions are not suitable to protect ferroconcrete structures from fire.

Resistance to corrosion is different for different materials, and therefore there are different anti-corrosion solutions. Regarding steel, which is used in both systems, corrosion is caused by formation of different salts on the surface of a steel element due to reaction of elements from the metal with other elements. Anti-corrosion methods include prevention of moisture and water collection by giving appropriate shapes to the elements and whole structures, or by reducing their emission when using the building, or by avoiding direct contact between unprotected steel with materials having different electro-chemical potential, e.g. aluminum. However, by being so vulnerable to the effects of external conditions, this material needs additional protective actions. They include two basic forms: paint layers and galvanizing.

These are unnecessary in ferroconcrete constructions because the concrete itself functions as a protective cover. Attention should be paid, however, to the width of gaps and thickness of concrete cover, which are regulated by norms and depend on the environment. According to the European norms, exposition classes are represented by the letter X and, depending on the environment, the number 0 when corrosion risk is absent, C – damage caused by carbonization, D – corrosion due to chlorides, S – effects of chlorides from seawater, F – elements exposed to cyclic freezing and thawing, and A – under chemical effect. Layers of concrete cover also depend on the class of applied cement and the number of checks carried out. The question of scratches is usually solved during the designing stage, by selecting adequate cross-sections of elements and amount of reinforcement.

Considering the above information, it can be concluded that anti-corrosive protection is similar to the ways of ensuring tolerance to high temperatures. Thus, steel constructions require use of different protection systems, while corrosion of ferroconcrete structures is prevented at the design stage by providing sufficiently thick concrete cover. Because the fireproof and anti-corrosive coatings on steel components can be combined, they were not analyzed separately, because the costs of painting steel surfaces would be similar. On the other hand, in our analysis of monolithic structures, the thickness of concrete cover was considered simultaneously regarding the unfavourable influence of the surroundings and an event of a fire.

Use of the construction

The major financial outlays which an investor must incur during the construction process should be amended by adding the costs needed to use and maintain a ready building object. Beside typical costs caused by maintenance, on a more or less same level each year, the analyzed model structures need periodic checks and repairs.

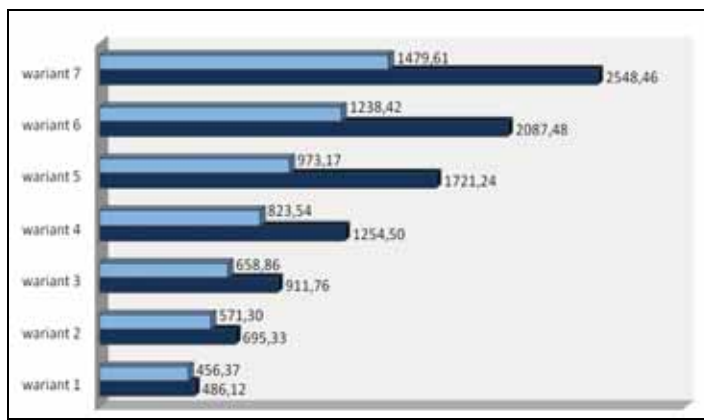


Fig. 8. Costs of renovating one steel and ferroconcrete frame after 10 years, for each of the span variants
Source: the author

The diagram in figure 8 shows differences in costs of renovation of the model solutions. With smaller spans, these costs are similar in both types of constructions, but as the span increases, the difference reaches 42%. In each variant, the financial inputs on renovation are

higher in the case of a steel structure, and differ by 6% to 42% from analogous reinforced constructions. Regarding both types of solutions in the variant with the maximum transverse span of columns, the difference rise by 81% and 69%, respectively. It is also possible to refer the calculated values to 1 m² of renovated surfaces. These data are included in the table below.

Tab. 4. Specification of costs of renovating 1 m² of steel and ferroconcrete constructions for particular variants

No of variant	Steel construction			Ferroconcrete construction		
	Total cost of renovation [PLN]	Area submitted to renovation [m ²]	Cost of renovation of 1m ² [PLN]	Total cost of renovation [PLN]	Area submitted to renovation [m ²]	Cost of renovation of 1m ² [PLN]
1	486,12	15,38	31,60	456,37	20,45	22,31
2	695,33	20,10	34,59	571,30	25,61	
3	911,76	24,35	37,45	658,86	29,53	
4	1254,50	30,54	41,08	823,54	36,91	
5	1721,24	38,93	44,21	973,17	43,62	
6	2087,48	44,96	46,43	1238,42	55,50	
7	2548,46	51,89	49,11	1479,61	66,31	

Source: the author

The data contained in the table verify the commonly accepted claim that reinforced concrete constructions are much more durable and under normal exploitation conditions do not require any major repairs during the planned usability life.

Costs of making the constructions

The total costs of constructions consist of various components. Out of the ones discussed above, the given specification contains costs of erecting the construction, costs of renovation and maintenance and costs of anti-corrosive and fireproof protection.

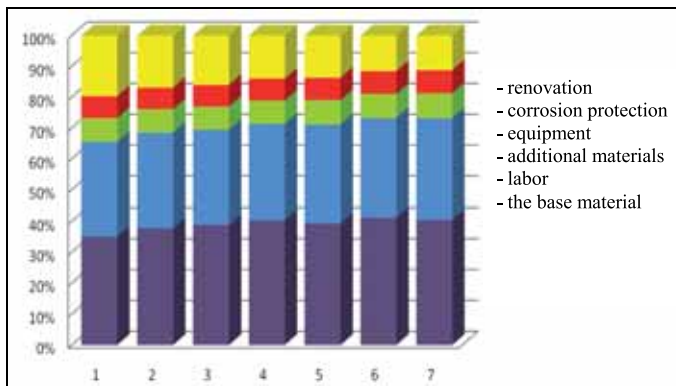


Fig. 9. Contribution of particular costs of building and using a single ferroconcrete frame in particular span size variants

Source: the author

In ferroconcrete constructions, the highest share to the total costs is contributed by the main construction material and labour – these costs are similar in all variants. The protection of a construction against corrosion or fire is minimal, almost negligible, which implies that it is very hardy to external environmental factors.

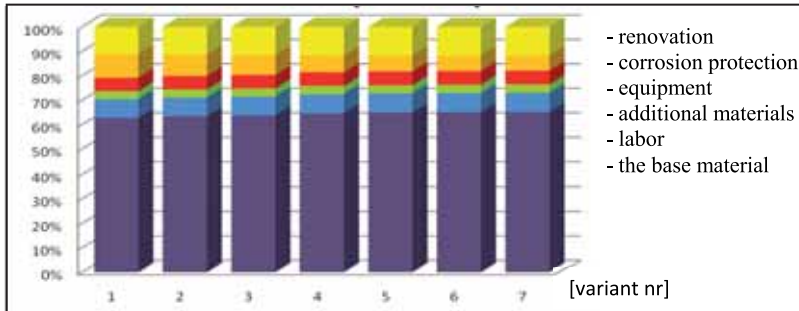


Fig. 10. Share of individual types of costs of building and using a single steel frame in particular span size variants *Source: the author*

Fig.10 shows a very high share of basic construction material in the total costs of erecting and maintaining a steel structure. Steel as a building material is very expensive. Also, notable is a higher percentage of costs of renovation and protection than in the case of ferroconcrete constructions. The other cost components are similar in both cases and do not increase notably as the span increases.

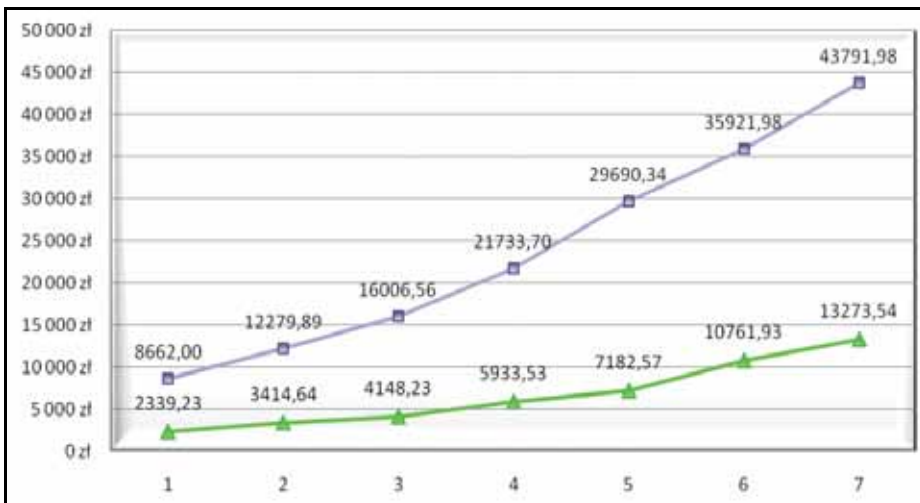


Fig. 11. Total costs of building and using a ferroconcrete frame and a steel frame relative to one frame in each variant *Source: the author*

The diagram in fig. 11 confirms our previous observations. Having analyzed all the variants, we can conclude that ferroconcrete constructions are a much more economical solution. Although the differences are small for constructions with smaller spans, it would be uneconomical to choose a steel construction when the span between columns is 18 m, as this solution is 70% more expensive.

The table below juxtaposes other aspects, which cannot be compared otherwise, for example as diagrams, because they are not mathematically comparable. The red colour highlights advantages.

Tab. 5. Main advantages and disadvantages of steel and ferroconcrete constructions

Ferroconcrete construction	Steel construction
<ul style="list-style-type: none"> • low costs of making and maintaining • small errors while building are reparable at relatively low cost, • long time to build, • the multi-component element sensitive to changes in loading direction, • large deviations of dimensions of elements, • difficulty in reproducing design assumptions, • much labour inputs to build, • many factors calling for care and attention on a construction site, • costly reinforcements of the construction, • the construction cannot be disassembled, • the material is practically unrecoverable, • large weight of the whole construction, • cross-sections of elements diminish the usable floor surface and cubic capacity, • difficulties during the assembly of installations inside the building. 	<ul style="list-style-type: none"> • high costs of making and maintenance, • each, even the smallest mistake causes serious consequences, • relatively short time to build, • the isotropic material resistant to changes in loading direction, • small deviations in dimensions of elements, • ease of reproducing design assumptions, • few activities that require control on a construction site, • quite simple and inexpensive ways to reinforce the construction, • possible disassembly of the construction, • the material can be recovered, • relatively light constructions, • cross-sections of elements need not decrease the usable floor area or cubic capacity, • easy to assemble installations in the building.

Source: the author

Analysis with the multi-criteria AHP method

The Analytic Hierarchy Process (AHP) is one of the multi-criteria analytic methods, with which it is possible to evaluate all available variants of an investment project. (Saaty 1990, 1994) The AHP approach enables the user to take into consideration various criteria which condition the attainability of the project's goal. By being a universal method, the AHP has proven practically useful in solving a broad scope of problems, from military through social and economic to technical ones. (Abu Dabous, Alkass 2008) The underlying provision of the method is that an overall goal is attainable by reaching subordinate goals, which lead to obtaining the main goal. Alternative solutions are considered, which – to a different extent- satisfy the expectations. How a given decision option fulfils the overall goal depends on the degree to which it satisfies the main criteria and, appropriately ranked, sub-criteria. Decomposition of a problem facilitates our evaluation and is the essence of the AHP method.

In this method, a problem is solved by going through three stages (steps), arranged in an integrated and logical sequence:

1. presenting the problem's structure and constructing a hierarchy model (determination of criteria),
2. evaluating the criteria on a nine-point scale by pairwise comparison and construction of an assessment matrix A (analysis of the matrix, determination of vectors of priorities),
3. evaluating and arranging the variants by setting the priorities (main weights), including the analysis of sub-priority vectors.

When applying the method, the number of criteria compared on the same level should be limited to just a few comparable ones so that it is possible to construct a cohesive matrix of comparisons. It is also necessary to assume some degree of simplification in modelling the analysed problem, to collaborate with experts and to review references as well as opinion surveys.

During the evaluation, all the criteria on a given level are compared in pairs and their mutual relations are established; thus, a decision must be made which of these criteria and to what extent will be more important for the execution of the planned project. The evaluation is achieved using an evaluation scale elaborated by Professor Thomas Saaty, which is presented below in a tab. 6.

Tab. 6. AHP fundamental scale *Source: (Saaty 1990, 1994)*

Score	Specification
9	Predominance of one criterion over the other is absolute and proven to the highest degree
7	One criterion is very strongly preferred to the other and the preference is proven in practice
5	One criterion is preferred to the other
3	One criterion is slightly more preferred to the other
1	Both criteria contribute to the same degree to attaining the goal
2,4,6,8	Intermediate values, used only when necessary

Source: (Saaty 1990, 1994)

The number of pairs creating the matrix and submitted to analysis depends on the number of defined criteria (tab. 7).

Tab. 7. Number of nodes a_{ij}

Number of criteria	1	2	3	4	5	6	7	n
Number of nodes	0	1	3	6	10	15	21	$\frac{n(n-1)}{2}$

Source: (Saaty 1990, 1994)

The next step involves construction of a comparison matrix A , in which we place the scores determined while evaluating the criteria. (Saaty 1990, 1994) The matrix has certain specific features: the diagonal consists of values equal one because it contains a comparison of each criterion to itself, $a_{ij} = 1$ for $i=j$; the elements a_{ij} are a reciprocal of the elements a_{ji} . Logically, all $a_{ij} > 0$. When the preferences (a_{ij}) are established, we can calculate elements $a_{ji} = \frac{1}{a_{ij}}$. The pairwise assessment and establishment of other elements enables the user to construct a preferences matrix. Below, a matrix constructed for 4 criteria is shown.

$$A = \begin{vmatrix} a_{11} = 1 & a_{12} & a_{13} & a_{14} \\ a_{21} = \frac{1}{a_{12}} & a_{22} = 1 & a_{23} & a_{24} \\ a_{31} = \frac{1}{a_{13}} & a_{32} = \frac{1}{a_{23}} & a_{33} = 1 & a_{34} \\ a_{41} = \frac{1}{a_{14}} & a_{42} = \frac{1}{a_{24}} & a_{43} = \frac{1}{a_{34}} & a_{44} = 1 \end{vmatrix} \quad [7]$$

In this case, for the number of criteria = 4, the number of nodes = 6.

The literature contains calculations formulas for the subsequent steps leading to the calculation of the value of a priority criterion.

These are:

Calculations of the value of a normalised matrix:

$$\overline{w}_{ij} = \frac{a_{ij}}{\sum_{i=1}^n a_{ij}} \quad [8]$$

Determination of the value of the vector of sub-priorities:

$$\overline{w}_j = \sum_{i=1}^n \overline{w}_{ij} a_{ij} \quad [9]$$

where:

$$\overline{w}_j = \frac{\sum_{i=1}^n \overline{w}_{ij}}{n} \quad i, j = 1 \dots n \quad [10]$$

To verify whether the above procedure has been correct, we determine:

- the matrix's own maximum value:

$$\lambda_{\max} = \frac{1}{w_i} \sum_{i=1}^n a_{ij} \overline{w}_j \quad [11]$$

- value of the consistency index:

$$C.I. = \frac{\lambda_{\max} - n}{n - 1} \quad [12]$$

- consistency ratio:

$$C.R. = \frac{C.I.}{R.I.}, \text{ where the CR should reach a value } < 10\%$$

R.I. - random index whose value depends on the 'n' number of compared components (tab. 8).

Tab. 8. Value of the random index (RI).

n	1	2	3	4	5	6	7	8	9	10
R.I.	0.00	0.00	0.58	0.90	1.12	1.24	1.32	1.41	1.45	1.49

Source: (Saaty 1990, 1994)

Conclusions

In the civil engineering practice, there are many ways of completing construction investment projects. Each construction can be built in a number of ways, which enables architects and designers to prepare different variants of planned buildings. The requirements set in front of building constructions, described above, show how wide is the range of analyses concerning the discussed solutions. The model construction can be made as a steel or monolithic ferroconcrete structure. The description of the construction given in this article demonstrates how differently the individual criteria are satisfied by the two technological variants. Analysis of the criteria could be a starting point for further analyses and, depending on the investor's expectations, either of the analyzed solutions can be implemented. Traditional methods have been amended with a calculation method which belongs to multi-criteria methods, namely the AHP approach. This is the method which – owing to its specific attitude to comparisons of analyzed criteria – enables us to see the problem via determination of advantages of one solution over the other, and can be successfully used in comparisons of the type dealt with in this paper.

References:

1. Ajdukiewicz A. 2011r. *Przegląd Budowlany*. „Aspekty trwałości i wpływu na środowisko w projektowaniu konstrukcji betonowych.”
2. Dąbrowski K., Stachurski W., Zieliński J.L. 1982. *Konstrukcje betonowe*. Arkady, Warszawa.
3. Giżejowski J., Ziółko J. i inni 2010. Praca zbiorowa; *Budownictwo ogólne. Stalowe konstrukcje budynków, projektowanie według eurokodów z przykładami obliczeń*. Arkady, Warszawa.
4. Górski W., Hojarczyk S. 1970. *Zarys ekonomiki konstrukcji stalowych*. Arkady, Warszawa.

5. Grabiec K., Bogucka J., Grabiec-Mizera T. 2001. *Obliczanie przekrojów w elementach betonowych i żelbetowych*. Arkady, Warszawa.
6. Łapko A., Jensen B. Ch. 2005. *Podstawy projektowania i algorytmy obliczeń konstrukcji żelbetowych*. Arkady, Warszawa.
7. Łubiński M., Filipowicz A., Żółtkowski W. 2003. *Konstrukcje metalowe. Część I. Podstawy projektowania*. Arkady, Warszawa.
8. Medwadowski J. i inni 1980. Praca zbiorowa; *Stalowe konstrukcje budowlane*. Państwowe Wydawnictwo Naukowe, Warszawa.
9. Robakiewicz M. 1969. *Ekonomika projektowania budynków przemysłowych*. Arkady.
10. Saaty T.L. 1990: How to Make a Decision: The Analytic Hierarchy Process. *European Journal of Operational Research* 48. pp. 9-26.
11. Szafranko E. 2013 "Application of the analytic hierarchy process (ahp) to evaluation of variants of a planned road investment project" ; *journal of international scientific publications: materials, methods & technologies*, volume 7, part1
12. E.K. Zavadskas, A. Kaklauskas, F. Peldschus, Z. Turskis, 2007: Multi-attribute assessment of road design solutions by using the COPRAS method, *The Baltic Journal of Road and Bridge Engineering*, 2, 4, 195-203,
13. Żybertowicz M., Bogucki W. 2010. *Tablice do projektowania konstrukcji metalowych*. Arkady.
14. PN-EN 1992-1-1:2008 *Eurokod2. Projektowanie konstrukcji z betonu. Część 1-1: Reguły ogólne i reguły dla budynków*. PKN, Warszawa.
15. PN-90/B-03200 *Konstrukcje stalowe. Obliczenia statyczne i projektowanie*. PKN, Warszawa.
16. PN-80/B-02010 *Obciążenia w obliczeniach statycznych. Obciążenie śniegiem*. PKN, Warszawa.
17. PN-77/B-02011:1977 *Obciążenia w obliczeniach statycznych. Obciążenie wiatrem*. PKN, Warszawa.
18. PN-EN-1992-1-2:2008 *Eurokod 2: Projektowanie konstrukcji z betonu. Część 1-2: Reguły ogólne. Projektowanie z uwagi na warunki pożarowe*. PKN, Warszawa.

POSSIBLE APPLICATIONS OF THE 3D LASER SCANNING TECHNOLOGY IN CIVIL ENGINEERING

Joanna A. Pawłowicz

University of Warmia and Mazury in Olsztyn, Faculty of Technical Sciences
Heweliusza Street 4/312, 10-724 Olsztyn, Poland
e-mail: jopaw@uwm.edu.pl

Summary:

Considering the constant drive to improve and accelerate building processes as well as possible applications of the latest technological achievements in civil engineering practice, the author has proposed to use 3D laser scanning in the construction industry. Field studies have been conducted on two buildings located on the university campus in Olsztyn, with the aim of verifying whether the said technology will find implementations in everyday work of civil engineers. Using a 3D laser scanner in a building process will provide an opportunity to accelerate certain activities, making the whole process more efficient. For example, data achieved through a 3D laser scanning process will facilitate making inventories of parameters of buildings in a very short time, will enable one to check irregularly shaped masses of earth, heavy and practically impossible to calculate precisely using traditional techniques. The other part of the research, performed in the laboratory, consisted of measurements of a model mound of earth. All the measurements were made with a 3D SkanStation C10 laser scanner manufactured by Leica. The data were analyzed. The results suggest that there are great opportunities for using the laser scanning technology in civil engineering.

Keywords: construction works, making inventories, earth masses, historical building, cloud of points, visualization, three-dimensional model.

Introduction

3D scanning is the state-of-the-art method based on laser technology, which creates endless opportunities for applications. Its main advantage is the rapid acquisition of huge amounts of data in a very short time, which makes it a much superior solution than any earlier measuring techniques. Terrestrial laser scanners easily find implementations in various branches of economy. The range of their capabilities means that they can be used in engineering geodesy, in specification of the parameters of buildings and building objects characterized by very complex shapes (e.g. historical buildings), in the research on deviations and deflections of building structures, but also in archeology or forensic science.

A 3D scanner is a device which analyzes in real time the measured building or surface area and collects data about the shape, texture or consistency of the object it scans and the surroundings. Properly performed scanning provides us with the data which can be processed, leading to the creation of a fully digital, three-dimensional image of the building. The trickiest part of the technology is to make accurate measurements of transparent, reflective, light-emitting or translucent surfaces because a laser beam is reflected from such surfaces in an uncontrollable manner, leading to an erroneous interpretation of the achieved information.

A 3D laser scanner is a teledetection system, which employs electromagnetic radiation emitted by the device itself. It belongs to the appliances called LIDAR (Light Detection and Ranging) equipment, while a ground laser scanner is called a TSL scanner (Terrestrial Laser Scanning). A scanner is an instrument which, once seated on a levelled and stable tripod, collects data while rotating around its own axis. Basically, it works by measuring the distance and angle between the device and the scanned object, using for this aim a laser beam which is reflected by an obstacle and returns to the instrument. The measured distance and angle allow us to visualize the scanned object by creating a point cloud with the set X, Y and Z coordinates, orientated in relation to the local set of coordinates of the laser. A cloud of points together with photographs used for reproduction of the texture of the building walls constitute a realistic visualization of the scanned building.

In this research, analytical data were collected by scanning two buildings, both situated in an area of protected architecture, which stand on the campus of the University of Warmia and Mazury in Olsztyn, called Kortowo. One is the house known as the 'Director's Villa' and the other one is now occupied by a post office. Both are listed buildings and are strictly protected as monuments of architecture. The two buildings were erected in the 1890s, as part of the then existing Asylum of the Mentally Insane.

The Villa (fig. 1) is a two-storey residential house, with a cellar and inhabitable attic. It stands in the north-eastern part of Kortowo. It is a brick building, raised on a polygonal plan, with an *avant-corps* located nearly axially, at the longitudinal and transversal axes of the main block, with a protruding wall base, finished with red kiln brick and decorated with yellow face brick laid in courses, with very carefully finished masonry bonds. The main block of the building is divided by *avant-corps* and breaks in the walls on each side of the building, and a winter garden, jutting out from the easternmost corner of the house and presenting a very complicated and decorative wooden structure. The building has a tiled roof on a timber rafter framing and a mixed construction.



Fig. 1. The villa, a view from the south (photo J. Pawłowicz 2011)

The other building, today a post office (fig. 2), used to contain flats. It stands in the north-eastern part of Kortowo, and the roof ridge runs parallel to the street. The walls are made of solid kiln brick and faced with brick joined with lime mortar. The building's roof rests on a purlin and rafter roof construction and is covered with Dutch roof tiles. This is a one-storey building with a habitable attic, made higher owing to the knee wall. There is a cellar under some of the building. The house was built on a nearly square plan.



Fig. 2. the post office building (photo J. Pawłowicz 2012)

Field assays

The preparation and execution of measurements in field must be preceded by surveying a given area. First of all, it is necessary to decide where to position the instrument and how to place the target discs, which during a later stage of data processing will help to combine the scans from all stations into one image. The scanner should be positioned so as to ensure that a laser beam can reach all details of a scanned object.. Wrong positioning or an insufficient number of scanning stations may lead to a situation when there are not enough data and the achieved three-dimensional picture of the analyzed object is incomplete. When the laser beam emitted from the device encounters an obstacle, which stops it from reaching the target, then so-called shadows or dead fields in a digital model of the object appear. Unfortunately, sometimes it is impossible to avoid such barriers as other buildings, stationary cars or plants. In addition to this, empty fields can also be created when the land parcel on which a building stands is too small. This was the case of the villa because it was impossible to move the scanner far enough to ensure that the angle at which the laser beam fell onto the building was not too sharp. As a result, there were some difficulties catching the measurements of the roof of the house. In this case, the objects which obscured the view were not only trees but also elements of the building itself (fig. 3). This is the problem which most often arises when measuring objects with complicated shapes and a complex body of the building.

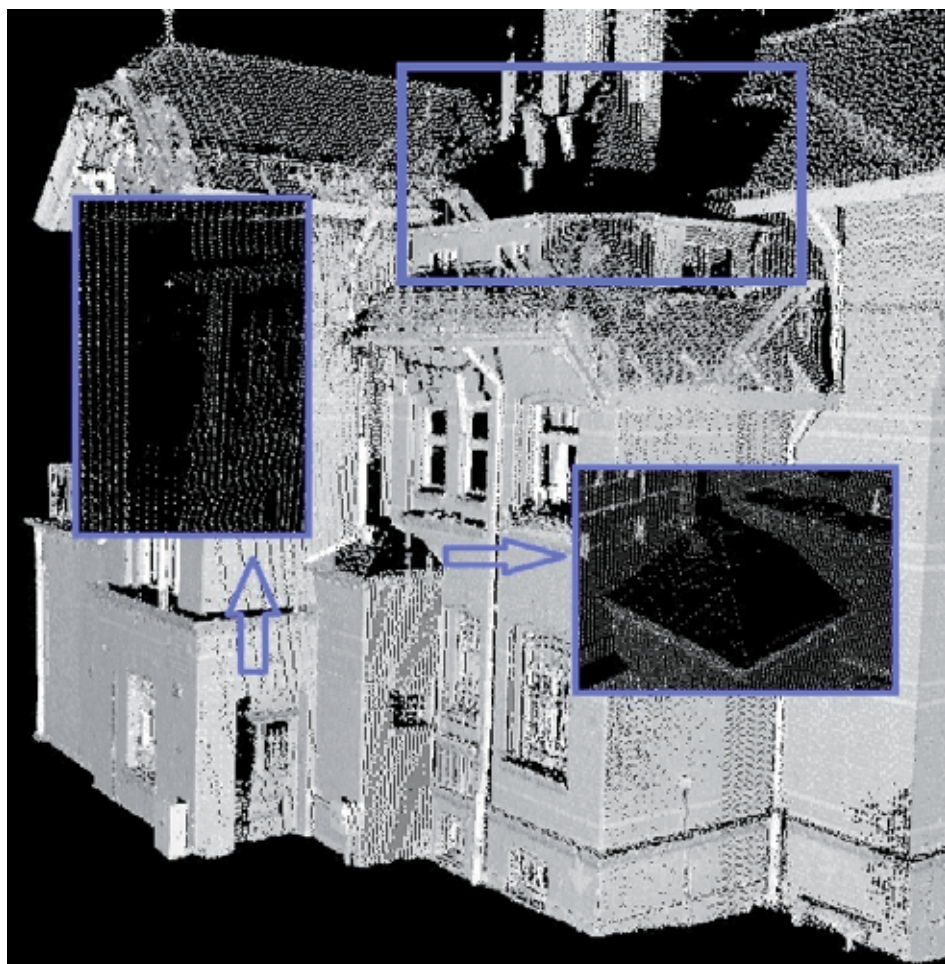


Fig. 3. Shadows on the villa.

Source: J. Pawłowicz, Z. Olek

Processing and analysis of the data

The data obtained during the measurements compose a point cloud, which is exported from the measuring device via a specialist software programme called Cyclon. When scans from all the stations are aligned and merged into a single model, and all unnecessary information is removed, it is possible to make almost instantly drawings of the building which will show all its component parts. Projections and cross-sections can be produced using the application called “a limit box”, which generates a hexagonal box with cutting edges. They can cut models of buildings at any site and create its vertical or horizontal cross-section (fig. 4), where it is possible to determine the dimensions: straight and oblique ones, diameters, arcs and any angles, etc.

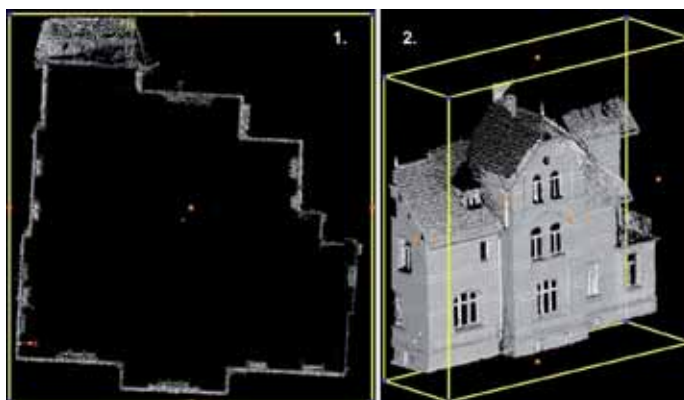


Fig. 4. Horizontal (1) and vertical (2) section through a building using limit box cutting edges (yellow lines).

Source: J. Pawłowicz, Z. Olek

Scanned interiors can also be represented as sections based on the contour of a point cloud cut with a reference plane. A point cloud can be cut in a number of ways, employing appropriate software applications. Owing to this solution, you can draw the contours of anything that is inside the building. The type of an option selected from the programme enables us to make a full (fig. 5) or contour (fig. 6) cross-section. The achieved drawings reveal many details, which can be measured and related to each other. This option is extremely useful when we need to make an inventory of a space characterized by a high degree of complexity, e.g. industrial buildings, or where access is difficult and it is impossible to make an inventory with classical methods (fig. 7).



Fig. 5. A projection of a room obtained using the application 'View Half-Space'.

Source: J. Pawłowicz, P. Ziółkowski



Fig. 6. A projection of a room obtained with the applications 'Cloud Shaded' and 'Cloud Silhouette'.
Source: J. Pawłowicz, P. Ziółkowski

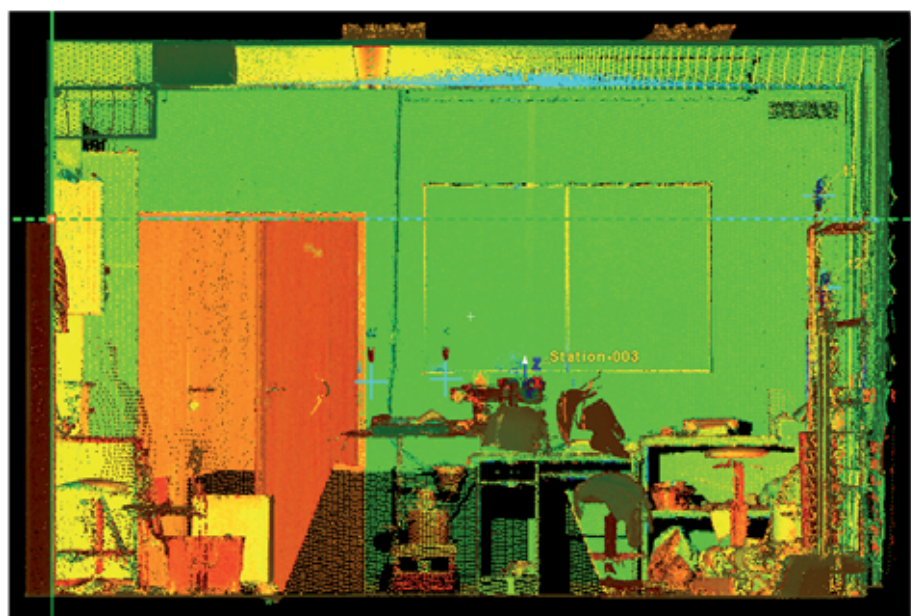


Fig. 7. A vertical cross-section through a room, using the application 'Cloud Shaded'.
Source: J.Pawłowicz, P.Ziółkowski

The data from scanning measurements also enable us to elaborate the axionometry of a building (fig. 8) or to visualize its facade walls (fig. 9). To this aim, we can employ a cloud of points obtained during field measurements, which constitutes a model of the objects, directly after the data from the individual stations are merged. The picture can be presented as a 'raw' cloud of points or a cloud with overlaid photographs, which additionally shows that colours and texture of the object.

The above information shows how easy it is to prepare technical documentation of an existing building. In the construction process, it is often necessary to elaborate such documents for a building when the original documentation is either missing or outdated. This is frequently the case when historical edifices and buildings are involved. Such documents are required for refurbishment, renovation, repairs or expansion of existing constructions. Based on the said documentation, architects and designers can work out a new design, while an estimator makes a costs analysis of a given investment. Moreover, such documentation must be made available when construction works will be awarded by a tender bid.

Three-dimensional laser scanning can help to prepare the documentation mentioned above, but it can also be deployed later to record stages of construction works and to monitor their progress when new buildings are erected. Documentation prepared with the aid of scanning technologies can act as proof for a building inspector or a construction site manager in case of any flaws. During the building works, some elements, e.g., reinforcement rods or wires, are hidden in concrete, which makes it a cumbersome venture to try and assess whether the reinforcement made is faithful to the design. Using a scanner for regular checks at consecutive stages of a building undertaking helps to determine later if everything has been done as planned, but also to capture flaws often invisible to the naked eye or found on covered elements. Having a scan of an element, before it is cast in concrete, we are able to see how the reinforcement structure was laid and to determine the parameter of used wires and rods. Furthermore, when we make scans alongside taking photographs which will show the texture of the object, it is also possible to assess the state of reinforcement at the moment it was covered in concrete, for example we can check whether it was not corroded, or if it was smooth or ribbed steel.

Recapitulating, it is obvious that using the 3D laser scanning technique for the purpose measuring and monitoring of a building is extremely helpful in civil engineering, as it can save us time as well as help to achieve better accuracy and safety of constructions works, and complete them in a shorter period of time.

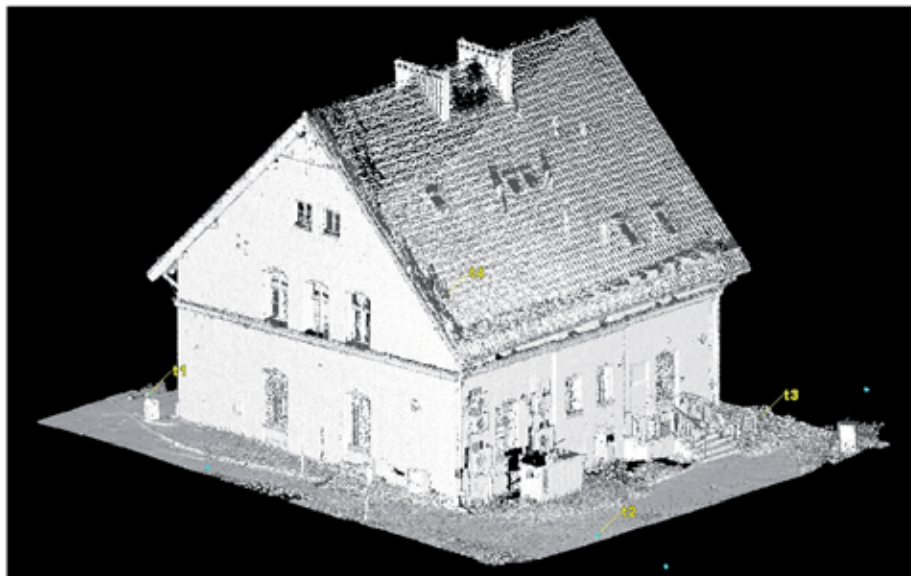


Fig. 8. An axionometric projection of the office building in Kortowo, without an overlaid texture.
Source: J.Pawłowicz, P.Ziółkowski



Fig. 9. A wall of the post office building with the texture.
Source: J.Pawłowicz, P.Ziółkowski

Measurements of volume of earth masses – laboratory assays.

Construction works often involve earthwork. The 3D laser scanning technology can also be successfully applied to control volumetric volume of earthen mounds and trenches. This part of the research was conducted in a laboratory. The objective was to determine what precision is attainable in measuring the volume of earthen material. The tests were carried out in the Laboratory for Testing Concrete, at the UWM in Olsztyn. A portion of 0.005 m^3 of medium grain aggregate was measured and used to make a mound. The mound was then scanned at high resolution. The higher the resolution, the denser and more accurate the point cloud obtained.

The experiment was conducted in two stages. First, high resolution scanning was performed at three laser measuring stations. Next, during the second, control stage, the measurements were taken at four stations but with medium resolution. Once the observations were completed, the data were exported to a computer. They served as a basis for making a model of the mound in the form of a point cloud (fig. 10).

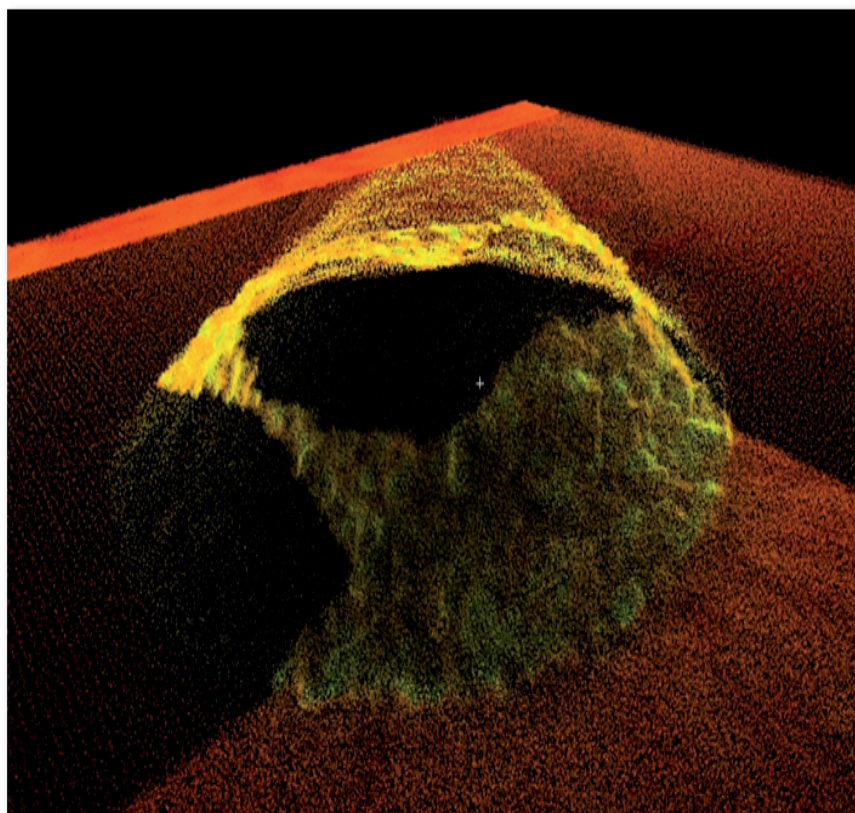


Fig. 10. A model of a mound of aggregate in the form of a point cloud.

Source: J.Pawłowicz, P.Ziółkowski

The volumetric volume was measurable once the cloud was transformed into a 'mesh' model, but to achieve this a TIN (Triangulated Irregular Network) mesh had to be overlaid. This is a mesh composed of triangles and each vertex of every triangle connects with points in a cloud, creating a surface. It is possible to modify the number of triangles in a model so as to reduce occlusions caused by matching noises appearing directly above the object to the Tin mesh (fig. 11). The default number of triangles is 105 of the basic model. Once the integration step is set, we can begin the volume of a mound. The result is given in m^3 (fig. 12).

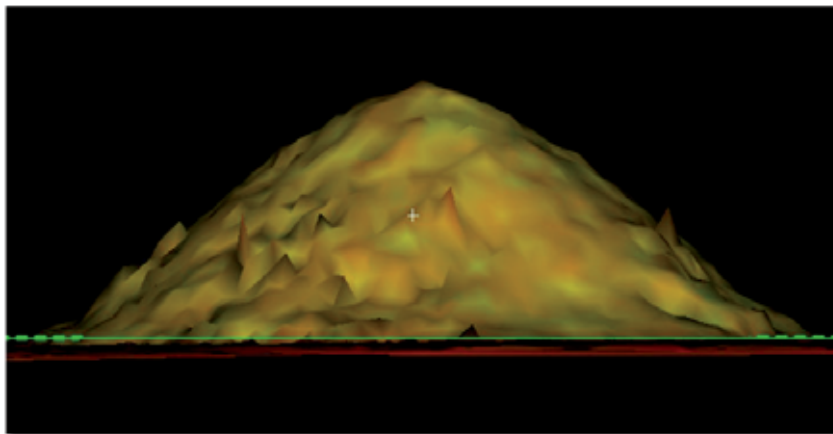


Fig. 11. A lateral view of the mound after overlaying and integrating TIN mesh.

Source: J.Pawłowicz, P.Ziółkowski

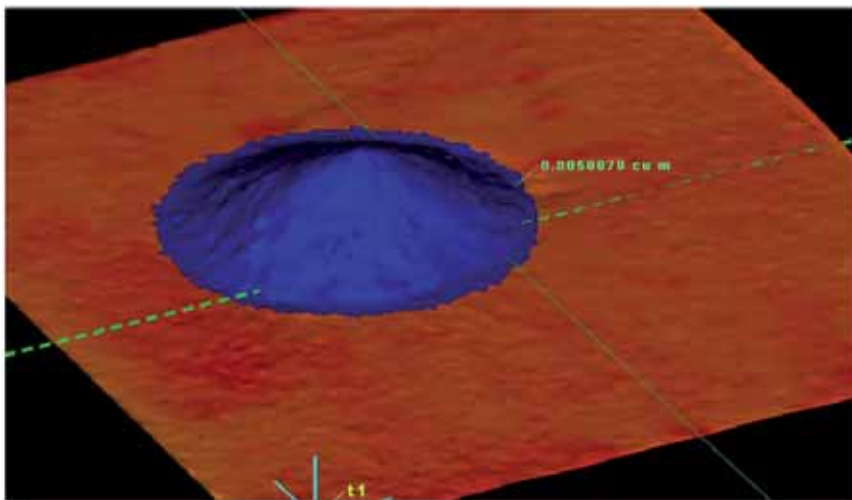


Fig. 12. Measuring the volume of a mound.

Source: J.Pawłowicz, P.Ziółkowski

The volumetric volume was measured at three integration steps: 0.1m, 0.05m, 0.01m. The degree of integration attained through decreasing the number of triangles in the mesh was determined consecutively at 100%, 10%, 8%, 6%, 4%, 2%, 1%, 0.5%. The results are contained in the tables below (tab. 1 and tab. 2).

Tab. 1. Results from test 1

Table of results from test 1			
Degree of diminished density of triangle mesh [%]	Model volume [m³]	Volume of the model	Difference in volume
Integration step– 0.10m			
100	0.005	0.0051668	-0.0001668
10		0.0050879	-0.0000879
8		0.0049888	0.0000112
6		0.0049749	0.0000251
4		0.0049803	0.0000197
2		0.0049701	0.0000299
1		0.0049674	0.0000326
0.5		0.0049576	0.0000424
Integration step– 0.05m			
100	0.005	0.0050249	-0.0000249
10		0.0050509	-0.0000509
8		0.0050499	-0.0000499
6		0.005043	-0.0000430
4		0.0050411	-0.0000411
2		0.005021	-0.0000210
1		0.005018	-0.0000180
0.5		0.0050099	-0.0000099
Integration step– 0.01m			
100	0.005	0.0050445	-0.0000445
10		0.004874	0.0001260
8		0.0049953	0.0000047
6		0.0050189	-0.0000189
4		0.0050182	-0.0000182
2		0.0050153	-0.0000153
1		0.0050087	-0.0000087
0.5		0.0050013	-0.0000013

Source: J. Pawłowicz, P. Ziolkowski

Tab. 2. Results from test 2.

Table of results from test 2			
Degree of diminished density of triangle mesh [%]	Model volume [m³]	Volume of the model	Difference in capacity
Integration step – 0.10m			
100	0.005	0.0050020	-0.0000020
10		0.0049558	0.0000442
8		0.0049517	0.0000483
6		0.0049456	0.0000544
4		0.0049327	0.0000673
2		0.004921	0.0000790
1		0.0049059	0.0000941
0.5		0.0049015	0.0000985
Integration step – 0.05m			
100	0.005	0.0048004	0.0001996
10		0.0047998	0.0002002
8		0.0047986	0.0002014
6		0.0048001	0.0001999
4		0.0048011	0.0001989
2		0.0048201	0.0001799
1		0.0048047	0.0001953
0.5		0.0048021	0.0001979
Integration step – 0.01m			
100	0.005	0.0048644	0.0001356
10		0.0048443	0.0001557
8		0.0048447	0.0001553
6		0.0048459	0.0001541
4		0.0048446	0.0001554
2		0.004841	0.0001590
1		0.0048354	0.0001646
0.5		0.0048246	0.0001754

Source: J. Pawłowicz, P. Ziolkowski

Based on the results of tests, the smallest difference in the volume of the mound model was determined, relative to the actual volume of the aggregate, and the result was 0.0000013m³, which corresponds to a deviation in the range of 0.026% of the model value. The mean deviation of all the variants of possible configurations during the processing of data was 0.274% for test 1 and 2.740% for test 2. Obviously, the 3D

laser scanning technology is suitable to measure volumes of earthen masses in civil engineering. Besides, a scan with a higher resolution of measurements yielded results more accurate by an order of values than observations with a laser device set at lower resolutions.

Summary and conclusions

While conducting field observations, it became obvious that time of day when scanning is done also matters. An engineer at a construction site, who often works in different weather conditions and different light intensity, must take into account the fact that time of day and weather conditions may affect the accuracy of recorded data.

Some of the measurements of one of the analyzed buildings were carried out in the afternoon and evening (from full sunlight to twilight). While analyzing the data, attention was drawn to the fact that the range of an area a laser can scan is much bigger under full sunlight than just before the sun sets or in the dark. These observations are presented in table 3.

Table.3. Relationship between the furthest point observed by a scanner and the sunlight falling on the building.

No	Hour of observations	Degree of sunlight	Distance to furthest measured point [m]
1	15.00	Full sunlight	291.263
2	16.30	Light cloud cover	245.701
3	18.00	Sunset	226.453
4	19.30	Twilight	194.911
5	21.00	Darkness	192.400

Source: J. Pawłowicz

Construction works are often carried out under changeable weather conditions, and a construction site is a difficult place for making any kind of measurements. A laser scanner is a device which will enable us to measure more precisely masses of earthen materials or control whether the building works are carried out correctly. However, as the above table shows, the distance to the furthest captured point decreases from full sunlight to twilight, and this can be considered as some kind of nuisance. On the other hand, observations with a laser scanner cannot be made facing the sun and under full exposure of the measured object to the source of light, because then unwanted noises can appear. These limitations mean that sometimes measurements need to be taken from a larger number of vantage points so as to reach all relevant 'nooks and corners'.

Finally, some light snowfall occurred during our observations. Atmospheric precipitation can also be a cause of serious problems. First of all, a laser scanner is a very sensitive instrument, full of electronic solutions, and should be protected from variable weather. Secondly, falling rain or snow which passes through a laser beam reflects the laser light and causes disturbances and distortions of a point cloud, known as 'noises' (fig. 13).

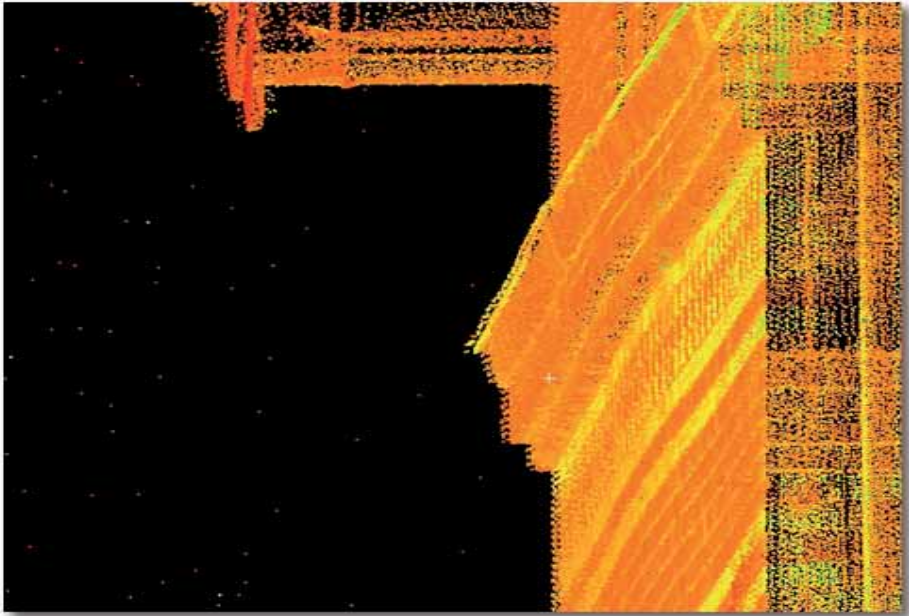


Fig. 13. Noise caused by snowfall during scanning,
Source: J. Pawłowicz, P. Ziolkowski

‘Noises’ are extra points, not connected to a model, which must be removed while processing data. The more noises, the less accurate the generated model. On the other hand, if a sufficiently dense cloud of points is measured, then some light atmospheric precipitation should not affect much the results of observations. Conversely, if the optical parts of a scanner are dirty or splashed with rainwater, then serious distortions of the final image may appear.

Noises are also created when some fragment of a laser beam falls on the edge of a measured object, as a result of which some impulse returns to the emitting device but some is reflected by another object, situated somewhere behind the target. This is known as an echo, which can be responsible for serious problems arising when we start processing data.

Despite the mentioned difficulties, it is doubtless that the 3D laser scanning technology proves useful in each of the analyzed situations. It is an exceptionally promising technology with endless applications in civil engineering, whose number and diversity are only limited by human imagination.

References:

1. Boroń A., Rzonca A., Wróbel A., (2007): *Metody fotogrametrii cyfrowej i skanowania laserowego w inwentaryzacji zabytków*. Roczniki Geomatyki, Tom V, Zeszyt 8;
2. Bojarowski K., Dumalski A., Kamiński W., Mroczkowski K., Trystuła J. (2008): *Ocena możliwości wykorzystania skanera laserowego ScanStation firmy Leica w badaniu deformacji obiektów budowlanych*; Czasopismo Techniczne, Wydawnictwo Politechniki Krakowskiej, Kraków 2008;
3. Dubik A. (1991): *Zastosowanie laserów*, Wydawnictwo Naukowo-Techniczne, Warszawa;
4. Kaspar M., Pospisil J., Stroner M., Kremen T., Tejkal M., (2004): *Laser Scanning in Civil Engineering and Land Surveying*, Vega s.r.o., Republika Czeska;
5. Kraszewski B. (2012) *Wykorzystanie naziemnego skaningu laserowego do inwentaryzacji pomieszczeń biurowych*; Instytut Geodezji i Kartografii, Zakład Fotogrametrii, Kraków;
6. Mitka B. (2007) *Możliwości zastosowania naziemnych skanerów laserowych w procesie dokumentacji i modelowania obiektów zabytkowych*; Instytut Geodezji i Kartografii, Zakład Fotogrametrii, Kraków;
7. Piechocki S., (1993) *Czyściec zwany Kortau*, Książnica Polska, Olsztyn.
8. Szafranko E. (1999) *Możliwości sterowania kosztami inwestycji za pomocą metod sieciowych*; Problemy Rozwoju Budownictwa, Kwartalnik IGM nr 4/1999;
9. Szafranko E. (2000) *Ekonomiczne aspekty remontów w budownictwie mieszkaniowym*; IX Konferencja naukowo-techniczna „Problemy remontowe w budownictwie ogólnym i obiektach zabytkowych”; Wrocław 7-9 grudnia 2000 r; materiały konferencyjne str. 459-465;

EXPERIMENTAL TESTS AND ANALYTICAL MODELS OF LIGHT WOOD-FRAMED BUILDINGS

Michał Baszeń, Czesław Miedziałowski

Białystok University of Technology, Faculty of Civil and Environmental Engineering,
Wiejska Street 45E, 15-351 Białystok, Poland
e-mail: m.baszen@kmb.pb.edu.pl

Summary:

Timber is excellent ecological material. It is biodegradable and not polluting the environment after destruction, but also it is very heterogeneous and has got various material properties. In opposition to concrete and steel structures the behavior of timber framed constructions is not properly recognized.

The authors presented in this paper a comprehensive overview of the problem of light wood-framed buildings. The wide range of experimental studies and the computational models of individual elements as well whole building in timber frame technology provided and developed in the world of science was presented.

The authors also presented the experimental tests provided at Białystok University of Technology. The range of studies, tested specimen and the results and conclusions was included in this paper. The developed numerical model using finite elements to describe behavior of wall and floor elements of wood-frame building was presented. The model had differences to previous models due to proposing the fasteners as beam elements as well the framing and sheathing as shell elements. The only nonlinear elements in proposed model were sheathing-to-framing connectors. The model was compared with the results from experimental studies and gave similar values.

The conclusions was ended this develop paper.

Keywords: light wood-framed building, experimental tests, analytical models, behaviour of timber walls and floors

Introduction

Buildings erected in lightweight timber frame technology account an insignificant segment of the construction market in Poland in opposition to the monolithic or precast concrete, structural masonry or steel structures. In contrast to other countries such as the United States, Canada, Japan and in Europe Germany or particularly the Nordic countries, this type of construction is very popular and still growing.

The popularity of this type of structure in the world comes from the environmental impact of material the buildings are made, of wood. In the United States, Canada or Finland huge tracts of coniferous forests provide excellent material not polluting environment and biodegradable. A significant feature of the timber is highly resistant to seismic impacts. In case of the Japanese islands exposed to a significant amount of shock, it is very important feature.

Of course the wood is not perfect material. Against positive features timber has negative. This material is susceptible for weather, biological conditions and depends on passing the time. Timber during use is drying unless the moisture protection. The drying

causes the change of transverse dimensions, appearance of gaps in the nodes resulting the higher flexibility and decrease the overall stiffness of the building.

Unlike steel almost homogeneous material or concrete characterized by a small variation of material characteristics, timber is very heterogeneous material. It is characterized by different compressive and tensile strength also dependent on the orientation of the fibers in the structural member.

Each tree grows in its own individual and unique way. In various trees the jars have different dimensions, the side branches appear in different places. This diversity makes the wood is obtained with similar parameters for each lot, but often differ quite significantly between different arts.

The wood frame structures are characterized by a multiplicity of connections, which distinguishes its from other types of constructions. It possible to distinguish connections between wall elements, wall and floor elements or wall and roof elements. Additionally in each structural elements exists connections between elements of timber frame as well the framing and sheathing.

The way the joints are made depends on what is connected. Components of the walls, floors or roofs are combined into one unit with shank fasteners, as nails, bolts, screw or staples. Increasingly the glued joints are used because of higher stiffness than nailed connection. In case of wall to wall, wall to floor or wall to roof connections appears the nodes connected by the bolts or screws but often the rigidity is increased by using woodworking joints.

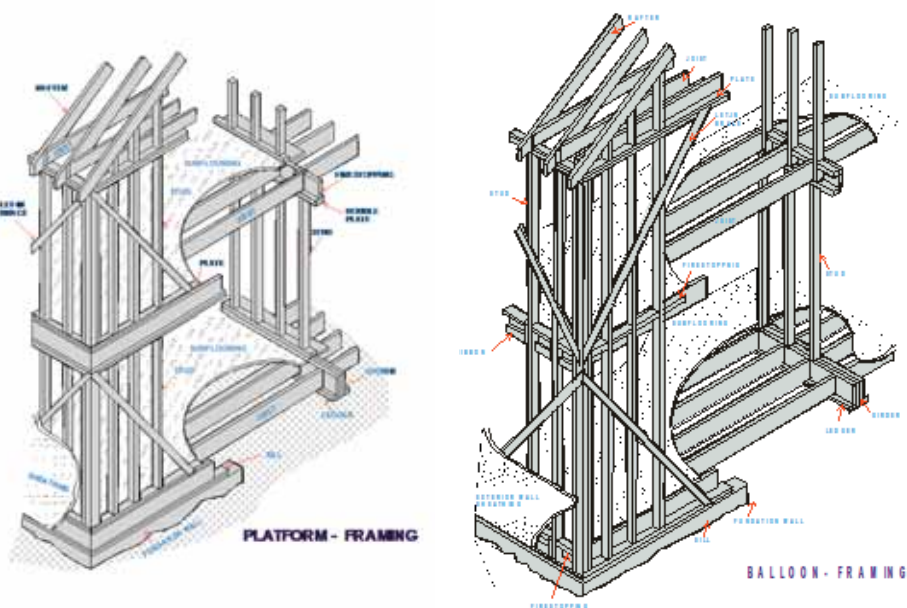


Fig. 1. System of wood-framed buildings: a) platform, b) balloon

The connection of elements in the structure is determined by the type of building that is erected. In platform framing system (Fig. 1a), the ceiling of the lower level is used as a working platform, in the construction of the walls of the next floor. In case of balloon framing system (Fig. 1b) the studs of the walls are raised to the height of the building and floor elements are created by connection of joists with the studs and sheathed by the panels of ceiling.

In balloon framing system it is possible to create joints which greater stiffness. It depends upon the construction of the joint as well as the numbers and type of fasteners used. Disadvantage of this system is reduce the height of the building to the length of timber arts used to create studs.

The opportunity to create high buildings limited only by capacity and stiffness of structural elements is possible using platform framing system. Additionally this system is perfect to use prefabrication, which reduce the time necessary to erect the building according to better implementation of capacity and stiffness of the structural elements.

Although the timber framed construction has more than 60 years, still the issue is accurate analysis of its behavior. The experimental tests and numerical analysis allowed to specify the behavior of construction work but still wide range of its characteristics remain unexplored.

A very important issue is the need to present the work of joints, as well its stiffness, which determines the stiffness of overall structure. The rigidity and thus the flexibility of joints determines the distribution of internal forces between the individual elements, affecting on structure behavior and its capacity.

The great importance for the joint stiffness is the passage of time and the associated drying of wood or the emergence of gaps. The gaps degrades connection accuracy, reduce its stiffness and affect onto overall stiffness of the building, which may result in excessive deformation or buckling.

Experimental tests

Wall elements

Starting from 40's of 20th century the experimental test of wood-frame structural elements were conducted. Initially the stiffness of walls was provided by corner anchoring or diagonally nailed timber plates. First recommendation for using sheathing panels appeared in guidelines publish in 1949.

Beginning from 50's the experimental studies focused on test of full-scale building. Soon the researchers found out the easier way to know behavior of wood-frame building is recognizing the behavior of individual elements as walls, floors or roofs.

The experimental tests allowed to observe many aspects of wood-frame structure work. The minimum thickness of sheathing was recognized as 9,5mm. The thickness greater then the limit allows to omit the buckling of panels (Dolan 1989). The limited length of shear wall which provides the cooperation in lateral load distribution is 1,22m (White 1995). The shear-walls of less length should be omitted in stiffness analysis of whole structure.

Influence of openings on element bearing capacity was studied. The empirical equations was developed to calculate the capacity of perforated elements (Sugiyama, Matsumoto, 1994). Property of proposed equations was experimentally verified (Johnson 1997).

Existence of openings affects on shear-wall bearing capacity so to prevent the element of failure it is necessary to use anchor bolts. Using anchoring along each opening increases the capacity and stiffness of shear-wall as well changes the destruction scheme. In the absence of anchoring destruction is uplifting studs and sheathing from bottom framing beam. Due to application the anchor bolts the destruction is provided as cutting the sheathing by the nails (Heine 1997).

The distance between edge of sheathing and lines of nailing affects on the capacity and stiffness. Lower distance causes the 20% less capacity and stiffness. The increase of capacity and stiffness is possible by applying more fasteners connecting sheathing with bottom framing beam (Salenikovich 2000).

The seismic response of wood-frame building is very important when the numbers of earthquakes is increasing. American guidelines ASCE Standard 41 (2007) use very conservative drift level to represent near collapse deformation at 3% limit drift. Experimental studies presented that using lateral braces increase the limit of inter-story drift to 7~10% level (Pei et. al., 2013).

The development of wood frame construction in Poland, as well as the emergence of companies manufacturing these buildings caused the desire to know the behavior of the structures. It resulted in a number of studies carried out at the Bialystok University of Technology (BUT). The aim was to describe the behavior of shear-walls and floor elements and create the calculation model for extensive analysis (Malesza 1997), (Baszeń 2004).

The first tests focused on the three panel shear wall (Malesza 1997). In opposition to more previous studies the structures was loaded by lateral as well vertical load simulating dead load and live loads of upper floors.

Three specimen 3,75m long and 2,75m high was loaded. The framing was made of pine wood class C-27. The studs and horizontal beams had 135x45mm transverse dimension. The stud spacing was 625mm. The framing was one-side sheathed by chipboard 12mm thick. The sheathing was divided to three separate panels 1,25m long and 2,75m high.

Framing connections were provided by two G 5/150 nails on each node. Sheathing-to-framing fasteners were G 2,7/65 nail with 150mm spacing on perimeter and 300mm spacing on the middle stud of each sheathing panels.

The experiment was conducted in three phases. The first phase was the beginning load at 10% destruction load level. In this phase the lateral and vertical loads were applied separately. The second phase was similar to first phase only the level of load was increased to 40%. In last phase the structure was loaded at the same time by lateral and horizontal loads until the destruction appears.

During the tests was observed that nonlinear behavior of sheathing-to-framing connectors affects the nonlinear behavior of the specimen. Shear wall work as plate-plane stress system. It is important due to load eccentricity. The influences on the plate state of work is conducted by sheathing thickness and fastener length.

The next experimental tests focused on aspect of opening in shear wall and its impact on capacity and stiffness of wall element. The second part of the study was the behavior of short length shear-wall (Baszeń 2004).

Four specimen with one sheathing panel 1,25m long by 2,75m high and three specimen 3,75m long by 2,75m high with three separate panels of sheathing was tested. The longer elements had in middle part the window opening (Fig.2).

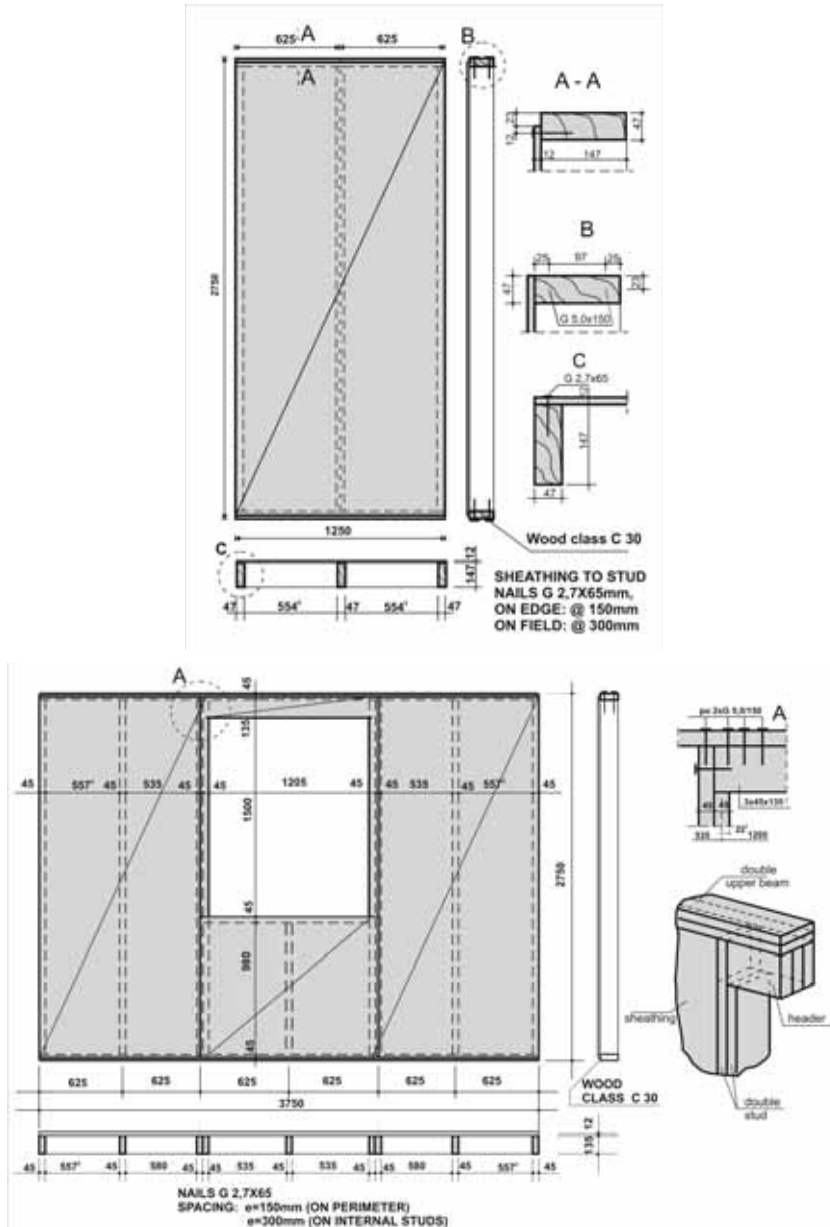


Fig. 2. Wall specimen: a) single wall, b) wall with opening

Framing was made of spruce wood class C-30. The dimensions of framing in single panel wall were 47x147mm, while in walls with opening were 45x135mm. As the sheathing was used chipboard 12mm thick divided to three separate panels with the same length.

Connection in framing was provided by two nail G 5/150 at each node. Sheathing-to-framing connection was made of G 2,7/65 nails with spacing 150mm on the perimeter and 300mm at middle stud.

In single wall the stud spacing was 602,5mm while in wall with opening 625mm. Additionally along the opening were built in two studs. The stud below the opening had length determined by the opening dimension. Additional horizontal beam was built in under opening. Over the opening was introduced the lintel made of three beams with the same dimensions as rest of framing. The lintel was based on the additional studs and connected with modular studs by the nails. The same system, configuration and phases of loads was used as at the previous studies.

During the studies was observed that wall with opening similar to full three panel wall from Malesza's test had accurate stiffness to prevent the destruction deflection. Single panel wall have had inaccurate stiffness to be included in lateral load distribution. That verified conclusions from previous studies (White 1995).

Force distribution between individual elements of wall with opening was at the same level, independent to type of loads. In single panel wall increase of loads, especially lateral, affect the decrease of sheathing in carrying the external load from 40% to 20% level. The decreasing was due to loss of capacity of fasteners.

The stress values in sheathing were greater in cross-section passing through the opening in opposition to cross-section under the opening. Stress in studs in wall with opening was less than in accurate wall without the opening. It depended on more studs in wall with opening.

Destruction of single panel wall followed by uplifting the stud at the same side as application of lateral load. Another scheme of destruction was the lost of sheathing-to-framing fasteners capacity at top corner opposite to lateral load.

Destruction of walls with opening followed by the lost of sheathing-to-framing fasteners capacity on the stud opposite to lateral load. Due to the existence of independent panels had also been the pressuring and the crushing of the panels.

Floor elements

Floor elements behave more like rigid body rather than elastic (Yokel et al., 1973), (Phillip et al., 1993). That is the reason why its have less deformation then wall elements. It results the designing is often limited to use of tabular summaries contained in design guidelines, for example, ATC (1981). The downside of using guidelines is taking into account only typical shape of building but exclude existence of openings. The problem also appears when the shape of building is different to rectangular.

Experimental study of floor elements started in the 50's of last century. One of the first test was carried out by Countryman (1952), later floors was investigated by Tissel (1967).

The first attempts to estimate openings impact on floor behavior was made in 1981. The tests were not conducted according to APA preferences, so the results were not properly verified (Tissel, Elliot, 1981).

Also in Japan wide studies over floor elements were conducted. Unfortunately most of the results were printed only in Japanese. The one of Japanese researchers, Kamiya, conducted wide experimental studies resulted proposed „membrane-to-brace” calculation model. The model gave results similar to experimental data as results calculated according to ATC guidelines (Kamiya 1990).

Next experiments allowed to develop the model to include existence and position of openings (Kamiya 1992). The aim of next step of floor element studies was concentration of shear force around openings and generation of axial forces in framing (Kamiya, Itani, 1998).

In BUT together with experimental studies of walls the test of floor elements were conducted. The same experimental stand were used as during wall tests, so floor elements was loaded in vertical position. The position of specimen allowed application only in-plane loads simulating lateral forces.

The were tested four specimen in two series by two elements. The dimensions of specimen was 2,75x3,75m for first series and 2,75x3,6m for the second (Fig.3).

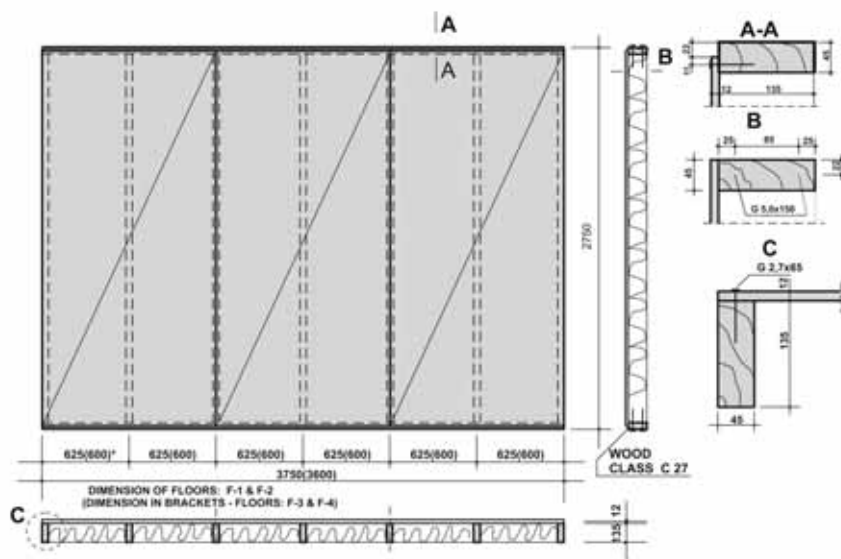


Fig. 3. Floor element

Framing was made of wood class C-27 with transverse dimension 45x135mm. Joist spacing was 625mm. As sheathing was used chipboard 12mm thick separated into three panels.

The connection of framing elements was made of G 5/150 nails by two fasteners on each node. The sheathing-to-framing connections were made of G 2,7/65 nails. The fasteners spacing were 50mm on the distance of 1m from the edge of specimen as well 100mm in the middle. The spacing of fasteners connecting sheathing to perimeter beam was 150mm.

During experimental test observed that sheathing is cooperating with framing in wider range than in wall elements. This is due to greater number of sheathing-to-framing fasteners and hence the greater stiffness of floor elements.

The stiffness of floors on low level of external load is very high, so nonlinear behavior of elements is not clearly visible as in case of wall elements.

Load distribution

Light wood-frame buildings are made of structural elements cooperating in carrying the external loads. Stiffness and capacity of whole structure is summation of each elements as walls, floors and roofs.

Walls are carrying the vertical forces from dead and live loads but also working under the lateral load from wind or seismic impacts transferred by floor elements. In both cases wall works as plane-stress element.

Floors also work in two ways. Live load makes the floor behave as plate while under lateral load submitted by perpendicular wall system, works as rigid beam.

The vertical load transmission on individual structural elements depends on how the floor lays on the walls as well the connection type (Lewicki 1979).

Under the lateral load from wind or seismic activities the distribution depends on the stiffness of individual elements. Capacity of single wall is linearly dependent to length. The stiffness change is describe by nonlinear function (Patton et al, 1985). Additionally in stiffness analysis of whole structure is necessary to omit existence of shear walls with length less than 1,22m (White 1995).

Stiffness of wall element is the function of framing, sheathing and nailing stiffness. More fasteners at each panel of sheathing increase the structure stiffness (Dolan 1989), (Baszeń et al., 2000). Increase of studs spacing decrease as well stiffness as the capacity. It depends on using less numbers of fasteners to connect sheathing with framing.

The important to the stiffness is the way the sheathing panels are shaped and nailed. Using continuous panels of sheathing increase overall stiffness of structural element (Dolan 1989), (Baszeń et al., 2000). Similar situation is observed for horizontal orientation of sheathing. The stiffness is 40% higher opposite to vertical orientation (Wolfe 1983). Increasing of the total stiffness is possible by consideration the existence of inner gypsum boards (Rose, Keith, 1996).

Joints

The nonlinear behavior of structural elements of wood-frame buildings is the result of fasteners nonlinearity.

The wall ability to carrying the external loads depends on sheathing-to-framing connection type. The most common fasteners despite high strength have a small cross-sectional area. That make the connection as most vulnerable component of the structure.

The first pay attention to it McCutcheon (1985). During experimental studies was observed the P-D function of fasteners is decisive for resistance to destruction.

The most important for structural element deflection is the destruction type of fasteners. Analyzing the various type of connectors there were obtained the nails are the best. Staples also meet the general criteria of capacity, but do not reach this level of capacity and stiffness as nails properly applied (Zacher, Gray, 1990).

To increase the capacity and stiffness of walls the glued connections are applied. This type of connection decrease flexibility of joints especially at destruction level of loads. Using glued connection with much higher capacity than traditionally nailed joints causes that nails serve as bonding until the adhesive reaches it's full capacity (Dolan, White 1992).

Destruction of joint could take different form. It may involve the bending of the fastener and pulling it out of framing or rely on sheathing's cut by nails as well as panel damage at the corners (Johnson 1997), (Heine, 1997), (Salenikovich 2000), (Baszeń 2004). The way the structure is loaded also affect on the joints destruction. Static loads cause damage by peeling sheathing of the wood frame and pulling out nails when dynamic load causes the joint damage by breaking the nails (Dinehart, Shenton, 1998).

Connection of two walls as well wall to floor is the most sensitive nodes of wood-frame building. Behavior of this kind of joints determine the behavior of whole building providing distribution of internal forces at individual elements and impact on overall building stiffness. Inadequate stiffness of the node despite the bearing capacity of structural elements could lead to disaster. Therefore most important is to determine the stiffness of this kind of nodes and develop an accurate model of its work.

The series of experimental studies of the joints to assess its stiffness was launched at BUT. In the first series focuses on the analysis of stud-to-beam connection behavior to calculate the flexibility of the joint (Fig. 4a). The next series focuses on connections of elements of two walls and floor (Fig. 4b). Future test will define the stiffness and flexibility of various types of connections in wood-frame buildings.



Fig. 4. Research scheme: a) stud-to-bottom beam connection, b) joists-to-walls connection

Building

Starting from 50's of last century the wide experimental studies of wood-frame buildings was carried out. Because of high cost the studies was provided only at limited scope so the results were not properly verified.

One of the first test was the experiment provided in Canada on one-story, basementless house with dimension 7,3x11m (Dorey, Schriever, 1957). The exterior sheathing was omitting and replaced by aluminium siding. The building was loaded by load simulating wind and snow. The study led to the conclusion that winds in excess of 90mph causes first cracks, while snow leads to failure occur in some parts of roof at 143% of design snow load.

Another experiment was conducted on full-scale two-story house representative of housing in the United States. The wood-frame structure was 14,3 m long by 7,9m wide (Yokel et al., 1973). Results from the tests of building under simulated wind loads presented that roof diaphragms behaved like a flexible diaphragm in opposite to second floor elements behaved more like a rigid body.

Two-story typical house full tests were conducted in Japan (Sugiyama et al., 1988). The building was 7,3m wide by 10m long. During the test there were examined the influence of wall sheathing around the openings on the racking resistance of the wall as well as the effect of shear walls placed perpendicular to the direction of lateral loading.

The researchers observed a little effect of differences in floor diaphragm openings on wall stiffness, whereas the increase of lateral stiffness as the result of addition of calcium silicate sidings to walls parallel to loading.

The next tests focused on the influence of different sheathing materials on stiffness of shear walls as well the effect of horizontal elements on load distribution to the shear walls (Phillip et al., 1993). The tested house was single-story structure with 4,9m wide and 9,8m long. There were observed increase of stiffness due to inner sheathing existence. The distribution of loads on longitudinal walls was greater in case when the floor elements exist opposite to situation the floor element was disassembled.

Analysis of the behavior of building structure resulted as experimental test of two-story wood-frame house (Fig. 5) (Malesza et al., 2002).

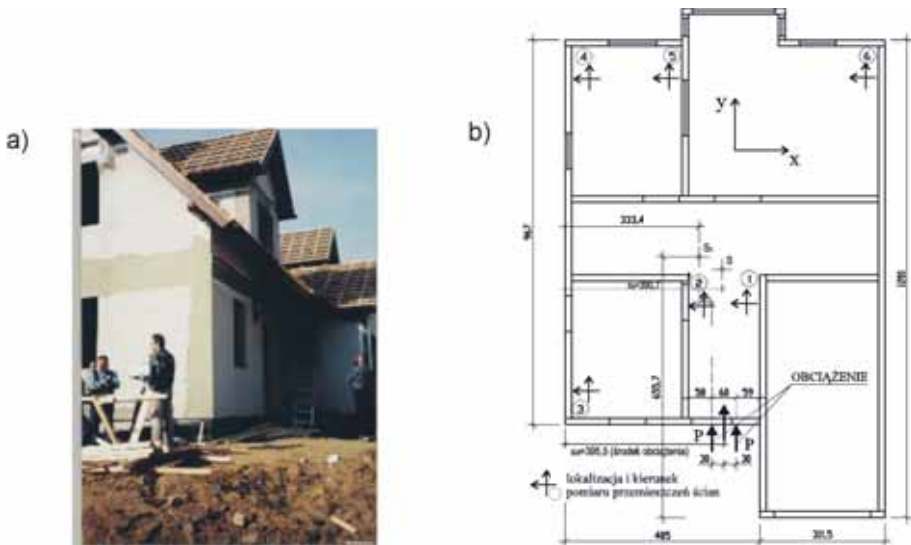


Fig. 5. Tested house (Malesza et al. 2002): a) view, b) plan of ground floor

The wall displacements under the lateral load were recorded. The lateral load simulating wind was applied as two concentrated forces (Fig. 5b). Displacements were observed at six points in longitudinal and perpendicular direction to loads. The load was assumed at design load. Results presented the building had accurate stiffness.

Major importance for wood-frame buildings is its resistance to seismic actions. South-western states of America or the Japanese islands are the places exposed to the risk of earthquakes. Therefore the experimental study was carried out to take into account the seismic response occurred during the earthquake in Kobe (Tanaka et al., 1998) and Southern California (Filiatrault 2010).

Mathematical models and numerical analysis

Wall elements

The high cost of experimental researches resulted in proposals of models describing wall behavior. For simpler cases mathematical equations was used while for more complex problem there were proposed model using finite elements.

First models assumed the fasteners behave linear (Tuomi, McCutcheon, 1978), (Gupta, Kuo, 1985). The models allowed to calculate stiffness or capacity of walls under lateral load. The nonlinear behavior of fasteners was observed during the comparative analysis of results of micro-scale tests and deflection function P-D of previously developed model (McCutcheon 1985).

The limitations of mathematical model made the next models were using finite element method. The rapid development of computer technology caused that large number of unknown is not the problem any more.

In models using finite elements the sheathing is described by plane stress elements, fasteners by system of springs, as well the wooden framing by beam elements (Foschi 1977), (White, Dolan, 1995), (Tarabia, Itani, 1997). More complex models took into account the impact pressure of sheathing panels (Tarabia, Itani, 1997), (Malesza, Miedziałowski, 2003).

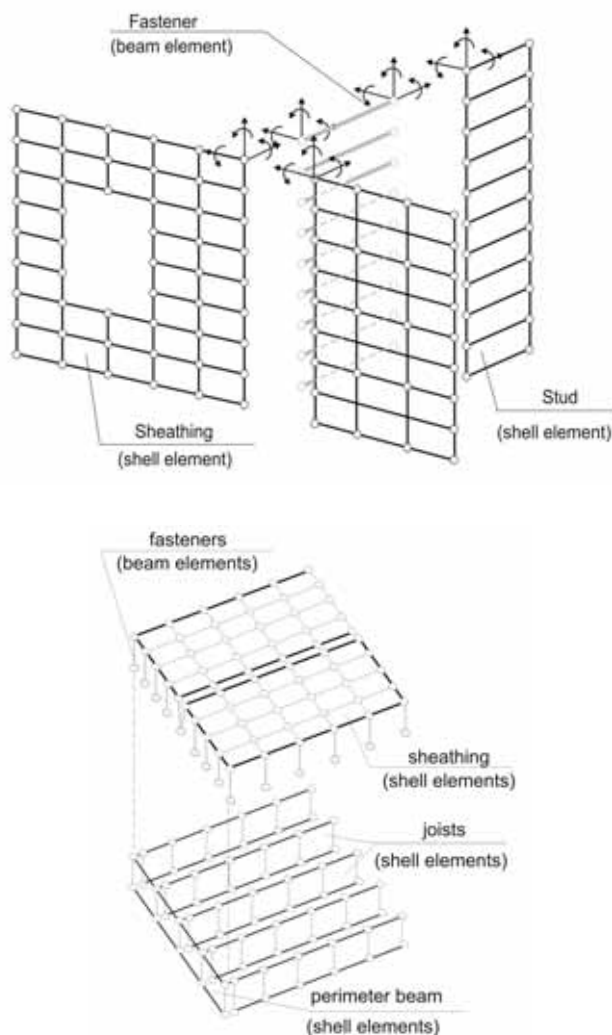


Fig. 6. Finite element model: a) wall element, b) floor element

The completely different approach was proposed in BUT. Timber elements and sheathing were described by shell elements as well the fasteners by the beam elements (Malesza 1997), (Baszeń 2004).

Proposed model was described using finite elements (Fig.6). In contrast to previous models describing fasteners by spring (Foschi 1977), (Dolan, White, 1995), (Tarabia, Itani, 1997), the new models proposed the connector as beam element with six degree of freedom. Slide of connector in the surrounding material influence in a decisive way to it's behavior as well the entire structure.

The main assumption was that only nonlinear elements were sheathing-to-framing connectors. The slide function is described by equation with constants determined from experimental tests.

$$N = (A + B \cdot \delta) \cdot \left[1 - e^{\left(\frac{C}{A} \delta \right)} \right] \quad (1)$$

This equation was used to determine the replacement stiffness of the beam element EA, EJ, GA, necessary for the element stiffness matrix.

Assuming that material of fastener is isotropic, the replacement modulus of elasticity was obtained from formula:

$$E = \xi \cdot C = \frac{l^3}{12J} \left[1 + \frac{3}{4} \cdot (1 + \nu) \alpha \left(\frac{d}{l} \right)^2 \right] \cdot C \quad (2)$$

where:

- C – flexibility of connection,
- J, l, d – respectively moment of inertia, length, diameter of fastener,
- α – shape coefficient, for circular cross-section 10/9,
- ν – Poisson's ratio.

Flexibility of connectors resulting from P-D curve affect on its nonlinearity. The nonlinearity was described by the change of modulus of elasticity. The nonlinear function was obtained separately for each fastener, as dependance between external load and deflection perpendicular to the fastener axis.

Proposed model was verified by the results obtained from experimental test. As a result of the comparative analysis, it was observed that the proposed model maps with high converge the structure deformation. The experimental and model P-D curves are of similar shape and the values are most similar at the destructive load level. A similar situation also occurred in the case of comparison of internal forces.

Floor elements

The wood-frame floors works in two dimensions. Vertical load is transmitted by sheathing to joists while the lateral load is absorbed directly by the perimeter beam and then transferred to joists which cooperate with sheathing. There is a partial effect of composite structure. Floor works as a T-shaped beam consisting of individual beams with collaborative part of sheathing. Flexibility of wooden joists allows for bi-directional operation and bi-directional bending.

The complex behavior of floor inspired the researchers to create the model describing this work. One of the first model was incorporated into FEAFL0 system. The model simplified the structure to system of crossing beams. The composite T-beams was representing joists while perpendicular beams with accurate width was representing sheathing (Thompson et al., 1977)

The next program was FAP using Fourier series to solve problem (Foschi 1982). Similarly FEAFL0 so FAP gave results consistent with the values of experimental studies, however, due to time-consuming calculations programs were not suitable for engineering applications.

The simplification was using the beam-to-spring analog model. In proposed model the sheathing was replaced by the single beam based by springs on multi-layer joists. Characteristics of springs was matched with deflection in mid-span of joists (McCutechon 1984). The development of this model allowed for consideration in the calculation appearance of gaps causes discontinuity of sheathing and thereby reducing the flexural stiffness (Friedley et al., 1997).

Another approach was presented in membrane-to-brace replacement method (Kamiya 1990). Model was based on the assumption that floor works as Vierendeel truss. The sheathing was replaced by compressed brace elements with stiffness according to sheathing material's properties as well connectors type and spacing. The results taken from model was similar to results calculated using ATC guidelines (1981).

Joints

Fasteners the most nonlinear structural elements of light wood-framed building were not analyzed as separate elements but as part of the general pattern of the walls or floors. The main tendency was to assume that the fasteners as springs.

In one of first models the fasteners were assumed as single spring. The connection between elements of timber frame was described as two degrees of freedom spring, when the sheathing-to-framing joint was described as three degrees of freedom spring (Foschi 1977).

More extended model was presented as the system of three springs (Dolan 1989). The extension of Dolan's model was system of independent springs (White, Dolan 1995). In next model also the system of two independent springs was used but additionally the different stiffness in three dimension was applied (Tarabia, Itani 1997).

Another approach was presented by the model proposed at Bialystok Technical University (Malesza 1997), (Baszeń 2004). In place of springs describing fasteners there were used beam elements with six degrees of freedom. The elements was simulating simple beams flexibly connected in sheathing and framing or both sides in framing. The nonlinearity was assumed only for connection between sheathing and framing.

Buildings

The developed numerical models of wall or floor elements encouraged researchers to develop proposed computational systems into models describing the entire building structure.

One of the first models predicting the behavior of whole building was model proposed by Gupta and Kuo (1987). Otherwise to previous models not including uplifting this model has allowed it. The results taken of the model had good agreement with the results from experimental tests.

Another model proposed was developed evaluate the seismic response of the light wood-frame buildings (Tarabia, Itani, 1997). The main part of the study was observing deformation of the structure and distribution of lateral loads among the shear-walls. The model assumed twofold plate and plane-stress state of structure work, provided that deformation in both states are independent. The sheathing movement was incorporated in the model. To prevent overlap of sheathing panels the contact elements was entered to the system.

Collins et al. (2005) proposed 3D nonlinear FE model of light frame buildings. The model was capable to predict the response of building from the global, as general displacement of building, to individual as behavior of single joint. The predicting ability was verified by experimental researches.

A completely different approach was used in the model proposed by Folz and Filiatrault (2004). The 3D building was degenerated into a 2D planar model using zero-height shear wall spring elements connected between adjacent diaphragms or the foundation. This numerical model has been used in computer program SAWS, which was verified by shake table tests performed on a full-scale two-story wood-frame house.

Most of the buildings constructed in lightweight timber frame technology in the United States was not design according to the earthquake engineering principles. Large window openings and garage doors made the first story soft, what prone the structure to large lateral movements. The need for analyzing the stability and seismic performance of soft-story houses have resulted in proposal 3D model by Pang and Ziaei (2012).

Conclusions

Despite wide range of experimental tests as well numerical analysis behavior of the light-frame wooden structures is still not thoroughly explored. The way its work as the whole structure is result of work of each individual structural elements.

The stiffness of walls, floor as well joints affect the behavior of the whole building. Features as higher stiffness of individual elements as selected joints can significantly affect the model of the building behavior. Knowledge of the model facilitate the designing, allows erecting the buildings much safer and cheaper, due to the optimal selection of the number as well the types of structural elements and connections.

The development of this type of construction, and thus the emergence of new and non-typical structures poses major challenges for designers. Large spans of floor elements, and thus a large cross-sections of the elements make the necessity to determine behavior of the structure, not necessarily working as common objects.

Prefabrication allows to reduction the time of building erection but forces necessity of very careful elements connection at the construction site.

This all makes it necessary to describe the model of the construction behavior what is possible using computational models. The need for proposed model verification necessitates the widest range of experimental tests.

References

1. American Society of Civil Engineers – ASCE (2007), *Seismic Rehabilitation of Existing Buildings (ASCE/SEI 41-06)*. Reston, Virginia.
2. Applied Technology Council (ATC) (1981), *Guidelines for the Design of Horizontal Wood Diaphragms*. Berkeley, USA.
3. Baszeń M., Malesza M., Miedziałowski Cz. (2000), *Rozkład naprężeń w poszyciu i słupkach drewnianej ściany szkieletowej z otworem*. Zeszyty Naukowe Politechniki Białostockiej. Budownictwo, Z.20, pp. 7-19.
4. Baszeń M. (2004), *Model obliczeniowy elementów z otworami konstrukcji szkieletowych budynków drewnianych z poszyciem wraz z weryfikacją doświadczalną*. PhD thesis, Białystok University of Technology, Białystok, Poland.
5. Collins, M., Kasal, B., Paevere, P., Foliente, G. (2005), *Three-Dimensional Model of Light Frame Wood Buildings. I: Model Description*. Journal of Structural Engineering, 131(4), pp 676–683.
6. Countryman D. (1952), *Lateral Tests on Plywood Sheathed Diaphragms*. Laboratory Report 55, Douglas Fir Plywood Association.
7. Dinehart D.W., Shenton III H.W. (1998), *Comparison of Static and Dynamic Response of Timber Shear Walls*. Journal of the Structural Engineering, 124(6), pp 686– 695.
8. Dolan J.D., White M.W. (1992), *Design Consideration for Using Adhesives in Shear Walls*. Journal of the Structural Engineering, ASCE, 118(12), pp 3473 – 3479.
9. Dolan J.D. (1989), *The Dynamic response of Timber Shear Walls*. PhD thesis. University of British Columbia, Vancouver, Canada.
10. Dorey D.B., Schriever W.R. (1957), *Structural Tests of a House Under Simulated Wind and Snow Loads*. ASTM Special Technical Report 210.
11. Filiatrault, A., Christovasilis, I., Wanitkorkul, A., van de Lindt, J. (2010). *Experimental Seismic Response of a Full-Scale Light-Frame Wood Building*. Journal of the Structural Engineering, 136(3), pp 246–254.
12. Folz, B. and Filiatrault, A. (2004). *Seismic Analysis of Wood-frame Structures. I: Model Formulation*. Journal of the Structural Engineering, 130(9), pp 1353–1360.
13. Foschi R.O. (1977), *Analysis of Wood Diaphragms and Trusses. I: Diaphragms*. Canadian Journal of the Structural Engineering, 4(3), pp 345–352.
14. Fridley K.J., Rosowsky D.V., Hong P. (1997), *Time-dependent service-load behavior of wood floors: analytical model*. Computers & Structures, 66(6), pp 847–860.
15. Gupta A.K., Kuo G.P. (1985), *Behavior of wood-framed shear walls*. Journal of the Structural Engineering, 111(8), pp 1722–1733.
16. Gupta A.K., Kuo G.P. (1987), *Modeling of a Wood-Framed House*. Journal of Structural Engineering, 113(2), pp 260–278.
17. Heine C.P. (1997), *Effect of Overturning Restraint on the Performance of Fully Sheathed and Perforated Timber Framed Shear Walls*. MSc thesis, Virginia Polytechnic Institute and State University, Blacksburg, USA.
18. Johnson A.C. (1997), *Monotonic and Cyclic Performance of Long Shear Walls with Openings*. MSc thesis, Virginia Polytechnic Institute and State University, Blacksburg, USA.

19. Kamiya F., Itani T. (1998), *Design of Wood Diaphragms with Openings*. Journal of Structural Engineering, 124(7), pp 839–848.
20. Kamiya F. (1990), *Horizontal Plywood Sheathed Diaphragms with Openings: Static Loading Tests and Analysis*. International Engineering Timber Conference, Tokyo, Japan, pp 502–509.
21. Kamiya F. (1992), *Study on Horizontal Diaphragms*. Annual Meeting of the Architectural Institute, Architectural Institute of Japan, Tokyo, Japan, pp 97–114.
22. Lewicki B. (1979), *Budynki wznoszone metodami uprzemysłowionymi: projektowanie konstrukcji i obliczenia*. Arkady, Warsaw, pp 755.
23. Malesza M., Miedziałowski Cz., Malesza J. (2002), *Badania doświadczalne konstrukcji nośnej szkieletowego budynku drewnianego*. XLVIII Konferencja Naukowa Komitetu Inżynierii Lądowej i Wodnej PAN i KN PZITB, Krynica, Poland, pp 163-170.
24. Malesza M., Miedziałowski Cz. (2003), *Discrete analytical models of the wood-framed with sheathing building structures and selected experimental test results*. Archives of Civil Engineering, 49(2), pp 213-240.
25. Malesza M. (1997), *Redystrybucja sił wewnętrznych i odkształcalność tarcz ściennych z nośnym drewnianym szkieletem i współpracującym poszyciem*. PhD thesis, Białystok University of Technology, Białystok, Poland.
26. McCutcheon W.J. (1984), *Deflection of uniformly loaded floors: A beam spring analog*. Research Paper FPL 449, U.S.D.A. Forest Product Laboratory, Madison.
27. McCutcheon W.J. (1985), *Racking Deformation in Wood Shear Walls*. Journal of the Structural Engineering, 111(2), pp 257-269.
28. Pang W., Ziaei E. (2012), *Nonlinear Dynamic Analysis of Soft-Story Light-Frame Wood Buildings*. Structures Congress 2012: pp 1767-1777.
29. Patton-Mallory M., Wolfe R.W., Soltis L.A., Gutkowski R.M. (1985), *Light Frame Shear Walls Length and Opening Effect*. Journal of the Structural Engineering, 111(10), pp 2227-2239.
30. Pei, S, van de Lindt J., Wehbe N., Liu H. (2013), *Experimental Study of Collapse Limits for Wood Frame Shear Walls*. Journal of the Structural Engineering, 139(9), pp 1489–1497.
31. Phillips T.L., Itani R.Y., McLean D.L. (1993), *Lateral Load Sharing by Diaphragms in Wood-Framed Buildings*. Journal of Structural Engineering, 119(5), pp 1556-1571.
32. Rose J.D., Keith E.L. (1996), *Wood Structural Panel Shear Walls with Gypsum Wallboard and Window/Openings*. APA Research Report 157.
33. Salenikov A.J. (2000), *The Racking Performance of Light-Frame Shear Walls*. PhD thesis, Virginia Polytechnic Institute and State University, Blacksburg, USA.
34. Sugiyama H., Andoh N., Uchisako T., Hirano S., Nakamara N. (1988), *Full Scale Test on a Japanese Type of Two-Story Wooden-Frame House Subject to Lateral Load*. Proceedings of 1988 International Conference on Timber Engineering. Forest Products Research Society, Madison, USA, Vol. 2, pp 55-61.
35. Sugiyama H., Matsumoto T. (1994), *Empirical Equations for the Estimation of Racking Strength of Plywood-Sheathed Wall with Opening*. Summaries of Technical Papers of Annual Meeting, Trans. of A.I.J.

36. Tanaka, Y., Ohashi, Y. Sakamoto, I. (1998), *Shaking Table Test of Full-scale Wood-frame House*. Proceedings of the 10th Earthquake Engineering Symposium Volume 2, Yokohama, Japan.
37. Tarabia A.M., Itani R.Y. (1997), *Static and Dynamic Modeling of Light-Frame Wood Buildings*. Computers & Structures, 63(2), pp 319-344.
38. Tissel J.R., Elliott J.R. (1981) *Plywood Diaphragms*. APA Laboratory Report 138.
39. Tissel J.R. (1967), *1966 Horizontal Plywood Diaphragm Tests*. APA Laboratory Report 106.
40. Tuomi R.L., McCutcheon W.J. (1978), *Racking strength of light-frame nailed walls*. Journal of the Structural Engineering, 104(7), pp 1131-1140.
41. White M.W., Dolan J.D. (1995), *Non-linear shear-wall analysis*. Journal of the Structural Engineering, 121(11), pp 1629-1635.
42. White M.W. (1995) *Parametric Study of Timber Shear Walls*. PhD thesis, Virginia Polytechnic Institute and State University, Blacksburg, USA.
43. Wolfe R.W. (1983), *Research Paper FLP 439 – Contribution of Gypsum Wallboards to Racking Resistance of Light-Frame Walls*. U.S. Department of Agriculture, Forest Product Laboratory.
44. Yokel F.Y., Hsi G., Sornes N.F. (1973), *Full Scale Test on Two-Story House Subjected to Lateral Load*. U.S. National Bureau of Standards, Washington, pp 1–26.
45. Zacher E.G., Gray R.G. (1990), *Lessons Learned from Dynamic Tests of Shear Panels*. In: Structural Design, Testing and Analysis, American Society of Civil Engineers, New York, USA, pp 134-142.

